Normal and malignant B-cells in acute lymphoblastic leukemia

Insight into clonal distrubution, minimal residual disease and normal B-cell recovery

Prisca M.J. Theunissen

The research for this thesis was performed within the framework of the Erasmus Postgraduate School Molecular Medicine.

The studies described in the thesis were performed at the Department of Immunology, Erasmus MC, University Medical Center Rotterdam, Rotterdam, The Netherlands and collaborating institutions.

The studies were financially supported by ERA-NET PrioMedChild, project 40-41800-98-027.

The printing of this thesis was supported by Erasmus MC.

ISBN: 978-94-91811-15-9

Illustrations: Prisca Theunissen
Cover: Prisca Theunissen
Lay-out: Daniëlle Korpershoek, Erna Moerland and Bibi van Bodegom
Printing: Haveka B.V., Alblasserdam, the Netherlands

Normal and malignant B-cells in acute lymphoblastic leukemia

Insight into clonal distribution, minimal residual disease and normal B-cell recovery

Normale en maligne B-cellen in acute lymfoblastische leukemie

Inzicht in klonale distributie, minimale restziekte en herstel van normale B-cellen

Proefschrift

ter verkrijging van de graad van doctor aan de
Erasmus Universiteit Rotterdam
op gezag van de rector magnificus

Prof.dr. H.A.P. Pols

en volgens besluit van het College voor Promoties.

De openbare verdediging zal plaatsvinden op
woensdag 21 december 2016 om 13.30 uur

door

Prisca Maria Josephina Theunissen

geboren te Bilzen, België

PROMOTIE COMMISSIE

Promotoren
Prof.dr. J.J.M. van Dongen

Overige leden
Dr. M. van der Burg
Prof.dr. T. Szczepański
Prof.dr. C.M. Zwaan

Copromotor
Dr. V.H.J. van der Velden

CONTENTS

Chapter 1

General Introduction

INTRODUCTION

The treatment of pediatric B-cell precursor acute lymphoblastic leukemia (BCP-ALL) has significantly improved over the last two decades. This has been achieved via new treatment strategies, which included the careful monitoring of treatment effectiveness via measurement of residual leukemic cells, i.e. minimal residual disease (MRD). A better understanding of the heterogeneity and tissue distribution of leukemic cells, the effect of BCP-ALL treatment on the normal B-cell system, and the immunophenotypic differences between malignant cells and their normal counterparts are important to further improve leukemia treatment. To study these topics, in-depth insight into the B-cell receptor (BCR), the immunophenotypic stages of normal B-cell differentiation/maturation, the pathobiology of BCP-ALL and the different techniques of MRD detection is required.

B-CELLS AND THE B-CELL RECEPTOR

B-cells are part of the adaptive immune system and are able to recognize specific antigens with their BCR. Upon encounter with the specific antigen, and with help of T-cells, B-cells become activated and differentiate to plasma cells that secrete immunoglobulins (Ig's) against the antigen. Furthermore, B-cells are able to refine their antigen-recognition and to generate immunological memory, resulting in an improved B-cell response upon re-encounter with the specific antigen. The BCR, and the related secreted Ig, is a Y-shaped molecule consisting of two identical heavy chains and two identical light chains (Figure 1a). Both the heavy chains and light chains are composed of a constant domain and a variable domain. The heavy chain is encoded by genes on the *IGH* locus (chromosome 14); its constant domain by one of the 9 constant genes (Cμ, Cδ, Cγ3, Cγ1, Cα1, Cγ2, Cγ4, Cε and Cα2) and its variable domain by the junction of a Variable (V), Diversity (D) and Joining (J) gene. The light chain is encoded by genes on either the *IGK* locus (chromosome 2), resulting in a κ-chain, or the *IGL* locus (chromosome 22), resulting in a λ-chain. The variable domain of the light chain is the result of transcription from the V-J gene junction on one these loci. The variable domains of the heavy chains and the light chains together form the two antigen-binding sites of the Ig. The constant domains of the two heavy chains together form the part of the BCR that can attach to other cells or molecules (e.g. complement). Depending on which of the 9 constant genes was transcribed, the secreted Ig can have different effector functions, including blockage of ligand-receptor interactions, cell lysis through activation of complement dependent cytotoxicity (CDC), interaction with Fc receptors on effector cells to initiate antibody dependent cellular cytotoxicity (ADCC) and opsonization of the pathogen to promote phagocytosis.

The above described V(D)J junctions are generated through a process called V(D)J-recombination. V(D)J-recombination includes the coupling of a specific V, (D) and J segment and the random insertion and deletion of nucleotides at the V-D and D-J or V-J junction (Figure 1b+c). This process is initiated by double stranded DNA breaks, mediated by recombination activating gene 1 and 2 (RAG1 and RAG2) enzymes. All V, D and J genes are flanked by recombination signal sequences (RSSs), which consist of a heptamer sequence, a spacer region of 12 or 23 base pairs, and a nonamer sequence. Rearrangements can only occur between RSSs with a different spacer length (12-23 rule). RAG1 and RAG2 enzymes recognize RSSs and introduce single strand breaks between the coding segment and the adjacent RSS. This results in hairpin ends at the site of the coding segment (coding ends) and blunt ends at the side of the RSS (signal ends). RAG1 and RAG2 remain associated with the coding and signal ends in a post-cleavage complex, which is critical for proper joining of the ends. The two coding ends are kept in close proximity by the MRN complex (MRE11, Rad50 and NBN), while ataxia-telangiectasia-mutated protein (ATM) induces cell cycle arrest and activation of DNA repair pathways [1,2]. Subsequently, Ku70, Ku80, DNA-dependent protein kinase (DNA-PKcs) and Artemis are recruited to the coding ends, resulting in cleavage of the hairpins by Artemis [3]. After opening the hairpins, endonucleases and terminal deoxynucleotidyl transferase (TdT) are able to delete and

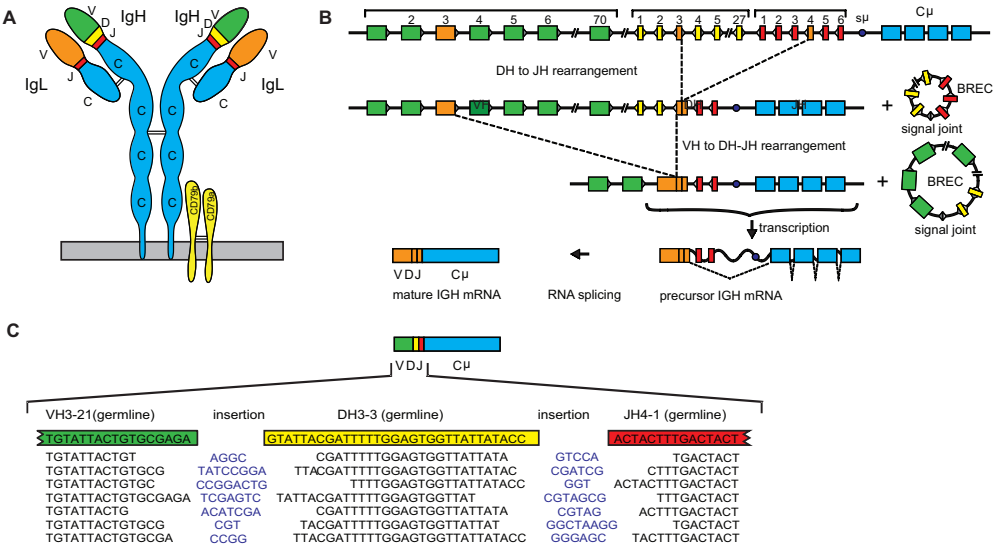

Figure 1.
A. Schematic representation of a BCR molecule, showing the constant domains and variable domains encoded by the V, D and J genes at the *IGH* locus.
B. Schematic representation of V(D)J recombination at the *IGH* locus.
C. Junctional diversity at the *IGH* locus. Examples of junctional diversity at the *IGH* locus, showing that nucleotides are deleted and non-templated nucleotides (blue) are added.

insert non-templated N-nucleotides. Lastly, a complex of DNA ligase V, XRCC4 and XLF ligates the two coding ends [4].

In theory, 38 to 46 functional Vh, 25 Dh, and 6 Jh genes can be combined, resulting in $>5.7\times10^3$ possible *IGH* gene rearrangements [5]. In turn, the IGH chain can be combined with one of the 200 possible *IGK* and 124 possible *IGL* gene rearrangements, resulting in a combinational diversity of $>1.8\times10^6$. The insertion and deletion of nucleotides at the junctions provide an additional junctional diversity of approximately 3 x 10^7. In total, this results in an estimated BCR diversity of $>10^{12}$ [5-7]. Besides these theoretical estimations, next generation sequencing (NGS) of the *IGH*, *IGK* and *IGL* loci was performed to study the naive BCR repertoire in healthy individuals [8]. One study showed a lower bound estimate of 2.2 x 10^5 diversity for the heavy chain diversity and 1.6 x 10^5 for the light chain diversity, suggesting a BCR of $>10^{10}$ [9]. However, the strict definition of diversity might have underestimated the total number of unique sequences in this study [9]. As a result of the large diversity of BCRs, B-cells with a vast number of antigen-specificities are generated.

NORMAL B-CELL DIFFERENTIATION/MATURATION

B-cell precursor differentiation in the bone marrow

B-cell precursors (BCPs) in the bone marrow (BM) differentiate through several differentiation stages to become mature B-cells, expressing a functional BCR. Based on the immunophenotypic and immunogenotypic changes during BCP differentiation, five stages (subsets) are classically defined (Figure 2). First, the pro-B stage, which is the first stage that expresses B-cell lineage markers and is characterized by the expression of CD22, cytoplasmic CD79a and Cd79b, and CD34 (but not yet CD10). In this stage, Dh-Jh rearrangements at the *IGH* locus occur, although Dh-Jh rearrangement were already found in common lymphoid progenitors [10,11]. Second, the pre-B-I stage, which is characterized by expression of CD19, CD10 and CD34. Also, TdT, the enzyme required for the random insertion of nucleotides during V(D)J-recombination, is expressed. In this stage, Vh to Dh-Jh rearrangements at the *IGH* locus are initiated. Only when an in-frame Vh-DhJh rearrangement is formed, transition to the next stage occurs. Third, the pre-B-II-Large stage, characterized by dim expression of CD20 and loss of CD34 and TdT expression. The presence of in-frame Vh-DhJh rearrangements results in the expression of a cytoplasmic Igμ heavy chain (cyIgμ). The cyIgμ is coupled to a VpreB surrogate light chain in the cytoplasm and expressed as a pre-BCR on the cell surface. Subsequent activation of the pre-BCR triggers proliferation of the pre-B-II-Large cells. During this stage, rearrangement processes are temporarily abrogated. Fourth, the pre-B-II-Small stage, characterized by complete CD34 negativity and loss of CD20 expression. In this stage, the pre-BCR is no

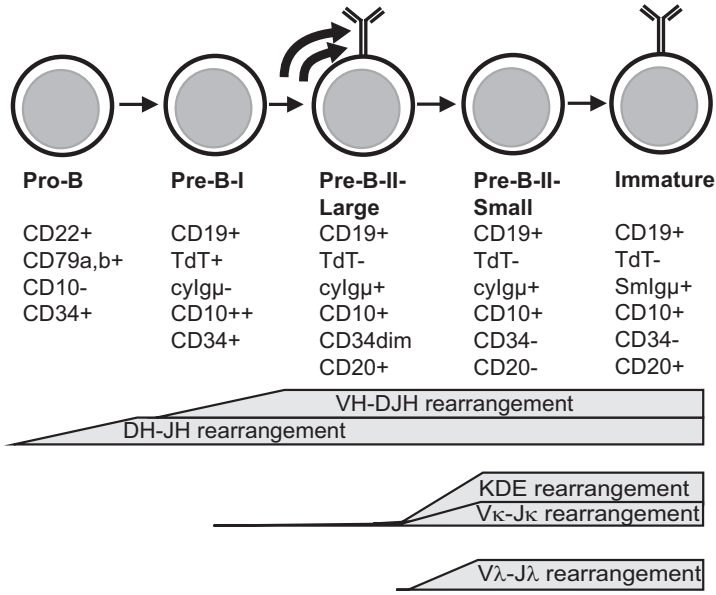

Figure 2.
Immunophenotypic stages of BCP differentiation. The most discriminative markers for each stage are indicated. Grey bars represent the initiation and continuation of rearrangements at the *IGH*, *IGK* and *IGL* locus.

longer expressed and Vκ-Jκ rearrangements at the *IGK* locus are initiated. If this results in an out-of-frame IGK-rearrangement at both alleles, part of the *IGK* gene is deleted (which is possible by two types of kappa deletion rearrangements: IntronRSS-KDE and Vκ-KDE) after which Vλ-Jλ rearrangements at the *IGL* locus will follow. Once an in-frame Vκ-Jκ or Vλ-Jλ rearrangement is formed, transition to the next stage occurs. Fifth, the immature stage, characterized by re-expression of CD20. In this stage, the presence of in-frame Vk-Jk or Vλ-Jλ rearrangements results in expression of a cytoplasmic Igκ respectively Igλ light chain. The Igμ heavy chain and the Igκ or Igλ light chain are combined in the cytoplasm and, if successfully coupled, expressed as a surface membrane IgM (SmIgM), i.e. a functional BCR, on the cell surface. Before migration out of the BM, B-cells with autoreactive BCRs are negatively selected via apoptosis or anergy (central tolerance checkpoint), resulting in a decrease of autoreactive B-cells from ~75% to ~45% and a decrease of polyreactive B-cells from ~55% to less than 10% [12]. Receptor editing, i.e. generation of a new light chain by recombination of an upstream V gene and downstream J gene, can rescue B-cells from negative selection. Later, at the transition from the new BM emigrant to the mature naive B cell stage in PB, the percentage of autoreactive B-cells is further reduced to ~20% (peripheral tolerance checkpoint) [12].

B-cell maturation in the periphery

Newly generated immature B-cells leave the BM and enter the peripheral blood (PB) in the form of transitional B-cells. In the periphery, further maturation of transitional B-cells (CD38++IgD+IgM+), via pre-naive B-cells (characterized by a slightly downregulated CD38 expression), to naïve mature B-cells (CD38dimIgD+IgM+) takes place [13,14]. Naive mature B-cells may migrate to lymphoid tissues, where they become activated after interaction with a specific antigen. After antigen encounter, four different maturation routes can be followed (Figure 3). First, naive mature B-cells can directly mature into plasmablasts (CD38++IgD-IgM+). Second, naive mature B-cells can enter a T-cell dependent germinal center (GC)-reaction in the lymphoid tissue, during which they undergo somatic hypermutation (SHM) to create a BCR with a higher antigen-affinity, and class switch-recombination (CSR) to change the isotype of the secreted Ig (depending on the type and location of the antigen).

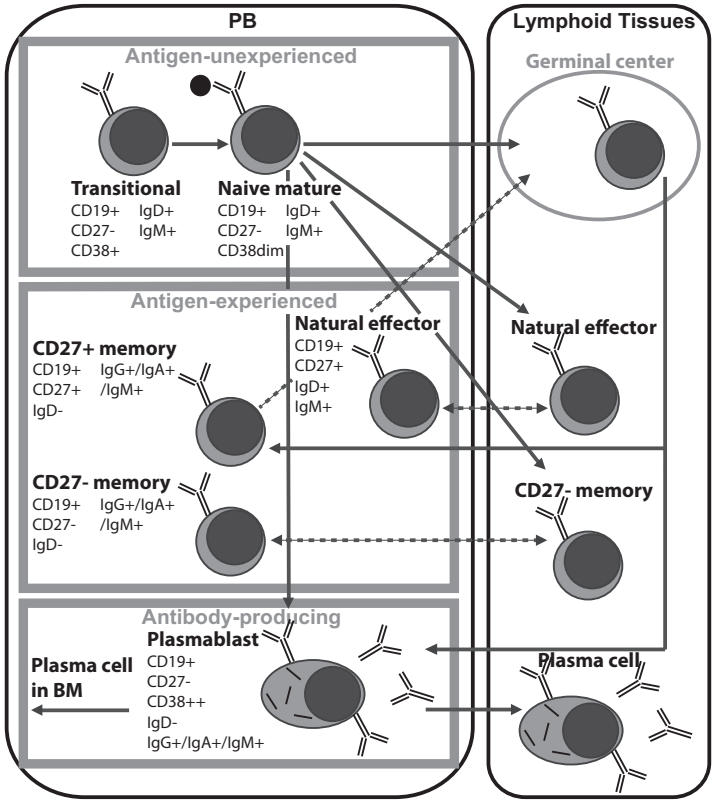

Figure 3.
Schematic overview of the different B-cell subsets in PB and lymphoid tissue. The immunophenotypic markers characteristic for each subset are shown. Solid arrows indicate the main differentiation routes, dashed arrows indicate migration routes.

As a result, plasmablasts (CD38++IgD- and IgG+, IgA+, IgM+ or IgE+) and memory B-cells (CD27+IgD- and IgG+, IgA+, IgM+ or IgE+) with a high affinity and an appropriate Ig-isotype are generated. Third, naive mature B-cells in the marginal zone of the spleen can, without the help of T-cells, develop into natural effector B-cells (CD27+IgD+IgM+) [15]. Fourth, naive mature B-cells in the mucosal lymphoid tissue can, without the help of T-cells, mature into CD27-IgA+ memory B-cells [16]. Plasmablasts generated via the first and second maturation route migrate to the BM, where they become Ig-secreting plasma cells (CD19+ or CD38++ and IgG+, IgA+, IgM+ or IgE+). Memory B-cells circulate through the BM, PB and lymphoid compartments. Upon antigen-encounter in the lymphoid tissue, memory B-cells become activated and can re-enter the GC-reaction, after which the second maturation route is repeated.

PEDIATRIC B-CELL PRECURSOR ACUTE LYMPHOBLAST LEUKEMIA

Epidemiology and clinical manifestation

Each year, approximately 100 children with BCP-ALL are diagnosed in the Netherlands. The incidence of pediatric BCP-ALL peaks between the ages of 2 and 5 years [17]. BCP-ALL is characterized by the clonal expansion of a malignantly transformed BCP and the subsequent suppression of the normal hematopoiesis in BM, resulting in anemia, thrombocytopenia and neutropenia [18]. As a consequence, children with BCP-ALL often present with pallor and fatigue, bruising or bleeding and recurrent infections. Furthermore, leukemic cells can disseminate to the testis and central nervous system, or infiltrate into lymph nodes, spleen and liver, which may result in lymphadenopathy and hepatosplenomegaly [18].

Pathobiology

The exact pathogenesis of BCP-ALL is still unclear. However, many genetic factors have been associated with the development of BCP-ALL. First, several polymorphic variants (*IKZF1*, *CEBPE, ARID5B*) and germline mutations (*PAX5, ETV6, TP53*) cause a genetic predisposition to ALL [17,19]. These gene variants contribute to the intrinsic vulnerability of BCPs to additional events that cause malignant transformation. Also, certain inherited genetic syndromes, such as Down syndrome, are associated with an increased risk of BCP-ALL [20]. In most BCP-ALL patients, the malignant transformation follows the 'multi-hit' model [17,19]. In this model, cytogenetic aberrancies, most commonly chromosomal translocations (e.g. *ETV6-RUNX1, BCR-ABL1*), are the initiating events. These translocations can already occur in utero and result in a chimeric protein with an aberrant function [21]. As secondary events, submicroscopic genetic lesions, such as mutations and deletions, are acquired in genes which encode regulators of lymphoid development or cell cycle, tumor

suppressors or lymphoid signaling molecules (e.g. *PAX5, IKZF1, EBF1*) [22,23]. Together, these events ultimately result in arrest of the BCP differentiation and uncontrolled proliferation.

During disease progression, multiple subclones can evolve from the ancestral BCP-ALL clone, as reported by studies showing different copy number alterations, chromosomal translocations and *IG* gene rearrangements within one BCP-ALL population [24-27]. According to the Darwinian selection model, subclones with additional genetic lesions that provide a survival advantage are positively selected. Consequently, a BCP-ALL population can contain one or few major clones as well as multiple smaller subclones, evolutionary connected to each other in a multi branch-like structure.

BCP-ALL subtypes

BCP-ALL can be classified into subtypes based on immunophenotype and cytogenetics. Based on immunophenotype, BCP-ALL cases are traditionally classified as pro-B ALL (CD10-cylgμ-), common ALL (CD10+cylgμ-) and pre-B ALL (CD10+cylgμ+). However, this classification has proven to be of limited clinical significance. Based on cytogenetic aberrancies, pediatric BCP-ALL cases are classified by the presence of an *ETV6-RUNX1* translocation, a *BCR-ABL1* translocation, a *TCF3-PBX1* translocation, a *MLL*-rearrangement, a translocation involving *MYC*-deregulation, hyperdiploidy (>50 chromosomes), hypodiploidy (<44 chromosomes) or none of these genetic aberrancies (not otherwise specified; NOS) (Figure 4) [28,29]. Of note, the frequency of *MLL*-rearrangements is particularly high (80%) among infants younger than 1 year [28].

Prognostic factors at diagnosis

The general prognosis for children with BCP-ALL is relatively good; the overall survival of children treated according to the Dutch Childhood Oncology Group (DCOG) ALL10 protocol was 92% [30]. However, depending on clinical features, genetic aberrancies and treatment response, the risk of relapse differs between patients [19]. With regard to clinical features, an age of >10 years, an age of <1 year and a white blood cell count of >50,000/uL at diagnosis are associated with an adverse prognosis. Several of the cytogenetic BCP-ALL subtypes are also associated with prognosis: a *TEL-AML1* translocation, hyperdiploidy, and some chromosome trisomies have a favorable prognosis, whereas a *BCR-ABL1* translocation, *MLL*-rearrangements and hypodiploidy have an adverse prognosis. Furthermore, a genetic alteration in *IKZF1*, which encodes the lymphoid transcription factor Ikaros, is associated with poor prognosis [31]. Finally, treatment response is a very important predictive factor. The presence of >1000 leukemic cells/uL in PB at eight days after start of therapy (prednisone response) is associated with poor prognosis. However, the strongest prognostic factor for relapse in children with BCP-ALL is the amount of residual leukemic cells, i.e. MRD, during the first months after start of treatment [32,33].

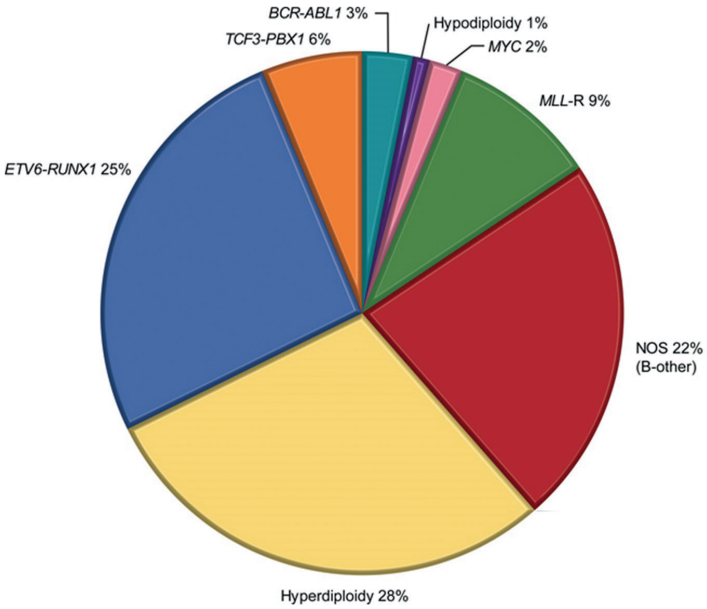

Figure 4.
Distribution of cytogenic subtypes of pediatric BCP-ALL (adapted from Bohjwani et al., Pediatr. Clin. North Am., 2015) [28].

Evaluation of treatment effectiveness as prognostic factor

MRD levels during the first months after start of therapy reflect the intrinsic drug sensitivity of the leukemic cells, the pharmacodynamics and pharmacogenomics of the host, the type of regimens administered and the treatment adherence [18]. Five-fold to ten-fold higher relapse rates were found in MRD-positive patients compared to MRD-negative patients when treated according to the same protocol (Figure 5). Moreover, within the MRD-positive patients, a high degree of MRD (>0.1%) was associated with a three-fold higher relapse rate when compared with patients with a low degree of MRD (<0.1%) [32]. MRD is generally monitored in BM samples, taken at different time points during therapy. In the Dutch protocols (DCOG), these time points are day 33, day 79, month 5, month 9 and month 12 after start of therapy. MRD levels at time points day 33 (during induction therapy) and day 79 (after induction therapy) determine to which risk group a patient will be assigned. Patients are assigned to the Standard Risk (SR) group if both time points are MRD negative, to the High Risk (HR) group if both time points are MRD positive with an MRD level of at least 10^{-3}, and to the Medium Risk (MR) group if one or both time points is/are MRD positive, provided that the MRD level at day 79 is less than 10^{-3}. Based on the risk group, patients are treated in different treatment arms; patients with a lower risk of

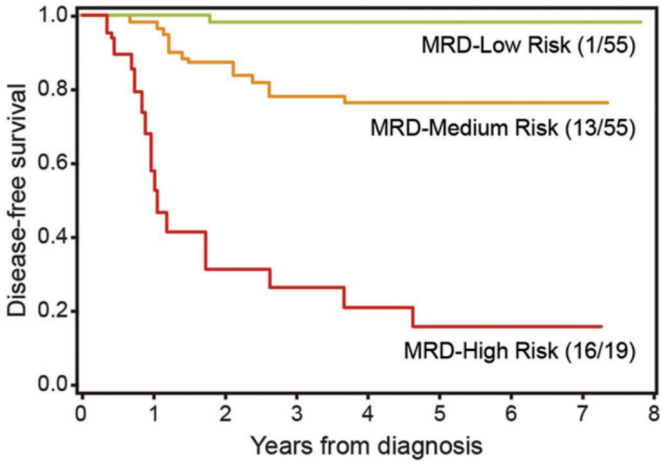

Figure 5.
Disease-free survival of MRD-based risk groups in children treated according to DCOG ALL8/ BFM/ AIEOP protocols (adapted from Van Dongen et al., Lancet, 1998) [32].

relapse undergo a less intensive treatment, resulting in less therapy-induced toxicity and morbidity [30,34].

Treatment

Although different treatment protocols exist (developed by different international consortia), most are based on the so-called Berlin-Frankfurt-Münster (BFM) backbone [35]. This backbone typically consists of an induction phase, an intensification/consolidation phase and a maintenance phase. The induction phase (4 to 6 weeks) is characterized by high doses of a glucocorticoid (prednisone or dexamethasone). This phase usually results in morphological remission (<5% leukemic cells in BM). The intensification phase (6 to 12 months) includes a combination of chemotherapeutic drugs that is designed to consolidate remission and prevent development of overt central nervous system leukemia [19]. Repeated courses of methotrexate are important during this treatment phase. The maintenance phase (18 to 30 months) consists of daily oral mercaptopurine or thioguanine and weekly oral methotrexate, in some protocols complemented by periodic pulses of glucocorticoid and vincristine [19]. Treatment of children in the HR group often involves stem cell transplantation. In this thesis, all included patients were treated according to the SR or MR treatment arm of the DCOG ALL10 or ALL11 protocol (Figure 6).

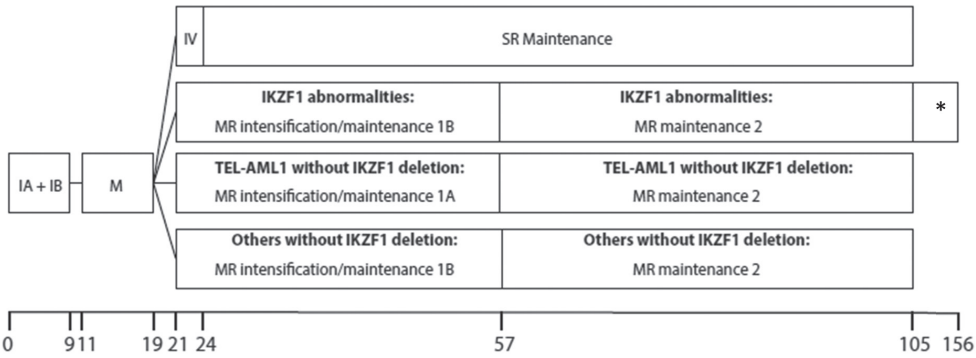

Figure 6.
DCOG ALL11 treatment protocol for children with BCP-ALL which are stratified into the SR or MR treatment arm. The number of weeks after diagnosis are indicated. 1A+1B: induction therapy. M: cycle M. *: extension of maintenance therapy with one year. The HR treatment arm is omitted, since HR patients were excluded from our studies (adapted from the DCOG ALL11 protocol, 2012).

Chemotherapy-induced suppression of humoral immunity

Although aimed to be directed against the leukemic cells, BCP-ALL therapy also affects the immune system, including normal B-cells. Already shortly after start therapy, hardly any BCPs and mature B-cells remain in BM respectively PB [36,37]. Consequently, patients develop hypogammaglobulinemia, which contributes to a high susceptibility to infections [38]. During intervals in therapy, regeneration of BCPs occurs, resulting in a temporary reappearance of early BCPs [39,40]. However, B-cell numbers in PB remain extremely low during therapy. After end of therapy, mature B-cell numbers and Ig levels quickly recover. However, the mature B-cell population shows an aberrant composition, characterized by a relative increase of naive mature B-cells, up to one year after end of therapy [37].

MINIMAL RESIDUAL DISEASE DETECTION

PCR-based MRD analysis

MRD detection is in Europe primarily performed by PCR-amplification of immunoglobulin (IG) or T-cell receptor (TR) gene rearrangements (www.EuroMRD.org) [41]. As described in the section 'B-cells and the B-cell receptor', the junctional regions of rearranged IG genes are unique for each B-cell. Since leukemic cells are derived from normal BCPs, leukemic cells will in most cases harbor IG gene rearrangements. Moreover, they can harbor certain TR gene rearrangements. Rearrangements and/or deletions of the *TRB*, *TRG* and *TRD* genes were found in 35%, 59% and 89% of BCP-ALL cases, respectively [42]. The high frequency (>90%) of cross-lineage TR gene rearrangements in BCP-ALL cells might be explained by

ongoing activity of the V(D)J recombination machinery after malignant transformation of a BCP [42]. Together, the IG and TR gene rearrangements present in a leukemic cell can be regarded as unique 'fingerprints' of that leukemic cell and thus as targets specific for residual leukemic cells [43].

In order to perform PCR-based MRD detection, the MRD targets (i.e. clonal IG/TR gene rearrangements) first need to be identified in the diagnosis sample. Therefore, singleplex or multiplex V-, D-, and J-primer sets are used to PCR amplify all potential *IGH*, *IGK*, *IGL*, *TRG*, *TRD* and *TRB* gene rearrangements [44]. Subsequently, heteroduplex analysis of the PCR products is performed (Figure 7a), which discriminates clonal IG/TR gene rearrangements (derived from leukemic clones) from polyclonal IG/TR gene rearrangements (derived from normal B-cells and T-cells). Next, the junctional regions of the clonal IG/TR gene rearrangements are sequenced. Based on these sequences, junctional region-specific oligonucleotides, so-called allele-specific oligonucleotides (ASOs), are designed [43,45]. Finally, ASO RQ-PCR is performed on follow up samples, resulting in the quantification of the clonal IG/TR gene rearrangement at a specific follow up time point (Figure 7b). This way, MRD levels can be detected with a sensitivity of 10^{-4} to 10^{-5}.

Advantages of PCR-based MRD detection are the relatively high sensitivity, the applicability to almost all patients and the already established standardization and quality assessment programs, whereas disadvantages are the laborious design of ASOs and the risk of losing MRD targets (due to oligoclonality or clonal evolution) [33].

Flow cytometric MRD analysis

MRD detection can also be performed by using flow cytometry (Figure 8). In 95% of the patients, leukemic cells can be recognized based on their aberrant marker expression. Leukemic cells can be discriminated from normal BCPs by the expression of BCP-ALL specific markers, e.g. CD123, CD66c and CD58, by overexpression or underexpression of B-cell differentiation markers, e.g. overexpression of CD10 or underexpression of CD81, or by asynchronous expression of B-cell differentiation markers, e.g. expression of TdT and high levels of CD20 [46-48]. Still, it can be difficult to discriminate residual leukemic cells from normal BCPs, since many markers are expressed similarly. Specific advantages of flow cytometric MRD detection include the potential to also analyze the normal BCP population while searching for MRD and the short time between sampling and availability of the MRD result [49]. However, disadvantages include the difficult discrimination between normal BCP and leukemic cells during therapy intervals (when regenerating BCPs might be abundantly present), the subjectivity in data analysis (e.g. differences in gating strategies) and data interpretation, the need for high cell numbers (to obtain a high sensitivity) and, in some cases, the onset of an immunophentoypic shift (e.g. a therapy-induced shift in marker expression levels during follow up) [33]. These disadvantages result in a moderate sensitivity

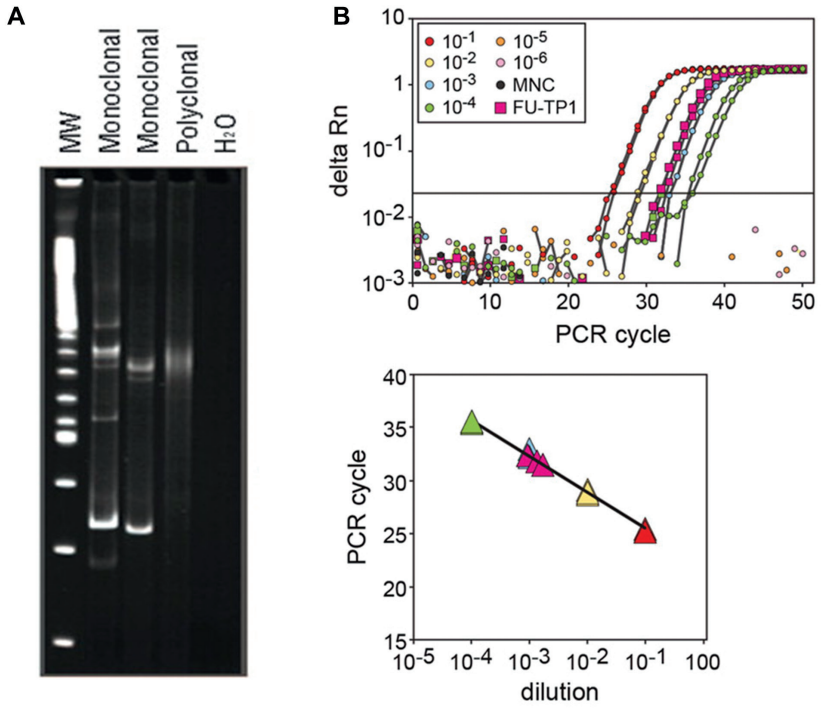

Figure 7.
A. In heteroduplex analysis, the junctional region heterogeneity of IG/TR gene rearrangements is exploited to distinguish between monoclonal and polyclonal lymphocyte expansions. In samples with clonal lymphocytes, the PCR products of rearranged IG/TR genes form, after reannealing, homoduplexes, causing relatively sharp bands. In contrast, in samples with polyclonal lymphocyte expansions, the PCR products form heteroduplexes, resulting in a background smear (Van Dongen et al., Leukemia, 2003) [44].
B. Example of an RQ-PCR MRD analysis using a Vd2-Dd2-Ja11 rearrangement as MRD target. The amplification plot (upper panel) shows the dilution experiment of the diagnosis sample and the measurement of the follow up sample (all performed in triplicate). The corresponding standard curve (lower panel) is based on the dilution experiment and allows calculation of the MRD level in the follow up sample (Van Dongen et al., Blood, 2015).

(>10^{-4} in the majority of cases) that is lower than that of PCR-based MRD detection. Studies which compared 4- to 6-color flow cytometric MRD detection with PCR-based MRD detection found, in absence of any cut-off, a concordance of 68% to 82% at early MRD time points (<3 months after start of therapy) [50-52]. Indeed, most discordant cases were found below 10^{-4}. To increase the sensitivity of flow cytometric MRD detection to a level comparable to that of PCR-based MRD detection (~10^{-5}), it is necessary to develop ≥8-color antibody panels, a procedure for high cell number acquisition, and new tools for objective data analysis.

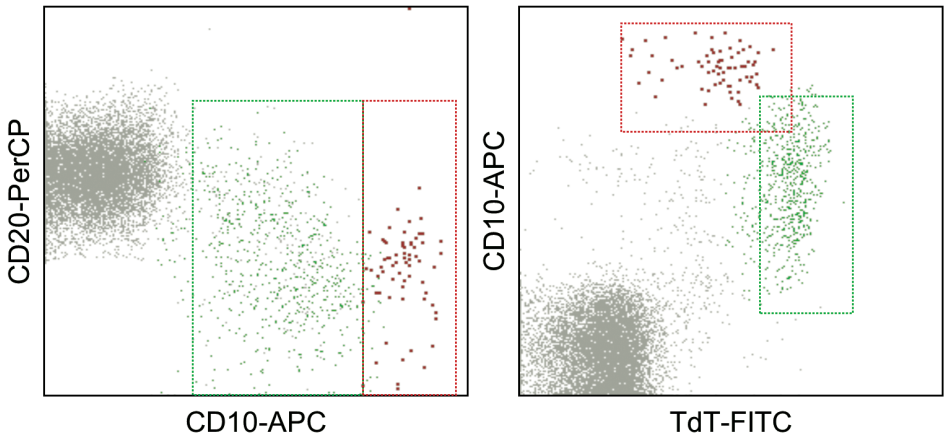

Figure 8.
Dot plots showing an example of flow cytometric MRD measurement at day 79 after start of BCP-ALL treatment. Red events indicate MRD (0.07% in total WBC). Green events indicate regenerating normal BCPs.

NGS-based MRD detection

Since recently, MRD detection is also possible by next generation sequencing of IG/TR gene rearrangements. After amplification of the IG/TR gene rearrangements by using V-, D-, and J-primer sets similar to those used for PCR-based MRD detection, high throughput sequencing of the PCR products can be performed by using different platforms. Commonly used in NGS-based studies on BCP-ALL MRD is the Illumina platform, which utilizes bridge amplification and reversible-terminator chemistry as important techniques [53,54]. Using the NGS-based approach, all IG/TR gene rearrangements present in the BCP-ALL sample are detected. At diagnosis, only the IG/TR gene rearrangements with a frequency of >5% are generally regarded as leukemia-derived (as opposed to normal lymphocyte-derived IG/TR gene rearrangements) [53]. During follow up, IG/TR gene rearrangements identified as leukemic at diagnosis can be retraced and quantified as MRD level. To correctly quantify the MRD level, the read count of each IG/TR gene rearrangement needs to be corrected for PCR amplification. This can be achieved by the so-called spike-in method, in which a known number of reference IG/TR gene rearrangements was added to each PCR reaction in order to determine the correction factor. Depending on the amount of DNA input, NGS-based MRD detection can reach a sensitivity between 10^{-4} and 10^{-5}. Advantages of NGS-based MRD detection are the relatively high sensitivity, the use of standard primers (rather than ASOs) and the ability to monitor all leukemic IG/TR gene rearrangements (which prevents potential loss of MRD targets). However, there are still some major concerns that need to be overcome before NGS-based MRD detection can be applied in clinical practice. First, it is still arbitrary how to discriminate IG/TR gene rearrangements derived from leukemic cells

from those derived from normal B-cell and T-cell clones and technical background. Second, since multiplex PCR reactions are prone to disproportional amplification, the frequency of a clonal IG/TR gene rearrangement might not be fully accurate. Third, standardization, quality assessment programs, and validation of NGS-based MRD detection in a multicenter and scientifically independent setting are still lacking [33].

AIMS AND OUTLINE OF THIS THESIS

In this thesis, we aimed to study both leukemic and newly generated normal B-cells in children with BCP-ALL, since a better understanding of the tissue distribution of leukemic cells, the effect of BCP-ALL treatment on normal B-cells and the immunophenotypic differences between malignant cells and their normal counterparts are important to further improve leukemia treatment. First, we focused on the leukemic B-cell population at BCP-ALL diagnosis. Recent NGS-based analysis of IG/TR gene rearrangements showed that the BCP-ALL population can consist of many more clones than previously thought. However, it is still unknown to what extent these clones are distributed throughout the body. Therefore, in **Chapter 2**, we study the number of BCP-ALL clones and their distribution throughout the BM and PB compartment, by using NGS-based IG/TR gene rearrangement analysis.

During BCP-ALL therapy, also the normal B-cell system is affected. As a result, both the BCP population in BM and mature B-cell population in PB are almost completely destroyed, and reconstitution of the B-cell system is needed. However, the complete differentiation/maturation pattern during B-cell reconstitution and the mechanism behind the relatively fast B-cell recovery after end of therapy (increased *de novo* BCP generation versus enhanced proliferation within a B-cell subset) is still unknown. In **Chapter 3**, we analyze in detail the B-cell subsets in both BM and PB during B-cell reconstitution, and study the degree of proliferation within different B-cell subsets during and after therapy.

Although the bulk of leukemic cells is effectively killed by chemotherapy, residual leukemic cells (i.e. MRD) can remain present. Adequate quantification of MRD is of utmost importance for stratification of patients into the different treatment arms. To quantify MRD by flow cytometry, BCP-ALL cells need to be discriminated from regenerating BCPs. However, studies on the immunophenotypes of regenerating BCPs in particular are very limited. **Chapter 4** provides a detailed description of the immunophenotypic maturation during normal B-cell differentiation and the immunophenotypic maturation during BCP regeneration in BM of BCP-ALL patients.

So far, the sensitivity of flow cytometric MRD detection has been inferior to that of PCR-based MRD detection. To increase the sensitivity of flow cytometric MRD detection,

a sample processing procedure allowing for the acquisition of high cell numbers, and an optimized ≥8-color antibody panel are required. In **Chapter 5**, we aim to identify new markers that can contribute to flow cytometric MRD detection in pediatric BCP-ALL. Subsequently, in **Chapter 6**, we develop a new single-tube antibody panel (8-colors) together with a new sample processing procedure, thereby increasing the sensitivity of flow cytometric MRD detection to $\leq 10^{-5}$.

Finally, we integrate all the findings presented in this thesis and discuss their implications for clinical practice in **Chapter 7**.

REFERENCES

1. de Jager M, van Noort J, van Gent DC, Dekker C, Kanaar R, Wyman C. Human Rad50/Mre11 is a flexible complex that can tether DNA ends. Mol Cell 2001 Nov; 8(5): 1129-1135.
2. Bakkenist CJ, Kastan MB. DNA damage activates ATM through intermolecular autophosphorylation and dimer dissociation. Nature 2003 Jan 30; 421(6922): 499-506.
3. van Gent DC, van der Burg M. Non-homologous end-joining, a sticky affair. Oncogene 2007 Dec 10; 26(56): 7731-7740.
4. Ahnesorg P, Smith P, Jackson SP. XLF interacts with the XRCC4-DNA ligase IV complex to promote DNA nonhomologous end-joining. Cell 2006 Jan 27; 124(2): 301-313.
5. H IJ, Wentink M, van Zessen D, Driessen GJ, Dalm VA, van Hagen MP, et al. Strategies for B-cell receptor repertoire analysis in primary immunodeficiencies: from severe combined immunodeficiency to common variable immunodeficiency. Front Immunol 2015; 6: 157.
6. Davis MM, Bjorkman PJ. T-cell antigen receptor genes and T-cell recognition. Nature 1988 Aug 4; 334(6181): 395-402.
7. van Dongen JJ, Wolvers-Tettero IL. Analysis of immunoglobulin and T cell receptor genes. Part I: Basic and technical aspects. Clin Chim Acta 1991 Apr; 198(1-2): 1-91.
8. Benichou J, Ben-Hamo R, Louzoun Y, Efroni S. Rep-Seq: uncovering the immunological repertoire through next-generation sequencing. Immunology 2012 Mar; 135(3): 183-191.
9. Glanville J, Zhai W, Berka J, Telman D, Huerta G, Mehta GR, et al. Precise determination of the diversity of a combinatorial antibody library gives insight into the human immunoglobulin repertoire. Proc Natl Acad Sci U S A 2009 Dec 1; 106(48): 20216-20221.
10. Rumfelt LL, Zhou Y, Rowley BM, Shinton SA, Hardy RR. Lineage specification and plasticity in CD19- early B cell precursors. J Exp Med 2006 Mar 20; 203(3): 675-687.
11. van Zelm MC, van der Burg M, de Ridder D, Barendregt BH, de Haas EF, Reinders MJ, et al. Ig gene rearrangement steps are initiated in early human precursor B cell subsets and correlate with specific transcription factor expression. J Immunol 2005 Nov 1; 175(9): 5912-5922.

12. Wardemann H, Yurasov S, Schaefer A, Young JW, Meffre E, Nussenzweig MC. Predominant autoantibody production by early human B cell precursors. Science 2003 Sep 5; 301(5638): 1374-1377.
13. Lee J, Kuchen S, Fischer R, Chang S, Lipsky PE. Identification and characterization of a human CD5+ pre-naive B cell population. J Immunol 2009 Apr 1; 182(7): 4116-4126.
14. Sims GP, Ettinger R, Shirota Y, Yarboro CH, Illei GG, Lipsky PE. Identification and characterization of circulating human transitional B cells. Blood 2005 Jun 1; 105(11): 4390-4398.
15. Weill JC, Weller S, Reynaud CA. Human marginal zone B cells. Annu Rev Immunol 2009; 27: 267-285.
16. Berkowska MA, Driessen GJ, Bikos V, Grosserichter-Wagener C, Stamatopoulos K, Cerutti A, et al. Human memory B cells originate from three distinct germinal center-dependent and -independent maturation pathways. Blood 2011 Aug 25; 118(8): 2150-2158.
17. Inaba H, Greaves M, Mullighan CG. Acute lymphoblastic leukaemia. Lancet 2013 Jun 1; 381(9881): 1943-1955.
18. Pui CH, Robison LL, Look AT. Acute lymphoblastic leukaemia. Lancet 2008 Mar 22; 371(9617): 1030-1043.
19. Hunger SP, Mullighan CG. Acute Lymphoblastic Leukemia in Children. N Engl J Med 2015 Oct 15; 373(16): 1541-1552.
20. Hertzberg L, Vendramini E, Ganmore I, Cazzaniga G, Schmitz M, Chalker J, et al. Down syndrome acute lymphoblastic leukemia, a highly heterogeneous disease in which aberrant expression of CRLF2 is associated with mutated JAK2: a report from the International BFM Study Group. Blood 2010 Feb 4; 115(5): 1006-1017.
21. Wiemels JL, Cazzaniga G, Daniotti M, Eden OB, Addison GM, Masera G, et al. Prenatal origin of acute lymphoblastic leukaemia in children. Lancet 1999 Oct 30; 354(9189): 1499-1503.
22. Mullighan CG, Goorha S, Radtke I, Miller CB, Coustan-Smith E, Dalton JD, et al. Genome-wide analysis of genetic alterations in acute lymphoblastic leukaemia. Nature 2007 Apr 12; 446(7137): 758-764.
23. Kuiper RP, Schoenmakers EF, van Reijmersdal SV, Hehir-Kwa JY, van Kessel AG, van Leeuwen FN, et al. High-resolution genomic profiling of childhood ALL reveals novel recurrent genetic lesions affecting pathways involved in lymphocyte differentiation and cell cycle progression. Leukemia 2007 Jun; 21(6): 1258-1266.
24. Swaminathan S, Klemm L, Park E, Papaemmanuil E, Ford A, Kweon SM, et al. Mechanisms of clonal evolution in childhood acute lymphoblastic leukemia. Nat Immunol 2015 Jul; 16(7): 766-774.
25. Anderson K, Lutz C, van Delft FW, Bateman CM, Guo Y, Colman SM, et al. Genetic variegation of clonal architecture and propagating cells in leukaemia. Nature 2011 Jan 20; 469(7330): 356-361.
26. Mullighan CG, Phillips LA, Su X, Ma J, Miller CB, Shurtleff SA, et al. Genomic analysis of the clonal origins of relapsed acute lymphoblastic leukemia. Science 2008 Nov 28; 322(5906): 1377-1380.
27. Gawad C, Pepin F, Carlton VE, Klinger M, Logan AC, Miklos DB, et al. Massive evolution of the immunoglobulin heavy chain locus in children with B precursor acute lymphoblastic leukemia. Blood 2012 Nov 22; 120(22): 4407-4417.
28. Bhojwani D, Yang JJ, Pui CH. Biology of childhood acute lymphoblastic leukemia. Pediatr Clin North Am 2015 Feb; 62(1): 47-60.

29. Wandt H, Haferlach T, Thiede C, Ehninger G. WHO classification of myeloid neoplasms and leukemia. Blood 2010 Jan 21; 115(3): 748-749; author reply 749-750.
30. Pieters R, de Groot-Kruseman H, Van der Velden V, Fiocco M, van den Berg H, de Bont E, et al. Successful Therapy Reduction and Intensification for Childhood Acute Lymphoblastic Leukemia Based on Minimal Residual Disease Monitoring: Study ALL10 From the Dutch Childhood Oncology Group. J Clin Oncol 2016 Jun 6.
31. van der Veer A, Waanders E, Pieters R, Willemse ME, Van Reijmersdal SV, Russell LJ, et al. Independent prognostic value of BCR-ABL1-like signature and IKZF1 deletion, but not high CRLF2 expression, in children with B-cell precursor ALL. Blood 2013 Oct 10; 122(15): 2622-2629.
32. van Dongen JJ, Seriu T, Panzer-Grumayer ER, Biondi A, Pongers-Willemse MJ, Corral L, et al. Prognostic value of minimal residual disease in acute lymphoblastic leukaemia in childhood. Lancet 1998 Nov 28; 352(9142): 1731-1738.
33. van Dongen JJ, van der Velden VH, Bruggemann M, Orfao A. Minimal residual disease diagnostics in acute lymphoblastic leukemia: need for sensitive, fast, and standardized technologies. Blood 2015 Jun 25; 125(26): 3996-4009.
34. van Tilburg CM, Sanders EA, Nibbelke EE, Pieters R, Revesz T, Westers P, et al. Impact of reduced chemotherapy treatment for good risk childhood acute lymphoblastic leukaemia on infectious morbidity*. Br J Haematol 2011 Feb; 152(4): 433-440.
35. Einsiedel HG, von Stackelberg A, Hartmann R, Fengler R, Schrappe M, Janka-Schaub G, et al. Long-term outcome in children with relapsed ALL by risk-stratified salvage therapy: results of trial acute lymphoblastic leukemia-relapse study of the Berlin-Frankfurt-Munster Group 87. J Clin Oncol 2005 Nov 1; 23(31): 7942-7950.
36. Nilsson A, De Milito A, Engstrom P, Nordin M, Narita M, Grillner L, et al. Current chemotherapy protocols for childhood acute lymphoblastic leukemia induce loss of humoral immunity to viral vaccination antigens. Pediatrics 2002 Jun; 109(6): e91.
37. van Tilburg CM, van der Velden VH, Sanders EA, Wolfs TF, Gaiser JF, de Haas V, et al. Reduced versus intensive chemotherapy for childhood acute lymphoblastic leukemia: impact on lymphocyte compartment composition. Leuk Res 2011 Apr; 35(4): 484-491.
38. Eyrich M, Wiegering V, Lim A, Schrauder A, Winkler B, Schlegel PG. Immune function in children under chemotherapy for standard risk acute lymphoblastic leukaemia - a prospective study of 20 paediatric patients. Br J Haematol 2009 Nov; 147(3): 360-370.
39. van Wering ER, van der Linden-Schrever BE, Szczepanski T, Willemse MJ, Baars EA, van Wijngaarde-Schmitz HM, et al. Regenerating normal B-cell precursors during and after treatment of acute lymphoblastic leukaemia: implications for monitoring of minimal residual disease. Br J Haematol 2000 Jul; 110(1): 139-146.
40. van Lochem EG, Wiegers YM, van den Beemd R, Hahlen K, van Dongen JJ, Hooijkaas H. Regeneration pattern of precursor-B-cells in bone marrow of acute lymphoblastic leukemia patients depends on the type of preceding chemotherapy. Leukemia 2000 Apr; 14(4): 688-695.

41. van der Velden VH, Cazzaniga G, Schrauder A, Hancock J, Bader P, Panzer-Grumayer ER, et al. Analysis of minimal residual disease by Ig/TCR gene rearrangements: guidelines for interpretation of real-time quantitative PCR data. Leukemia 2007 Apr; 21(4): 604-611.
42. Szczepanski T, Beishuizen A, Pongers-Willemse MJ, Hahlen K, Van Wering ER, Wijkhuijs AJ, et al. Cross-lineage T cell receptor gene rearrangements occur in more than ninety percent of childhood precursor-B acute lymphoblastic leukemias: alternative PCR targets for detection of minimal residual disease. Leukemia 1999 Feb; 13(2): 196-205.
43. van der Velden VH, Hochhaus A, Cazzaniga G, Szczepanski T, Gabert J, van Dongen JJ. Detection of minimal residual disease in hematologic malignancies by real-time quantitative PCR: principles, approaches, and laboratory aspects. Leukemia 2003 Jun; 17(6): 1013-1034.
44. van Dongen JJ, Langerak AW, Bruggemann M, Evans PA, Hummel M, Lavender FL, et al. Design and standardization of PCR primers and protocols for detection of clonal immunoglobulin and T-cell receptor gene recombinations in suspect lymphoproliferations: report of the BIOMED-2 Concerted Action BMH4-CT98-3936. Leukemia 2003 Dec; 17(12): 2257-2317.
45. Pongers-Willemse MJ, Verhagen OJ, Tibbe GJ, Wijkhuijs AJ, de Haas V, Roovers E, et al. Real-time quantitative PCR for the detection of minimal residual disease in acute lymphoblastic leukemia using junctional region specific TaqMan probes. Leukemia 1998 Dec; 12(12): 2006-2014.
46. Gaipa G, Basso G, Biondi A, Campana D. Detection of minimal residual disease in pediatric acute lymphoblastic leukemia. Cytometry B Clin Cytom 2013 Nov-Dec; 84(6): 359-369.
47. Campana D, Coustan-Smith E. Detection of minimal residual disease in acute leukemia by flow cytometry. Cytometry 1999 Aug 15; 38(4): 139-152.
48. Szczepanski T, van der Velden VH, van Dongen JJ. Flow-cytometric immunophenotyping of normal and malignant lymphocytes. Clin Chem Lab Med 2006; 44(7): 775-796.
49. Coustan-Smith E, Campana D. Immunologic minimal residual disease detection in acute lymphoblastic leukemia: a comparative approach to molecular testing. Best Pract Res Clin Haematol 2010 Sep; 23(3): 347-358.
50. Denys B, van der Sluijs-Gelling AJ, Homburg C, van der Schoot CE, de Haas V, Philippe J, et al. Improved flow cytometric detection of minimal residual disease in childhood acute lymphoblastic leukemia. Leukemia 2013 Mar; 27(3): 635-641.
51. Gaipa G, Cazzaniga G, Valsecchi MG, Panzer-Grumayer R, Buldini B, Silvestri D, et al. Time point-dependent concordance of flow cytometry and real-time quantitative polymerase chain reaction for minimal residual disease detection in childhood acute lymphoblastic leukemia. Haematologica 2012 Oct; 97(10): 1582-1593.
52. Malec M, van der Velden VH, Bjorklund E, Wijkhuijs JM, Soderhall S, Mazur J, et al. Analysis of minimal residual disease in childhood acute lymphoblastic leukemia: comparison between RQ-PCR analysis of Ig/TcR gene rearrangements and multicolor flow cytometric immunophenotyping. Leukemia 2004 Oct; 18(10): 1630-1636.

53. Faham M, Zheng J, Moorhead M, Carlton VE, Stow P, Coustan-Smith E, et al. Deep-sequencing approach for minimal residual disease detection in acute lymphoblastic leukemia. Blood 2012 Dec 20; 120(26): 5173-5180.
54. Ladetto M, Bruggemann M, Monitillo L, Ferrero S, Pepin F, Drandi D, et al. Next-generation sequencing and real-time quantitative PCR for minimal residual disease detection in B-cell disorders. Leukemia 2014 Jun; 28(6): 1299-1307.

Chapter 2

Antigen receptor sequencing of paired bone marrow samples shows homogeneous distribution of acute lymphoblastic leukemia subclones

Prisca M.J. Theunissen[1], David van Zessen[1, 2], Andrew P. Stubbs[2], Malek Faham[3], Michel Zwaan[4], Jacques J.M. van Dongen[1, $,*] and Vincent H.J. van der Velden[1,*]

[1]Department of Immunology, Erasmus MC, University Medical Center Rotterdam, Rotterdam, The Netherlands
[2]Department of Bioinformatics, Erasmus MC, University Medical Center Rotterdam, Rotterdam, The Netherlands
[3]Adaptive Biotechnologies Corp, South San Francisco, CA
[4]Department of Pediatric Oncology, Sophia Children's Hospital/Erasmus MC, University Medical Center Rotterdam, Rotterdam, The Netherlands
[$]Present address: department of Immunohematology & Blood Transfusion, Leiden University Medical Center, Leiden, The Netherlands

* Shared senior authorship (equal contribution)

Submitted

ABSTRACT

In B-cell precursor acute lymphoblastic leukemia (BCP-ALL), the initial leukemic cells share the same immunoglobulin (IG) and T-cell receptor (TR) gene rearrangements. However, due to ongoing rearrangement processes, leukemic cells with different IG/TR gene rearrangement patterns can develop, resulting in subclone formation. We studied BCP-ALL subclones and their distribution in the bone marrow (BM) and peripheral blood (PB) compartments.

We used next generation sequencing to study IG/TR gene rearrangements (*IGH*, *IGK*, *TRG*, *TRD*, *TRB*) in seven paired BM samples and five paired BM-PB samples from seven respectively five newly diagnosed BCP-ALL patients.

Background-thresholds were defined, which enabled identification of leukemic IG/TR gene rearrangements down to very low levels. Paired BM-BM analysis showed oligoclonality in all seven patients and up to 34 leukemic clones per patient. Additional analysis of evolutionary-related *IGH* gene rearrangements revealed up to 171 leukemic clones per patient. The percentage of leukemic IG/TR gene rearrangements present in both BM samples ranged from 87% to 100% per patient (excluding 46% for Vδ-Dδ rearrangements in a patient with *TCF3-PBX1*). Paired BM-PB analysis showed that 98% of all leukemic IG/TR gene rearrangements in BM were also found in PB (excluding 78% for Vδ-Dδ rearrangements in an infant with *MLL-ENL*). Remarkably, the vast majority of leukemic IG/TR gene rearrangements had a similar frequency in the paired BM-BM and BM-PB samples (<5-fold frequency difference). Together, these results indicate that BCP-ALL is generally highly oligoclonal. Nevertheless, almost all BCP-ALL clones, even the minor subclones, are homogeneously distributed throughout the BM and PB compartment.

INTRODUCTION

During B-cell and T-cell differentiation, genes that encode the B-cell receptor (immunoglobulin; IG) and the T-cell receptor (TR) are rearranged, respectively. This process of IG and TR gene rearrangement includes the assembly of Variable (V), Diversity (D) and Joining (J) gene segments and the random insertion and deletion of nucleotides between these gene segments [1,2], resulting in unique V(D)J junctions. In normal B-cells and T-cells, productive V(D)J exons encode the antigen-binding domains of the IG and TR molecules. The large diversity of V(D)J junctions contributes significantly to the large diversity of IG and TR molecules, thereby providing the B- and T-lymphocytes with a wide variety of antigen specificities.

B-cell precursor acute lymphoblastic leukemia (BCP-ALL) arises from a malignantly transformed B-cell precursor (BCP) [3]. Therefore, BCP-ALL cells contain IG gene rearrangements in the vast majority of cases [4]. Additionally, most BCP-ALL cells also harbor certain TR gene rearrangements, which are uncommon in normal BCPs [5-7]. Since BCP-ALL is thought to arise from a single cell, a BCP-ALL population is expected be monoclonal with regard to IG/TR gene rearrangements, i.e. to consist of cells which all share the same IG/TR gene rearrangements. However, continuing rearrangement processes and V-segment replacements that occur in normal BCP cells can also occur during the development of BCP-ALL [8-10]. As a result, a BCP-ALL population can be oligoclonal, i.e. can contain subclones with IG/TR gene rearrangements that deviate from those in the initial leukemic cell.

Previously, several studies analyzed IG/TR gene rearrangements in BCP-ALL diagnosis samples by using PCR-based methods in combination with Southern blot (SB), which allowed identification of clonal IG/TR gene rearrangements down to the level of 1-5% [11,12]. In these studies, oligoclonality was detected in 40% of patients when analyzing the *IGH* and *TRD* loci and in 10-20% of patients when analyzing the *IGK* and *TRB* loci [11-13]. With regard to complete *IGH* gene rearrangements, a maximum of 9 clonal rearrangements could be found per patient [14]. More recently, *IGH* gene rearrangements in BCP-ALL at diagnosis were analyzed with highly sensitive next generation sequencing (NGS), which showed that many more clonal *IGH* gene rearrangements (up to 4024) can be present in a single patient [15]. However, in NGS studies of IG/TR gene rearrangements in BCP-ALL patients, it is difficult to discriminate leukemic rearrangements at low-frequency levels from the background of normal lymphocyte-derived rearrangements and from technical artifacts. Furthermore, NGS-based analysis of gene rearrangements other than complete *IGH* gene rearrangements, has, to the best of our knowledge, so far not been performed in patients with BCP-ALL. Therefore, the degree of oligoclonality in BCP-ALL patients, especially at low-frequency level, remains unclear.

BCP-ALL subclones may develop at different locations in the body, after which they may disseminate throughout the bone marrow (BM) and peripheral blood (PB) compartment. Whereas minimal residual disease (MRD) levels were shown to be comparable between paired BM samples during follow up [16], limited data is available on the distribution of BCP-ALL clones at the time of diagnosis. Our early SB study on IG/TR gene rearrangements in paired BM-PB samples at diagnosis, reported that in five out of ten oligoclonal patients, subclonal *IGH* gene rearrangements were found in BM, but not in the corresponding PB sample [17]. However, the relative frequency of these subclonal *IGH* gene rearrangements in PB might have been too low to be detected with SB. Therefore, it is still unknown to what extent BCP-ALL clones are distributed throughout the BM and PB compartments.

Here, we studied the distribution of leukemic clones in BCP-ALL patients by performing NGS of IG/TR gene rearrangements on paired BM-BM samples as well as paired BM-PB samples.

MATERIALS AND METHODS

Patient and control samples

BM and PB samples from in total 12 children with newly diagnosed BCP-ALL were collected from the Erasmus MC - Sophia Children's Hospital in Rotterdam (Supplementary Table 1). These samples included 7 left BM-right BM pairs i.e. BM from the left respectively right pelvic bone of the same patient, and 5 BM-PB pairs, all taken at initial diagnosis. One BM sample from a healthy child (residual material from a donor for allogenic BM transplantation), two BM samples from BCP-ALL patients at one year after end of therapy and 5 regenerating BM samples from T-ALL patients at day 79 and month 5 during therapy were collected, to be used as control samples. All control samples were MRD negative according to allele-specific oligonucleotide PCR assays, which were described previously [4,18]. All samples were obtained according to the guidelines of the local Medical Ethics Committees and in line with the Declaration of Helsinki Protocol.

Next generation sequencing by the Adaptive Biotechnologies method

Genomic DNA was isolated from BM and PB mononuclear cells (MNCs) by the QIAamp DNA Mini Kit (Qiagen, Hilden, Germany).

A detailed description of the NGS-based immunosequencing method was published elsewhere [19]. Briefly, a DNA quantity of 420-480 ng, corresponding to 70,000-80,000 MNCs, was used for the amplification of complete *IGH* gene rearrangements (Vh-DJh) and a DNA quantity of 120-180 ng, corresponding to 20,000-30,000 MNCs, was used for the amplification of incomplete *IGH* gene rearrangements (Dh-Jh), *IGK* gene rearrangements

(Vκ-Jκ, Vκ-KDE, intronRSS-KDE), *TRG* gene rearrangements (Vγ-Jγ), *TRD* gene rearrangements (Vδ-Dδ, Dδ-Dδ) and *TRB* gene rearrangements (Vβ-Jβ). These rearrangements were amplified in a first PCR reaction of 25 cycles, using locus-specific primer sets [20]. Next, 1/100 of these PCR products was further amplified in a second PCR reaction of 14 cycles, using universal primers complementary to the adaptors which were linked to the locus-specific primers with sample-identifiers. The final PCR products were sequenced by using the Illumina platform. Low-quality reads were filtered out and sequences with a single read were excluded [19]. For each sequence, the absolute read count, i.e. the read count corrected for PCR amplification by the spike-in method, was calculated (Supplementary Methods). Also the frequency for each sequence was determined. Importantly, the frequency represents a fraction of the rearranged genes of the involved locus, rather than a fraction of all, including germline, IG and TR genes, as is the case in SB and PCR-based IG/TR gene rearrangement analysis (Supplementary Methods).

NGS clonal variant comparison pipeline and data analysis

We developed a new analysis tool (PRISCA: PRecISe Clonal Analysis) in Galaxy [21] to compare sequences from paired and triplicate samples (Supplementary Methods). The graphical output from this tool was used for further data analysis.

Background-thresholds were determined based on the maximum absolute read count of normal lymphocyte-derived rearrangements in regenerating BM and normal BM samples. Since read counts of normal lymphocyte-derived rearrangements are expected to be lower in diagnosis BM than in regenerating BM or normal BM (due to overgrow of the leukemic population), these thresholds can be reliably applied to BCP-ALL BM samples at diagnosis. In order to use the thresholds in the analysis of BCP-ALL BM samples at diagnosis, the thresholds were expressed as a frequency of the total reads of the involved IG/TR gene rearrangement. The IG/TR gene rearrangements at diagnosis were subsequently analyzed according to the criteria described in the Supplementary Methods.

RESULTS

Normal and regenerating BM samples define thresholds for the exclusion of normal lymphocyte-derived IG/TR gene rearrangements

For in-depth analysis of IG/TR gene rearrangements in BCP-ALL patients, it is necessary to discriminate the IG/TR gene rearrangements derived from leukemic clones from the background that also contains IG/TR gene rearrangements derived from normal B-cell and T-cell clones. We therefore aimed to define "read count thresholds" (RCTs) above which we can fairly assume normal lymphocyte-derived IG/TR gene rearrangements to be absent. To

define these RCTs, we determined the maximum absolute read counts (i.e. the read count corrected for amplification) of normal lymphocyte-derived IG/TR gene rearrangements in eight non-leukemic BM samples, i.e. a normal BM sample from a healthy child, two normal BM samples from BCP-ALL patients one year after end of therapy, and five regenerating BM samples from T-ALL patients during therapy intervals (reflecting a background with potentially high numbers of early BCPs). Importantly, regenerating BM samples did not contain residual leukemic IG/TR gene rearrangements (as determined by the absence of leukemic IG/TR gene rearrangements which were found by NGS in the corresponding diagnosis sample; data not shown). Analysis of complete *IGH* gene rearrangements showed that the maximum read count of complete *IGH* gene rearrangements in the non-leukemic BM samples was 26 (Figure 1). The *IGH* Vh-DJh RCT was therefore set at 30 reads. The same strategy was applied to the other types of IG/TR gene rearrangements, resulting in an RCT of 30 reads for Dh-Jh rearrangements, 70 reads for Vκ-Jκ rearrangements, 40 reads for Vκ-KDE rearrangements, 170 reads for intronRSS-KDE rearrangements, 50 reads for Vγ-Jγ rearrangements, 20 reads for Vδ-Dδ rearrangements, 30 reads for Dδ-Dδ rearrangements and 30 reads for Vβ-Jβ rearrangements (Supplementary Figure 1). The relatively high maximum read count of intronRSS-KDE rearrangements was probably due to the limited junctional variability of intronRSS-KDE rearrangements. Importantly, these RCTs are dependent on DNA input and are therefore not universal, but specific for our data.

Samples run in triplicate show that our thresholds also exclude IG/TR gene rearrangements derived from technical artifacts

We aimed to evaluate whether IG/TR gene rearrangements with a read count above the RCTs were truly clonal, i.e. were derived from leukemic clones and not from technical artifacts (non-clonal rearrangements whose read counts were insufficiently corrected after PCR amplification). We therefore performed three independent NGS-runs on the same sample, based on the fair assumption that IG/TR gene rearrangements can be regarded as clonal if present in all three samples or if present in two of the three samples (since small clones can coincidently be absent in a sampling volume). Analysis of complete *IGH* gene rearrangements in a BM sample at diagnosis showed that all complete *IGH* gene rearrangements with a read count above the previously defined RCT, and thus considered to be derived from leukemic clones, were present in all three replicates, indicating that these were not technical artefacts (Figure 2). Analysis of the other IG/TR gene rearrangement types in this diagnosis sample showed the same (Supplementary Figure 2). Thus, by using these RCTs, we ensured that the included rearrangements (above the RCT) were very likely to be derived from leukemic clones (as opposed to normal lymphocytes or technical artefacts), thereby accepting that leukemic rearrangements with a read count below the RCT will be ignored. Analysis of IG/TR gene rearrangements in three replicates of a regenerating BM

sample from a T-ALL patient showed, as expected, that none of the rearrangements had a read count above the RCT. Nevertheless, part of the IG/TR gene rearrangements with a read count below the RCT were present in two or three of the replicates, and could thus be derived from normal B-cell or T-cell clones (Supplementary Figure 3).

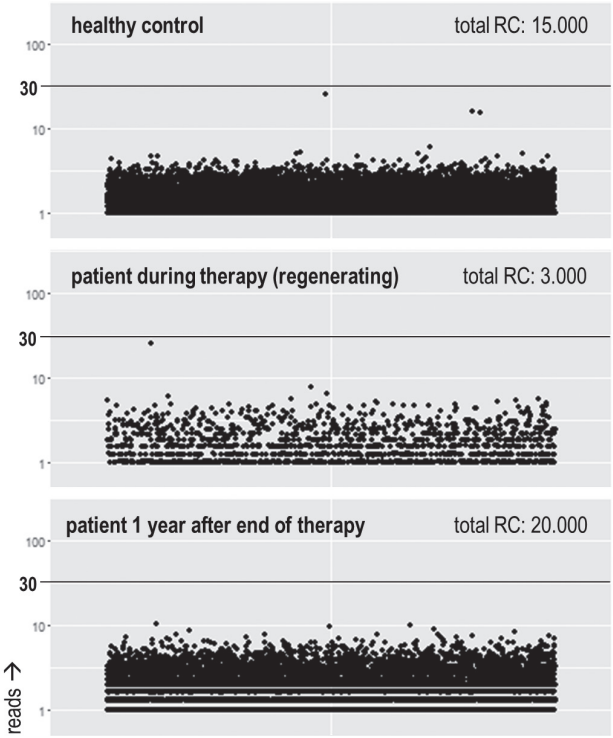

Figure 1.
Read counts of Vh-DJh rearrangements in BM from a healthy child, a T-ALL patient at a therapy interval (regenerating BM) and a BCP-ALL patient at one year after end of therapy (representative examples of the in total 8 non-leukemic BM samples). Each dot represents a single rearrangement. Vh-DJh with a read count of <1 (caused by amplification-correction) were displayed as rearrangements with a read count of 1. The black line indicates the established threshold for Vh-DJh rearrangements.
Regenerating BM showed structurally lower numbers of unique Vh-DJh rearrangements compared to healthy control BM and BM one year after end of therapy. This was also true for Vκ-Jκ, Vκ-KDE and intronRSS-KDE rearrangements, but not Dh-Jh rearrangements (Supplementary Figure 1). This was expected, since the B-cell population in regenerating BM mainly consists of pre-B-I cells [31,32].

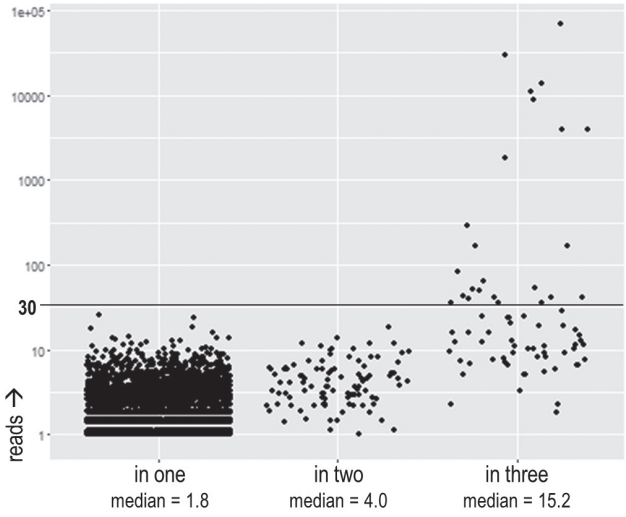

Figure 2.
Read counts of Vh-DJh rearrangements in BM replicates from a BCP-ALL patient at diagnosis. This BM was sequenced in triplicate, resulting in IGH gene rearrangements that were found in one, in two or in all three replicates. Each dot represents a single rearrangement. Vh-DJh rearrangements with a read count of <1 (caused by amplification-correction), were displayed as rearrangements with a read count of 1. The black line indicates the previously defined threshold for Vh-DJh rearrangements (30 reads).

Paired BM samples show homogeneous distribution of BCP-ALL, also for small subclones

Next, we aimed to analyze the number and particularly the tissue distribution of clones in BCP-ALL patients. Therefore, we performed NGS of IG/TR gene rearrangements in paired BM samples (from the left and the right pelvic bone) from newly diagnosed BCP-ALL patients (n=7). By applying the previously described thresholds (now expressed as frequency) and analysis criteria (Supplementary Methods) to Vh-DJh rearrangements, oligoclonality was detected in six out of seven BCP-ALL patients (Figure 3). The number of index clones ranged from 1 to 5 (median: 1), whereas the total number of (sub)clones ranged from 2 to 34. With regard to distribution of the clones, 84% (74 out of 88) of all leukemic Vh-DJh rearrangements were present in both BM samples, ranging from 76% to 100% per patient (Figure 3; Table 1). Importantly, 61 out of the 74 (82%) paired leukemic Vh-DJh rearrangements had a comparable frequency (<5-fold difference) in the two BM samples. Among the 13 paired leukemic Vh-DJh with a frequency of >5% (index clones), all Vh-DJh rearrangements had a comparable frequency in the two BM samples. The leukemic Vh-DJh rearrangements which were present in only one of the two samples, all had a very low frequency below 0.2% and often shared a common Dh-Jh stem with a paired leukemic Vh-DJh rearrangement (see below). Analysis of the other types of IG/TR gene rearrangements also showed that the vast majority of the leukemic rearrangements were

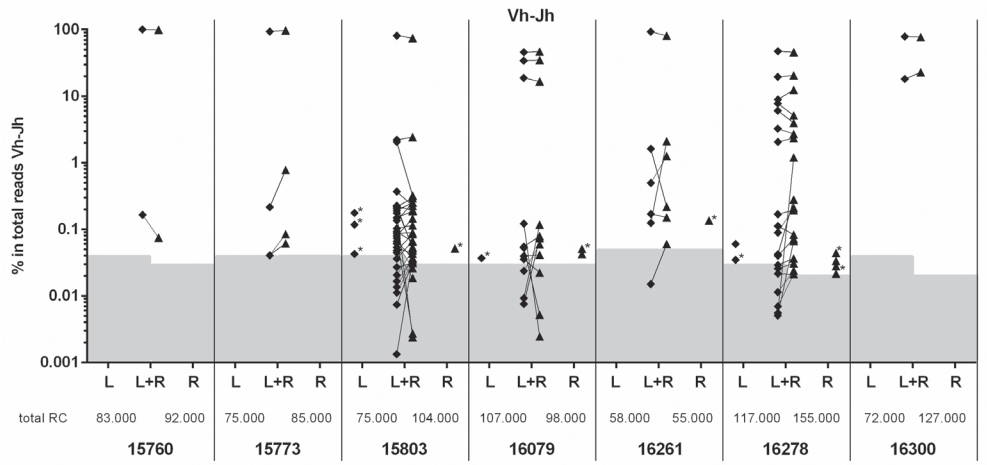

Figure 3.
Frequencies of leukemic Vh-DJh rearrangements in paired BM samples (left and right pelvic bone) from BCP-ALL patients at diagnosis. For each leukemic Vh-DJh rearrangement, the presence in both BM samples (L+R) or in only one of the two BM samples (L or R) is indicated. The background-area which also contains Vh-DJh rearrangements derived from normal B-cell clones is indicated for each sample (grey). Asterisks indicate that these Vh-DJh rearrangement share a common Dh-Jh stem with a paired leukemic Vh-DJh rearrangement.

paired: 4 out of 5 (80%) Dh-Jh rearrangements, 8 out of 8 (100%) Vκ-Jκ rearrangements, 8 out of 8 (100%) Vκ-KDE rearrangements, 3 out of 3 (100%) intronRSS-KDE rearrangements, 55 out of 57 (96%) Vγ-Jγ rearrangements, 30 out of 45 (67%) Vδ-Dδ rearrangements, 8 out of 9 (89%) Dδ-Dδ rearrangements and 11 out of 11 (100%) Vβ-Jβ rearrangements (Supplementary Figure 4). Importantly, 171 out of all 199 (86%) paired leukemic IG/TR gene rearrangements showed a comparable frequency in the two BM samples. The overall results per patient are summarized in Table 1.

Analysis of leukemic Dh-Jh stems at very low frequency levels suggests even higher numbers of homogeneously distributed subclones

We subsequently aimed to estimate the number of leukemic IG/TR gene rearrangements that were present at very low frequencies and that were, based on the background-threshold, excluded from previous analyses. Therefore, we visualized all paired complete *IGH* gene rearrangements, irrespective of their frequency (i.e. also with a frequency below the threshold). Only paired *IGH* gene rearrangements (i.e. present in both BM samples) were visualized in order to exclude potential technical artifacts. The resulting graph showed that, besides the previously detected paired *IGH* gene rearrangements, many more paired *IGH* gene rearrangements were present below the threshold (Figure 4). However, a paired *IGH* gene rearrangement below the threshold can be either derived from a leukemic clone or derived from a normal mature B-cell clone which had been distributed throughout

Table 1. Number and distribution of leukemic clones at BCP-ALL diagnosis.

	ID_15760	ID_15773	ID_15803	ID_16079	ID_16261	ID_16278	ID_16300	total
	#clones paired/total	#clones paired/total	#clones paired/total	#clones paired/total	#clones paired/total	#clones paired/total	#clones paired/total	#clones paired/total
Vh-Jh	2 / 2 (100%)	4 / 4 (100%)	30 / 34 (88%)	11 / 14 (79%)	6 / 7 (86%)	19 / 25 (76%)	2 / 2* (100%)	74 / 88 (84%)
Dh-Jh	-	-	4 / 5 (80%)	-	-	-	-	4 / 5 (80%)
Vκ-Jκ	-	-	0 / 0 (NA)	-	2 / 2 (100%)	5 / 5 (100%)	1 / 1 (100%)	8 / 8 (100%)
Vκ-KDE	1 / 1 (100%)	1 / 1 (100%)	1 / 1 (100%)	1 / 1 (100%)	-	2 / 2 (100%)	2 / 2* (100%)	8 / 8 (100%)
Intr-KDE	-	-	-	-	3 / 3 (100%)	-	-	3 / 3 (100%)
Vγ-Jγ	2 / 2* (100%)	3 / 3 (100%)	0 / 0 (NA)	21 / 22 (96%)	5 / 5 (100%)	19 / 20 (95%)	5 / 5 (100%)	55 / 57 (96%)
Vδ-Dδ	1 / 1 (100%)	-	12 / 26 (46%)	9 / 9 (100%)	-	8 / 9 (89%)	-	30 / 45 (67%)
Dδ-Dδ	-	-	-	6 / 7 (86%)	-	-	2 / 2 (100%)	8 / 9 (89%)
Vβ-Jβ	-	3 / 3 (100%)	1 / 1 (100%)	4 / 4 (100%)	1 / 1 (100%)	-	2 / 2 (100%)	11 / 11 (100%)
total	6 / 6 (100%)	11 / 11 (100%)	48 / 67 (72%)	52 / 57 (91%)	17 / 18 (94%)	53 / 61 (87%)	14 / 14 (100%)	201 / 234 (86%)

- : total RC <1000

*: monoclonal, but bi-allelic for involved rearrangement type

The number of leukemic Vh-DJh, Dh-Jh, Vκ-Jκ, Vκ-KDE, intronRSS-KDE, Vγ-Jγ, Vδ-Dδ, Dδ-D and Vβ-Jβ rearrangements and the percentage of these leukemic rearrangements that was homogeneously distributed (found in both BM samples), in BCP-ALL patients at diagnosis. Intr-KDE = intronRSS-KDE.

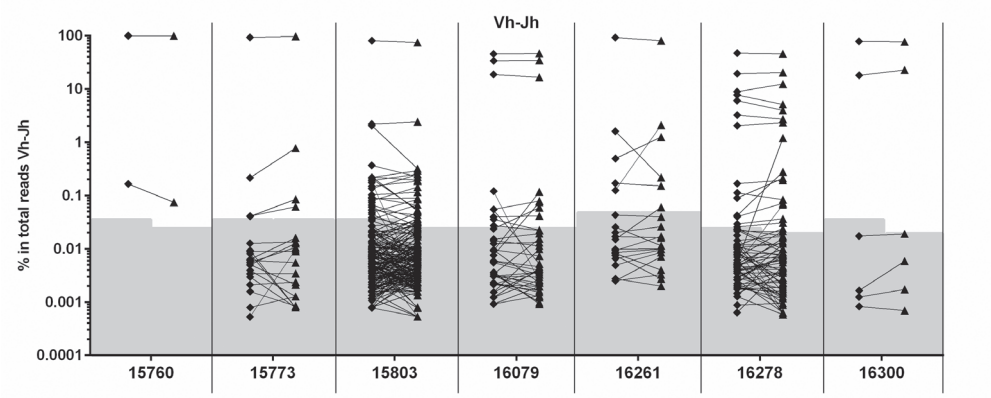

Figure 4.
Frequencies of Vh-DJh rearrangements in paired BM samples (left and right pelvic bone) from BCP-ALL patients at diagnosis. All paired Vh-DJh rearrangements are shown, i.e. with a frequency above as well as below the threshold. Per sample, the background-area is indicated in grey.

the BM compartment. To discriminate, at sub-threshold level, leukemia-derived *IGH* gene rearrangements from normal B-cell derived *IGH* gene rearrangements, we searched for common Dh-Jh stems. An *IGH* gene rearrangement below the threshold that shared a common Dh-Jh stem with a leukemic *IGH* gene rearrangement above the threshold was considered leukemic too (since both were derived from the same ancestral clone). This analysis showed that, on top of the leukemic *IGH* gene rearrangements found in the previous analyses (above the threshold), even more leukemic *IGH* gene rearrangements are present at very low frequency-levels (below the threshold) (summarized in Figure 5). The exact number of leukemic *IGH* gene rearrangement per patient remains unknown, since the origin (leukemia or mature B-cell derived) of the *IGH* gene rearrangements with a frequency below the threshold and without a common Dh-Jh stem could not be determined. Of note, the *IGH* gene rearrangements with a common Dh-Jh stem often also had a common V-D junction, indicating that V to D-J joining as well as Vh-replacement had taken place.

Paired BM-PB samples confirm the homogeneous distribution of BCP-ALL clones via PB

The above data indicate that BCP-ALL clones are distributed homogeneously over the BM compartment, implying that migration via PB is required. Therefore, we investigated whether leukemia-derived IG/TR gene rearrangements detected in BM can also be found in PB. To do so, we performed NGS of IG/TR gene rearrangements in paired BM–PB samples from newly diagnosed BCP-ALL patients (n=5). Leukemic IG/TR gene rearrangements found in the BM sample (i.e. with a frequency above the previously established thresholds) were searched in the corresponding PB sample and classified as 'paired' when also present

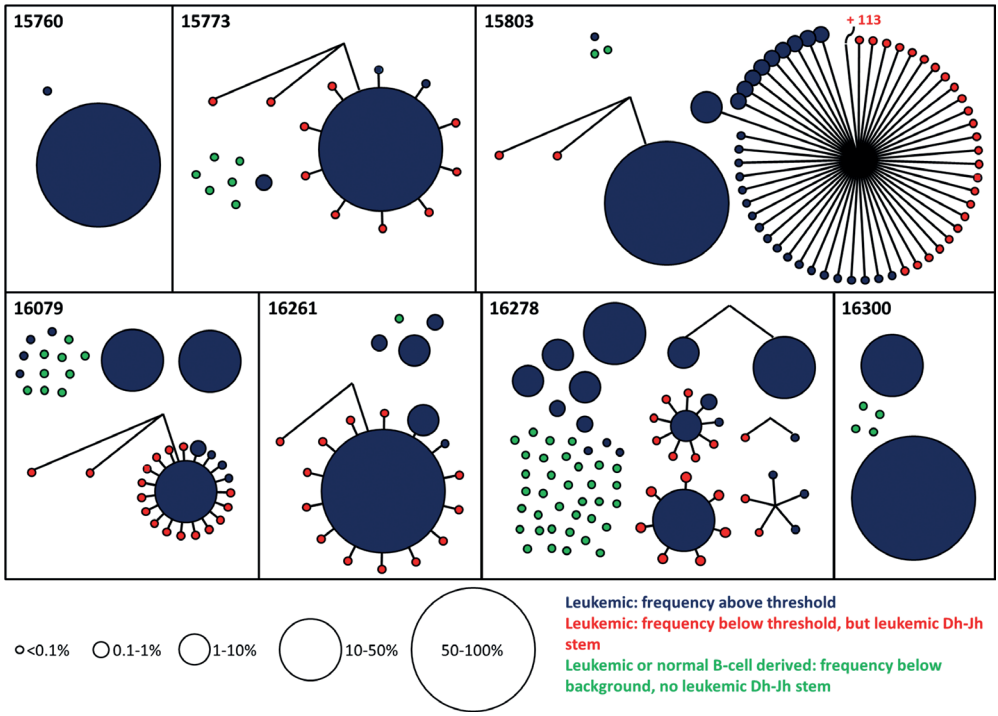

Figure 5.
Schematic representation of the relations between Vh-DJh rearrangements, based on common Dh-Jh stems, in BM samples from BCP-ALL patients at diagnosis. The size of the circle represents the frequency of the Vh-DJh rearrangement. The blue or red color indicates a leukemic origin (blue; based on frequency, red; based on a common Dh-Jh stem), whereas the green color indicates small clones of unknown origin (no leukemic Dh-Jh stem).

in the PB sample. Analysis of complete *IGH* gene rearrangements showed that 98% (43 out of 44) of all leukemic Vh-DJh rearrangements were paired (Figure 6). Of note, 42 out of the 43 (98%) paired leukemic Vh-DJh rearrangements had a comparable frequency (<5-fold difference) in the two corresponding samples. The only leukemic Vh-DJh rearrangement present in the BM sample but not in the PB sample, had a frequency of 0.04% and shared a common Dh-Jh stem with a paired leukemic Vh-DJh rearrangement. Analysis of the other IG and TR gene rearrangement types also showed that the majority of the leukemic rearrangements were paired: 30 out of 32 (94%) Dh-Jh rearrangements, 2 out of 2 (100%) Vκ-Jκ rearrangements, 1 out of 1 (100%) Vκ-KDE rearrangements, 9 out of 9 (100%) Vγ-Jγ rearrangements, 320 out of 403 (79%) Vδ-Dδ rearrangements, 17 out of 17 (100%) Dδ-Dδ rearrangements and 4 out of 4 (100%) Vβ-Jβ rearrangements (no clonal intronRSS-KDE rearrangements were found) (Supplementary Figure 5). Together, 411 out of all 426 (96%) paired leukemic IG/TR gene rearrangements showed a comparable frequency between the BM and the corresponding PB sample.

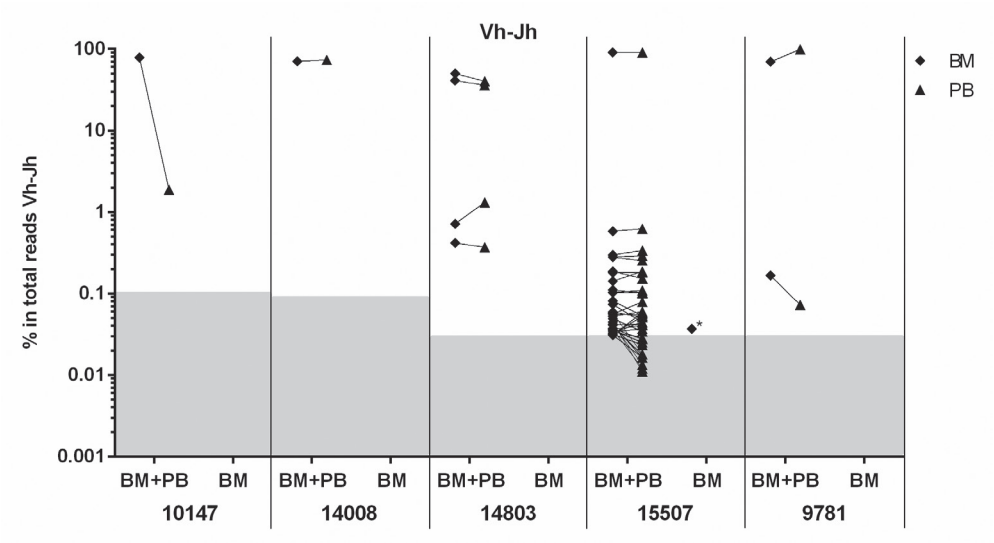

Figure 6.
Frequencies of leukemic Vh-DJh rearrangements in paired BM-PB samples from BCP-ALL patients at diagnosis. For each leukemic Vh-DJh rearrangement in the BM sample (above the background-threshold), the presence in both samples (BM+PB) or in only the BM sample (BM) is indicated. Diamonds represent Vh-DJh rearrangements found in BM, triangles represent Vh-DJh rearrangements found in PB. Per sample, the background-area is indicated in grey.

DISCUSSION

To study the number of clones and their distribution in patients with BCP-ALL, we performed NGS of IG/TR gene rearrangements in paired BM-BM and BM-PB samples at diagnosis. First, we aimed to carefully define background-thresholds (RCTs), which exclude normal lymphocyte-derived IG/TR gene rearrangements when using an identical amount of DNA per sample. Therefore, we determined the maximum read count of these normal lymphocyte-derived IG/TR gene rearrangements in non-leukemic BM, i.e. healthy control BM, regenerating BM, and BM one year after end of therapy. Second, by analysing a BCP-ALL sample at diagnosis in triplicate, we confirmed that all IG/TR gene rearrangements with a read count above the preset RCT represented clonal IG/TR gene rearrangements, and not technical artifacts. Of note, RCTs could not exclude IG/TR gene rearrangements derived from normal lymphocyte expansions directed against leukemic cells, since these expansions were probably not present in the studied MRD negative follow up samples (and certainly not in the healthy control BM sample). However, since many Vh-DJh rearrangements shared a common stem with an index clone and since, besides clonal TR gene rearrangements, also clonal IG gene rearrangements were observed (whereas

reactive expansions against leukemic cells would be mainly of T-cell origin), it is likely that most IG/TR gene rearrangements with read counts above the RCTs are of leukemic origin.

Analysis of IG/TR gene rearrangements in paired BM-BM diagnosis samples showed that all seven patients were oligoclonal. Remarkably high numbers of leukemic Vh-DJh, Vγ-Jγ and Vδ-Dδ rearrangements per patient could be detected (e.g. up to 34 leukemic Vh-DJh rearrangements). Even higher numbers of leukemic rearrangements per patient were detected when common Dh-Jh stem (junction sequence) analysis was used to also include Vh-DJh rearrangements below the background-threshold (up to 171 leukemic Vh-DJh rearrangements). Previous studies which used SB to analyze IG/TR gene rearrangements reported that only 40% of the ALL-patients were oligoclonal, with maximally 9 leukemic rearrangements per patient [11,14]. The discrepancies between these previous findings and our current results can be explained by the difference in sensitivity of the applied methods. A more recent study that used NGS to analyze *IGH* gene rearrangements showed, in line with our results, that far more *IGH* gene rearrangements per patient can be found when analysis down to very low frequency-levels is allowed [15]. However, in contrast with our results, this study also reported on a few patients (4 out of the 51 studied patients) in which more than thousand leukemic *IGH* gene rearrangements were found. Patients with such exceptionally high numbers of *IGH* gene rearrangements were not present in our study, which is probably related to the lower number of patients analyzed. Anyway, we showed that the number of leukemic IG/TR gene rearrangements per BCP-ALL patient is considerably higher than previously observed.

IG/TR gene rearrangements are used as PCR targets for MRD detection [22-26]. Insight into subclone formation and distribution of these subclones might improve selection of MRD targets. Our current findings indicate that MRD targets have so far been selected from only a small part of the total number of leukemic IG/TR gene rearrangements present at diagnosis, i.e. from those that were sufficiently large to be detected by PCR-based methods (index clones with a frequency >5%). Still, more than 90% of the relapsed cases had maintained the IG and TR targets selected at diagnosis [25]. Apparently, monitoring of only the index clones might be sufficient to predict relapse in most BCP-ALL patients. Furthermore, our observation that the vast majority of leukemic clones could be detected both in BM and PB implies that also PB samples may reliably be used for NGS-based selection of MRD targets.

By analyzing paired BM samples, we showed that the vast majority of the leukemic rearrangements were present in both BM samples and that their frequency was generally similar in both samples. The few leukemic rearrangements that were present in only one of the two samples generally had a low frequency (<2%). Probably, also these low-frequent clones were present in the whole BM compartment, but were absent in one of the two samples based on statistical chance. By analyzing paired BM-PB samples (from other patients), we showed that almost all leukemic rearrangements that were present in BM,

were also present in PB, generally at a similar frequency. As an exception to the above results, relatively many leukemic Vδ-Dδ rearrangements in patient 15803 (child with a *TCF3-PBX1* translocation) and in patient 15507 (infant with an *MLL-ENL* translocation) were present in only one of the paired samples (54% and 22%, respectively). Since infants with a *MLL-R* translocation are known to be a distinct form of ALL (e.g. more oligoclonal) [27,28], the specific genetic aberrancies might be associated with the deviating results on Vδ-Dδ rearrangements [29].

NGS-based IG/TR gene rearrangement analysis in paired BM-BM and BM-PB samples from newly diagnosed BCP-ALL patients has, to our knowledge, not been performed previously. Our early SB study on IG gene rearrangements in paired BM-PB samples of newly diagnosed BCP-ALL patients showed that relatively many leukemic *IGH* gene rearrangements were detected in the BM sample, but not or in a lower frequency in the corresponding PB sample [17], which seems to contradict our current results. However, this discrepancy is probably due to technical differences between SB and NGS (as described in the Materials and Methods section).

Together, our paired BM-BM and paired BM-PB NGS analyses showed that almost all leukemic rearrangements are present in comparable frequencies in the BM and PB compartment. We did not study leukemic IG/TR gene rearrangements in tissues other than BM or PB. However, it might be speculated that extramedullary dissemination is different from distribution within the BM and PB compartment, since only clones with specific characteristics (e.g. homing receptors) are able to migrate to extramedullary sites [30].

In conclusion, by using NGS data in combination with carefully defined thresholds, we were able to study leukemic IG/TR gene rearrangements down to a low level (0.01%-0.1%), without the interference of background-rearrangements. By studying paired BM-BM and paired BM-PB samples, we showed that the relative quantity of IG/TR gene rearrangements within the total (rearranged) BCP-ALL population is generally similar throughout the BM compartment and between BM and PB. Apparently, after their development at different BM sites in the body, almost all clones within a BCP-ALL population, even the small subclones, disseminate homogeneously via PB throughout the BM compartment.

ACKNOWLEDGEMENTS

We gratefully thank Arjan Lankester and the involved technicians of the Laboratory for Medical Immunology, in particular Rianne Noordijk, Patricia Hoogeveen and Maaike de Bie. We acknowledge Auke Beishuizen for providing BM samples from the BCP-ALL patients. The research for this manuscript was (in part) performed within the framework

of the Erasmus Postgraduate School Molecular Medicine and was financially supported by PrioMedChild, project 40-41800-98-027.

REFERENCES

1. Tonegawa, S., Somatic generation of antibody diversity. Nature, 1983. 302(5909): p. 575-81.
2. Alt, F.W., et al., VDJ recombination. Immunol Today, 1992. 13(8): p. 306-14.
3. Pui, C.H., D. Campana, and W.E. Evans, Childhood acute lymphoblastic leukaemia--current status and future perspectives. Lancet Oncol, 2001. 2(10): p. 597-607.
4. van der Velden, V.H. and J.J. van Dongen, MRD detection in acute lymphoblastic leukemia patients using Ig/TCR gene rearrangements as targets for real-time quantitative PCR. Methods Mol Biol, 2009. 538: p. 115-50.
5. Chen, Z., et al., Human T cell gamma genes are frequently rearranged in B-lineage acute lymphoblastic leukemias but not in chronic B cell proliferations. J Exp Med, 1987. 165(4): p. 1000-15.
6. Szczepanski, T., et al., Cross-lineage T cell receptor gene rearrangements occur in more than ninety percent of childhood precursor-B acute lymphoblastic leukemias: alternative PCR targets for detection of minimal residual disease. Leukemia, 1999. 13(2): p. 196-205.
7. Fronkova, E., et al., Lymphoid differentiation pathways can be traced by TCR delta rearrangements. J Immunol, 2005. 175(4): p. 2495-500.
8. Choi, Y., et al., Clonal evolution in B-lineage acute lymphoblastic leukemia by contemporaneous VH-VH gene replacements and VH-DJH gene rearrangements. Blood, 1996. 87(6): p. 2506-12.
9. Moreira, I., et al., Heterogeneity of VH-JH gene rearrangement patterns: an insight into the biology of B cell precursor ALL. Leukemia, 2001. 15(10): p. 1527-36.
10. Stankovic, T., et al., Clonal diversity of Ig and T-cell receptor gene rearrangements in childhood B-precursor acute lymphoblastic leukaemia. Leuk Lymphoma, 2000. 36(3-4): p. 213-24.
11. Beishuizen, A., et al., Multiple rearranged immunoglobulin genes in childhood acute lymphoblastic leukemia of precursor B-cell origin. Leukemia, 1991. 5(8): p. 657-67.
12. van der Velden, V.H., et al., TCRB gene rearrangements in childhood and adult precursor-B-ALL: frequency, applicability as MRD-PCR target, and stability between diagnosis and relapse. Leukemia, 2004. 18(12): p. 1971-80.
13. van der Velden, V.H., et al., Age-related patterns of immunoglobulin and T-cell receptor gene rearrangements in precursor-B-ALL: implications for detection of minimal residual disease. Leukemia, 2003. 17(9): p. 1834-44.
14. Beishuizen, A., et al., Analysis of Ig and T-cell receptor genes in 40 childhood acute lymphoblastic leukemias at diagnosis and subsequent relapse: implications for the detection of minimal residual disease by polymerase chain reaction analysis. Blood, 1994. 83(8): p. 2238-47.
15. Gawad, C., et al., Massive evolution of the immunoglobulin heavy chain locus in children with B precursor acute lymphoblastic leukemia. Blood, 2012. 120(22): p. 4407-17.

16. van der Velden, V.H., et al., Impact of two independent bone marrow samples on minimal residual disease monitoring in childhood acute lymphoblastic leukaemia. Br J Haematol, 2006. 133(4): p. 382-8.
17. Beishuizen, A., et al., Differences in immunoglobulin heavy chain gene rearrangmeent patterns between bone marrow and blood samples in childhood precursor B-acute lymphoblastic leaukemia at diagnosis. Leukemia, 1993. 7(6): p. 60-3.
18. van der Velden, V.H., et al., Analysis of minimal residual disease by Ig/TCR gene rearrangements: guidelines for interpretation of real-time quantitative PCR data. Leukemia, 2007. 21(4): p. 604-11.
19. Faham, M., et al., Deep-sequencing approach for minimal residual disease detection in acute lymphoblastic leukemia. Blood, 2012. 120(26): p. 5173-80.
20. Faham, M., Methods of monitoring conditions by sequence analysis; US 2011/0207135 A1. 2011, Sequenta, inc.: United States
21. Afgan, E., et al., The Galaxy platform for accessible, reproducible and collaborative biomedical analyses: 2016 update. Nucleic Acids Res, 2016. 44(W1): p. W3-W10.
22. Szczepanski, T., et al., Minimal residual disease in leukaemia patients. Lancet Oncol, 2001. 2(7): p. 409-17.
23. van Dongen, J.J., et al., Prognostic value of minimal residual disease in acute lymphoblastic leukaemia in childhood. Lancet, 1998. 352(9142): p. 1731-8.
24. van der Velden, V.H., et al., Detection of minimal residual disease in hematologic malignancies by real-time quantitative PCR: principles, approaches, and laboratory aspects. Leukemia, 2003. 17(6): p. 1013-34.
25. Pieters, R., et al., Successful Therapy Reduction and Intensification for Childhood Acute Lymphoblastic Leukemia Based on Minimal Residual Disease Monitoring: Study ALL10 From the Dutch Childhood Oncology Group. J Clin Oncol, 2016.
26. van Dongen, J.J., et al., Minimal residual disease diagnostics in acute lymphoblastic leukemia: need for sensitive, fast, and standardized technologies. Blood, 2015. 125(26): p. 3996-4009.
27. Bardini, M., et al., Clonal variegation and dynamic competition of leukemia-initiating cells in infant acute lymphoblastic leukemia with MLL rearrangement. Leukemia, 2015. 29(1): p. 38-50.
28. Jansen, M.W., et al., Immunobiological diversity in infant acute lymphoblastic leukemia is related to the occurrence and type of MLL gene rearrangement. Leukemia, 2007. 21(4): p. 633-41.
29. Brumpt, C., et al., The incidence of clonal T-cell receptor rearrangements in B-cell precursor acute lymphoblastic leukemia varies with age and genotype. Blood, 2000. 96(6): p. 2254-61.
30. van der Velden, V.H., et al., New cellular markers at diagnosis are associated with isolated central nervous system relapse in paediatric B-cell precursor acute lymphoblastic leukaemia. Br J Haematol, 2016. 172(5): p. 769-81.
31. van Lochem, E.G., et al., Regeneration pattern of precursor-B-cells in bone marrow of acute lymphoblastic leukemia patients depends on the type of preceding chemotherapy. Leukemia, 2000. 14(4): p. 688-95.
32. van Wering, E.R., et al., Regenerating normal B-cell precursors during and after treatment of acute lymphoblastic leukaemia: implications for monitoring of minimal residual disease. Br J Haematol, 2000. 110(1): p. 139-46.

SUPPLEMENTARY METHODS

Calculation of absolute read count and frequency

To determine the absolute read count of a sequence, i.e. the read count of a sequence corrected for PCR amplification, a known number of reference sequences was added to each PCR reaction. This resulted in a factor of difference between the number of reference sequences that was added and the read count after sequencing. Per gene rearrangement type, this factor was used to correct the read count of each patient sequence.

To determine the frequency of a sequence, the individual read count of that sequence was divided by the total read count for that gene rearrangement type in a sample. However, to calculate the frequency of a sequence from the *IGK* locus or *TRD* locus, the individual read count of the sequence was divided by the sum of the Vk-Jk, Vk-KDE and INTRSS-KDE total read counts respectively the sum of the Vd-Dd and Dd-Dd total read counts.

Frequencies of IG/TR gene rearrangements in NGS versus SB or PCR

Using PCR and SB, the frequency of leukemic rearrangements is determined within all IG and TR genes of the tested MNC's, including germline (non-rearranged) IG and TR genes. In contrast, NGS determines the frequency of a leukemic rearrangement within the rearranged genes of a specific locus, without measurement of the germline genes. The number of non-leukemic MNCs is often higher in PB than in BM. Consequently, using PCR or SB, the frequency of a leukemic rearrangement is often lower in PB than in BM, whereas using NGS, the frequency is generally similar between PB and BM.

PRISCA tool in Galaxy

As input file, a list of all unique sequences with their associated sample ID, patient ID, gene rearrangement type, frequency and absolute read count was used. During a step-wise bioinformatic process, sequences that were identical between the paired/triplicate samples were linked. Importantly, sequences were defined as identical if all nucleotides were similar. Only a difference in length of the sequence was accepted (e.g. a sequence which aligns 100% to another sequence, but is two nucleotides shorter, is considered identical). The graphical output from this tool displays the frequency of each sequence and its presence in only one or in more samples. PRISCA was developed in R (version 3.1.2) and on Galaxy (version v15.10). The PRISCA tool is freely available for use at https://bioinf-galaxian.erasmusmc.nl/galaxy without the need to login and it can be installed on an existing Galaxy server through the Galaxy toolshed [1].

Analysis criteria

The IG/TR gene rearrangements at diagnosis were analyzed according to the following criteria: First, rearrangements were not further analyzed in case of a total read count of less than 1,000 (since no IG or TR gene rearrangements with a frequency above the background-threshold were present in these cases). Second, rearrangements were classified as 'paired' when present in both corresponding (BM-BM or BM-PB) samples. Third, a rearrangement was regarded as leukemia-derived, if the frequency of the rearrangement or the frequency of at least one of the paired rearrangements was higher than the threshold. Fourth, a leukemia-derived rearrangement was considered to be derived from an index clone if the frequency was >5% and from a subclone if the frequency was <5%. Fifth, a patient was considered oligoclonal if: 1. More than two leukemic rearrangements of the same rearrangement type were found, or 2. Two leukemic rearrangements of the same rearrangement type were found and their frequency differed with more than a factor 5 (to take variation due to PCR amplification into account).

SUPPLEMENTARY TABLE

Supplementary Table 1. Patient/sample characteristics.

type of comparison	ID number	gender	age at diagnosis	immunophentypic classification	cytogenetic aberrancy	tumor load BM
Left BM - Right BM	15760	m	12	common-ALL	iAMP	96%
	15773	f	9	common-ALL	*ETV6-RUNX1*	90%
	15803	m	1	pre-B-ALL	*TCF3-PBX1*	71%
	16079	m	8	common-ALL	*ETV6-RUNX1* hyperdiploid	70%
	16261	f	3	common-ALL	*ETV6-RUNX1*	85%
	16278	f	3	common-ALL	-	69%
	16300	f	4	common-ALL	*ETV6-RUNX1*	88%
BM - PB	10147	f	18	common-ALL	-	65%
	14008	f	7	common-ALL	hyperdiploid	97%
	14803	f	4	pre-B-ALL	hyperdiploid	56%
	15507	f	0	pro-B-ALL	*MLL-ENL*	100%
	9781	f	5	common-ALL	hyperdiploid	87%

SUPPLEMENTARY FIGURES

Supplementary Figure 1.
Read counts of Dh-Jh, Vκ-Jκ, Vκ-KDE, intronRSS-KDE, Vγ-Jγ, Vδ-Dδ, Dδ-Dδ and Vβ-Jβ rearrangements in BM from a healthy child, BM from a representative T-ALL patient at a therapy interval (regenerating BM; n=5) and BM from a representative BCP-ALL patient at one year after end of therapy (n=2). Each dot represents a single rearrangement. Rearrangements with a read count of <1 (caused by amplification-correction) were displayed as rearrangements with a read count of 1. The black line indicates the threshold for the involved type of rearrangement.

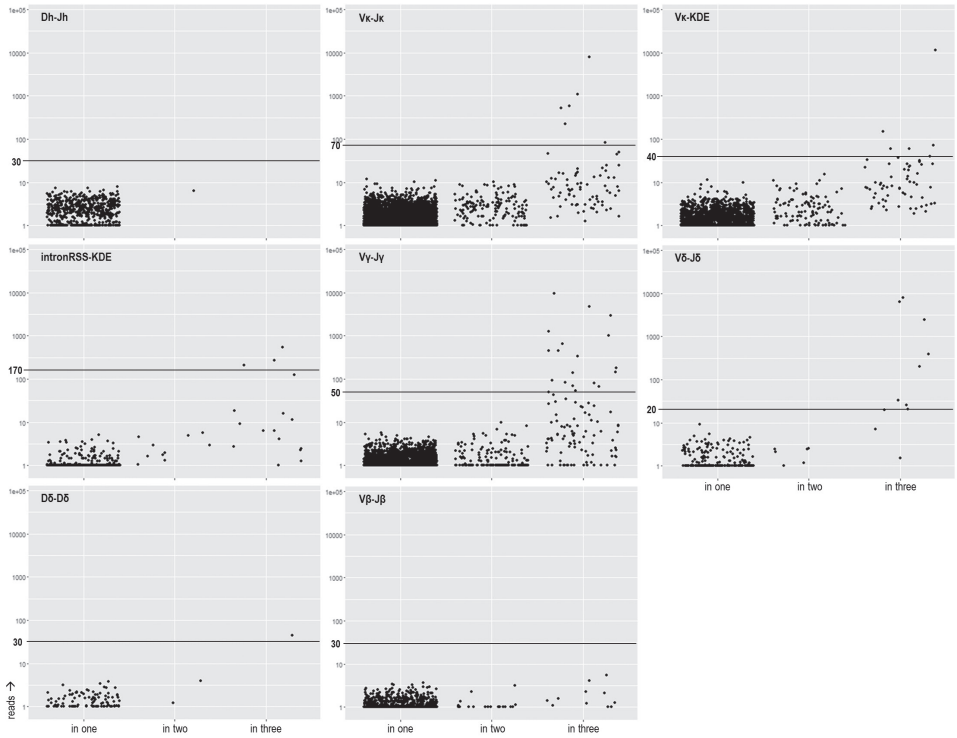

Supplementary Figure 2.
Read counts of Dh-Jh, Vκ-Jκ, Vκ-KDE, intronRSS-KDE, Vγ-Jγ, Vδ-Dδ, Dδ-Dδ and Vβ-Jβ rearrangements in BM from a BCP-ALL patient at diagnosis. Each dot represents a single rearrangement. This BM was sequenced in triplicate, resulting in rearrangements that were found in one, in two or in all three of the replicates. Rearrangements with a read count of <1 (caused by amplification-correction) were displayed as rearrangements with a read count of 1. The black line indicates the previously defined threshold for the involved type of rearrangement.

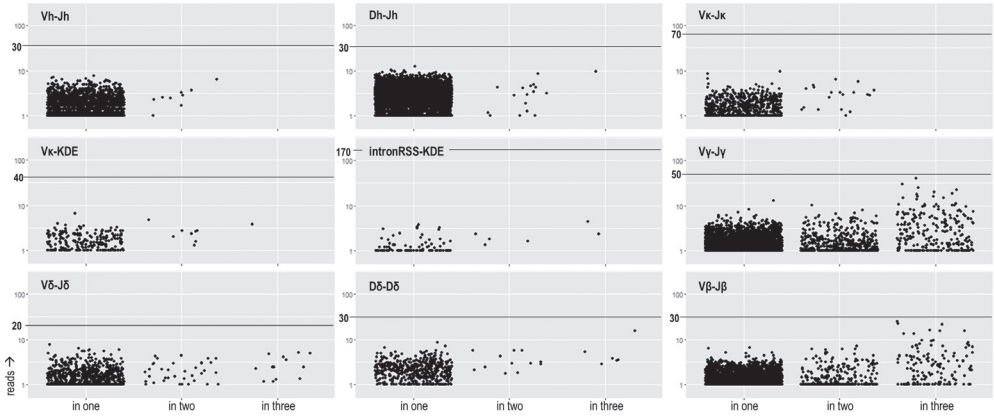

Supplementary Figure 3.
Read counts of Vh-DJh, Dh-Jh, Vκ-Jκ, Vκ-KDE, intronRSS-KDE, Vγ-Jγ, Vδ-Dδ, Dδ-Dδ and Vβ-Jβ rearrangements in regenerating BM from an T-ALL patient at a therapy interval. This BM was sequenced in triplicate, resulting in rearrangements that were found in one, in two or in all three of the replicates. Rearrangements with a read count of <1 (caused by amplification-correction), were displayed as rearrangements with a read count of 1. The black line indicates the previously defined threshold for the involved type of rearrangement.

A

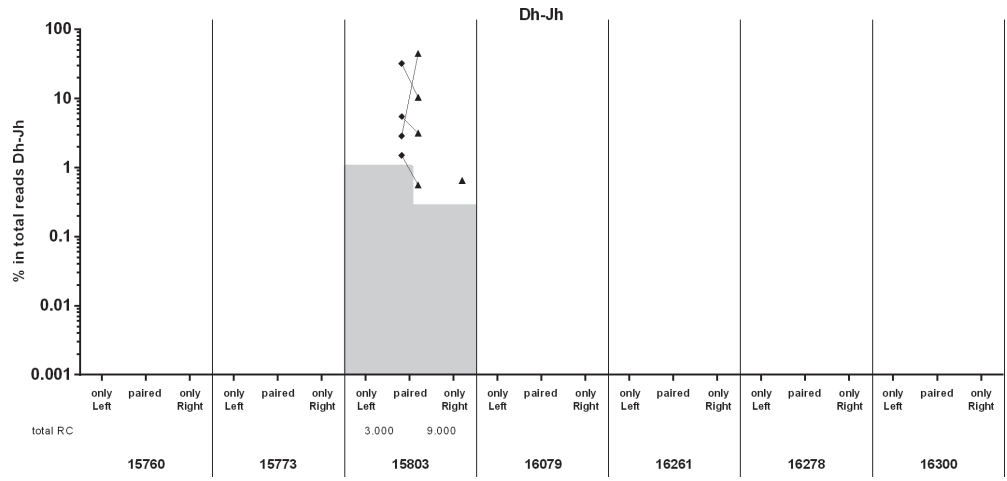

B

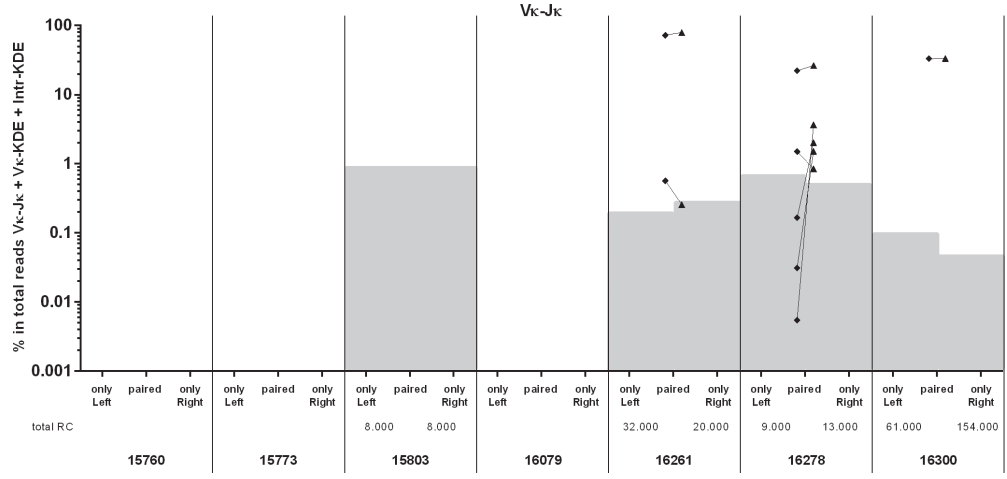

Supplementary Figure 4.

C

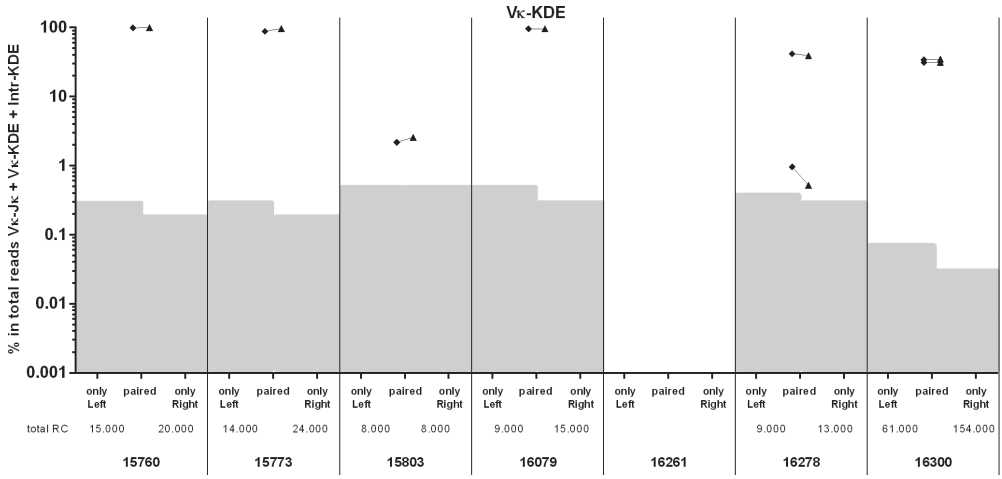

D

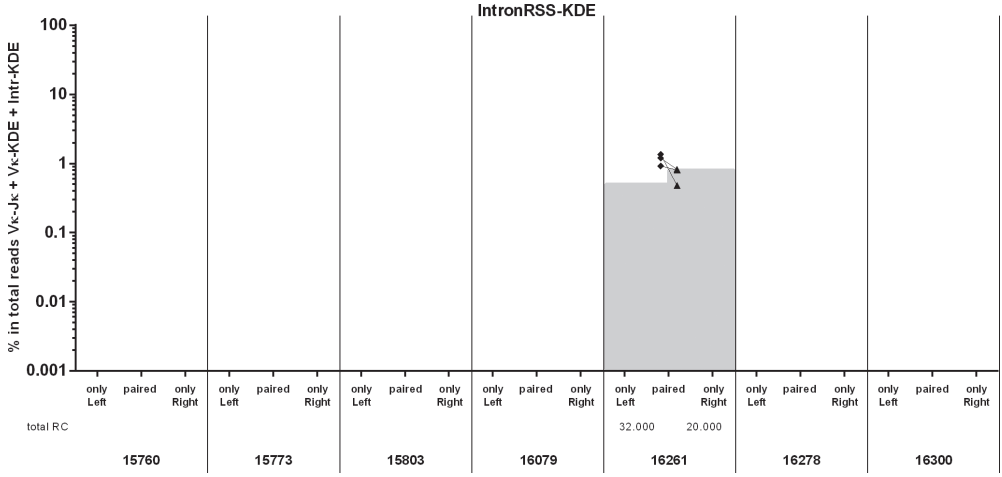

Supplementary Figure 4 (continued).

E

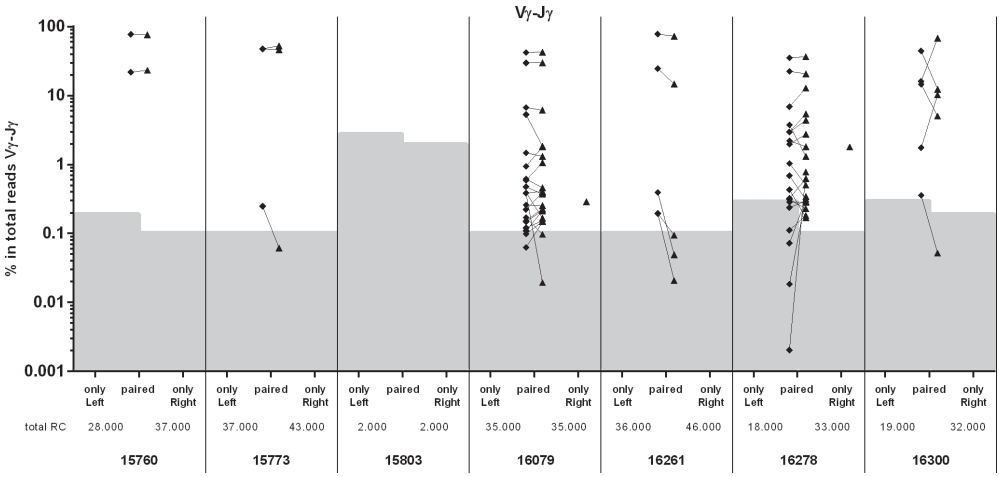

F

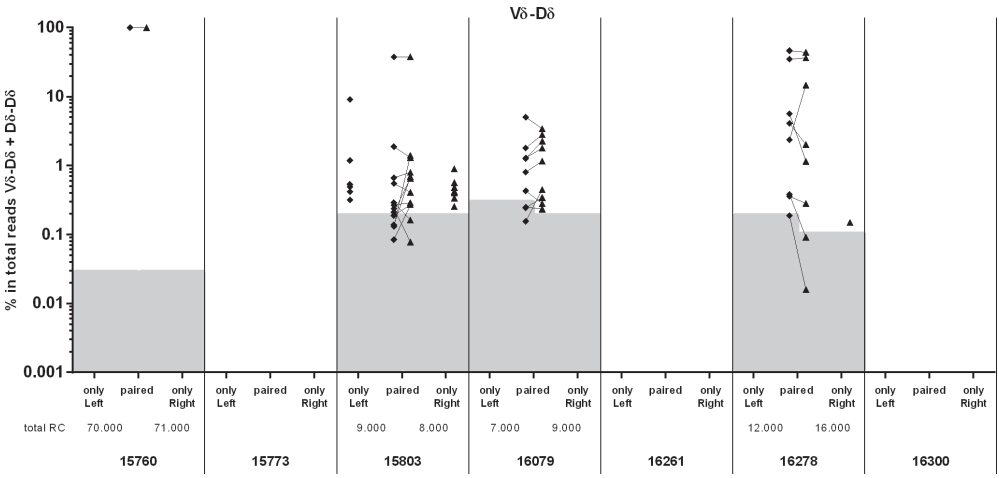

Supplementary Figure 4 (continued).

G

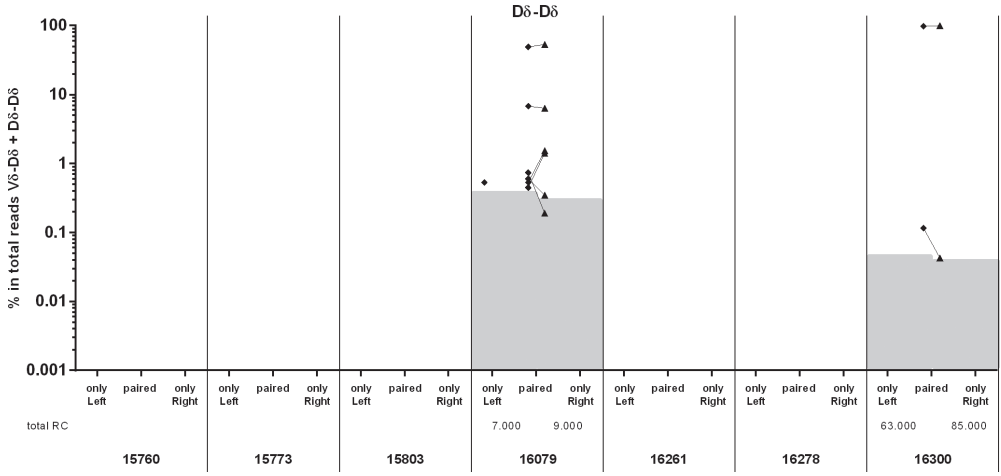

H

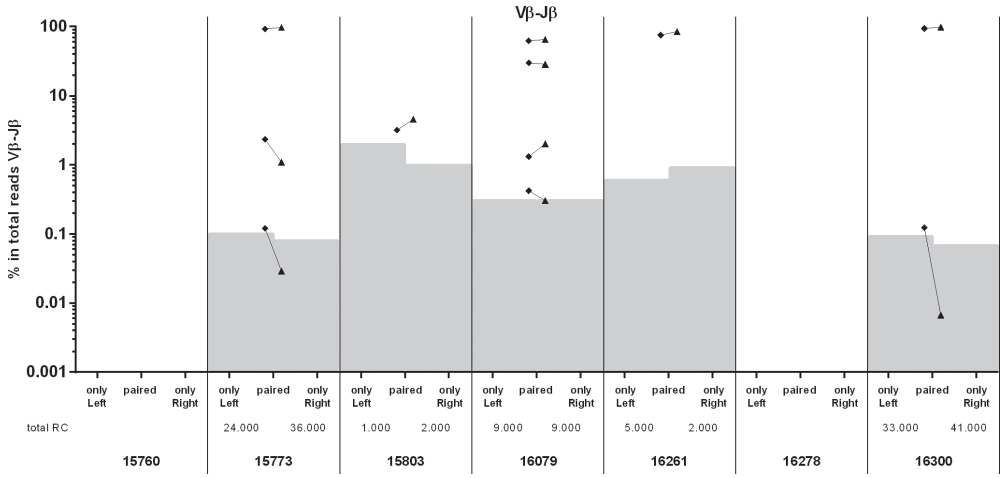

Supplementary Figure 4 (continued).
Frequencies of leukemic Dh-Jh, Vκ-Jκ, Vκ-KDE, intronRSS-KDE, Vγ-Jγ, Vδ-Dδ, Dδ-Dδ and Vβ-Jβ rearrangements in paired BM samples (left and right pelvic bone) from BCP-ALL patients at diagnosis. For each leukemic rearrangement, the presence in both BM samples (paired) or in only one of the two BM samples is indicated. The background-area which also contains IG/TR gene rearrangements derived from normal B-cell and T-cell clones is indicated for each sample (grey).

A

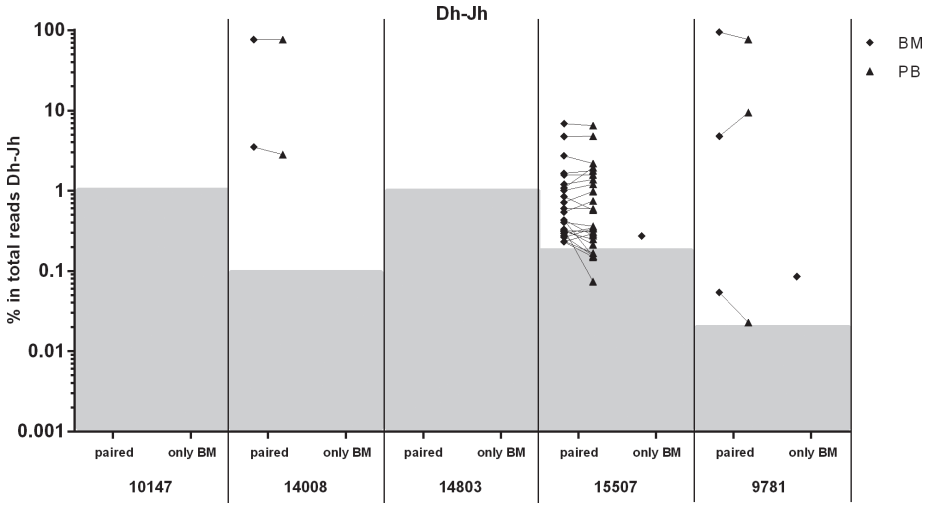

B

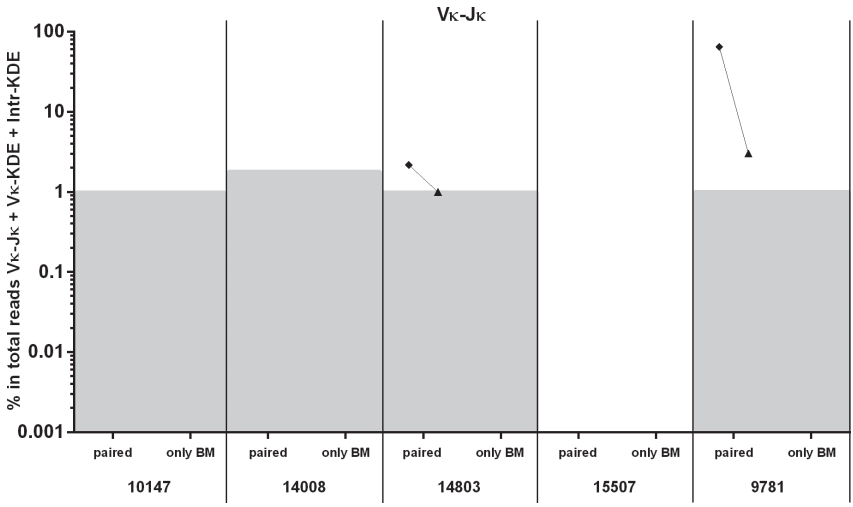

Supplementary Figure 5.

C

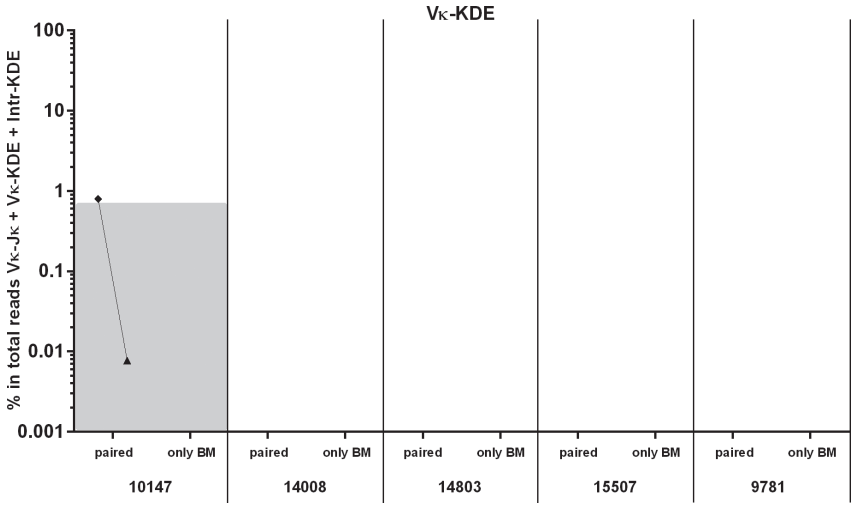

D

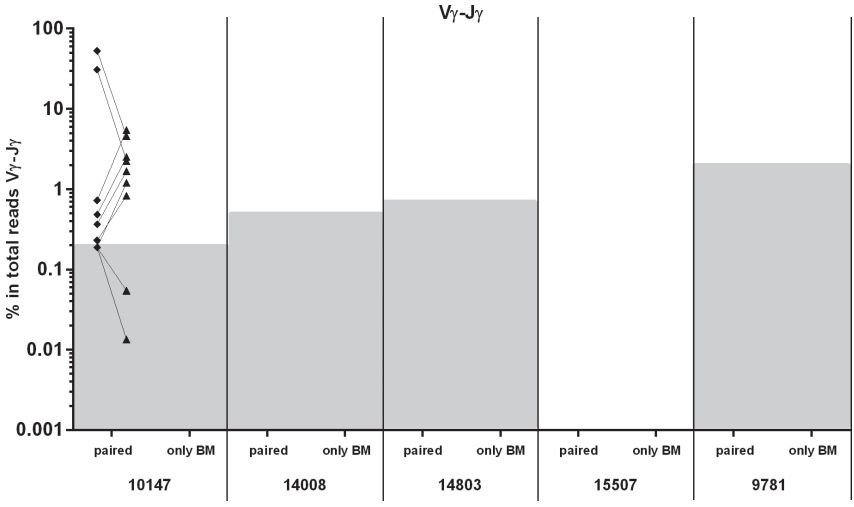

Supplementary Figure 5 (continued).

E

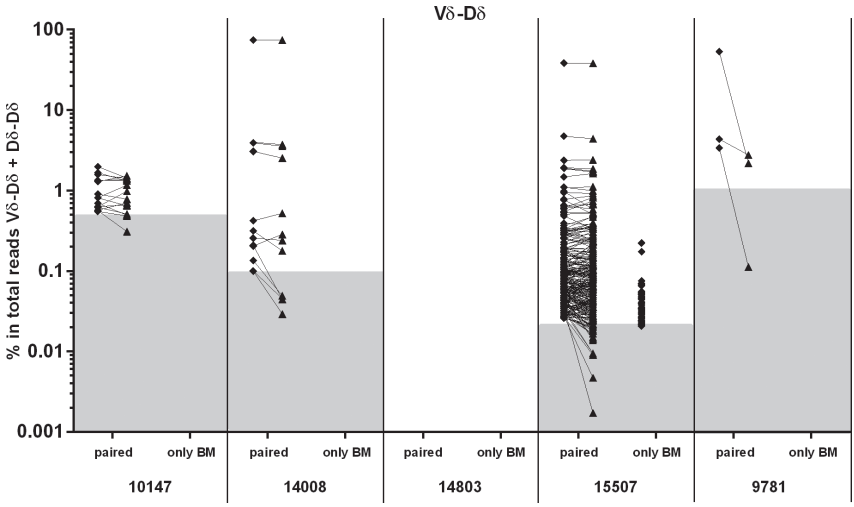

F

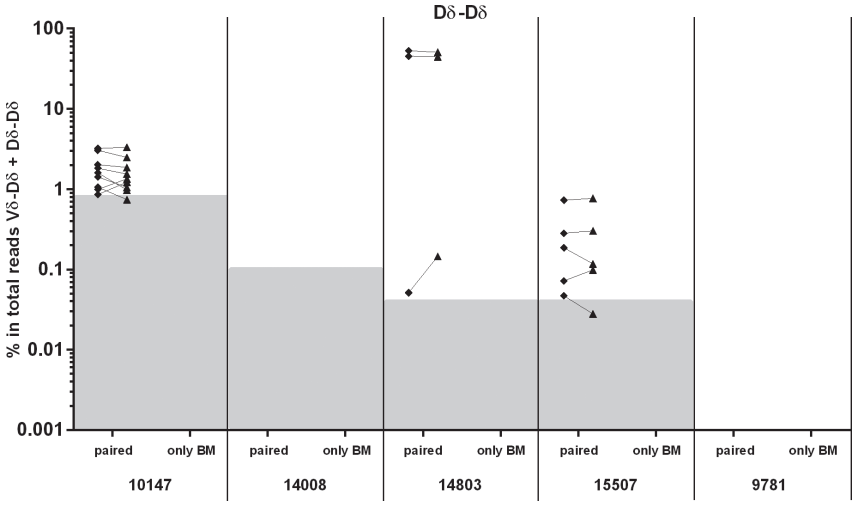

Supplementary Figure 5 (continued).

G

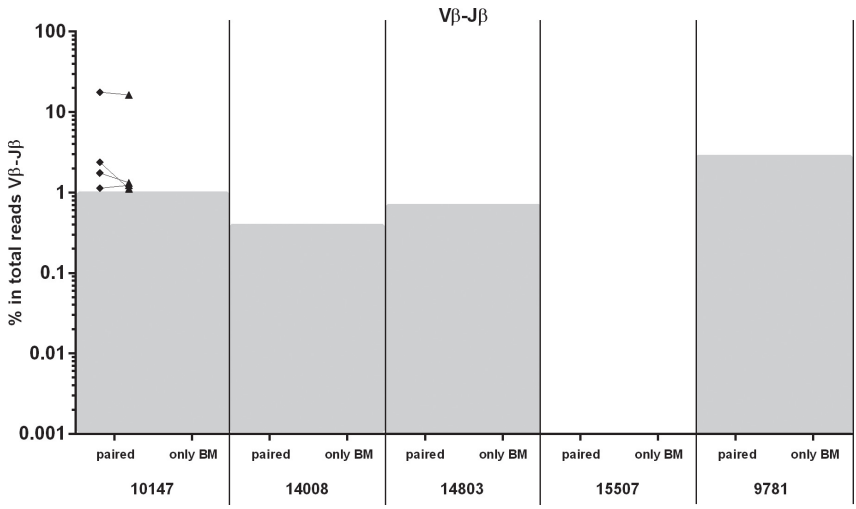

Supplementary Figure 5 (continued)
Frequencies of leukemic Dh-Jh, Vκ-Jκ, Vκ-KDE, Vγ-Jγ, Vδ-Dδ, Dδ-Dδ and Vβ-Jβ rearrangements in paired BM-PB samples from BCP-ALL patients at diagnosis. For each leukemic rearrangement in the BM sample (i.e. with a frequency above the BM threshold), the presence in both samples (paired) or in only the BM sample is indicated. Diamonds represent rearrangements found in BM, triangles represent rearrangements found in PB. The BM background-area which also contains IG/TR gene rearrangements derived from normal B-cell and T-cell clones is indicated for each sample (grey). IntronRSS-KDE rearrangements with a frequency above the threshold were absent in all patients.

REFERENCES

1. Blankenberg, D., et al., Dissemination of scientific software with Galaxy ToolShed. Genome Biol, 2014. 15(2): p. 403.

Chapter 3

Understanding the reconstitution of the B-cell compartment in bone marrow and blood after treatment for B-cell precursor acute lymphoblastic leukemia

Prisca M.J. Theunissen[1], Anouk van den Branden[1], Alita van der Sluijs-Gelling[2], Valerie de Haas[2], Auke Beishuizen[3], Jacques J.M. van Dongen[1] and Vincent H.J. van der Velden[1]

[1]Department of Immunology, Erasmus MC, University Medical Center Rotterdam, Rotterdam, The Netherlands
[2]Dutch Childhood Oncology Group, The Hague, The Netherlands
[3]Department of Pediatric Hematology and Oncology, Sophia Children's Hospital/Erasmus MC, University Medical Center Rotterdam, Rotterdam, The Netherlands

Submitted to Br J Haematol (minor revisions)

ABSTRACT

A better understanding of the reconstitution of the B-cell compartment during and after treatment for B-cell precursor acute lymphoblastic leukemia (BCP-ALL) will help to assess the immunological status and needs of posttreatment BCP-ALL patients. Therefore, we aimed to study the composition and proliferation of both the B-cell precursor (BCP) population in bone marrow (BM) and mature B-cell population in peripheral blood (PB) during and after BCP-ALL therapy. Eight-color flow cytometry was used to identify BCP and mature B-cell subsets. Cell-cycle analysis using DRAQ5 and proliferation history analysis using the KREC-assay were performed to study B-cell proliferation. We found a normal BCP differentiation pattern and a delayed formation of classical CD38dim naive mature B-cells, natural effector B-cells and memory B-cells in patients after chemotherapy. This B-cell differentiation/maturation pattern was strikingly similar to that during initial B-cell development in healthy infants. Tissue-resident plasma cells appeared to be partly protected from chemotherapy. Also, we found that the fast recovery of naive mature B-cell numbers after chemotherapy was the result of increased *de novo* BCP generation, rather than enhanced proliferation within a BCP subset or within the naive mature B-cell subset. These results indicate that posttreatment BCP-ALL patients will eventually reestablish a B-cell compartment with a composition and a B-cell receptor repertoire similar to that in healthy children. However, the infant-like B-cell differentiation/maturation during reconstitution also implies a temporarily absent memory B-cell compartment shortly after end of therapy. Our data suggest that revaccination might be beneficial in posttreatment BCP-ALL patients.

INTRODUCTION

Normal B-cell differentiation in the bone marrow (BM) is a tightly controlled process in which B-cell precursors (BCPs) differentiate through the pro-B, pre-B-I, pre-B-II-Large and pre-B-II-Small stage, to finally become immature BCPs, which express a functional B-cell receptor (BCR) [1-3]. These are released in the peripheral blood (PB) as transitional B-cells which can further mature in the lymphoid tissues and spleen to become naive mature, natural effector and memory B-cells (Figure 1) [4].

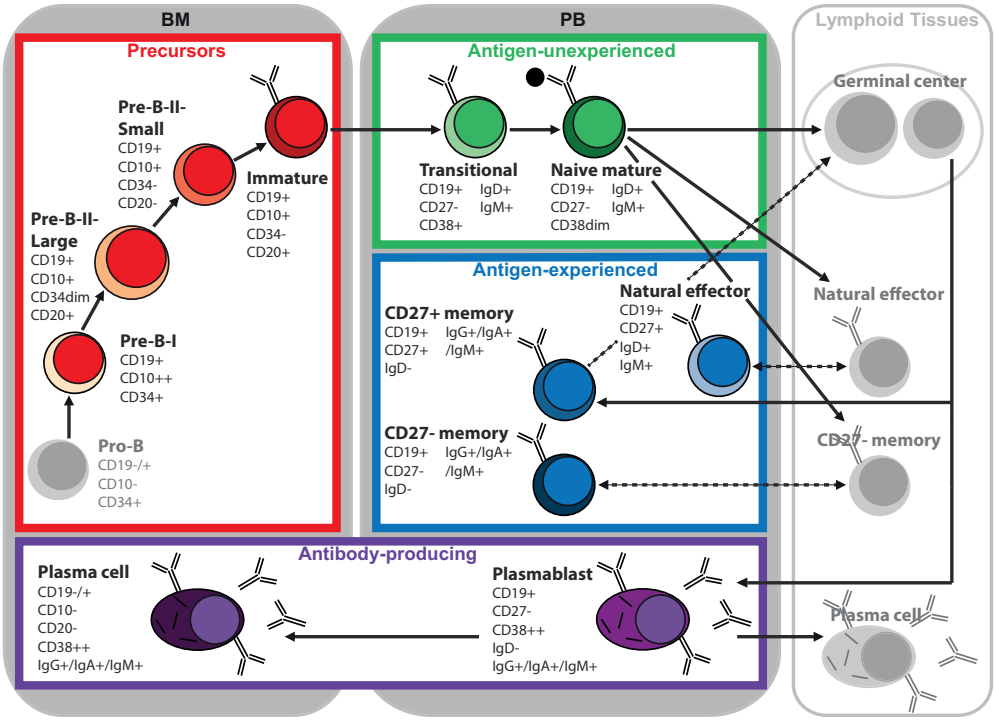

Figure 1.
Schematic overview of the different B-cell subsets in BM, PB and lymphoid tissue. The immunologic markers characteristic for each subset are shown. Solid arrows indicate the main differentiation routes, dashed arrows indicate migration routes. For reasons of clarity, an arrow indicating direct differentiation of the naive mature B-cell subset into the plasmablast subset and arrows indicating migration of memory B-cells and plasma cells between the compartments are omitted. The specific colors for the different B-cell subsets are consistently applied throughout the different figures in the results section. The grey parts are not investigated in this study.

The normal B-cell compartment can be severely affected in patients receiving chemotherapy regimens, resulting in a compromised humoral immunity and consequently a high vulnerability to infections [5, 6]. Profound B-lymphocytopenia as a result of chemotherapy was previously reported in patients with solid tumors treated with docetaxel, patients with breast cancer treated with anthracycline-based regimens and patients with acute leukemia treated with multidrug chemotherapy [7-13].

In patients treated for B-cell precursor acute lymphoblastic Leukemia (BCP-ALL), regeneration of BCPs in BM and recovery of all mature B-cell subsets in PB is needed in order to restore humoral immunity after chemotherapy. Previous studies on BM of ALL patients found that chemotherapy dramatically decreased BCP numbers, but that BCP regeneration occurred in between treatment phases and after end of ALL therapy [12,13]. In between treatment phases, the regenerating BCP population consisted mainly of pre-B-I BCPs, while after end of therapy, also BCPs in later differentiation stages reappeared [12,13]. Furthermore, the total percentage of BCPs was higher in regenerating BM of ALL patients than in BM of healthy controls [14,15]. Previous studies on PB of ALL patients found normal to high levels of transitional and naive mature B-cells in PB shortly after end of therapy, while hardly any natural effector and memory B-cells were observed during the first year after end of therapy [9,10].

Since these studies reported on the composition of the B-cell populations in either BM or PB of ALL patients, it is unclear whether the total (BM and PB) B-cell differentiation/maturation pattern after chemotherapy is similar to that in healthy individuals. Importantly, an abnormal differentiation/maturation pattern could hinder the reestablishment of a well-functioning B-cell compartment in the long-term. Also, since proliferation of normal B-cells in ALL patients has so far not been studied, it is unknown whether the degree of B-cell proliferation in patients after chemotherapy is similar to that in healthy individuals. Enhanced proliferation of BCPs and/or naive mature B-cells in order to quickly restore B-cell numbers could possibly result in a B-cell compartment with a less diverse naive BCR repertoire.

Here, we aimed to get more insight into the reconstitution of the B-cell compartment after profound B-lymphocytopenia induced by BCP-ALL chemotherapy. We therefore studied, by performing more detailed analyses than previously done, the composition and the proliferation of B-cell populations in both the BM and the PB compartment at different time points during and after BCP-ALL therapy.

METHODS

Patient and healthy control samples

In total, 198 PB samples and 132 BM samples from 81 pediatric BCP-ALL patients (aged 1 to 18 years old) were collected (Supplementary Table 1). All patients were treated according to the Standard Risk (SR) or Medium Risk (MR) treatment arm of the Dutch Childhood Oncology Group (DCOG) ALL10 or ALL11 protocol, which contain the following key drugs: prednisone, dexamethasone, vincristine, daunorubicin, asparaginase, cyclophosphamide, cytarabine, mercaptopurine and doxorubicin [16]. Patients with Down syndrome, patients assigned to the Ikaros positive-treatment arm and patients assigned to the High Risk (HR) treatment arm of the DCOG-ALL11 protocol were excluded, since treatment of these patients differs significantly from the large group of remaining BCP-ALL patients. BM samples from six healthy children (aged 1 to 12 years old) that were BM stem cell donor for their siblings with parental informed consent and with approval of the Medical Ethical Committee of the Leiden University Medical Center (protocol P08.001) were used as healthy control BM. PB samples from (young) adults were used as healthy control PB, since PB samples from healthy children were not available. All samples were collected with informed-consent and/or according to the guidelines of the Medical Ethical Committee of Erasmus MC.

Immunophenotyping

Eight-color flow cytometry was performed on BM and PB samples after bulk-lysing with ammonium chloride and subsequent staining with the antibody panels as described in Supplementary Table 2. The samples were measured on a LSRFortessa or FACSCanto II flow cytometer (BD Biosciences, Erembodegem, Belgium) using FACS-Diva software (BD Biosciences). Data were analyzed with Inificyt Software (Cytognos, Salamanca, Spain). The immunophenotypic definitions of the different B-cell subsets are shown in Figure 1.

Cell-cycle analysis

Post-Ficoll mononuclear cells (MNCs) from BM samples were stained with antibodies directed against cell-surface markers, labeled with DNA-intercalating agent DRAQ5 (3 uL, BioStatus, Shepshed, UK), and intracellularly stained after fixation and permeabilization with Fix&Perm reagents (An der Grub, Vienna, Austria). Antibody panels are described in Supplementary Table 2. Samples were measured (low speed, linear scale in APC channel) on a LSRFortessa (BD Biosciences), using FacsDIVA software (BD Biosciences). Using Inifinicyt Software (Cytognos), the percentage of cells with high DRAQ5 expression (cells in S/G2/M-phase) was determined within each BCP subset.

Molecular analysis of replication history

Post-Ficoll MNCs from BM and PB samples were stained with the antibody panels described in Supplementary Table 2. Pre-B-II-Small and immature BCP fractions (BM) and naive mature B-cell fractions (PB) were sorted using the FACSAriaIII Cell Sorter (BD Biosciences) and FACSDiva software (BD Biosciences). The gating strategies for sorting of the naive mature B-cell subset and different CD38-related stages within the naive mature B-cell subset are described in Supplementary Figure 1. DNA was isolated from the sorted cell fractions with the Mammalian Genomic DNA Miniprep Kit (Sigma-Aldrich, St. Louis, Missouri, USA) according to instructions of the manufacturer. The kappa-deleting recombination excision circle (KREC)-assay was performed on the sorted cell fractions as described previously [17].

Statistical analysis

The Mann-Whitney U test in Prism 5.0 software (GraphPad, La Jolla, California, USA) was used. A P-value of less than 0.05 was considered statistically significant.

RESULTS

Composition of the BCP population in BM during and after therapy

At day 15 and at day 33, induction therapy caused a complete loss of BCPs and a very low total WBC count in BM (Figure 2a). At day 79 and month 5, the preceding therapy intervals induced BCP regeneration. However, the intervals were too short to achieve a complete BCP differentiation, resulting in relatively high percentages of early pre-B-I BCPs and a relatively low percentage of total BCPs (less than one third of that in healthy children) (Figure 2a+b). From month 5 onwards, continuous maintenance therapy resulted in very low percentages of BCPs at month 9 and month 12. One year after end of therapy, the percentage of total BCPs in BM and the relative distribution of the BCP subsets within the BCP population had normalized (time points after end of therapy are indicated with # in the figures).

Composition of the B-cell population in PB during and after therapy

Since B-cell numbers in PB of children vary with age, B-cell numbers in PB of patients were expressed as percentage of the age-matched reference value. At day 15 and day 33, transitional B-cells had already completely disappeared and absolute numbers of naive mature B-cells, natural effector B-cells, memory B-cells and plasmablasts had dropped far below the normal reference values (Figure 3). From day 79 until end of therapy, hardly any mature B-cells, except for plasmablasts, were present (in both SR patients and MR patients,

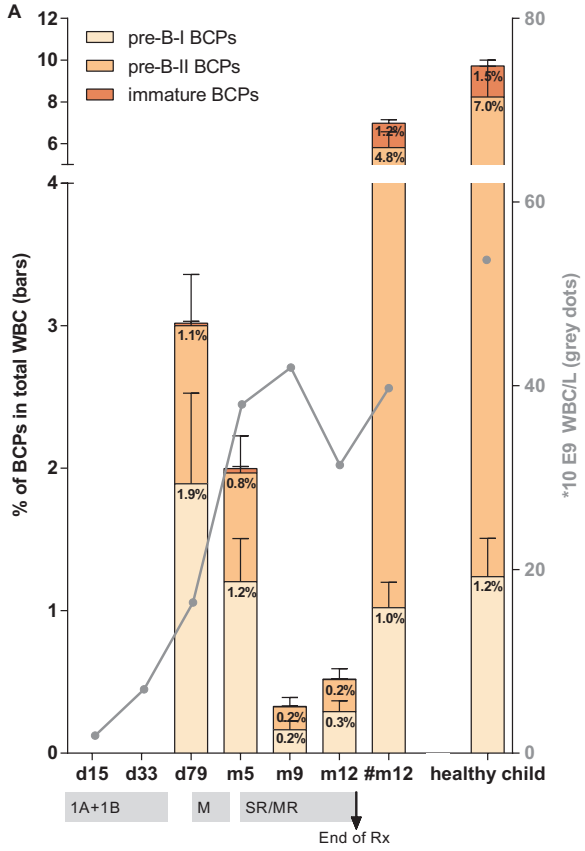

Figure 2.
A. Percentage of pre-B-I, pre-B-II and immature BCPs in total BM WBC, in patients at different time point during therapy (n>15 per time point), in patients at one year after end of therapy (n=7) and in healthy children (n=6). The grey curve correlates to the right y-axis and shows the average WBC count per time point. Treatment phases are indicated below the x-axis. Bars represent mean values with SEMs.

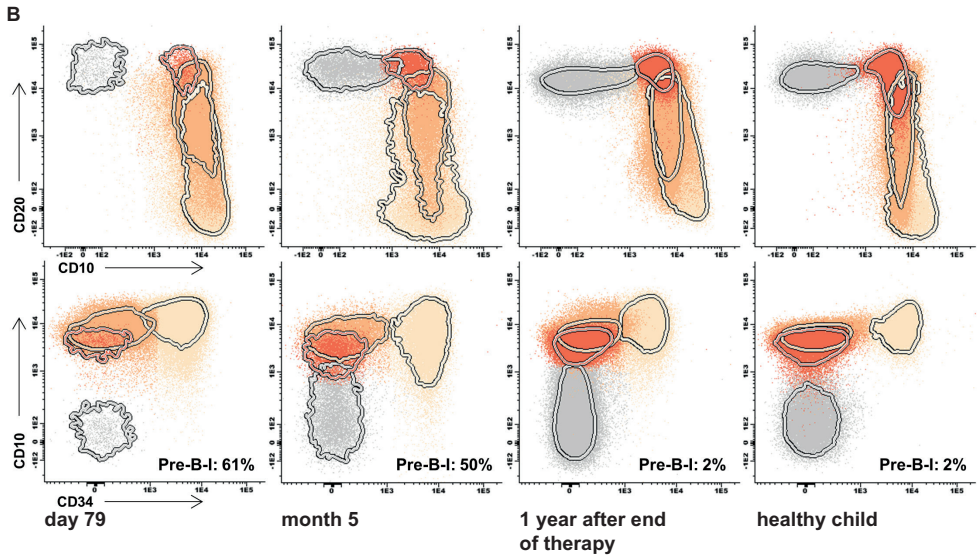

Figure 2 (continued).
B. Dot plots showing representative examples of the CD19+ B-cell population (plasma cells excluded) in BM of a patient at day 79, a patient at month 5, a patient at one year after end of therapy and a healthy child. Contours indicate 1.5 SD. The percentage of pre-B-I BCPs within the total CD19+ B-cell population in BM is shown.

although numbers were slightly higher in SR patients; data not shown). Remarkably, plasmablasts returned to normal or high numbers in half of the patients at day 79 and month 5. At 6 weeks after end of therapy, transitional B-cells reappeared, exceeding normal reference values, while the other mature B-cell subsets remained at very low levels. At three months after end of therapy, also naive mature B-cell numbers exceeded the normal reference values. Until one year posttreatment, transitional and naive mature B-cell numbers remained above normal reference values, whereas numbers of natural effector B-cells and memory B-cells increased, but remained below normal reference values.

Link between B-cell subsets in BM and PB during and after therapy

We next aimed to link the results on BCP subsets in BM to the results on mature B-cell subsets in PB. At day 15 and day 33, BCPs were absent in BM, but low numbers of naive mature B-cells were still present in PB (Figure 4a). At day 79 and at month 5, only very few immature BCPs were formed during regeneration in BM, resulting in only very few transitional and naive mature B-cells in PB. During the remaining months of therapy, BCPs in BM and transitional and naive mature B-cells in PB were virtually absent. At one year after end of therapy, a BCP population comparable to that in healthy children had been reestablished in BM, resulting in high numbers of transitional and naive mature B-cells in PB.

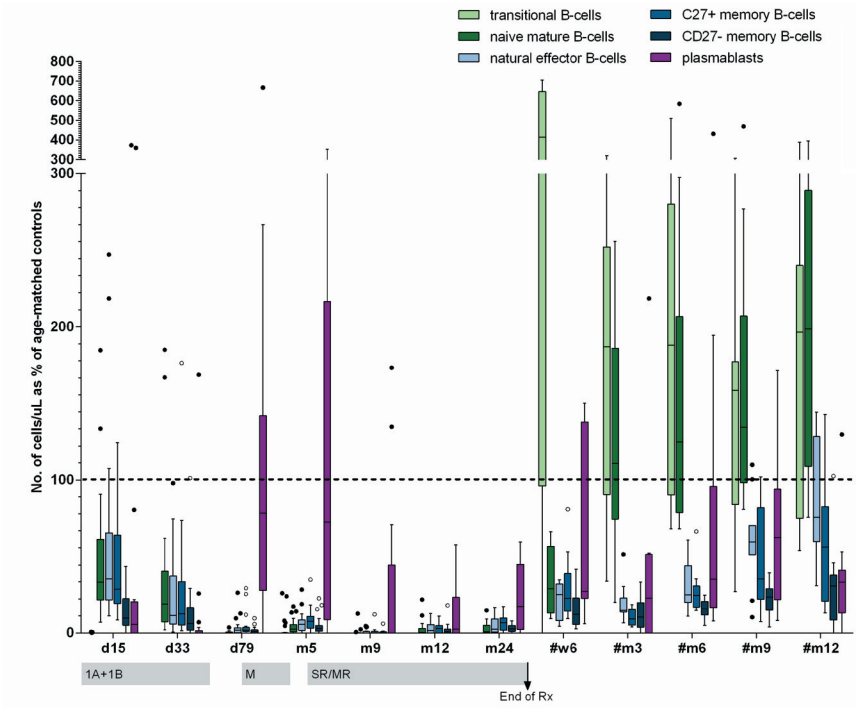

Figure 3.
Absolute numbers of mature B-cells expressed as a percentage of the aged-matched reference value (medians of healthy children), at different time points during therapy (n>15 per time point) and after end of therapy (n>10 per time point). Boxes show medians with 2nd and 3rd quartiles. Whiskers show the most extreme values within 1.5 times the interquartile ranges. Values more than 1.5 times the interquartile ranges are plotted individually.

Changes in plasma cell numbers in BM and plasmablast numbers in PB occurred more or less synchronously (Figure 4b). Particularly the increase in plasmablasts at day 79 and month 5 in PB was paralleled by an increase of plasma cells in BM. The immunoglobulin-isotype subset distribution of the plasmablast population varied slightly at different time points, but both IgM+ plasmablasts and class-switched IgA+ and IgG+ plasmablasts remained present during and after therapy (Figure 4c).

No enhanced proliferation during BCP regeneration in BM

To evaluate whether proliferation is enhanced during BCP regeneration, we determined the degree of proliferation per BCP subset by measuring the percentage of cells in the S/G2/M-phase. As expected, pre-B-II-Large BCPs showed the highest degree of proliferation (Figure 5). Remarkably, also pro-B and pre-B-I BCPs showed a significant degree of proliferation. Pre-B-II-Small and immature BCPs showed hardly any proliferation (<5%; data not shown). Importantly, pre-B-I and pre-B-II-Large BCPs in regenerating BM (day 79 and month 5) proliferated to the same extent as pre-B-I and pre-B-II-Large BCPs in

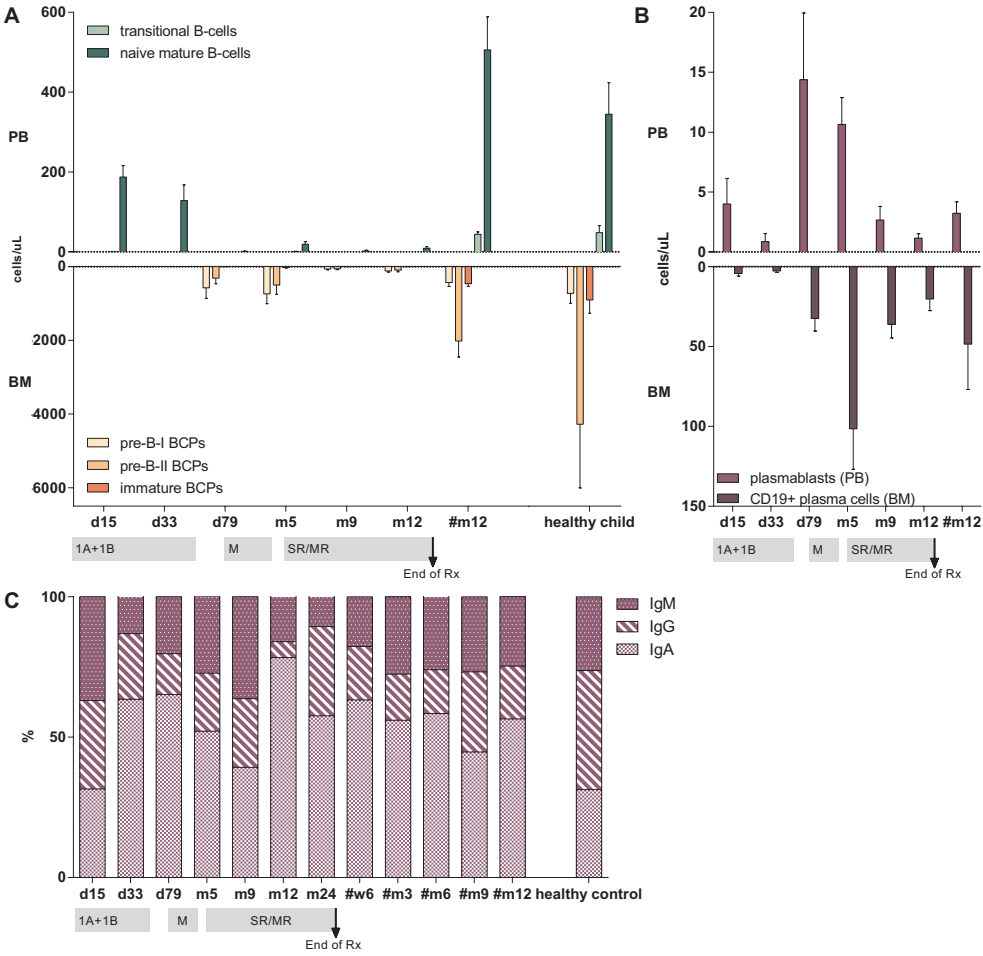

Figure 4.
A. Absolute numbers of BCPs per microliter in BM and absolute number of transitional and naive mature B-cells per microliter in PB at different time points during therapy (BM and PB: n>15 per time point) and at one year after end of therapy (BM n=7; PB n=11). Bars represent mean valus with SEMs. Transitional and naive mature B-cell numbers in PB of healthy children are based on literature [18].
B. Absolute numbers of plasmablasts in PB and CD19+ plasma cells in BM, at different time points during therapy (BM and PB: n>15 per time point) and at one year after end of therapy (BM n=7; PB n=11). Bars represent mean values with SEMs.
C. Percentage of the immunoglobulin-isotype subsets within total plasmablasts in PB. n>5 per time point. Immunoglobulin-isotype percentages in PB of healthy controls are based on literature [24].

healthy control BM. Small differences in pro-B BCP proliferation between regenerating BM and healthy control BM could be attributed to the limited number of healthy controls with sufficient pro-B BCPs (n=3). KREC-analysis confirmed that pre-B-II-Small and immature BCPs in non-regenerating BM did not proliferate (data not shown). KREC-analysis of

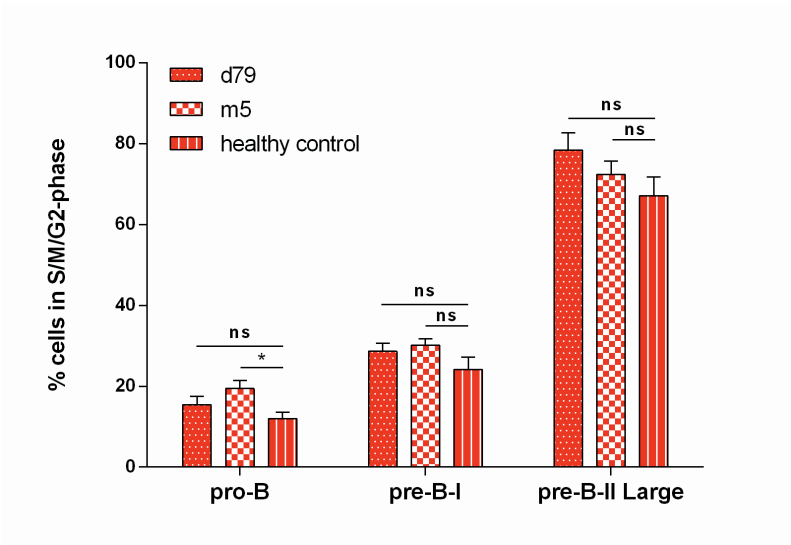

Figure 5.
Percentage of S/G2/M-cells within the pro-B BCP subset (CD34+CD19-CD36/CD123-CD22+), pre-B-I BCP subset (CD19+CD10+IgM-cyIgM-) and pre-B-II-Large BCP subset (CD19+CD10+IgM-cyIgM+cyCD179a+) in BM at day 79 (n=9), BM at month 5 (n=10) and BM from healthy controls (n=7; 3 children, 4 adults). Bars represent mean values with SEMs. *p<0.05.

pre-B-II-Small and immature BCPs in regenerating BM could not be performed due to very low numbers of these cells at day 79 and month 5.

No enhanced proliferation in the naive mature B-cell subset during and after therapy

To evaluate the replication history of the naive mature B-cells at different time points during and after therapy, KREC-analysis was performed. This analysis showed that the naive mature B-cell subset in all day-15 and day-33 PB samples, and some month-5 PB samples, seemed to have undergone a higher number of cells divisions than the naive mature B-cell subset in healthy control PB samples (Figure 6a). After end of therapy, the number of cell divisions of the naive mature B-cell subset was not significantly different from that in healthy controls. However, more detailed analysis showed that the variations in the observed number of cell divisions appeared to be related to the variable composition of the naive B-cell subset at the different time points. The larger the proportion of CD38low naive mature B-cells, the higher the number of cell divisions (Figure 6b+c). This correlation between CD38 expression and replication within the naive mature B-cell subset was confirmed by separately analyzing CD38high, CD38dim and CD38low naive mature B-cells from healthy control PB (Figure 6d). Thus, the naive mature B-cells in patients during and after therapy showed a similar number of cell divisions as the corresponding naive mature B-cells (i.e. with the same CD38 expression) in healthy controls.

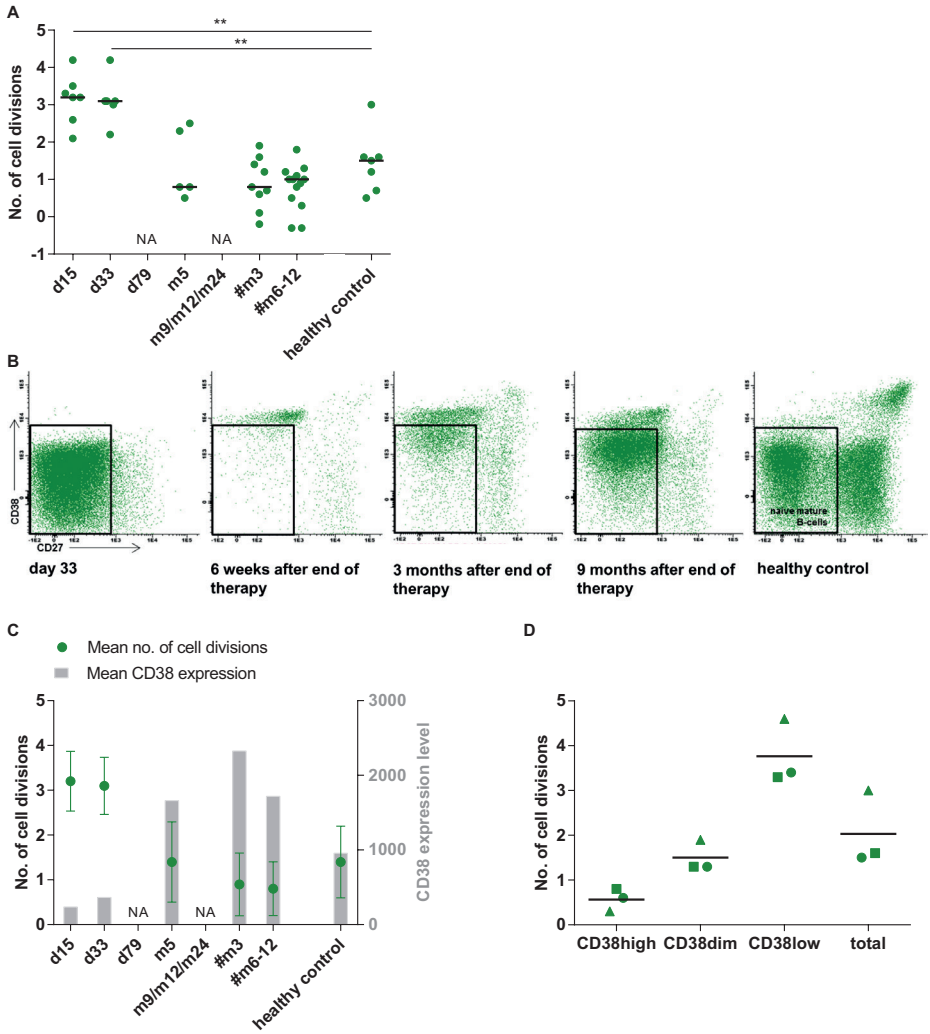

Figure 6.

A. Number of cell divisions after IGK IntronRSS-KDE rearrangement in the naive mature B-cell subset, at different time points during and after therapy. Each dot represents a patient. Medians are shown. **p<0.01. Naive B-cell numbers at 6 weeks after end of therapy were too low for KREC-analysis. Healthy controls are young adults, but previous studies showed that the median number of naive mature B-cell replications in adults was similar to that in children [39,40].

B. Dot plots showing representative examples of the CD19+ B-cell population in PB of a patient at day 33, a patient at 6 weeks after end of therapy, a patient at 3 months after end of therapy, a patient at 9 months after end of therapy and a healthy control. As a reference, the CD38 expression of naive mature B-cells in healthy controls is indicated with a black square.

C. Correlation between CD38 expression and the number of cell divisions in the naive mature B-cell subset, at different time points during and after therapy. Green circles represent mean numbers of cell divisions (with SD), corresponding to right y-axis. Grey bars represent mean levels of CD38 expression, corresponding to left y-axis.

D. Comparison of the number of cell divisions between CD38high, CD38dim, CD38low and total naive B-cells in PB from healthy controls. Each symbol corresponds to one of the three healthy controls. Medians are shown.

The subset distribution of the mature B-cell population in PB after end of therapy is similar to that in PB of infants

Since our results indicated that virtually the entire B-cell compartment had to be rebuilt after end of BCP-ALL treatment, we compared the subset distribution of the mature B-cell population in PB of patients at 0-6 months or 6-12 months posttreatment with that of healthy infants that were 0-6 months and 6-12 months of age, respectively (infant reference values from literature [18]). We did not further subdivide the naive mature B-cell subset into the different CD38-based maturation stages, since infant reference values for these subpopulations do not exist. This comparison showed that the subset distribution of the mature B-cell population in patients after end of therapy, aged 4 years and older, paralleled that in healthy infants (Figure 7).

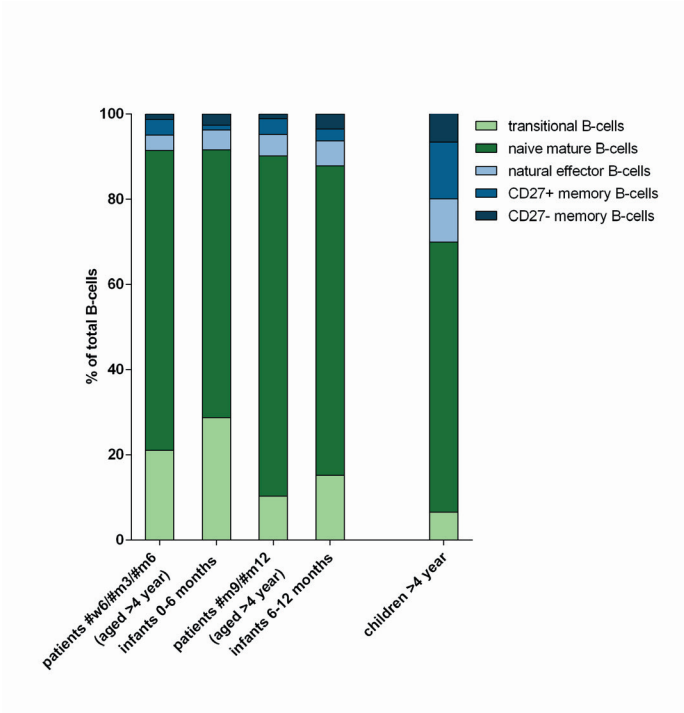

Figure 7.
Distribution of the B-cell subsets within the total mature B-cell population in PB of patients after end of therapy compared to that in PB of healthy infants. Since the age of the included ALL patients is >4 years, healthy children >4 years old are used as a reference. The subset distribution in infants and children > 4 years are based on normal reference values in literature [18].

DISCUSSION

BCP-ALL treatment has a dramatic impact on the normal B-cell compartment. We aimed to understand reconstitution of the B-cell compartment after BCP-ALL therapy. We therefore performed a detailed study on the composition of the B-cell population and the degree of proliferation in the specific B-cell subsets at different time points during and after ALL therapy. Of importance, we studies B-cells in both BM and PB, which to our best knowledge has not been done before.

Our results on the dynamics of B-cell subsets in BM and PB during and after ALL-therapy showed that chemotherapy dramatically affected the BCP population in BM and the mature B-cell population in PB, which was in agreement with previous studies [9-13]. The two therapy intervals (with a duration of one week and two weeks, respectively) were too short to achieve complete BCP differentiation in BM and therefore too short to replenish PB with new mature B-cells. These results were in line with previous results on BCP recovery in ALL patients treated according to the DCOG ALL8 protocol [12,13]. In posttreatment PB, we showed a relatively fast recovery of transitional and naive mature B-cell numbers (within 6 weeks and 3 months, respectively), but a delayed recovery of natural effector and memory B-cell numbers. In previous studies, a similar pattern of mature B-cell recovery after chemotherapy was found in patients treated for ALL (according to older protocols), in patients treated for other types of cancer (e.g. breast cancer) and, remarkably, in patients who had received a stem cell transplantation (SCT) after chemotherapeutic conditioning [8-10,19-22]. These data indicate that once B-cell recovery is induced (at a variable time point depending on the type of preceding chemotherapy or SCT), reconstitution of the B-cell compartment follows a consistent pattern. Our data indicate that between two and six weeks of BCP regeneration are needed to generate new transitional B-cells. Subsequently, less than six weeks are necessary to restore normal levels of naive mature B-cells. However, more than one year is required to reestablish normal levels of antigen-experienced B-cells, such as memory B-cells.

In some patients, an increase of plasmablasts in PB was observed during therapy intervals, which correlated with an increase of plasma cells in BM. A large part of these plasmablasts were class-switched and predominantly of the IgA-isotype. Since memory B-cell numbers in PB remained very low, also during therapy intervals, plasmablasts reappearing at day 79 and month 5 had to be derived from long-lived plasma cells in the tissue. Studies on antibody levels in ALL patients showed that vaccination-induced immunoglobulins were, although decreased, still present after therapy [23]. Other studies showed that, in steady-state conditions, long-lived plasma cells in BM and tissue recirculate in PB [24,25]. Together, these data suggest that some long-lived plasma cells residing in the

tissue, in particular IgA-plasma cells in the mucosal surfaces, are protected from cytotoxic therapy and are able to recirculate as plasmablasts in PB during and after BCP-ALL therapy.

Since regenerating BM samples from children directly after end of therapy were not available, we used regenerating BM samples taken at therapy intervals (day 79 and month 5) to study the role of BCP proliferation in the reconstitution of the B-cell compartment after BCP-ALL therapy. We found that BCPs in BM of patients at day 79 and month 5 proliferated at a similar rate as BCPs in BM of healthy individuals. Proliferation of BCPs during B-cell recovery after ALL chemotherapy was not studied before. However, other proliferation studies found, in line with our results, that early lymphoid precursors in cytopenia-induced reactive BM samples and early BCPs in regenerating/infant BM samples (mixed group) proliferated at a similar rate as their equivalents in healthy adult BM [26,27]. These data indicate that the increased percentage of pre-B-I BCPs in regenerating BM after chemotherapy (although less pronounced in our data than in previous studies) is not caused by enhanced proliferation but rather by a larger influx of non-committed stem cells into the B-cell lineage. This way, BCP regeneration after chemotherapy is likely to result in the reestablishment of a diverse naive BCR repertoire (i.e. not narrowed by enhanced proliferation).

Our results on B-cell replication in PB showed that the naive mature B-cell subset was composed of naive B-cells with different levels of maturation. Maturation within the naive mature B-cell subset was characterized by a decrease in CD38 expression and an increase in number of passed replication cycles. The naive mature B-cell subset present shortly after start of therapy (at day 15 and day 33) consisted of residual CD38low naive mature B-cells with a relatively high number of replications. In contrast, the naive mature B-cell subset present directly after end of chemotherapy predominantly consisted of newly generated CD38high naive mature B-cells with a low number of replications. Variations in replication number of the total naive mature B-cell subset were therefore caused by the variable composition of the naive mature B-cell subset at the different time points and not by a changed degree of B-cell proliferation. Thus, the proliferation history of the naive mature B-cells in PB of patients during and after therapy was similar to that in PB of healthy individuals. To our knowledge, no previous studies exist on mature B-cell proliferation or on BCR repertoire formation after ALL therapy. A study on immune reconstitution after SCT showed that the proliferation history of naive mature B-cells after autologous SCT was also similar to that in healthy individuals [28]. In another SCT-study, a restricted BCR repertoire was found during the first year after SCT, but this was most likely the result of low numbers of sequenced *IGH* gene-rearrangements early posttransplant [29]. These data indicate that recovery of the naive mature B-cell numbers after BCP-ALL therapy is the result of *de novo* B-cell generation, rather than enhanced proliferation within the naive B-cell subset, resulting in the reestablishment of a diverse naive BCR repertoire after therapy.

Comparing our data on reconstitution of the mature B-cell population after BCP-ALL therapy with literature data on development of the mature B-cell population in infants, we found remarkable similarities. Firstly, we found that, also in infants, natural effector and memory B-cell numbers remained low until at least one year after birth. Moreover, the subset distribution of the mature B-cell population in patients at a certain time point after end of therapy was almost identical to that in infants at the same time point after birth. This comparison between posttreatment patients and infants has not been performed previously, but SCT-studies showed that the B-cell subset distribution during reconstitution after SCT was also similar to that during the first year of life [19-21]. Secondly, we found, as already discussed, that almost all newly generated naive mature B-cells during the first half year after end of chemotherapy were CD38high (indicating a low degree of maturation), while the first CD38dim naive mature B-cells only appeared after six to nine months posttreatment. Previous studies showed that also in cord blood (and in PB of patients in the first half year after SCT), almost all naive mature B-cells were CD38high [20,30,31]. CD38high B-cells represent pre-naive B-cells, which are in an intermediate stage between the CD38bright transitional B-cells and the classical CD38dim naive mature B-cells [30,31]. It is unlikely that the transition from pre-naive to classical naive mature B-cell stage takes more than six months (longer than the life-span of a naive mature B-cell). Thus, it seems that pre-naive B-cells in PB of patients during the first half year after end of therapy are, similar to those in PB of infants, temporarily less able to mature to the CD38dim naive mature B-cell stage. Possibly, this is due to a lack of contact with germinal centers, which were found to be decreased in both neonates and patients after chemotherapeutic conditioning regimens [19,32,33]. Together, these data indicate that the recovery of the B-cell subsets in patients after BCP-ALL therapy is similar to the initial development of the B-cell subsets in infants. Since the DCOG ALL10 and ALL11 protocols consist of a backbone that is derived from the Berlin-Frankfurt-Münster (BFM) protocol, our results can presumably be generalized to all BCP-ALL patients treated according to a BFM-based protocol.

Thus, although we showed that residual plasma cells might still be present in the tissue after end of BCP-ALL therapy, previous studies showed that these plasma cells do not produce protective levels of immunoglobulins anymore in a significant part of the patients [23,34]. Also, we showed that the B-cell population shortly after BCP-ALL therapy was, similar to that in healthy infants, lacking natural effector B-cells and memory B-cells. In healthy infants, this inexperienced B-cell population is supported by the national vaccination programs starting from the second month after birth [35-38]. Therefore, revaccination might also be beneficial in BCP-ALL patients shorty after end of therapy.

ACKNOWLEDGMENTS

We thank the involved technicians of the Laboratory for Medical Immunology, in particular Romana Jugooa, Gonnie Paulides, Jeanet Hogervorst, Jeroen te Marvelde, Claudia Hagens, Jolanda Doekharan and André Bijkerk. We gratefully acknowledge the department of Pediatric Oncology/Hematology for their support in the collection of patient samples, in particular Nel de Jongh-den Braber and Rolinda Stigter. We thank Arjan Lankester from the department of Pediatrics at the Leiden University Medical Center for kindly providing BM samples from SCT donors. We acknowledge Edwin Sonneveld of the Dutch Childhood Oncology Group for kindly providing additional clinical data. This study was financially supported by PrioMedChild, project 40-41800-98-027.

REFERENCES

1. Ghia P, ten Boekel E, Sanz E, de la Hera A, Rolink A, Melchers F. Ordering of human bone marrow B lymphocyte precursors by single-cell polymerase chain reaction analyses of the rearrangement status of the immunoglobulin H and L chain gene loci. J Exp Med 1996 Dec 1; 184(6): 2217-2229.
2. van Zelm MC, van der Burg M, de Ridder D, Barendregt BH, de Haas EF, Reinders MJ, et al. Ig gene rearrangement steps are initiated in early human precursor B cell subsets and correlate with specific transcription factor expression. J Immunol 2005 Nov 1; 175(9): 5912-5922.
3. Anzilotti C, Kienzler AK, Lopez-Granados E, Gooding S, Davies B, Pandit H, et al. Key stages of bone marrow B-cell maturation are defective in patients with common variable immunodeficiency disorders. J Allergy Clin Immunol 2015 Aug; 136(2): 487-490 e482.
4. Pieper K, Grimbacher B, Eibel H. B-cell biology and development. J Allergy Clin Immunol 2013 Apr; 131(4): 959-971.
5. Steele TA. Chemotherapy-induced immunosuppression and reconstitution of immune function. Leuk Res 2002 Apr; 26(4): 411-414.
6. Lehrnbecher T, Koehl U, Wittekindt B, Bochennek K, Tramsen L, Klingebiel T, et al. Changes in host defence induced by malignancies and antineoplastic treatment: implication for immunotherapeutic strategies. Lancet Oncol 2008 Mar; 9(3): 269-278.
7. Kotsakis A, Sarra E, Peraki M, Koukourakis M, Apostolaki S, Souglakos J, et al. Docetaxel-induced lymphopenia in patients with solid tumors: a prospective phenotypic analysis. Cancer 2000 Sep 15; 89(6): 1380-1386.
8. Verma R, Foster RE, Horgan K, Mounsey K, Nixon H, Smalle N, et al. Lymphocyte depletion and repopulation after chemotherapy for primary breast cancer. Breast Cancer Res 2016; 18(1): 10.

9. van Tilburg CM, van der Velden VH, Sanders EA, Wolfs TF, Gaiser JF, de Haas V, et al. Reduced versus intensive chemotherapy for childhood acute lymphoblastic leukemia: impact on lymphocyte compartment composition. Leuk Res 2011 Apr; 35(4): 484-491.
10. Eyrich M, Wiegering V, Lim A, Schrauder A, Winkler B, Schlegel PG. Immune function in children under chemotherapy for standard risk acute lymphoblastic leukaemia - a prospective study of 20 paediatric patients. Br J Haematol 2009 Nov; 147(3): 360-370.
11. Wiegering V, Frank J, Freudenberg S, Morbach H, Schlegel PG, Eyrich M, et al. Impaired B-cell reconstitution in children after chemotherapy for standard or medium risk acute precursor B-lymphoblastic leukemia. Leuk Lymphoma 2014 Apr; 55(4): 870-875.
12. van Wering ER, van der Linden-Schrever BE, Szczepanski T, Willemse MJ, Baars EA, van Wijngaarde-Schmitz HM, et al. Regenerating normal B-cell precursors during and after treatment of acute lymphoblastic leukaemia: implications for monitoring of minimal residual disease. Br J Haematol 2000 Jul; 110(1): 139-146.
13. van Lochem EG, Wiegers YM, van den Beemd R, Hahlen K, van Dongen JJ, Hooijkaas H. Regeneration pattern of precursor-B-cells in bone marrow of acute lymphoblastic leukemia patients depends on the type of preceding chemotherapy. Leukemia 2000 Apr; 14(4): 688-695.
14. McKenna RW, Asplund SL, Kroft SH. Immunophenotypic analysis of hematogones (B-lymphocyte precursors) and neoplastic lymphoblasts by 4-color flow cytometry. Leuk Lymphoma 2004 Feb; 45(2): 277-285.
15. McKenna RW, Washington LT, Aquino DB, Picker LJ, Kroft SH. Immunophenotypic analysis of hematogones (B-lymphocyte precursors) in 662 consecutive bone marrow specimens by 4-color flow cytometry. Blood 2001 Oct 15; 98(8): 2498-2507.
16. Pieters R, de Groot-Kruseman H, Van der Velden V, Fiocco M, van den Berg H, de Bont E, et al. Successful Therapy Reduction and Intensification for Childhood Acute Lymphoblastic Leukemia Based on Minimal Residual Disease Monitoring: Study ALL10 From the Dutch Childhood Oncology Group. J Clin Oncol 2016 Jun 6.
17. van Zelm MC, Szczepanski T, van der Burg M, van Dongen JJ. Replication history of B lymphocytes reveals homeostatic proliferation and extensive antigen-induced B cell expansion. J Exp Med 2007 Mar 19; 204(3): 645-655.
18. van Gent R, van Tilburg CM, Nibbelke EE, Otto SA, Gaiser JF, Janssens-Korpela PL, et al. Refined characterization and reference values of the pediatric T- and B-cell compartments. Clin Immunol 2009 Oct; 133(1): 95-107.
19. Avanzini MA, Locatelli F, Dos Santos C, Maccario R, Lenta E, Oliveri M, et al. B lymphocyte reconstitution after hematopoietic stem cell transplantation: functional immaturity and slow recovery of memory CD27+ B cells. Exp Hematol 2005 Apr; 33(4): 480-486.
20. Small TN, Keever CA, Weiner-Fedus S, Heller G, O'Reilly RJ, Flomenberg N. B-cell differentiation following autologous, conventional, or T-cell depleted bone marrow transplantation: a recapitulation of normal B-cell ontogeny. Blood 1990 Oct 15; 76(8): 1647-1656.

21. Bosch M, Khan FM, Storek J. Immune reconstitution after hematopoietic cell transplantation. Curr Opin Hematol 2012 Jul; 19(4): 324-335.
22. Castiello MC, Scaramuzza S, Pala F, Ferrua F, Uva P, Brigida I, et al. B-cell reconstitution after lentiviral vector-mediated gene therapy in patients with Wiskott-Aldrich syndrome. J Allergy Clin Immunol 2015 Sep; 136(3): 692-702 e692.
23. van Tilburg CM, Sanders EA, Rovers MM, Wolfs TF, Bierings MB. Loss of antibodies and response to (re-) vaccination in children after treatment for acute lymphocytic leukemia: a systematic review. Leukemia 2006 Oct; 20(10): 1717-1722.
24. Caraux A, Klein B, Paiva B, Bret C, Schmitz A, Fuhler GM, et al. Circulating human B and plasma cells. Age-associated changes in counts and detailed characterization of circulating normal CD138- and CD138+ plasma cells. Haematologica 2010 Jun; 95(6): 1016-1020.
25. Mei HE, Yoshida T, Sime W, Hiepe F, Thiele K, Manz RA, et al. Blood-borne human plasma cells in steady state are derived from mucosal immune responses. Blood 2009 Mar 12; 113(11): 2461-2469.
26. Campana D, Janossy G. Proliferation of normal and malignant human immature lymphoid cells. Blood 1988 May; 71(5): 1201-1210.
27. Matarraz S, Fernandez C, Albors M, Teodosio C, Lopez A, Jara-Acevedo M, et al. Cell-cycle distribution of different cell compartments in normal versus reactive bone marrow: a frame of reference for the study of dysplastic hematopoiesis. Cytometry B Clin Cytom 2011 Nov; 80(6): 354-361.
28. van Hoeven V. Lymphocyte dynamics in healthy and lymphopenic conditions. 2015.
29. Logan AC, Gao H, Wang C, Sahaf B, Jones CD, Marshall EL, et al. High-throughput VDJ sequencing for quantification of minimal residual disease in chronic lymphocytic leukemia and immune reconstitution assessment. Proc Natl Acad Sci U S A 2011 Dec 27; 108(52): 21194-21199.
30. Lee J, Kuchen S, Fischer R, Chang S, Lipsky PE. Identification and characterization of a human CD5+ pre-naive B cell population. J Immunol 2009 Apr 1; 182(7): 4116-4126.
31. Sims GP, Ettinger R, Shirota Y, Yarboro CH, Illei GG, Lipsky PE. Identification and characterization of circulating human transitional B cells. Blood 2005 Jun 1; 105(11): 4390-4398.
32. Bemark M, Holmqvist J, Abrahamsson J, Mellgren K. Translational Mini-Review Series on B cell subsets in disease. Reconstitution after haematopoietic stem cell transplantation - revelation of B cell developmental pathways and lineage phenotypes. Clin Exp Immunol 2012 Jan; 167(1): 15-25.
33. Pihlgren M, Tougne C, Bozzotti P, Fulurija A, Duchosal MA, Lambert PH, et al. Unresponsiveness to lymphoid-mediated signals at the neonatal follicular dendritic cell precursor level contributes to delayed germinal center induction and limitations of neonatal antibody responses to T-dependent antigens. J Immunol 2003 Mar 15; 170(6): 2824-2832.
34. Lehrnbecher T, Schubert R, Allwinn R, Dogan K, Koehl U, Gruttner HP. Revaccination of children after completion of standard chemotherapy for acute lymphoblastic leukaemia: a pilot study comparing different schedules. Br J Haematol 2011 Mar; 152(6): 754-757.
35. Patel SR, Ortin M, Cohen BJ, Borrow R, Irving D, Sheldon J, et al. Revaccination of children after completion of standard chemotherapy for acute leukemia. Clin Infect Dis 2007 Mar 1; 44(5): 635-642.

36. Zignol M, Peracchi M, Tridello G, Pillon M, Fregonese F, D'Elia R, et al. Assessment of humoral immunity to poliomyelitis, tetanus, hepatitis B, measles, rubella, and mumps in children after chemotherapy. Cancer 2004 Aug 1; 101(3): 635-641.
37. Zengin E, Sarper N. Humoral immunity to diphtheria, tetanus, measles, and hemophilus influenzae type b in children with acute lymphoblastic leukemia and response to re-vaccination. Pediatr Blood Cancer 2009 Dec; 53(6): 967-972.
38. Ercan TE, Soycan LY, Apak H, Celkan T, Ozkan A, Akdenizli E, et al. Antibody titers and immune response to diphtheria-tetanus-pertussis and measles-mumps-rubella vaccination in children treated for acute lymphoblastic leukemia. J Pediatr Hematol Oncol 2005 May; 27(5): 273-277.
39. Driessen GJ, van Zelm MC, van Hagen PM, Hartwig NG, Trip M, Warris A, et al. B-cell replication history and somatic hypermutation status identify distinct pathophysiologic backgrounds in common variable immunodeficiency. Blood 2011 Dec 22; 118(26): 6814-6823.
40. Driessen GJ, Ijspeert H, Weemaes CM, Haraldsson A, Trip M, Warris A, et al. Antibody deficiency in patients with ataxia telangiectasia is caused by disturbed B- and T-cell homeostasis and reduced immune repertoire diversity. J Allergy Clin Immunol 2013 May; 131(5): 1367-1375 e1369.

SUPPLEMENTARY TABLES AND FIGURE

Supplementary Table 1. Characteristics of the 81 BCP-ALL patients collected from the Sophia Children's hospital in Rotterdam.

Characteristic	n	%
Age at diagnosis		
<1 year	0	0
1-10 years	67	83
>10 years	14	17
Sex		
male	50	62
female	31	38
WBC in PB at diagnosis		
<50.000/uL	74	91
>50.000/uL	7	9
Immunophenotype		
pro-B ALL	0	0
common ALL	61	75
pre-B ALL	20	25
Cytogenetics*		
TCF3-PBX1	0	0
MLL-rearranged	0	0
hyperdiploidy	31	38
TEL-AML1	26	32
normal	18	22
unknown	6	7

* Patients with *IKZF1* mutation, *BCR-ABL* fusion gene and patients with Down syndrome were excluded from this study since their treatment protocol is significantly different

Supplementary Table 2A. Antibody panels used for flow cytometry.

PB/ BV421	PO/ BV510	BV605	FITC	PE	PerCP-Cy5.5	PE-Cy7	APC	APC-H7/ APC-C750	Labeling for:
CD27	IgM	-	IgG	IgD	CD45	CD19	IgA	CD38	Immunophenotyping PB
CD20	CD45	-	CD81	-	CD34	CD19	CD10	CD38	Immunophenotyping BM
CD20	IgM	CD19	CD34	CD10	-	-	DRAQ5	-	Cell-cycle analysis tube 1
CD10	IgM	CD19	cyIgM	cy-CD179a	-	-	DRAQ5	-	Cell-cycle analysis tube 2
-	CD34	CD19	CD36+ CD123	CD22	-	-	DRAQ5	-	Cell-cycle analysis tube 3
CD27	-	-	-	IgD	-	CD19	(CD5)	CD38	Sort naive mature B-cells
-	CD45	-	CD34	CD20	IgM	CD19	CD10	-	Sort BCP subsets BM

Supplementary Table 2B. Detailed antibody characteristics.

Marker	Fluorochrome	Clone	Supplier	Volume per test
CD5	APC	UCHT2	Biolegend	25 uL (20x diluted)
CD10	APC	HI10a	BD Biosciences	5uL
CD10	BV421	HI10a	Biolegend	1 uL
CD10	PE	ALB1	Beckman Coulter	20 uL
CD123	FITC	AC145	Miltenyi Biotech	10 uL
CD179a	PE	4G7	Beckman Coulter	25 uL (50x diluted)
CD19	PE-Cy7	J3-119	Beckman Coulter	5 uL
CD19	BV605	SJ25C1	BD Biosciences	5 uL
CD20	PB	2H7	Biolegend	1 uL
CD20	PE	L27	BD Biosciences	2.5 uL
CD22	PE	S-HCL-1	BD Biosciences	10 uL
CD27	BV421	M-T271	BD Biosciences	1 uL
CD34	PerCP-Cy5.5	8G12	BD Biosciences	7uL
CD34	BV510	581	Biolegend	5 uL
CD34	FITC	8G12	BD Biosciences	10 uL
CD36	FITC	CLB-IVC7	Sanquin	5 uL
CD38	APC-H7	HB7	BD Biosciences	3 uL
CD38	APC-C750	LS198-4-3	Beckman Coulter	1uL
CD45	PerCP-Cy5.5	2D1	BD Biosciences	5 uL
CD45	PO	HI30	Invitrogen	5uL
CD81	FITC	JS81	BD Biosciences	5 uL
IgA	APC	IS11-8E10	Miltenyi Biotech	5 uL (50x diluted)
IgD	PE	Polyclonal	SBA	2.5 uL (5x diluted)
IgG	FITC	G18-145	BD Biosciences	2.5 uL
IgM	FITC	Polyclonal	SBA	25 uL (50x diluted)
IgM	BV510	MHM-88	Biolegend	1.5 uL
IgM	PerCP-Cy5.5	MHM-88	Bioloegend	2.5 uL

DNA dye				
DRAQ5	similar to APC	-	Biostatus	3 uL

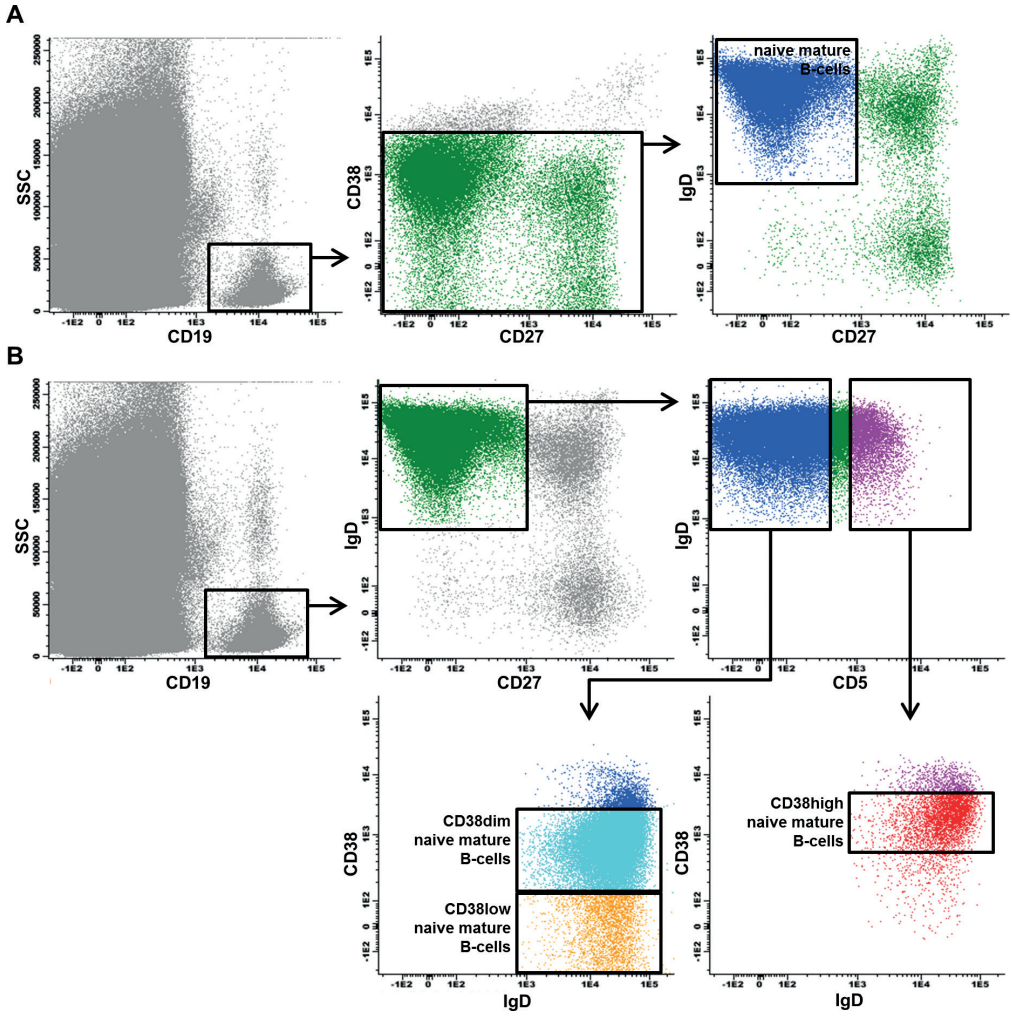

Supplementary Figure 1.
A. Stepwise gating strategy used for sorting of the naive mature B-cell subset.
B. Stepwise gating strategy used for sorting of CD38high, CD38dim and CD38low naive mature B-cells in healthy control PB. To improve separation of CD38high from CD38dim naive mature B-cells, CD5-APC was added to the antibody panel which was previously used to sort the total naive mature B-cell subset.

Chapter 4

Detailed immunophenotypic analysis of B-cell precursors in regenerating bone marrow of children treated for acute lymphoblastic leukemia reveals new subsets: implications for minimal residual disease detection

Prisca M.J. Theunissen[1], Łukasz Sędek[2], Valerie de Haas[3], Tomasz Szczepański[2], Alita van der Sluijs-Gelling[3], Ester Mejstrikova[4], Michaela Nováková[4], Tomas Kalina[4], Quentin Lecrevisse[5], Alberto Orfao[5], Arjan C. Lankester[6], Jacques J.M. van Dongen[1,7] and Vincent H.J. van der Velden[1], on behalf of the EuroFlow Consortium

[1]Department of Immunology, Erasmus MC, University Medical Center Rotterdam, Rotterdam, The Netherlands
[2]Department of Pediatric Hematology and Oncology, Zabrze, Medical University of Silesia (SUM), Katowice, Poland
[3]Dutch Childhood Oncology Group, The Hague, The Netherlands
[4]Department of Pediatric Hematology and Oncology, 2nd Faculty of Medicine, Charles University (DPH/O) and University Hospital Motol, Prague, Czech Republic
[5]Cancer Research Center (IBMCC-CSIC), Department of Medicine and Cytometry Service, University of Salamanca (USAL) and Institute of Biomedical Research of Salamanca (IBSAL), Salamanca, Spain
[6]Department of Pediatrics, Leiden University Medical Center, Leiden, The Netherlands
[7]Department of Immunohematology and Blood Transfusion, Leiden University Medical Center, Leiden, The Netherlands

Submitted

ABSTRACT

Flow cytometric detection of minimal residual disease (MRD) in children with B-cell precursor acute lymphoblastic leukemia (BCP-ALL) requires discrimination between residual leukemic cells and B-cell precursors (BCPs) which regenerate during therapy intervals. Therefore, detailed knowledge on the immunophenotypes of normal and regenerating BCPs is crucial. In this study, EuroFlow-based 8-color flow cytometry and new analysis tools were used to first characterize the immunophenotypic maturation of normal BCPs in bone marrow (BM) from healthy children. This resulted in a continuous multiparametric pathway consisting of 7 maturation stages, including transition phases that formed the missing links between the conventional B-cell differentiation stages. This pathway was subsequently used as a reference to characterize the immunophenotypic maturation of regenerating BCPs in BM from children treated for BCP-ALL. Within regenerating BCPs, we identified pre-B-I cells that expressed low or dim CD34 levels, in contrast to the classical CD34high pre-B-I cell immunophenotype. These CD34-/dim pre-B-I cells were relatively abundant in regenerating BM (11-85% within the pre-B-I subset), while hardly present in healthy control BM (9-13% within the pre-B-I subset; p=0.0027). Furthermore, analysis of BCP-ALL diagnosis samples showed that part of the BCP-ALL cases (23%) immunophenotypically overlapped with CD34-/dim pre-B-I cells. Our results indicate that newly identified CD34-/dim pre-B-I cells in regenerating BM can be mistaken for residual BCP-ALL cells, which could potentially result in false-positive MRD outcomes. Therefore, regenerating BM, in which CD34-/dim pre-B-I cells are relatively abundant, should be used as reference frame in flow cytometric MRD measurements.

INTRODUCTION

B-cell precursors (BCPs) in bone marrow (BM) differentiate to mature B-cells, which are released into peripheral blood (PB). Based on classical immunophenotyping, BCP differentiation can be subdivided into a pro-B (CD22+CD19-CD34+), pre-B-I (CD19+CD10highCD34+), pre-B-II-Large (CD19+CD10+CD34-CD20high), pre-B-II-Small (CD19+CD10+CD34-CD20low) and immature (CD19+CD10+Igκ/λ+) stage [1-3]. The percentages of BCPs in BM of healthy individuals are variable and decline with age [4,5].

B-cell precursor acute lymphoblastic leukemia (BCP-ALL) is a clonal expansion of a malignantly transformed BCP cell. Therapy in BCP-ALL patients targets the malignant cells, but also affects the remaining normal BCP population. However, normal BCPs are able to regenerate during therapy intervals and after end of therapy. During BCP regeneration, the BCP population is relatively increased [6-8].

To determine treatment response and subsequent prognosis in children treated for BCP-ALL, minimal residual disease (MRD) measurements are performed [9-11]. Flow cytometry is one of the methods used for MRD detection, in which residual leukemic cells are recognized based on their aberrant immunophenotype [12-17]. Since the immunophenotype of leukemic cells resembles that of BCPs, it is particularly difficult to detect residual leukemic cells during therapy intervals, i.e. when regenerating BCPs are abundantly present [18-20]. Leukemic cells can be discriminated from regenerating BCPs by the expression of BCP-ALL specific markers, by overexpression or underexpression of B-cell differentiation markers or by asynchronous expression of B-cell differentiation markers [8,21-26].

In this study, we first aimed to map the immunophenotypic maturation of normal BCPs in BM from healthy children. Previous studies on normal B-cell differentiation, using 4-color to 6-color immunostainings, provided a consensus model, in which four to five discrete BCP stages could be discerned [1-4,26-28]. However, BCPs which expressed a combination of differentiation markers that did not fit into any of these stages were observed in BM from healthy individuals [29,30]. These BCPs might represent transition phases between the well-defined BCP stages.

Secondly, we aimed to characterize the immunophenotypic maturation of regenerating BCPs in children treated for BCP-ALL, since this will result in a better discrimination between leukemic cells and regenerating BCPs and consequently may improve flow cytometric MRD detection. Most of the previous studies on regenerating BCPs during and after ALL therapy focused on the relative ratios between the known BCP stages [4,6,7,29,31]. Studies that specifically evaluated the immunophenotypic maturation of regenerating BCPs used 3-color or 4-color flow cytometry, which is not sufficient for a detailed analysis [4,29,31].

In this study, we used a single 8-color immunostaining and EuroFlow-based multivariate analysis strategies [32] to visualize the immunophenotypic maturation of normal BCPs in

healthy children as a continuous multiparametric pathway, which was subsequently used to characterize the immunophenotypic maturation of regenerating BCPs in children treated for BCP-ALL.

METHODS

BM samples from healthy children and BCP-ALL patients

BM was obtained from three healthy children (all male; aged 2, 5 and 13 years old) that were BM stem cell donor for their siblings with parental informed consent and with approval of the medical ethical committee of the Leiden University Medical Center (protocol P08.001). Twenty-eight diagnosis BM samples and 32 follow up BM samples were collected from pediatric BCP-ALL patients treated according to the Dutch Childhood Oncology Group (DCOG) ALL11 protocol and assigned to the standard risk (SR) treatment group or medium risk (MR) treatment group. The follow up BM samples were acquired during the interval after induction therapy (at 3 months after start of therapy, n=10), during the interval after therapy phase M (at 5 months after start of therapy, n=19) and at one year after end of therapy (n=3) (Supplementary Figure 1) [6,7]. All follow up BM samples were MRD negative, as determined by real-time quantitative PCR analysis of rearranged immunoglobulin and T-cell receptor genes [33,34]. Samples were obtained according to the guidelines of the local Medical Ethics Committees and in line with the Declaration of Helsinki Protocol.

EuroFlow-based immunophenotyping

BM samples were bulk-lysed with ammonium chloride. Subsequently, at least 3 x 10^6 leukocytes per tube were stained with the following antibodies: CD20-PB (2H7; Biolegend, San Diego, California, USA), CD45-PO (HI30; Invitrogen, Carlsbad, California, USA), Terminal deoxynucleotidyl Transferase (TdT)-FITC (HT-6; DAKO, Glostrup, Denmark), SmIgκ-PE (polyclonal; Cytognos, Salamanca, Spain), SmIgλ-PE (polyclonal; Cytognos), CyIgμ-PerCP Cy5.5 (MHM-88; Biolegend), CD19-PE Cy7 (J3-119; Beckman Coulter, Brea, California, USA), CD34-APC (8G12; BD Biosciences, Erembodegem, Belgium), CD10-APC C750 (HI10a; Cytognos). Cell surface markers were stained first, followed by staining of intracellular markers using Fix&Perm reagents (An der Grub, Wien, Austria) [32]. At least 1 x 10^6 events were acquired on a FACSCanto-II flow cytometer (BD Biosciences) using FACSDiva software (BD Biosciences). Flow cytometric data were analyzed with Infinicyt Software (Cytognos), using different approaches which are described in detail within the Results section [32,35].

High-speed cell sorting

One normal BM sample and two regenerating BM samples were stained with the same antibodies as described above and by applying the Foxp3/Transcription-Factor-Staining Buffer Set for intracellular staining (resulting in a higher DNA yield than after applying Fix&Perm reagents). One additional BM sample with a very low WBC count was stained for only surface markers, in order to further optimize DNA yield (intracellular markers were not required due to absence of BCPs beyond the pre-B-I stage). After sorting of the selected BCP fractions (FACSAria-III, BD Biosciences), DNA was extracted using the Mammalian Genomic DNA Miniprep Kit (Sigma-Aldrich, St. Louis, Missouri, USA).

GeneScan analysis of IGH gene rearrangements

IGH gene rearrangements in the sorted BCP fractions were amplified with BIOMED2-primers and subsequently analyzed with GeneScan as described previously [2,36]. The presence of high frequencies of in-frame rearrangements could be deduced from triplet spacing of the GeneScan peaks [2,36].

Statistical methods

The Mann-Whitney U test in Prism 5.0 software was used (GraphPad, La Jolla, California, USA).

RESULTS

Detailed analysis of the normal BCP differentiation

We first aimed to evaluate the immunophenotypic maturation of normal CD19+ BCPs. Therefore, B-cell populations from three BM samples of healthy children were merged in an Automatic Population Separator (APS) and analyzed with the Infinicyt maturation tool (Supplementary Methods). This resulted in a multiparametric maturation pathway consisting of an arbitrary number of 20 immunophenotypic stages (Figure 1a). The expression levels of the individual differentiation markers in each stage were visualized in a maturation diagram (Figure 1c). Stages in which the individual differentiation markers showed similar expression levels were then combined, resulting in a total of 7 distinct immunophenotypic stages (Figure 1b). These 7 maturation stages formed a continuous multiparametric pathway, in which each stage gradually evolved into the next: Stage 1 BCPs expressed high levels of the early progenitor markers CD34 and CD10, low levels of the mature B-cell markers CD45 and CD20, and high levels of TdT, an enzyme which is only detectable at high levels during *IGH* gene rearrangements. Stage 1 BCPs did not yet express cylgμ and Igκ/λ, markers which can only be present after formation of a functional

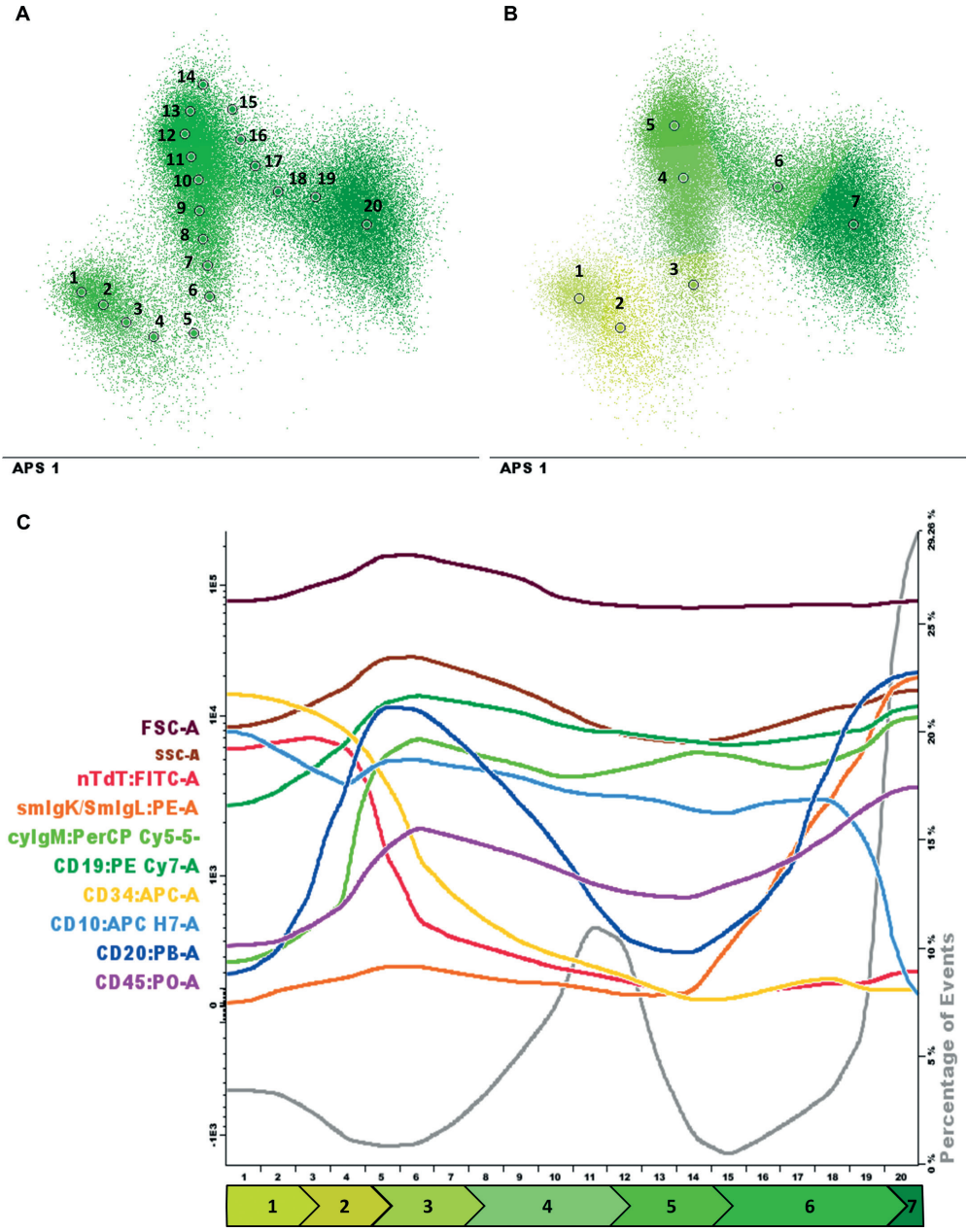
A
B
APS 1
APS 1
C
FSC-A
SSC-A
nTdT:FITC-A
smIgK/SmIgL:PE-A
cyIgM:PerCP Cy5-5-
CD19:PE Cy7-A
CD34:APC-A
CD10:APC H7-A
CD20:PB-A
CD45:PO-A
Percentage of Events

Figure 1.

A. Automatic, multiparametric analysis of a CD19+ B-cell population (merge from 3 healthy children) in an APS-plot, resulting in a B-cell maturation pathway. The B-cell maturation pathway was automatically separated into 20 stages, ranging from the least mature (1) to the most mature (20) immunophenotype.

B. By combining stages with comparable immunophenotypes, the arbitrary 20 stages were reduced to 7 distinct maturation stages.

C. FSC, SSC and expression levels of eight differentiation markers during the B-cell maturation pathway shown in (A) and (B). The seven distinct B-cell maturation stages are shown below the plot. Additionally, the grey line, corresponding to the right y-axis, shows the percentage of cells within the total B-cell population for each maturation stage.

IGH gene rearrangement or functional *IGK/IGL* gene rearrangement, respectively. This first immunophenotypic stage matches the classical pre-B-I stage. In stage 2, progressively more BCPs became cylgμ-positive, and BCPs expressed higher levels of CD20 and slightly lower levels of CD10, while still remaining TdT-positive and CD34-positive. This stage seems to represent the transition from the pre-B-I to the pre-B-II-Large stage. In stage 3, all BCPs showed cylgμ positivity, dim levels of CD45 and high levels of CD20, while the expression of CD34 and TdT had decreased, although not yet to the lowest level. In combination with a larger cell size (high FSC), this immunophenotype is typical for the pre-B-II-Large stage. From stage 3 onwards, BCPs remained cylgμ-positive as a result of a successful *IGH* gene rearrangement. In stage 4, BCPs had become fully TdT-negative and CD34-negative, while remaining CD20dim, suggesting a transition stage between the pre-B-II-Large and the pre-B-II-Small stage. From stage 4 onwards, BCPs remained CD34-negative and TdT-negative. In stage 5, CD20 expression had dropped to low levels, resulting in an immunophenotype which matches the conventional pre-B-II-Small stage. In stage 6, BCPs expressed Igκ/λ as a result of a successful *IGK/IGL* gene rearrangement. This Igκ/λ expression occurred together with increased expression of CD45 and re-expression of CD20, which is characteristic for the immature stage. Finally, in stage 7, B-cells had lost their CD10 expression, while levels of Igκ/λ , CD45 and CD20 remained high, which is in accordance with the immunophenotype of mature B-cells. The immunophenotype of each of the 7 maturation stages was confirmed within conventional two-dimensional dot plots (Supplementary Figure 2).

The immunophenotypic maturation of regenerating BCPs differs from that of normal BCPs

We next aimed to evaluate to what extent the immunophenotypic maturation of regenerating BCPs is similar to that of normal BCPs. Therefore, regenerating BM from BCP-ALL patients at 3 months (n=10) and 5 months (n=19) after start of therapy and at one year after end of therapy (n=3) were analyzed. Principal component analysis was used to immunophenotypically compare regenerating BCPs (present at 3 and 5 months after start

of treatment) with normal BCPs based on FSC, SSC and all eight differentiation markers together. After exclusion of Igκ/λ-positive immature BCPs and mature B-cells (stage 6 and 7; hardly present in regenerating BM), the regenerating BCPs of each patient were visualized in an APS-plot with a fixed normal BCP maturation pathway (Figure 2). As expected, BM samples taken at 3 and 5 months after start of therapy showed a shift in distribution towards the pre-B-I subset (also shown in conventional dot plots in Supplementary Figure 3). Surprisingly, 80% of the regenerating BM samples taken at 3 months after start of therapy (n=10) and 89% of the regenerating BM samples taken at 5 months after start of therapy (n=19) showed an immunophenotypic maturation that deviated from the normal BCP maturation pathway (Figure 2a and b). In these samples, more than 5% (up to 73%) of the regenerating BCPs was located outside the 2SD boundaries of the normal BCP maturation pathway. All regenerating BCPs outside the 2SD boundaries were, according to the conventional dot plots, cyIgμ-negative and TdT-positive. Of note, these cells could not represent pro-B cells, since CD19-negative cells were excluded from this analysis. These results indicated that the cells with an aberrant immunophenotype were probably part of the pre-B-I subset. In contrast, BM samples taken at one year after end of therapy showed a fully normal immunophenotypic maturation, virtually completely overlapping the normal BCP maturation pathway (Figure 2c).

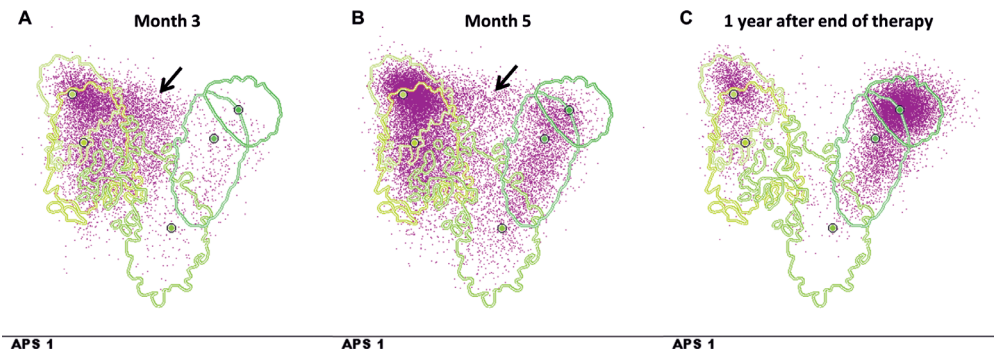

Figure 2.

APS-plots with representative examples of the patients' BCP population (purple) at 3 months after start of therapy (**A**), at 5 months after start of therapy (**B**) and at 1 year after end of therapy (**C**) plotted against the fixed 2SD contours of the normal BCP maturation pathway (shades of green). Stage 6 and 7 (Igκ/λ-positive immature BCPs and mature B-cells, respectively), which are virtually absent in regenerating BM, were excluded. Arrows indicate regenerating BCPs with an immunophenotype that deviates from the normal BCP maturation pathway.

The regenerating pre-B-I subset contains a high percentage of CD34-/dim cells

To evaluate which surface markers caused the regenerating pre-B-I cells to deviate from the normal pre-B-I cells, regenerating pre-B-I cells and normal pre-B-I cells were gated based on cyIgμ-TdT+ and were compared in an unsupervised and balanced APS (Figure 3a). This analysis showed that, out of all individual markers, CD34 differed the most between normal and regenerating pre-B-I cells (Figure 3b). Evaluation of CD34 expression in conventional dot plots showed that the difference in CD34 expression was the result of a significantly higher percentage of CD34-/dim cells within the pre-B-I subset in regenerating BM at month 3 (median 34%; range 12-85%) and month 5 (median 25%; range 11-82%) than in normal BM (median 10%; range 9-13%) (Figure 4a+c). In normal BM, the CD34-/dim pre-B-I cells accounted for less than 2% of the total BCP population, which explains why these cells were not regarded as a separate immunophenotypic stage in the above described normal BCP maturation pathway. The percentage of CD34-/dim cells within the regenerating pre-B-I subset varied widely between patients, but was unrelated to the cellularity of the BM sample, the total percentage of B-cells in the BM sample and the exact length of the preceding therapy interval, which was very consistent (data not shown). Additionally, also regenerating BM from a patient with central nervous system Non-Hodgkin lymphoma two weeks after end of a high-dose methotrexate chemotherapy cycle, showed a high percentage of CD34-/dim cells within the pre-B-I subset (Figure 4b).

A

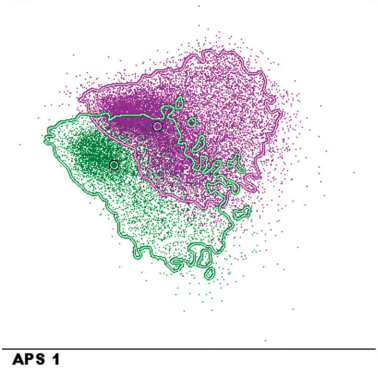

B

PC1		PC2	
Parameter	**Significance**	**Parameter**	**Significance**
CD34:APC	**27.35**	**CD34:APC**	**21.96**
CD20:PB	23.60	FSC-A	17.11
CD10:APC C750	11.78	cyIgM:PerCP Cy5-5	12.70
FSC-A	10.36	CD20:PB	11.93
CD19:PE Cy7	7.71	FSC-H	10.97
CD45:PO	6.74	SSC	7.80
FSC-H	6.32	smIgK/SmIgL:PE	4.53
smIgK/SmIgL:PE	2.56	CD19:PE Cy7	4.46
cyIgM:PerCP Cy5-5	1.83	nTdT:FITC	3.22
SSC	1.54	CD45:PO	2.89
nTdT:FITC	0.22	CD10:APC C750	2.43

Figure 3.

A. An unsupervised APS-plots showing a representative example of the separation between normal pre-B-I cells (green; cyIgμ-TdT+) and regenerating pre-B-I cells (purple; cyIgμ-TdT+). Medians and 2SD contours are indicated.

B. APS-plot information showing the contribution of each differentiation marker to the separation between normal and regenerating pre-B-I cells shown in panel A.

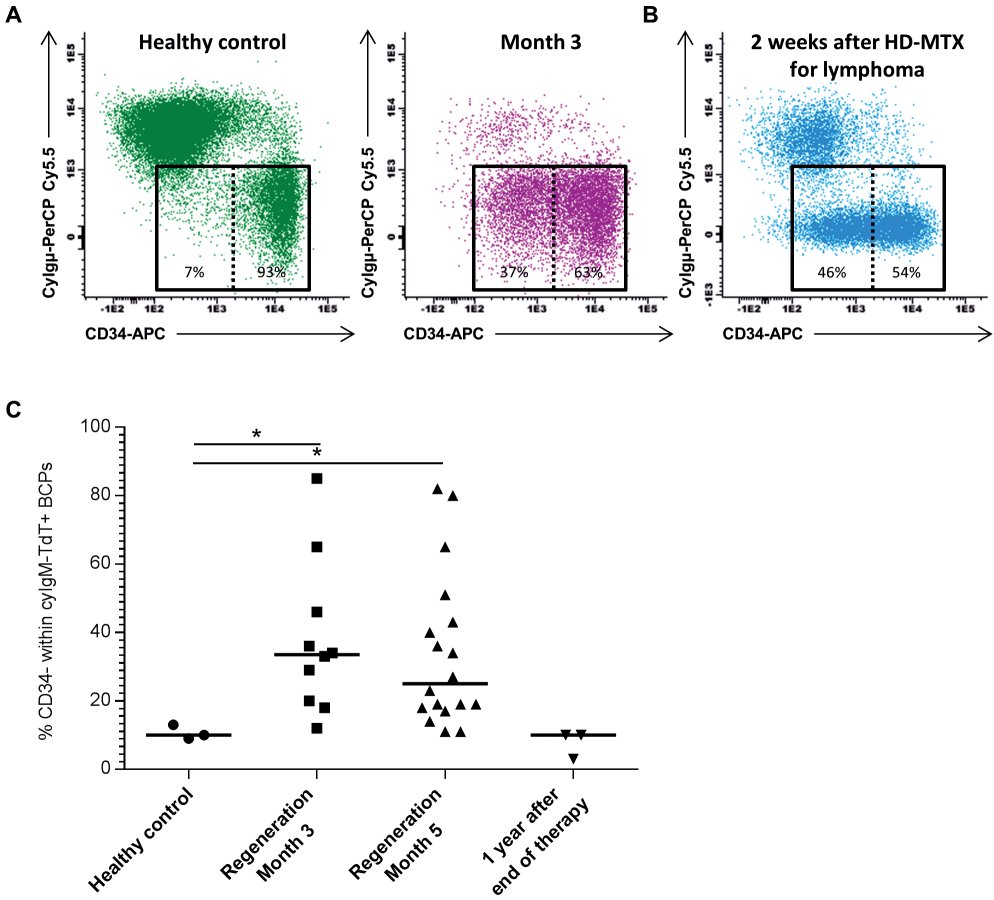

Figure 4.

A. Dot plots showing the CD34 and cylgμ expression of CD19+ B-cells in a representative BM sample from a healthy child and a pediatric BCP-ALL patient at 3 months after start of therapy. The percentages of CD34-/dim cells and CD34+ cells within the TdT+ pre-B-I subset (indicated by the rectangle) are shown.

B. Dot plot showing the CD34 and cylgμ expression of CD19+ B-cells in BM from an adult treated for a central nervous system lymphoma, two weeks after HD-MTX chemotherapy. The percentages of CD34-/dim cells and CD34+ cells within the TdT+ pre-B-I subset (indicated by the rectangle) are shown.

C. Scatter plots showing the percentage of CD34-/dim cells within the pre-B-I subset in BM from 3 healthy children, 10 pediatric BCP-ALL patients at 3 months after start of therapy (Regeneration Month 3), 19 pediatric BCP-ALL patients at 5 months after start of therapy (Regeneration Month 5) and 3 pediatric BCP-ALL patients at 1 year after end of therapy. Horizontal lines represent the median values.

Cell-cycle analysis showed absence of sub-G1 peaks in CD34-/dim pre-B-I cells from regenerating BM samples (both at month 3 (n=5) and month 5 (n=5)), indicating that these cells were non-apoptotic (data not shown). GeneScan analysis of *IGH* gene rearrangements showed an irregular size distribution pattern (without clear triplet spacing) in CD34-/dim cyIgμ-TdT+ BCPs sorted from regenerating BM samples (n=3), indicating that selection for in-frame *IGH* gene rearrangements had not yet occurred in these cells (Figure 5). A similar

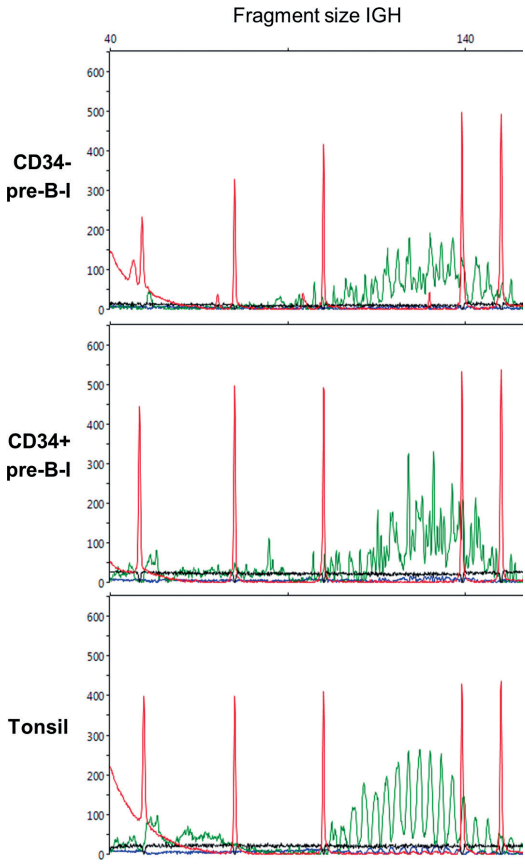

Figure 5.

GeneScan diagrams showing the size distribution of complete *IGH* gene rearrangements (green) of CD34-/dim pre-B-I cells and CD34+ pre-B-I cells in BM from a pediatric BCP-ALL patient at 5 months after start of therapy and, to compare, of mature B cells in a tonsil from a healthy control. Internal size standard peaks are shown in red. Similar results were found in another month-5 BM sample and supported by an additional month-5 BM sample in which only the CD34-/dim cyIgμ-TdT+ fraction contained sufficient cells. The number of BM samples in this experiment was limited, since almost all regenerating BM samples showed a low cellularity and a low percentage of BCPs within total WBC, which hindered the sorting of sufficient CD34+ cyIgμ-TdT+ and CD34-/dim cyIgμ-TdT+ cells.

irregular size distribution pattern of *IGH* gene rearrangements was found in CD34+ cyIgμ-TdT+ BCPs sorted from regenerating BM samples (n=2) and a normal BM sample (n=1) (data not shown). These data confirmed that CD34-/dim cyIgμ-TdT+ BCPs were, as already assumed based on immunophenotypic analyses, part of to the pre-B-I subset.

BCP-ALL cells can also express a CD34-/dim cyIgμ-TdT+ immunophenotype

Finally, we wanted to investigate whether BCP-ALL cells can immunophenotypically overlap with regenerating CD34-/dim pre-B-I cells. Therefore, BCP-ALL populations (n=26) and the CD34-/dim pre-B-I cell population (merge of n=29) were separated in an APS which only took the expression of cyIgμ, TdT and CD34 into account. This analysis showed that, based on these three markers, 6 out of 26 BCP-ALL cases (23%) had a median that overlapped with the CD34-/dim pre-B-I cells, i.e. expressed a CD34-/dim cyIgμ-TdT+ immunophenotype (Figure 6).

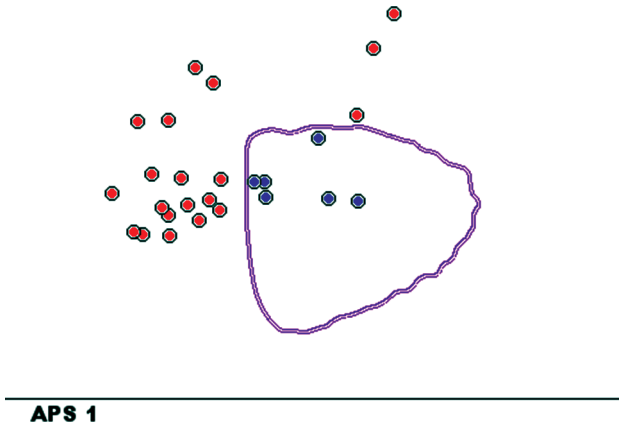

Figure 6.

APS-plot showing the 2SD contours of a CD34-/dim pre-B-I cell population (purple; merge of CD34-/dim pre-B-I cells of 29 patients) and the medians of 26 pediatric BCP-ALL cases. The BCP-ALL cases with a median which overlaps the regenerating CD34-/dim pre-B-I cell population are indicated in blue.

DISCUSSION

In order to improve discrimination between residual leukemic cells and the background of BCPs in BM of patients treated for BCP-ALL, we studied the immunophenotypic maturation of normal and regenerating BCPs.

Therefore, we designed an 8-color antibody panel that allowed us to optimally characterize the full immunophenotypic B cell differentiation in a single tube analysis. For

this antibody panel, we selected antibodies against markers that were most contributing to the key processes in BCP development, that is, first, the production of a functional cylgμ chain (which needs TdT), and secondly the production of the light chains (Igκ/λ) [1]. To further discriminate the different subsets, we used cell membrane markers previously shown to allow recognition of specific subsets [2,3]: CD19 (B-cells beyond the pro-B cell stage), CD34 (pre-B-I cells), CD10 (immature B-cells), CD20 (mature B-cells) and CD45 (increased expression during differentiation). Our analysis of the immunophenotypic maturation of normal BCPs revealed a stage ('stage 2') in which BCPs were TdT-positive and therefore classically defined as pre-B-I, but in which a small fraction of the BCPs already contained cylgμ. Furthermore, the BCPs in this stage were CD20dim. These findings are in contrast with the conventional model on human B-cell differentiation, in which all TdT+ BCPs are cylgμ-negative and CD20-negative [1-4,26-28]. However, other studies also observed BCPs with combined expression of TdT, cylgμ and, if studied, CD20 [29,30]. Probably, this stage represents a transition phase between the pre-B-I and pre-B-II-Large stage. Secondly, our analysis showed a stage ('stage 4') in which BCPs had passed the pre-B-II-Large immunophenotype, but in which BCPs were still Igκ/λ-negative. Furthermore, the BCPs in this stage gradually lost their CD20 expression. This stage probably represents a transition phase between the pre-B-II-Large and pre-B-II-Small stage. Together, only by using a single 8-color tube in combination with multiparametric analyses, we were able to identify the above described B-cell differentiation subsets.

Analysis of regenerating BM from children treated for BCP-ALL showed that the subset distribution of the regenerating BCP population (present during therapy intervals at 3 and 5 months after start of therapy) had shifted towards the early maturation stages. This finding was in accordance with previous studies [6,7]. More surprisingly, by analyzing regenerating BM, we identified pre-B-I cells with low or dim CD34 expression. The pre-B-I origin was supported by the presence of complete *IGH* gene rearrangements which were not yet selected for in-frame rearrangements. None of the three previous studies on the immunophenotype of BCPs in regenerating BM reported on TdT+ BCPs (pre-B-I cells) with a low CD34 expression. However, in two of these studies, regenerating BCPs were not directly compared with normal BCPs from healthy individuals [4,31]. Moreover, only 3- or 4-color flow cytometry was used [4,29,31]. These aspects might explain why the CD34-/dim pre-B-I cells in regenerating BM have been overlooked in these studies. Apparently, multicolor flow cytometry (at least >4 colors) is necessary to achieve a detailed immunophenotypic characterization of BCPs.

Although CD34-/dim pre-B-I cells were initially not identified within the normal BCP maturation pathway, we were later able to find low numbers of these cells in BM from healthy controls. By comparing pre-B-I cells in regenerating BM from BCP-ALL patients at 3 months and 5 months after start of therapy with those in BM from healthy controls,

we showed that the percentage of CD34-/dim cells within the pre-B-I subset was much higher in regenerating BM than in BM from healthy controls. A relatively high percentage of CD34-/dim cells within the pre-B-I subset was also found in regenerating BM from an adult treated for lymphoma. These data indicate that an increased percentage of CD34-/dim pre-B-I cells is a characteristic of BCP regeneration and is independent of the type of preceding therapy.

The mechanism behind the increase of CD34-/dim pre-B-I cells during BCP regeneration remains unclear. The presence of CD34-/dim pre-B-I cells in healthy control BM indicates that the reduced expression of CD34 on pre-B-I cells is not caused by chemotherapeutic drugs. Also, we found that the frequency of hematotoxic side effects was similar between patients with a very high percentage of CD34-/dim pre-B-I cells and all other patients. This suggests that the reduced expression of CD34 is also not caused by toxic damage of the BM niche, which contains ligands for CD34 molecules. Hypothetically, CD34-/dim pre-B-I cells might represent pre-B-I cells that are negatively selected based on two unproductive *IGH* gene rearrangements, but are not yet apoptotic. During normal hematopoiesis, these cells may only form a minor subset of the total BCP population. During regeneration, a high number of BCPs differentiates simultaneously. By sampling at the time this 'wave' reaches the pre-B-I stage, the CD34-/dim pre-B-I cells may represent a relatively large part of the total BCP population, mainly consisting of pre-B-I cells.

Finally, our results showed that a significant part of the BCP-ALL cases (23%) expressed a CD34-/dim cyIgμ-TdT+ immunophenotype. Previous studies already described BCP-ALL cases which were negative for CD34, while negative for cyIgμ or positive for TdT [21,37]. Since CD34-/dim pre-B-I cells show a marker-expression pattern that is asynchronous according to the current B-cell differentiation model, these BCPs can be mistaken for leukemic cells with a CD34-cyIgμ-TdT+ immunophenotype. Consequently, the presence of CD34-/dim pre-B-I cells in regenerating BM at MRD follow up time points could potentially result in a false-positive MRD outcome. Therefore, BCPs from regenerating BM, in which CD34-/dim pre-B-I cells are relatively abundant, should be used as the normal reference in flow cytometric MRD detection (rather than BCPs from healthy control BM, in which CD34-/dim pre-B-I cells are scarce). Also, since the expression of differentiation markers on BCP-ALL cells overlaps with regenerating BCPs, MRD detection can be more reliable when also based on the expression of BCP-ALL specific markers. Therefore, within the EuroFlow Consortium, new 8-color antibody panels are currently being developed to optimize discrimination between BCP-ALL and the background of regenerating BCPs.

ACKNOWLEDGMENTS

We gratefully thank the involved technicians of the Laboratory for Medical Immunology, in particular Romana Jugooa, Gonnie Paulides, Jeanet Hogervorst, Jeroen te Marvelde, Claudia Hagens, Jolanda Doekharan and André Bijkerk. The research for this manuscript was (in part) performed within the framework of the Erasmus Postgraduate School Molecular Medicine and was financially supported by PrioMedChild, project 40-41800-98-027. This study was performed within the EuroFlow Consortium, the EU-supported LSHB-CT-2006-018708 FP6 Specific Targeted Research Project, which obtained sustainability based on income from the development of intellectual property and related patents, which have been licensed to industry. The work was supported through AZV (15-28525A) to EM and to MN.

REFERENCES

1. Ghia P, ten Boekel E, Sanz E, de la Hera A, Rolink A, Melchers F. Ordering of human bone marrow B lymphocyte precursors by single-cell polymerase chain reaction analyses of the rearrangement status of the immunoglobulin H and L chain gene loci. J Exp Med 1996 Dec 1; 184(6): 2217-2229.
2. van Zelm MC, van der Burg M, de Ridder D, Barendregt BH, de Haas EF, Reinders MJ, et al. Ig gene rearrangement steps are initiated in early human precursor B cell subsets and correlate with specific transcription factor expression. J Immunol 2005 Nov 1; 175(9): 5912-5922.
3. Noordzij JG, de Bruin-Versteeg S, Comans-Bitter WM, Hartwig NG, Hendriks RW, de Groot R, et al. Composition of precursor B-cell compartment in bone marrow from patients with X-linked agammaglobulinemia compared with healthy children. Pediatr Res 2002 Feb; 51(2): 159-168.
4. McKenna RW, Washington LT, Aquino DB, Picker LJ, Kroft SH. Immunophenotypic analysis of hematogones (B-lymphocyte precursors) in 662 consecutive bone marrow specimens by 4-color flow cytometry. Blood 2001 Oct 15; 98(8): 2498-2507.
5. Bras AE, van den Heuvel-Eibrink MM, van der Sluijs-Gelling AJ, Coenen EA, Wind H, Zwaan CM, et al. No significant prognostic value of normal precursor B-cell regeneration in paediatric acute myeloid leukaemia after induction treatment. Br J Haematol 2013 Jun; 161(6): 861-864.
6. van Lochem EG, Wiegers YM, van den Beemd R, Hahlen K, van Dongen JJ, Hooijkaas H. Regeneration pattern of precursor-B-cells in bone marrow of acute lymphoblastic leukemia patients depends on the type of preceding chemotherapy. Leukemia 2000 Apr; 14(4): 688-695.
7. van Wering ER, van der Linden-Schrever BE, Szczepanski T, Willemse MJ, Baars EA, van Wijngaarde-Schmitz HM, et al. Regenerating normal B-cell precursors during and after treatment of acute lymphoblastic leukaemia: implications for monitoring of minimal residual disease. Br J Haematol 2000 Jul; 110(1): 139-146.

8. Gaipa G, Basso G, Biondi A, Campana D. Detection of minimal residual disease in pediatric acute lymphoblastic leukemia. Cytometry B Clin Cytom 2013 Nov-Dec; 84(6): 359-369.
9. Kamps WA, van der Pal-de Bruin KM, Veerman AJ, Fiocco M, Bierings M, Pieters R. Long-term results of Dutch Childhood Oncology Group studies for children with acute lymphoblastic leukemia from 1984 to 2004. Leukemia 2010 Feb; 24(2): 309-319.
10. Conter V, Bartram CR, Valsecchi MG, Schrauder A, Panzer-Grumayer R, Moricke A, et al. Molecular response to treatment redefines all prognostic factors in children and adolescents with B-cell precursor acute lymphoblastic leukemia: results in 3184 patients of the AIEOP-BFM ALL 2000 study. Blood 2010 Apr 22; 115(16): 3206-3214.
11. Mejstrikova E, Fronkova E, Kalina T, Omelka M, Batinic D, Dubravcic K, et al. Detection of residual B precursor lymphoblastic leukemia by uniform gating flow cytometry. Pediatr Blood Cancer 2010 Jan; 54(1): 62-70.
12. van Dongen JJ, van der Velden VH, Bruggemann M, Orfao A. Minimal residual disease diagnostics in acute lymphoblastic leukemia: need for sensitive, fast, and standardized technologies. Blood 2015 Jun 25; 125(26): 3996-4009.
13. Coustan-Smith E, Sancho J, Hancock ML, Boyett JM, Behm FG, Raimondi SC, et al. Clinical importance of minimal residual disease in childhood acute lymphoblastic leukemia. Blood 2000 Oct 15; 96(8): 2691-2696.
14. Karawajew L, Dworzak M, Ratei R, Rhein P, Gaipa G, Buldini B, et al. Minimal residual disease analysis by eight-color flow cytometry in relapsed childhood acute lymphoblastic leukemia. Haematologica 2015 Jul; 100(7): 935-944.
15. Obro NF, Ryder LP, Madsen HO, Andersen MK, Lausen B, Hasle H, et al. Identification of residual leukemic cells by flow cytometry in childhood B-cell precursor acute lymphoblastic leukemia: verification of leukemic state by flow-sorting and molecular/cytogenetic methods. Haematologica 2012 Jan; 97(1): 137-141.
16. Lucio P, Gaipa G, van Lochem EG, van Wering ER, Porwit-MacDonald A, Faria T, et al. BIOMED-I concerted action report: flow cytometric immunophenotyping of precursor B-ALL with standardized triple-stainings. BIOMED-1 Concerted Action Investigation of Minimal Residual Disease in Acute Leukemia: International Standardization and Clinical Evaluation. Leukemia 2001 Aug; 15(8): 1185-1192.
17. Denys B, van der Sluijs-Gelling AJ, Homburg C, van der Schoot CE, de Haas V, Philippe J, et al. Improved flow cytometric detection of minimal residual disease in childhood acute lymphoblastic leukemia. Leukemia 2013 Mar; 27(3): 635-641.
18. Mirkowska P, Hofmann A, Sedek L, Slamova L, Mejstrikova E, Szczepanski T, et al. Leukemia surfaceome analysis reveals new disease-associated features. Blood 2013 Jun 20; 121(25): e149-159.
19. Sedek L, Bulsa J, Sonsala A, Twardoch M, Wieczorek M, Malinowska I, et al. The immunophenotypes of blast cells in B-cell precursor acute lymphoblastic leukemia: how different are they from their normal counterparts? Cytometry B Clin Cytom 2014 Sep; 86(5): 329-339.

20. Dworzak MN, Froschl G, Printz D, Mann G, Potschger U, Muhlegger N, et al. Prognostic significance and modalities of flow cytometric minimal residual disease detection in childhood acute lymphoblastic leukemia. Blood 2002 Mar 15; 99(6): 1952-1958.
21. Hurwitz CA, Loken MR, Graham ML, Karp JE, Borowitz MJ, Pullen DJ, et al. Asynchronous antigen expression in B lineage acute lymphoblastic leukemia. Blood 1988 Jul; 72(1): 299-307.
22. Lucio P, Parreira A, van den Beemd MW, van Lochem EG, van Wering ER, Baars E, et al. Flow cytometric analysis of normal B cell differentiation: a frame of reference for the detection of minimal residual disease in precursor-B-ALL. Leukemia 1999 Mar; 13(3): 419-427.
23. Campana D, Coustan-Smith E. Detection of minimal residual disease in acute leukemia by flow cytometry. Cytometry 1999 Aug 15; 38(4): 139-152.
24. Szczepanski T, van der Velden VH, van Dongen JJ. Flow-cytometric immunophenotyping of normal and malignant lymphocytes. Clin Chem Lab Med 2006; 44(7): 775-796.
25. Seegmiller AC, Kroft SH, Karandikar NJ, McKenna RW. Characterization of immunophenotypic aberrancies in 200 cases of B acute lymphoblastic leukemia. Am J Clin Pathol 2009 Dec; 132(6): 940-949.
26. van Lochem EG, van der Velden VH, Wind HK, te Marvelde JG, Westerdaal NA, van Dongen JJ. Immunophenotypic differentiation patterns of normal hematopoiesis in human bone marrow: reference patterns for age-related changes and disease-induced shifts. Cytometry B Clin Cytom 2004 Jul; 60(1): 1-13.
27. Loken MR, Shah VO, Dattilio KL, Civin CI. Flow cytometric analysis of human bone marrow. II. Normal B lymphocyte development. Blood 1987 Nov; 70(5): 1316-1324.
28. Sevilla DW, Emmons FN, Bai X, Colovai A, Bhagat G, Alobeid B. The pattern of cytoplasmic IgM expression in the context of the three currently recognised maturational stages of hematogones. Leuk Lymphoma 2009 Apr; 50(4): 642-644.
29. Dworzak MN, Fritsch G, Fleischer C, Printz D, Froschl G, Buchinger P, et al. Multiparameter phenotype mapping of normal and post-chemotherapy B lymphopoiesis in pediatric bone marrow. Leukemia 1997 Aug; 11(8): 1266-1273.
30. Campana D, Janossy G. Proliferation of normal and malignant human immature lymphoid cells. Blood 1988 May; 71(5): 1201-1210.
31. Babusikova O, Zeleznikova T, Kirschnerova G, Kankuri E. Hematogones in acute leukemia during and after therapy. Leuk Lymphoma 2008 Oct; 49(10): 1935-1944.
32. Kalina T, Flores-Montero J, van der Velden VH, Martin-Ayuso M, Bottcher S, Ritgen M, et al. EuroFlow standardization of flow cytometer instrument settings and immunophenotyping protocols. Leukemia 2012 Sep; 26(9): 1986-2010.
33. van der Velden VH, van Dongen JJ. MRD detection in acute lymphoblastic leukemia patients using Ig/TCR gene rearrangements as targets for real-time quantitative PCR. Methods Mol Biol 2009; 538: 115-150.

34. van der Velden VH, Cazzaniga G, Schrauder A, Hancock J, Bader P, Panzer-Grumayer ER, et al. Analysis of minimal residual disease by Ig/TCR gene rearrangements: guidelines for interpretation of real-time quantitative PCR data. Leukemia 2007 Apr; 21(4): 604-611.
35. Pedreira CE, Costa ES, Lecrevisse Q, van Dongen JJ, Orfao A, EuroFlow C. Overview of clinical flow cytometry data analysis: recent advances and future challenges. Trends Biotechnol 2013 Jul; 31(7): 415-425.
36. van Dongen JJ, Langerak AW, Bruggemann M, Evans PA, Hummel M, Lavender FL, et al. Design and standardization of PCR primers and protocols for detection of clonal immunoglobulin and T-cell receptor gene recombinations in suspect lymphoproliferations: report of the BIOMED-2 Concerted Action BMH4-CT98-3936. Leukemia 2003 Dec; 17(12): 2257-2317.
37. Pui CH, Hancock ML, Head DR, Rivera GK, Look AT, Sandlund JT, et al. Clinical significance of CD34 expression in childhood acute lymphoblastic leukemia. Blood 1993 Aug 1; 82(3): 889-894.

SUPPLEMENTARY FIGURES

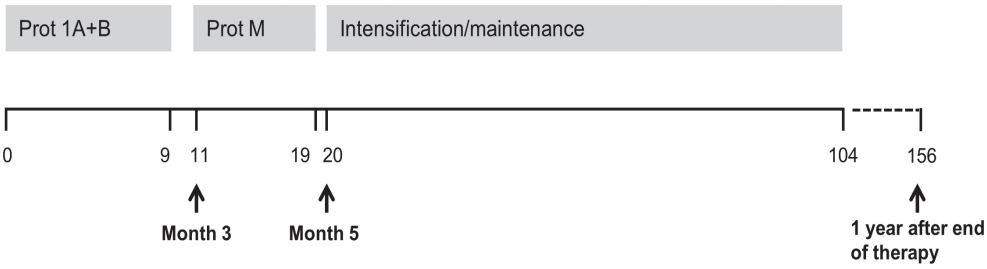

Supplementary Figure 1.

Simplified scheme of the BCP-ALL treatment for SR and MR patients according to the DCOG ALL11 protocol. Arrows indicate the sampling time points for the BM samples in this study. Prot 1A+B: protocol 1A+B, consisting of induction therapy. Prot M: protocol M.

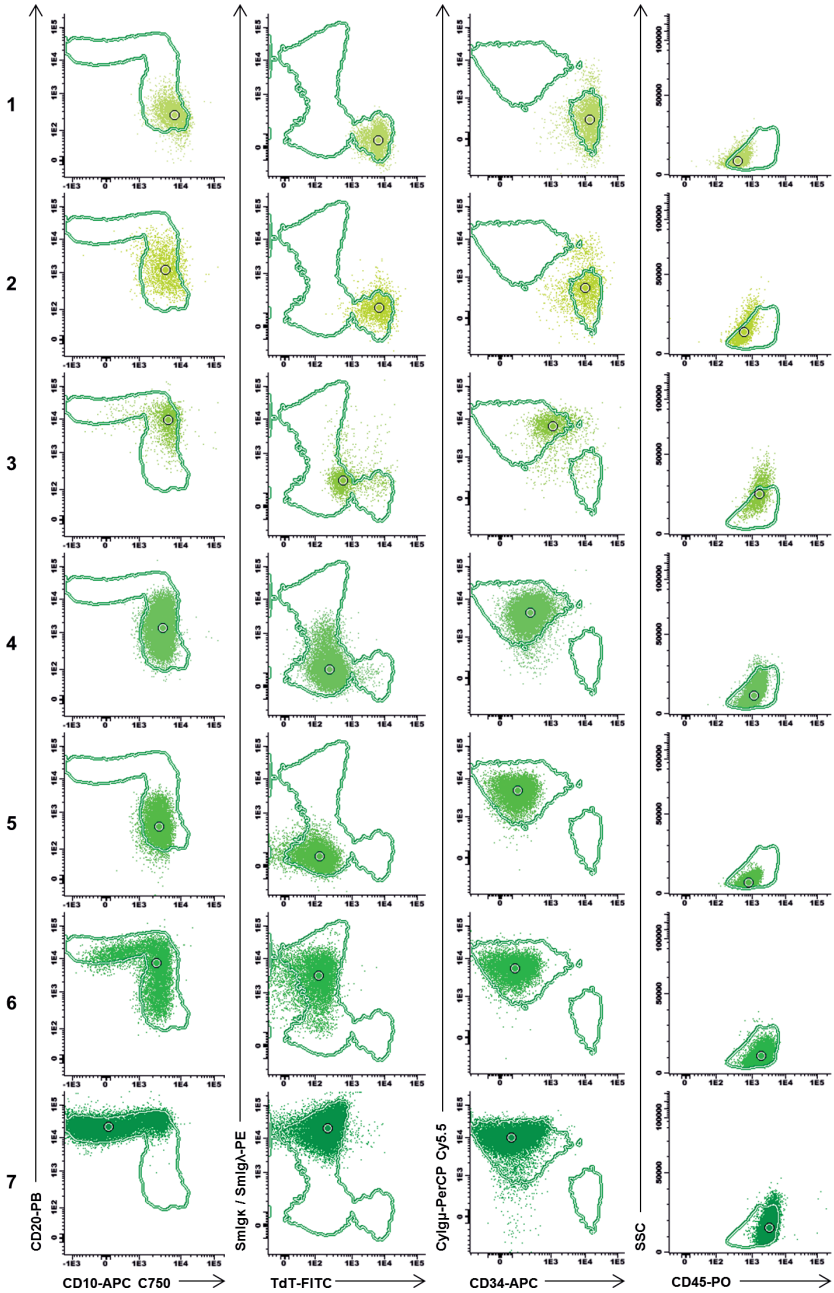

Supplementary Figure 2.

Dot plots showing the expression levels of individual markers for each of the maturation stages (1 t/m 7) previously identified in a multidimensional APS-plot. The 2SD contours of the total CD19+ B-cell maturation pathway are shown.

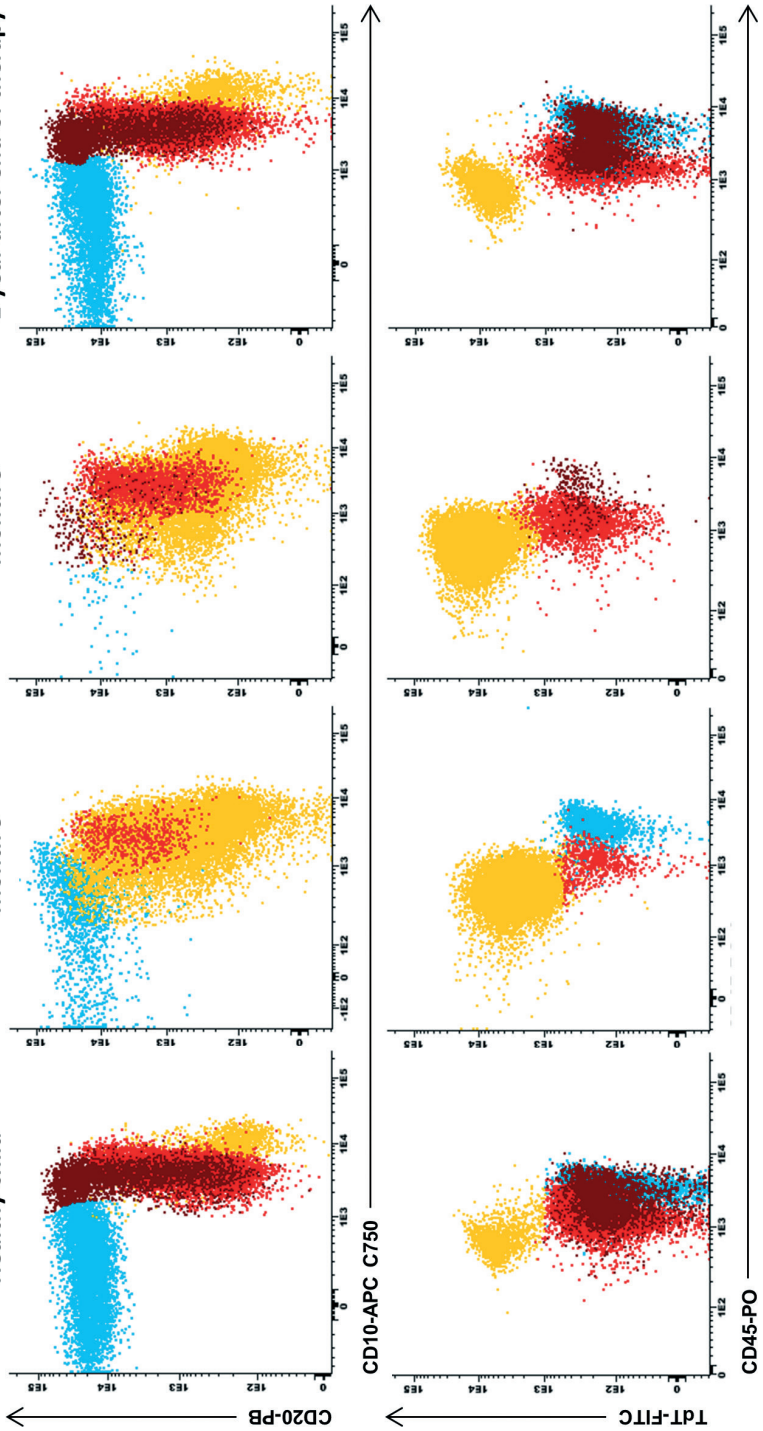

Supplementary Figure 3.

Dot plots showing the distribution of the pre-B-I (yellow; CD10+TdT+Igκ/λ-), pre-B-II (red; CD10+TdT-Igκ/λ-), immature B-cell (brown; CD10+TdT-Igκ/λ+) and mature B-cell (light blue; CD10-Igκ/λ+CD20+) subsets within the total B-cell population, in representative BM samples from a healthy child, a BCP-ALL patient at 3 months after start of therapy, a BCP-ALL patient at 5 months after start of therapy and a BCP-ALL patient at 1 year after end of therapy. The pre-B-II-Large and pre-B-II-Small subsets were not gated individually, since full separtation of these two subsets based on conventional gating strategies is impossible.

SUPPLEMENTARY METHODS

Analysis of the immunophenotypic B-cell maturation using Infinicyt Software-tools

CD19- pro-B-cells were excluded. The CD19+ populations of three BM samples from healthy children were digitally merged to create one representative normal B-cell population. The merged normal B-cell population was visualized in an APS-plot. The maturation tool in Inifinicyt Software was applied on the merged normal B-cell population, subdividing it into consecutive maturation stages based on forward scatter, side scatter and all eight differentiation markers. This resulted in a single multiparametric B-cell maturation pathway.

Chapter 5

Pattern of expression of CD73, CD86 and CD304 in normal vs. leukemic B-cell precursors: utility as stable minimal residual disease markers for treatment monitoring in childhood B-cell precursor acute lymphoblastic leukemia

Łukasz Sędek[1]*, Prisca Theunissen[2]*, Elaine Sobral da Costa[3], Alita van der Sluijs-Gelling[4], Ester Mejstrikova[5], Giuseppe Gaipa[6], Alicja Sonsala[1], Magdalena Twardoch[1], Elen Oliveira[3], Michaela Novakova[5], Chiara Buracchi[6], Jacques J.M. van Dongen[2], Alberto Orfao[7], Vincent H.J. van der Velden[2] and Tomasz Szczepański[1], on behalf of the EuroFlow Consortium.

[1] Department of Pediatric Hematology and Oncology, Medical University of Silesia, Zabrze, Poland
[2] Department of Immunology, Erasmus MC, University Medical Center Rotterdam (Erasmus MC), Rotterdam, The Netherlands
[3] Pediatrics Institute IPPMG, Faculty of Medicine, Federal University of Rio de Janeiro, Rio de Janeiro, Brazil
[4] Dutch Childhood Oncology Group, The Hague, Netherlands
[5] Department of Pediatric Hematology and Oncology, 2nd Faculty of Medicine, Charles University (DPH/O), Prague, The Czech Republic
[6] Centro Ricerca Tettamanti, Clinica Pediatrica Università di Milano-Bicocca, Monza, Italy
[7] Cancer Research Center (IBMCC-CSIC), Department of Medicine and Cytometry Service, University of Salamanca (USAL) and Institute of Biomedical Research of Salamanca (IBSAL), Salamanca, Spain

* ŁS and PT contributed equally

Submitted

ABSTRACT

Background Proper distinction between leukemic blasts and normal B-cell precursors (BCP) is critical for optimized treatment of BCP acute lymphoblastic leukemia (ALL), which justifies the need of identification of new markers, differentially expressed on normal BCP and leukemic blasts.

Methods We performed a multicenter analysis of CD73, CD86 and CD304 expression levels on leukemic blasts in 282 pediatric BCP-ALL patients and on normal BCP. To determine the antigen expression levels, we used a quantitative scale, based on normalized median fluorescence intensity measure.

Results CD73 was expressed at higher level than on pooled normal BCP in 71/108 BCP-ALL patients (66%), whereas CD304 and CD86 in 94/202 (47%) and 35/100 (35%) patients, respectively. The expression of CD304 was detected at similar percentages in common- and pre-B-ALL subgroups, at significantly higher frequencies than in the pro-B-ALL subgroup. A significant association (p=0.001) was found between CD304 expression and the presence of the *ETV6-RUNX1* fusion gene. Interestingly, both CD73 and CD304 showed a negative association with *MLL* gene rearrangements (p=0.02 and 0.002, respectively). The expression levels of CD73 and CD86 at day 15 after starting therapy vs. diagnosis were constant or higher in 26/33 (79%) and 22/47 (47%) of cases, respectively. In turn, CD304 showed decreased expression levels during follow-up in 94% of cases, but was still positive in 61% of cases.

Conclusions This multicenter EuroFlow study shows that CD73, CD86 and CD304 are overexpressed in a substantial number of BCP-ALL patients and that these markers are relatively stable during treatment, which may contribute to improved MRD analysis.

INTRODUCTION

Acute leukemias (AL) are a heterogeneous group of hematological malignancies, characterized by the neoplastic expansion of immature precursor cells (blasts) of lymphoid or myeloid lineage origin. The most frequent type of AL in children is acute lymphoblastic leukemia (ALL) which results from the malignant transformation of B or T lymphoid precursor cells. Among the two subtypes, B-cell-precursor (BCP) ALL is more prevalent, representing around 85% of all pediatric ALL patients [1-3]. BCP represent a cell compartment in the bone marrow which is morphologically recognized as hematogones. In normal bone marrow, BCP form a continuous maturation pathway consisting of three major maturational stages, all of which show CD19 expression: pre-B-I cells, pre-B-II cells and immature/transitional B-cells, respectively. Leukemic blasts in BCP-ALL share many phenotypic features with normal BCP. Despite this, the expression levels of BCP-associated antigens commonly assessed in BCP-ALL (e.g. CD10, CD20, CD34, TdT, CD22, CD38, CD45) are frequently altered in variable degree, as detected by the multiparametric flow cytometry (FC) technique [4]. In the past decades, it has been shown that immunophenotypic differences between normal BCP and leukemic blasts, i.e., the leukemia-associated immunophenotypes (LAIPs), can be found in virtually all (up to 98%) BCP-ALL patients [5]. Despite this high frequency, these differences may be either very subtle or modulated by treatment-induced up- or downregulation of unstable markers such as CD10, CD20, CD34 throughout therapy [6,7,8]. Furthermore, following different types of chemotherapy, normal BCP might represent a significant and variable proportion of all bone marrow cells, which could cause additional difficulties in distinguishing BCP from minimal residual disease (MRD) that might be present in the bone marrow of BCP-ALL patients during therapy [4,9,10]. Proper FC-based distinction between leukemic blasts and normal BCP is critical for reliable treatment decisions in BCP-ALL, which justifies the need for identifying new stable markers which are differentially expressed on leukemic blasts vs. normal BCP in a significant fraction of BCP-ALL patients.

Based on the analysis of the leukemia cell surface proteome [11] and genome-wide gene expression screening of leukemic cells vs. normal BCP [12], novel markers for more efficient MRD monitoring in ALL have been recently identified. Here, we selected three of such candidate markers (CD73, CD86 and CD304), in order to assess their power to discriminate leukemic blasts from normal BCP, their stability during early follow-up time points (day +15 of induction therapy) and thereby, their potential utility for MRD monitoring. For this purpose, we performed a multicenter, standardized FC validation study and compared the expression of these three markers on leukemic blasts from a large series of pediatric BCP-ALL patients (including different immunologic and genetic subtypes) with that on normal BCP from non-leukemic bone marrow samples. In order to evaluate the utility of individual markers, we used the normalized median fluorescence intensity

(nMFI) scale [4], rather than the classical percentage-positivity-based reporting method. This approach is particularly helpful for the quantification of differences in antigen expression between leukemic blasts and normal BCP, thus facilitating their distinction in subsequent follow-up MRD studies. Given that for almost two decades MRD is regarded as one of the most powerful independent prognostic factors in BCP-ALL and is currently used for risk group stratification [13], studies on new phenotypic features of leukemic cells might contribute to improving MRD detection and fine-tuning the treatment intensity in these patients.

MATERIALS AND METHODS

Patients and controls

The overall study group comprised 282 children (male/female ratio of 1.06 and median age of 4 years) with newly-diagnosed BCP-ALL from 6 different pediatric hemato-oncology centers belonging to the EuroFlow Consortium: Medical University of Silesia in Katowice (Zabrze, Poland), Erasmus Medical Center (Rotterdam, The Netherlands), Dutch Childhood Oncology Group (The Hague, The Netherlands), Federal University of Rio de Janeiro (Rio de Janeiro, Brazil), Charles University (Prague, The Czech Republic) and University of Milan-Bicoca (Monza, Italy). The entire study, including data analysis strategies and interpretation of the results, was collectively designed by all involved EuroFlow centers during regular meetings. All involved centers measured samples and provided FCS 3.0 data files of BCP-ALL patient samples which were analyzed centrally at Medical University of Silesia in Katowice (Zabrze, Poland). Expression patterns of the examined antigens were investigated within different EGIL BCP-ALL subtypes, i.e., pro-B-, common- and pre-B –ALL, and genetic subgroups of BCP-ALL, i.e., presence vs. absence of *MLL* gene rearrangements and other relevant chromosomal translocations such as t(12;21), t(9;22), t(1;19) with their respective fusion gene products (*ETV6-RUNX1*, *BCR-ABL1*, *TCF3-PBX1*, respectively) as well as hyperdiploidy and hypodiploidy. Not all studied antigens were assessed in every patient (Table 1) and genetic data were also not available for all cases, which explains the differences in the total number of cases per specific genetic subgroup (Table 2). A control group of 19 bone marrow samples from children with benign hematologic conditions such as thrombocytopenia and neutropenia, subjected to bone marrow aspiration for diagnostic purposes at all involved centers was studied in parallel. The current study was approved by the local ethics committees and informed consent was given by each child or their parent/guardian, following the Declaration of Helsinki.

Sample preparation and quality control

Bone marrow samples were subjected to the EuroFlow standardized lyse/wash sample preparation protocols [14] and stained with an 8-color, 2-tube panel of fluorochrome-conjugated mouse anti-human antibodies, containing a backbone of 6 common markers: CD34/PerCP-Cy5.5, clone 8G12 (BD Biosciences, San Jose, CA, USA), CD19/PE-Cy7, clone J3-119 (Beckman Coulter, Brea, CA, USA), CD10/APC, clone HI10a (BD Biosciences), CD38/APC-Ax750, clone LS198-4-3 (Beckman Coulter), CD20/Pacific Blue, clone 2H7 (Biolegend, San Diego, CA, USA), CD45/Pacific Orange, clone HI30 (Life Technologies, Carlsbad, CA, USA). Additionally, tube 1 contained CD86/FITC, clone FUN-1 (BD Pharmingen) and CD304/PE, clone 12C2 (Biolegend) antibodies, while tube 2 contained the CD73/PE, clone AD2 (BD Pharmingen, San Jose, CA, USA) antibody. Erythrocyte lysis was performed after staining the samples using FACS Lyse solution (BD Biosciences). Stained samples were measured with FACSCanto II or LSR II flow cytometers (BD Biosciences) available at each participating center, which had been set-up and calibrated following the standardized EuroFlow guidelines and protocols [15]. During the study, each cytometer was subjected to daily quality assessment using fluorescent beads (Sphero Rainbow Calibration Particles; Spherotech, Lake Forest, IL, USA) of the same lot and the EuroFlow guidelines for monitoring instrument performance in order to ensure the reproducibility of the obtained stainings [15]. All contributing centers were subjected to the regular external quality assessment trials including assessment of standardized instrument settings, reagent panels, and sample preparation protocols, which ensured a high degree of data comparability. For data analysis the Infinicyt software was used (Cytognos SL, Salamanca, Spain).

Determination of reference populations and antigen expression levels in nMFI units

The levels of expression of CD73, CD86 and CD304 on leukemic blasts, the 3 major stages of maturation of normal BCP (pre-B-I, pre-B-II and immature B-cells) and mature B/T/NK lymphocytes, were assessed on a nMFI scale, based on a previously described concept [4]. To create a complete frame of reference of expression, antigen-specific negative and positive reference cell populations (internal controls) were determined. Therefore, positive reference cell populations for CD73, CD86 and CD304 antigens consisted of: the subset of CD73-positive mature B lymphocytes, plasma cells (PC) and plasmacytoid dendritic cells (pDC), respectively. In contrast, mature B/T/NK lymphocytes and the CD73-negative subset of B/T/NK lymphocytes were used as negative reference cell populations for CD86, CD304 and CD73 antigens, respectively (Figure 1 and Supplementary Table 1).

Briefly, the median of the MFI obtained for each marker on the negative reference populations was assigned an nMFI score of 0, whereas the median of the MFI obtained for the corresponding positive reference populations was assigned an arbitrary nMFI score of 10. To normalize the scale, the median of the MFI of the negative reference populations

was subtracted from the median of the MFI of the corresponding positive reference populations per marker. Subsequently, the obtained MFI ranges were divided into 10 equal linear scale intervals, corresponding to a single step on the nMFI scale. Such normalization of MFI measure enabled us to build individual scales of expression for each antigen on leukemic blasts and normal BCP, enabling also the detection of antigen overexpression (i.e., expression higher than on the positive reference population). The nMFI scores of 0–1 were assigned as negative (absence of expression), the nMFI scores of 2–3 were equivalent to heterogeneous-negative-to-dim expression, and the nMFI scores of 4–6 and 7–10 were classified as dim and strong expression, respectively. Finally, nMFI values exceeding 10 reflected antigen overexpression compared to the corresponding positive reference cell population (Figure 2). In parallel, classical, 3-step expression notation was used, in which cases with heterogeneous-negative-to-dim and dim expression were altogether classified as "dim", whereas cases with strong expression and overexpression were classified as"bright" (Table 1).

Stability of CD73, CD86, CD304 and other antigens at early follow-up time points

Expression of CD73, CD86, CD304 and other frequently used MRD markers (i.e., CD34, CD10, CD20) were evaluated for stability of their expression levels at day +15 of induction therapy (MRD15). Since the expression of the backbone markers was not normalized, comparisons were based on absolute MFI values (Figure 5, Supplementary Figure 1). The absolute MFI of all examined antigens was assessed at diagnosis (Dx) and at day +15 in MRD-positive cases. Subsequently, median MFI and ratio of paired MRD15/Dx cases was calculated. Only cases that were positive (MFI>150) at diagnosis for CD73 (n=33), CD86 (n=47), CD304 (n=31), CD34 (n=50), CD10 (n=50) and CD20 (n=23) were included in this part of the study (Figure 5, Table 3 and Supplementary Figure 1).

Statistical methods

The non-normal distribution of nMFI values obtained for all markers analyzed was confirmed by the Shapiro-Wilk's test. To determine the statistical significance of differences in the expression levels of the examined antigens within different immunologic and genetic subgroups of BCP-ALL cases in ordinal nMFI units, the Mann-Whitney U test was applied. Additionally, Bonferroni's p-value corrections were applied for multiple comparisons performed for the same data matrices. For the expression levels given in classical, 3-step notation, Pearson chi-square test was used. Statistical significance was set at $p \leq 0.05$. All statistical analyses were performed centrally at Medical University of Silesia in Katowice (Zabrze, Poland), using the Statistica 8.0 software (Statsoft, Tulsa, OK, USA).

RESULTS

Expression of CD73, CD86 and CD304 on positive and negative reference cell populations

PC expressed the highest levels of CD86 among all cell populations identified in normal bone marrow (median nMFI of 10 (range: 6–25)), being higher than those of normal pDC (median nMFI of 2 (range: 1–3)). Mature lymphocytes (B and T/NK) showed very low CD86 expression levels (median nMFI of 1 (range: 0–1)), and therefore used as the negative reference cell types for CD86. As expected, the highest levels of CD304 expression (median nMFI of 10 (range: 4–22)) were found for pDC, which is a lineage-specific marker, also known as BDCA4. None of bone marrow mature lymphocytes showed CD304 expression (median nMFI of 0), although some expression of this marker was observed on PC (median nMFI of 2 (range: 1–3)). Expression of CD73 was observed in a distinct subset of mature B as well as T/NK lymphocytes (mean percentage of CD73-positive cells of 74% (range 41%–88%) and 26% (range 10%–39%), respectively), with a significantly higher CD73 expression levels on the former cell population (median nMFI of 10 (range: 4–19) vs. 3 (range: 3–5), respectively). Based on these results, the subset of CD73-positive mature B-cells was selected as the positive reference population for this marker (Figures 1–2 and Supplementary Table 1).

Expression of CD73, CD86 and CD304 on normal BCP

Based on the above defined criteria for positivity (nMFI≥2, or at least dim expression in classical notation), normal BCP either did not express or expressed very low levels of CD73, CD86 and CD304 antigens (Figure 1). In detail, CD86 and CD304 were expressed at low levels (median nMFI of 1 (range: 0–2) for both markers) only by pre-B-I cells (CD34+) and only in a fraction of all control bone marrow samples analyzed. Pre-B-II and immature B-cells did not express CD86 and CD304 (median nMFI of 0 (range: 0–2) and 0.5 (range: 0–1), respectively). In contrast, CD73 was very weakly expressed only on pre-B-II and immature B-cells (median nMFI of 1 (range: 0–1)), which therefore was consistently classified as negative (Figures 1–3, and Supplementary Table 1).

Expression of CD73, CD86 and CD304 on leukemic blasts

CD73 was the most frequently expressed antigen on BCP-ALL blasts, being positive (nMFI≥2, or showing at least dim expression in classical notation) in 71/108 (66%) patients. These positive cases showed a CD73 expression that was higher than that of all pooled BCP types (Figure 3 and Supplementary Table 1). However, in most cases, CD73 was expressed at rather low levels; heterogeneous (partial) negative-to-dim and dim CD73 expression (nMFI range: 2–6, or dim in classical notation) was observed in 43/108 (40%) patients,

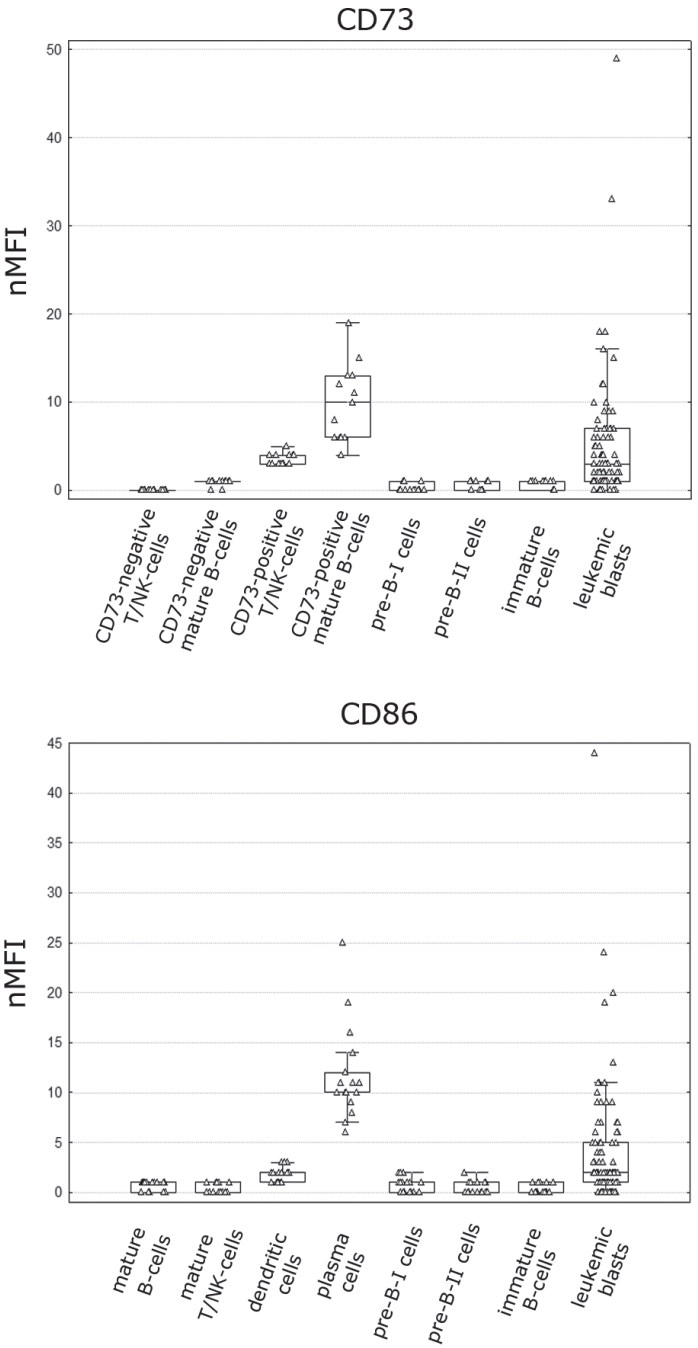
CD73
nMFI
50
40
30
20
10
0
CD73-negative T/NK-cells
CD73-negative mature B-cells
CD73-positive T/NK-cells
CD73-positive mature B-cells
pre-B-I cells
pre-B-II cells
immature B-cells
leukemic blasts
CD86
nMFI
45
40
35
30
25
20
15
10
5
0
mature B-cells
mature T/NK-cells
dendritic cells
plasma cells
pre-B-I cells
pre-B-II cells
immature B-cells
leukemic blasts

Figure 1.

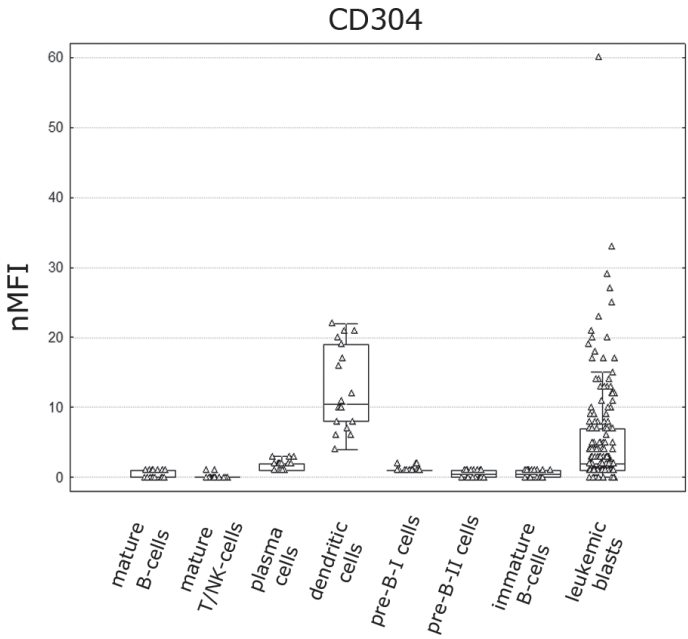

Figure 1 (continued).

Normalized, nMFI-based expression levels of CD73, CD86 and CD304 on normal bone marrow cells and leukemic blasts.

whereas strong positivity and overexpression of CD73 (nMFI≥7, or bright expression in classical notation) was identified in 28/108 (26%) patients (Figures 1–3 and Table 1).

CD304 and CD86 were, compared to CD73, expressed in a slightly lower percentage of BCP-ALL cases: 119/202 (59%) and 58/100 (58%) patients, respectively. Due to the fact that CD304 and CD86 exhibited low expression levels on pre-B-I and pre-B-II cells in a fraction of all control bone marrow samples (nMFI range: 0–2), expression of these markers on leukemic blasts was considered to be higher than normal when the nMFI values were ≥ 3. Thus, in 94/202 (47%) and 35/100 (35%) patients, CD304 respectively CD86 were expressed at higher levels than on normal pooled BCP (Figure 3). However, CD304 more frequently showed strong positivity and overexpression (nMFI≥7, or bright expression) than CD86, i.e., in 56/202 (28%) vs. 17/100 (17%) patients, respectively (Figures 1–3 and Table 1).

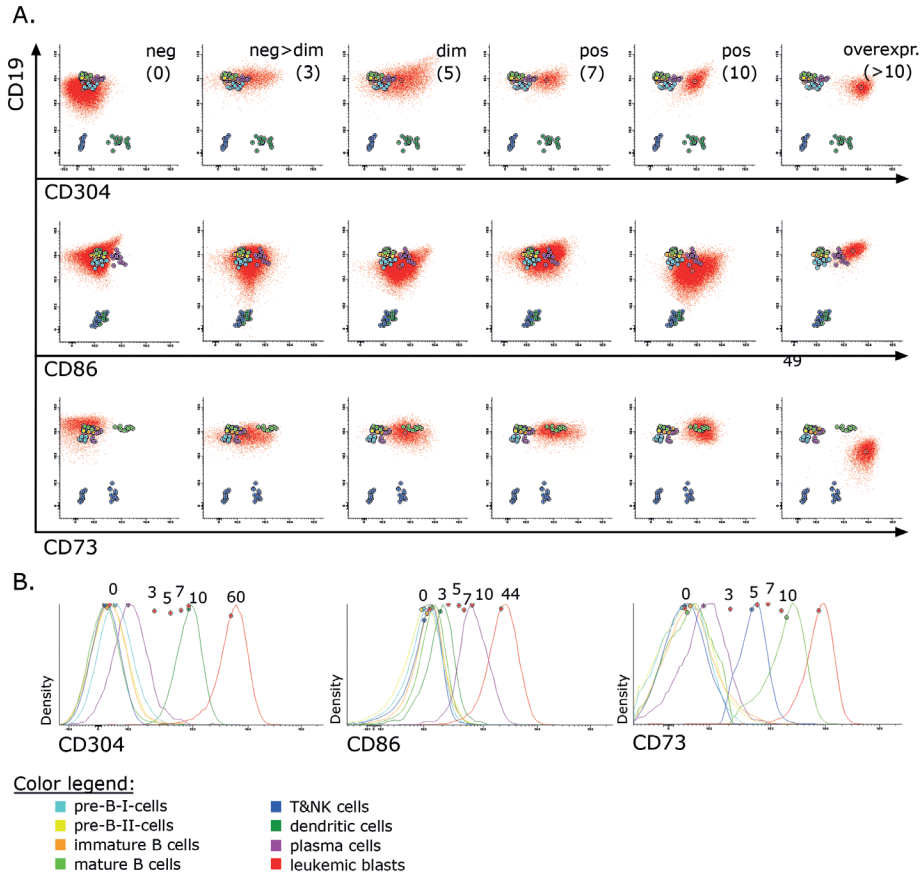

Figure 2.

Illustrating bivariate dot plots (**A.**) and single parameter histograms (**B.**) of the different patterns of expression (nMFI scores) of CD73, CD86 and CD304, observed on leukemic BCP-ALL blasts. The red dots in panels A and B represent BCP-ALL blasts with different nMFI compared to different reference cell types; for clarity, the histograms in panel B only show the highest nMFI values of BCP-ALL blasts.

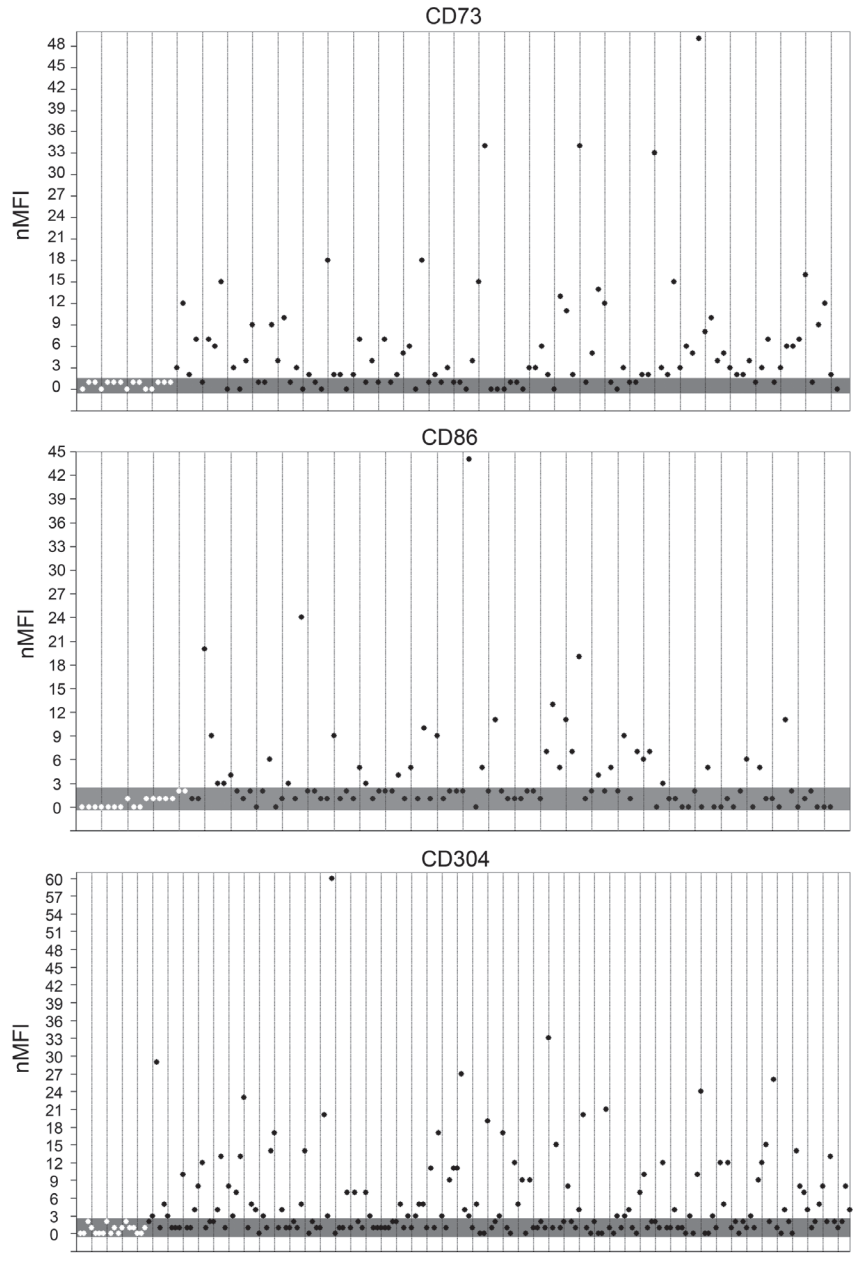

Figure 3.

Expression of CD73, CD86 and CD304 on normal BCP (white dots) vs. leukemic blasts (black dots) in nMFI units The shaded area corresponds to the nMFI spread detected among normal bone marrow BCP.

Table 1. Overall expression profile of CD73, CD86 and CD304 on leukemic BCP-ALL blasts in nMFI-based scale and in classical, 3-step notation (between square parentheses).

Marker expression notation	CD73 (n=108)	CD86 (n=100)	CD304 (n=202)
negative (nMFI: 0–1) [negative]	37 (34%)	42 (42%)	83 (41%)
overall positive (nMFI ≥2)	71 (66%)	58 (58%)	119 (59%)
heterogeneous-negative-to-dim expression (nMFI: 2–3) [dim]	27 (25%)	28 (28%)	41 (20%)
dim expression (nMFI: 4–6) [dim]	16 (15%)	13 (13%)	22 (11%)
strong/bright expression (nMFI: 7–10) [bright]	12 (11%)	9 (9%)	22 (11%)
overexpression (nMFI ≥11) [bright]	16 (15%)	8 (8%)	34 (17%)

Results expressed as number of cases (percentage)

Expression of CD73, CD86 and CD304 in different immunologic subgroups of BCP-ALL defined by the EGIL classification

Data on the immunologic subtype of BCP-ALL was available for 274 (97%) patients, out of which 18 (7%) had pro-B-ALL, 184 (67%) had common-ALL and 72 (26%) had pre-B-ALL. Overall, similar median nMFI values, median nMFI values of positive cases, expression rates (nMFI≥2, or at least dim in classical notation) and overexpression rates (nMFI≥11) were observed for CD73 and CD304 between common- and pre-B-ALL cases. Of these two markers, only CD304 showed significantly higher expression within common- and pre-B-ALL compared to that observed within pro-B-ALL (nMFI of CD304-positive cases of 5 and 7 vs. 2, respectively, p=0.0007 and p=0.0017, respectively; Figure 4, Supplementary Table 2, Supplementary Table 3). Regarding CD86, a similar percentage of positive cases was observed among all three immunologic subgroups of BCP-ALL, the highest median nMFI of CD86-positive cases being observed among pro-B-ALL cases (nMFI of 7 vs. 3 and 4 for common-ALL and pre-B-ALL, respectively), however without reaching statistical significance (Figure 4, Supplementary Table 2 and Supplementary Table 3).

Expression of CD73, CD86 and CD304 in different genetic subgroups of BCP-ALL

The frequency of expression (i.e., nMFI≥2, or at least dim in classical notation) of CD73, CD86 and CD304 was compared among previously defined genetic subgroups of BCP-ALL (Table 2). Overall, a significant association (p=0.001) was found between CD304 expression measured in nMFI scale and the presence of the *ETV6-RUNX1* fusion gene: CD304 was positive in 21/25 (84%) *ETV6-RUNX1*-positive cases with a median nMFI of 7 (range: 2–26) vs. positive in 62/117 (53%) *ETV6-RUNX1*-negative cases, with a median nMFI of 5 (range: 2–60; Table 2, Supplementary Table 4). Among *MLL*-rearranged BCP-ALL patients, a slightly different expression of CD86 was observed: 5/7 (71%) *MLL*-rearranged patients were

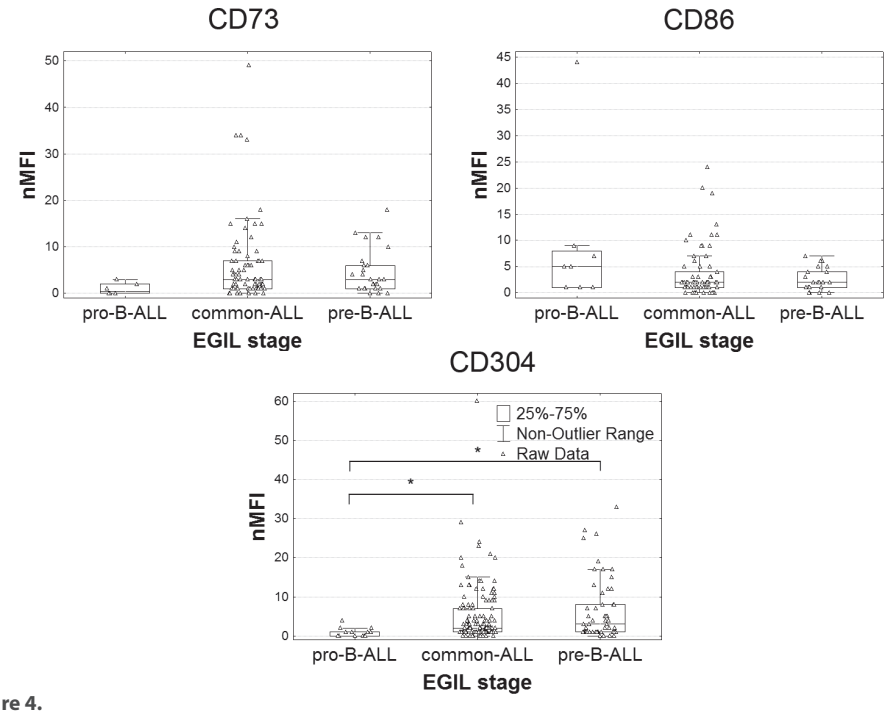

Figure 4.

Expression levels (nMFI values) of CD73, CD86 and CD304 in different immunologic subgroups of BCP-ALL as defined by the EGIL classification. * p<0.05.

CD86-positive with a median nMFI of 7 (range: 5–44), vs. 46/77 (60%) of the *MLL*-negative patients (median nMFI of 3 (range: 2–24)), although these differences did not reach statistical significance (p=0.09). Interestingly, both CD73 and CD304 showed a negative association with *MLL* gene rearrangements (p=0.02 and p=0.002, respectively): CD73 was positive in 50/74 (68%) *MLL*-negative patients (nMFI of 5.5 (range: 2–49)), while only in 2/6 (33%) of the *MLL*-rearranged patients (nMFI of 2.5 (range: 2–3)); similarly, expression of CD304 was observed in 93/152 (61%) *MLL*-negative patients (nMFI of 7 (range: 2–60)), but only in 2/9 (22%) *MLL*-rearranged patients (nMFI of 3 (range: 2–4)). No statistically significant associations were observed between the pattern of antigen expression of hyperdiploid BCP-ALL cases vs. the remaining genetic subgroups of BCP-ALL (i.e., *BCR-ABL1*-positive, *TCF3-PBX1*-positive, hypodiploidy), which were individually too small (1–3 cases (1.5–3.6%) per specified antigen subgroup) to draw reliable conclusions on potential associations with specific expression patterns for any of the three antigens investigated. However, both CD86 and CD304 were positive in all 3 *BCR-ABL1*-positive cases, with a median nMFI of 3

Table 2. Expression of CD73, CD86 and CD304 in different genetic subgroups of BCP-ALL.

	CD73-pos (%)	CD73-pos median nMFI (range)	CD86-pos (%)	CD86-pos median nMFI (range)	CD304-pos (%)	CD304-pos median nMFI (range)
MLL-rearranged						
neg	50/74 (68%)	5.5 (2–49)	46/77 (60%)	3 (2–24)	93/152 (61%) *	7 * (2–60)
pos	2/6 (33%)	2.5 (2–3)	5/7 (71%)	7 (5–44)	2/9 (22%) *	3 * (2–4)
ETV6-RUNX1						
neg	37/58 (64%)	6 (2–49)	40/62 (65%)	5 (2–44)	62/117 (53%) *	5 * (2–60)
pos	12/18 (67%)	3.5 (2–15)	5/8 (63%)	2 (2–9)	21/25 (84%) *	7 * (2–26)
BCR-ABL1						
neg	52/80 (65%)	5 (2–49)	48/81 (60%)	4 (2–44)	92/157 (59%)	6 (2–60)
pos	0 (0%)	–	3/3 (100%)	3 (2–10)	3/3 (100%)	10 (4–14)
TCF3-PBX1						
neg	44/64 (69%)	4.5 (2–49)	33/52 (64%)	3 (2–44)	70/116 (60%)	7 (2–60)
pos	0/2 (0%)	–	0 (0%)	–	0/2 (0%)	–
hypodiploidy						
neg	27/44 (61%)	5 (2–34)	25/47 (53%)	3 (2–20)	57/93 (61%)	8 (2–33)
pos	17/25 (68%)	4 (2–49)	14/18 (78%)	3 (2–44)	24/44 (55%)	4 (2–60)
hypodiploidy						
neg	41/67 (61%)	5 (2–49)	37/64 (58%)	3 (2–44)	79/131 (60%)	7 (2–60)
pos	1/1 (100%)	9 (9)	1/1 (100%)	2 (2)	0/2 (0%)	–

pos – positive, neg – negative; * $p<0.05$ between positive vs. negative cases for individual genetic aberrations (Mann-Whitney U-test). Results expressed as number of cases /total cases (percentage) unless otherwise specified.

(range: 2–10, or dim expression) and 10 (range: 4–14, or bright expression), respectively (Table 2, Supplementary Table 4).

No statistically significant association was found between antigen overexpression (exceeding the expression observed on the relevant positive reference cell type, i.e., nMFI≥11) and any specific genetic subgroup of BCP-ALL (data not shown).

Stability of CD73, CD86, CD304 and other antigens at early follow-up MRD time points

Evaluation of CD86, CD73 and CD20 expression levels at MRD15 vs. diagnosis, showed constant or higher median MFI for CD86 in 22/47 (47%), for CD73 in 26/33 (79%) and for CD20 in 19/23 (83%) patients. The median MFI MRD15/Dx ratio for CD86 equaled 1.4, while

for CD73 and CD20 reached 5.5 and 4.3, respectively, which points out that CD86 was only slightly upregulated in comparison to CD73 and CD20. Despite this, complete loss of CD86 expression at day +15 was observed in only 2/47 (4%) cases. In contrast, the expression of the remaining markers (i.e., CD304, CD34, CD10) decreased in the majority of cases after therapy (median MFI MRD15/Dx ratio of 0.4, 0.5 and 0.3, respectively; Table 3). Of note, CD304 expression decreased in 29/31 (94%) cases, and was completely lost in 10/31 (32%) cases. Despite the decrease in CD304 expression levels, this marker still remained positive in 19/31 (61%) cases (Table 3 and Figure 5). Interestingly, when cases which were negative

Table 3. Stability of expression of selected antigens at day +15 of induction treatment (MRD15).

	CD73 (n=33)	CD86 (n=47)	CD304 (n=31)	CD34 (n=50)	CD10 (n=50)	CD20 (n=23)
stable or increased expression	26 (79%)	22 (47%)	2 (6%)	5 (10%)	0 (0%)	19 (83%)
decreased expression	7 (21%)	25 (53%)	29 (94%)	45 (90%)	50 (100%)	4 (17%)
loss of expression	1 (3%)	2 (4%)	10 (32%)	2 (4%)	0 (0%)	1 (4%)
median MFI ratio (MRD15/Diagnosis)	5.5	1.4	0.4	0.5	0.3	4.3

MFI – median fluorescence intensity. Results expressed as number of cases (percentage) unless otherwise specified. Only cases at least slightly positive at initial diagnosis (MFI>150) were shown.

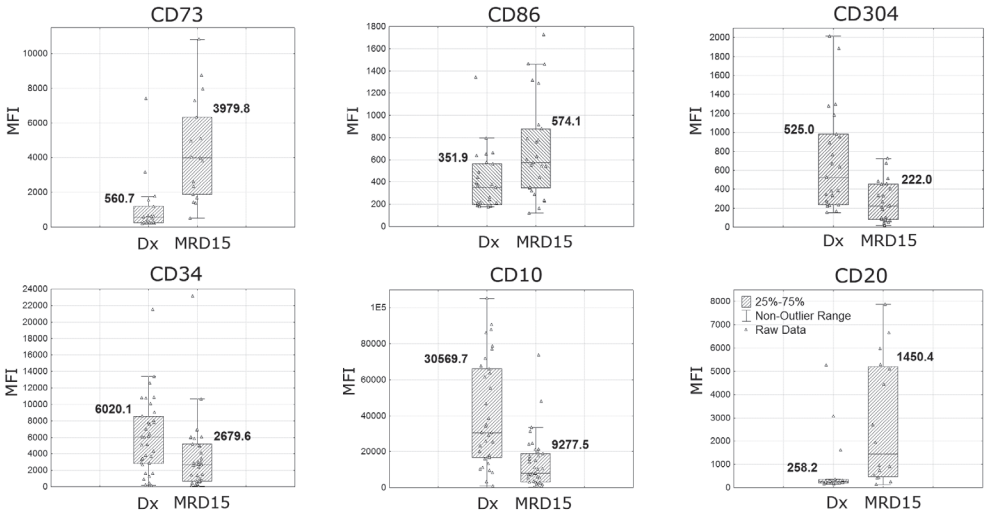

Figure 5.

Levels of expression of different markers at diagnosis (Dx) and at day +15 of induction treatment (MRD15) for cases that showed positivity at initial diagnosis (MFI>150). Boxes cover the interquartile range (25%–75%) and whiskers the non-outlier range. The numbers above the boxes correspond to mean MFI values of the particular antigens at Dx and MRD15.

at diagnosis for a particular antigen were also considered, the percentage of cases with an increased MRD15/Dx ratio for CD86 and CD304 raised up to 53% and 24%, respectively, suggesting that expression of these markers can be upregulated in a significant proportion of cases, even when it was absent at diagnosis (Supplementary Figure 1).

DISCUSSION

MRD evaluated during early phases of treatment is currently the most significant predictive factor for relapse and thereby forms the basis for patient risk stratification in most ALL treatment protocols contemporarily used worldwide, particularly in childhood ALL [16-20]. Therefore, it is critical to optimize currently used MRD detection techniques, particularly FC-based MRD approaches. In this regard, identification of new candidate markers for improved distinction between normal BCP and leukemic blasts still remains a challenge in order to increase the applicability, as well as both specificity and sensitivity of the assay. An ideal candidate marker should exhibit differential expression on normal BCP and leukemic blasts and remain stable during treatment in order to overcome the immunophenotypic switches frequently observed for the most commonly used MRD markers [7,9,12,21]. Further optimization of the FC assay can be achieved by increasing the number of markers combined in a tube and by improved data analysis software enabling assessment of multiple (up to 12 or even more) antigens simultaneously [22,23].

Analysis of leukemia cell surface proteome and genome-wide gene expression screening of leukemic cells against normal BCP have proven to be powerful techniques to search for potential candidate MRD markers in ALL [11,12]. Thus, these studies have highlighted the potential utility of many new markers, of which CD73, CD86 and CD304 have here been investigated in detail, as potentially useful targets for MRD monitoring in childhood BCP-ALL. For this purpose we used a prospective, multicenter and standardized FC approach based on the EuroFlow techniques and tools [14,15]. Since the same EuroFlow instrument settings, sample preparation and data acquisition protocols [15] were followed at each participating center, we were able to apply highly standardized approaches for data analysis, including normalization of MFI values on a pooled group of patients and controls, with the use of innovative Infinicyt software tools [15,22,23].

Overall, our results are consistent with previously reported data on the differential expression patterns of CD73, CD86 and CD304 in normal BCP vs. leukemic blasts from BCP-ALL patients. The pattern of expression of CD304 on normal BCP from our cohort of control bone marrow was concordant to that reported by Meyerson et al. [25] and Solly et al. [26]; in this regard, our results confirmed variably weak/partial CD304 expression on pre-B-I cells, which progressively decreased with BCP maturation, becoming negative

on mature B-cells (Figure 1, Supplementary Table 1). The frequency of cases with strong expression and overexpression (nMFI≥7, or bright expression)) of CD304 on leukemic blasts in our childhood BCP-ALL patients was 28%, in line with the results reported by Coustan-Smith et al. [12] and Meyerson et al. [25] In contrast, Solly et al. [26] reported that CD304 was overexpressed in 24/50 (48%) patients, and expressed on >80% of CD45lowCD19+ leukemia cells in 18/50 (36%) of BCP-ALL patients [26]. This frequency is slightly higher than that observed in the current study. These differences might be due to the fact that the patient group in the study by Solly et al. was composed of both pediatric and adult BCP-ALL patients, while both our and the other two former studies were all based on childhood ALL patients.

Regarding CD73, two-thirds of our cases showed expression of this marker. This frequency of CD73-positive cases is slightly higher than that previously reported by others (54.5% [12] and 41.8% [27]), even when the expression of CD73 was assessed in specific immunological subgroups of BCP-ALL as defined by the EGIL classification (e.g. 33%, 67% and 69% CD73-positive pro-B-, common- and pre-B-ALL patients were found in our series vs. 35%, 45.5% and 50% patients in the series of Wang et al. [27], respectively). Of note, this latter series also included adult BCP-ALL patients. In this regard, it should be highlighted that common-ALL and pre-B-ALL cases showed similar rates and levels of CD73 expression, in line with previous findings by Wieten et al. [28]. Interestingly, Wang et al. [27] observed increasing expression of CD73 along with the maturation of normal BCP, reaching the highest CD73 expression levels on part of the mature B-cells. Although such increased expression of CD73 along BCP maturation was not clearly visible in our study, we confirmed the bimodal expression pattern for CD73 on mature B-lymphocytes, in addition to bone marrow T/NK lymphocytes (Figure 1, Figure 2, Supplementary Table 1).

Data on CD86 expression is more limited. Coustan-Smith et al. [12] have previously reported expression of this marker in around half of all childhood BCP-ALL patients, as confirmed in our study.

As stated above, differences between studies with regard to the frequency of positivity for individual markers, might be related to the age composition of the patient group included in different study reports. In addition, the differences might also be associated with different criteria used to define positivity, or the sensitivity of the specific antibody reagents used [12,25–27]. Although we used a commensurate positivity criterion of nMFI≥2 or at least dim in the classical notation (i.e., higher than that observed on normal BCP), this might not be directly comparable to a given MFI cutoff for positivity, or another definition of high vs. low expression based on the ratio between the MFI of a positive cell population and the negative (e.g., isotype) control signals used in other studies.

The pattern of expression of the three markers investigated in the current study showed limited associations with the genetic subgroups of BCP-ALL: 1) the relationship between

CD304 expression and *ETV6-RUNX1* gene rearrangements, which has also been reported by Solly et al. [26] (but not confirmed by Coustan-Smith et al. [12]) and, 2) the inverse relationship between *MLL* gene rearrangements and both CD73 and CD304 expression reported here for the first time. Of note, the above mentioned associations were proven with the use of two statistical approaches. Coustan-Smith et al. [12] reported a marginal association (p=0.09) between CD86 expression and hyperdiploidy in BCP-ALL patients, which could not be confirmed in our series (Table 2).

It should be noted that relatively high expression levels of CD86 and CD304 were detected in our three *BCR-ABL1*-positive cases, but differences vs. *BCR-ABL1*-negative patients did not reach statistical significance, probably due to the low number of *BCR-ABL1*-positive cases. Solly et al. [26] found a higher frequency of *BCR-ABL1*-positive cases among the CD304+ vs. the CD304– patient groups (32% and 5% of patients, respectively); Meyerson et al. [25] revealed a higher frequency of CD304-positivity among *BCR-ABL1*-positive than among negative patients (90% vs. 68%, respectively). However, these differences did not reach statistical significance in neither study (p-values of 0.08 and 0.09, respectively).

In order to further confirm the potential utility of the three markers evaluated here for MRD monitoring, we assessed the stability of their expression during the early phases of therapy, along with other frequently used MRD markers such as CD34, CD10 and CD20. MRD results at day +15 of induction therapy was chosen to assess the stability of marker expression, as on one hand MRD measurements at day +15 directly provide clinically useful information about response to therapy of BCP-ALL patients in most ALL treatment protocols [16–20], and on the other hand, MRD-positivity levels higher than 0.1% are observed at this time point in the majority of patients, which ensures more reliable comparative analyses than at later time points with lower rates and lower levels of MRD-positivity. Of the three new markers evaluated, CD73 turned out to be the most stable, being expressed at the same or higher levels at day +15 in around 80% of cases, with virtually no complete loss of expression observed. The expression levels of CD86 remained stable in around half of the cases, while only two patients showed complete loss of CD86 expression at day +15. In turn, CD304 expression was the least stable at follow-up – its expression level decreased in the majority of cases, however in more than half of them, the leukemic blasts still remained CD304-positive (Table 3).

To date, there is only a limited number of studies in which the stability of CD73, CD86 and CD304 has been investigated in detail during follow-up. Stability of CD304 expression on leukemic blasts after therapy has been previously reported by Solly et al., however in this study levels of CD304 in diagnosis samples were compared with that in relapsed samples and only on a relatively small patient cohort [26]. Meyerson et al. [25] and Coustan-Smith et al. [12] concluded that CD304 might potentially represent a useful MRD marker, based mainly on its relatively high overexpression rate at diagnosis, although stability of

CD304 during therapy was not investigated. In this regard, our results showed that CD304 overexpression at diagnosis does not always predict stability of this aberrant marker, even at early time points (day +15 of induction therapy). Despite the fact that decreased expression of CD304 was observed in some cases, it does not rule out this antigen as a good marker for MRD monitoring, particularly because expression of CD304, as well as of CD86, was also found to increase in cases in which leukemic blasts at diagnosis were negative for these markers. This is also true for CD73, for which we found the highest stability and the highest median MRD15/Diagnosis MFI ratio, confirming what has also been previously reported for CD73 by Wang et al. [27] Increased expression during follow-up is of particular importance, as it may considerably facilitate MRD identification. Phenotypic modulation (switch) is a relatively common finding during treatment, and might occur in up to 70% of all BCP-ALL patients [8,10,21], mainly due to down- or upregulation of well-established MRD markers by steroid-induced blast cell maturation. As a consequence, decreased expression of "immaturity" markers like CD34 and CD10, together with upregulation of differentiation-associated antigens such as CD20, have been recurrently reported during the early phases of treatment (day +15 and day +33) [6,7,9,11,19,29–31]. In order to overcome this problem, it is recommended that multiple aberrant markers, representing LAIP at diagnosis, should be followed, so that at least one LAIP will remain stable.

Finally, a recent study of Theunissen et al. (Blood 2016 – under review) evaluated the applicability of CD73 and CD304 antigens based on testing of 319 MRD bone marrow samples from BCP-ALL patients, in parallel with molecular IG/TR gene PCR-based MRD monitoring. In order not to increase the number of fluorochromes required for the most reliable follow-up approach for BCP-ALL patients, this study combined both markers in the same tube with the same fluorochrome, which did not affect background staining. The use of the antibody combination containing CD73 and CD304, together with the use of a bulk lysis protocol enabling the collection of more than 3 million cells, resulted in comparable results as obtained by IG gene rearrangement-based MRD approach.

In summary, here we confirm and extend on previous findings about the potential utility of three candidate markers for MRD monitoring in BCP-ALL and prove the usefulness of a standardized approach to generate convergent and comparable flow cytometric data at multiple centers for fast and reproducible evaluation of relatively large numbers of samples. Our results provide useful, quantitative information on the expression of CD73, CD86 and CD304 antigens on different cell types, including normal BCP. Our study also proves that aberrant expression/overexpression of CD73, CD86 and CD304 occurs in a significant percentage of BCP-ALL patients; increased expression of CD73 and CD304 being particularly associated with specific immunological subtypes of BCP-ALL (common- and pre-B-ALL), whereas CD304 expression is particularly frequent among *ETV6-RUNX1*-positive cases. In addition, our results suggest that CD73 expression exhibits more frequently stable

or increased levels than CD86 and CD304 during the early phases of therapy, which proves the former one to be a promising marker for MRD monitoring in BCP-ALL patients.

ACKNOWLEDGEMENTS

The authors EM[5] and MN[5] were supported by the Czech Republic national BCP-ALL MRD grant AZV, no. 15-28525A. TS[1] and ŁS[1] were supported by internal grants from the Medical University of Silesia and Iskierka Foundation (Katowice, Poland). PT[2], TS[1] and ŁS[1] were financially supported by ERA-NET PrioMedChild project (no. 40-41800-98-027). Part of this research was performed within the framework of the Erasmus Postgraduate School Molecular Medicine. The authors declare no conflict of interest. ŁS[1] and PT[2] have contributed equally to this study.

REFERENCES

1. Pieters R, Carroll WL. Biology and treatment of acute lymphoblastic leukemia. Pediatr Clin North Am 2008; 55: 1–20
2. Onciu M. Acute lymphoblastic leukemia. Hematol Oncol Clin N Am 2009; 23:655–674
3. Szczepański T, van der Velden VHJ, van Dongen JJM. Classification systems for acute and chronic leukaemias. Best Pract Res Clin Haematol 2003; 16: 561–582
4. Sędek Ł, Bulsa J, Sonsala A, Twardoch M, Wieczorek M, Malinowska I, Derwich K, Niedźwiecki M, Sobol-Milejska G, Kowalczyk JR, Mazur B, Szczepański T. The immunophenotypes of blast cells in B-cell precursor acute lymphoblastic leukemia: how different are they from their normal counterparts? Cytometry B Clin Cytom 2014; 86B: 329–339
5. Campana D. Role of minimal residual disease monitoring in adult and pediatric acute lymphoblastic leukemia. Hematol Oncol Clin North Am 2009; 23(5): 1083–1098
6. Gaipa G, Basso G, Maglia O, Leoni V, Faini A, Cazzaniga G, Bugarin C, Veltroni M, Michelotto B, Ratei R, Coliva T, Valsecchi MG, Biondi A, Dworzak MN; I-BFM-ALLFCM-MRD Study Group. Drug-induced immunophenotypic modulation in childhood ALL: Implications for minimal residual disease detection. Leukemia 2005; 19: 49–56
7. Dworzak MN, Gaipa G, Schumich A, Maglia O, Ratei R, Veltroni M, Husak Z, Basso G, Karawajew L, Gadner H, Biondi A. Modulation of antigen expression in B-cell precursor acute lymphoblastic leukemia during induction therapy is partly transient: Evidence for a drug-induced regulatory phenomenon. Results of the AIEOPBFM-ALL-FLOW-MRD-Study Group. Cytometry B Clin Cytom 2010; 78B: 147–153

8. Slamova L, Starkova J, Fronkova E, Zaliova M, Reznickova L, van Delft FW, Vodickova E, Volejnikova J, Zemanova Z, Polgarova K, Cario G, Figueroa M, Kalina T, Fiser K, Bourquin JP, Bornhauser B, Dworzak MN, Zuna J, Trka J, Stary J, Hrusak O, Mejstrikova E. CD2-positive B-cell precursor acute lymphoblastic leukemia with an early switch to the monocytic lineage. Leukemia 2014; 28(3): 609–620
9. Gaipa G, Basso G, Biondi A, Campana D. Detection of minimal residual disease in pediatric acute lymphoblastic leukemia. Cytometry B Clin Cytom 2013; 84B: 359–369
10. Mejstrikova E, Fronkova E, Kalina T, Omelka M, Batinic D, Dubravcic K, Pospisilova K, Vaskova M, Luria D, Cheng SH, Ng M, Leung Y, Kappelmayer J, Kiss F, Izraeli S, Stark B, Schrappe M, Trka J, Stary J, Hrusak O. Detection of residual B precursor lymphoblastic leukemia by uniform gating flow cytometry. Pediatr Blood Cancer 2010; 54(1): 62-70
11. Mirkowska P, Hofmann A, Sędek Ł, Slamova L, Mejstrikova E, Szczepański T, Schmitz M, Cario G, Stanulla M, Schrappe M, van der Velden VHJ, Bornhauser BC, Wollscheid B, Bourquin JP. Leukemia surfaceome analysis reveals new disease-associated features. Blood 2013; 121(25): 149–159
12. Coustan-Smith E, Song G, Clark C, Key L, Liu P, Mehrpooya M, Stow P, Su X, Shurtleff S, Pui CH, Downing JR, Campana D. New markers for minimal residual disease detection in acute lemphoblastic leukemia. Blood 2011; 117(23): 6267–6276
13. Szczepański T. Why and how to quantify minimal residual disease in acute lymphoblastic leukemia? Leukemia 2007; 21: 622–626
14. van Dongen JJM, Lhermitte L, Böttcher S, Almeida J, van der Velden VHJ, Flores-Montero J, Rawstron A, Asnafi V, Lecrevisse Q, Lucio P, Mejstřikova E, Szczepański T, Kalina T, de Tute R, Brüggemann M, Sędek Ł, Cullen M, Langereak AW, Mendonca A, Macintyre E, Martin-Ayuso M, Hrusak O, Vidriales MB, Orfao A. EuroFlow antibody panels for standardized n-dimensional flow cytometric immunophenotyping of normal, reactive and malignant leukocytes. Leukemia 2012; 26: 1908–1975
15. Kalina T, Flores-Montero J, van der Velden VHJ, Martin-Ayuso M, Böttcher S, Ritgen M, Almeida J, Lhermitte L, Asnafi V, Mendonca A, de Tute R, Cullen M, Sędek Ł, Vidriales MB, Perez JJ, te Marvelde JG, Mejstřikova E, Hrusak O, Szczepański T, van Dongen JJM, Orfao A. EuroFlow standardization of flow cytometer instrument settings and immunophenotyping protocols. Leukemia 2012; 26:1986–2010
16. Pui CH. Treatment of acute lymphoblastic leukemia. N Engl J Med 2006; 354: 166–178
17. Campana D. Minimal residual disease monitoring in childhood acute lymphoblastic leukemia. Curr Opin Hematol 2012; 19: 313–318
18. Brüggemann M, Gökbuget N, Kneba M. Acute lymphoblastic leukemia: monitoring minimal residual disease as a therapeutic principle. Semin Oncol 2012; 39(1): 47–57
19. Basso G, Veltroni M, Valsecchi MG, Dworzak MN, Ratei R, Silvestri D, Benetello A, Buldini B, Maglia O, Masera G, Conter V, Arico M, Biondi A, Gaipa G. Risk of relapse of childhood acute lymphoblastic leukemia is predicted by flow cytometric measurement of residual disease on day 15 bone marrow. J Clin Oncol 2009; 27: 5168–5174
20. Kusenda J, Fajtova M, Kovarikova A. Monitoring of minimal residual disease in acute leukemia by multiparametric flow cytometry. Neoplasma 2014; 61(2): 119–127

21. Chen W, Karandikar NJ, McKenna RW, Kroft SH. Stability of leukemia-associated immunophenotypes in precursor B-lymphoblastic leukemia/lymphoma: A single institution experience. Am J Clin Pathol 2007; 127: 39–46
22. Flores-Montero J, Flores LS, Paiva B, Puig N, García O, Böttcher S, van der Velden VHJ, Pérez-Morán JJ, Vidriales MB, García-Sanz R, Jimenez C, González M, Martinez-López J, Mateos AC, Grigore GE, Fluxá R, Caetano J, Sędek Ł, del Cañizo MC, Bladé J, Lahuerta JJ, Aguilar C, Bárez A, Gracía A, Labrador J, Leoz P, Aguilera-Sanz C, San-Miguel J, Mateos MV, Durie B, van Dongen JJM, Orfao A, on behalf of the EuroFlow Consortium and the International Myeloma Foundation. Next Generation Flow (NGF) for High-Sensitive and Standardized Detection of Minimal Residual Disease in Multiple Myeloma. Blood 2016 [in press].
23. Denys B, van der Sluijs-Gelling AJ, Homburg C, van der Schoot CE, de Haas V, Philippe J, Pieters R, van Dongen JJM, van der Velden VHJ. Improved flow cytometric detection of minimal residual disease in childhood acute lymphoblastic leukemia. Leukemia 2013; 27: 635–641
24. van Dongen JJM, van der Velden VHJ, Bruggemann M, Orfao A. Minimal residual disease diagnostics in acute lymphoblastic leukemia: need for sensitive, fast, and standardized technologies. Blood 2015; 125(26): 3996–4009
25. Meyerson HJ, Blidaru G, Edinger A, Osei E, Schweitzer K, Fu P, Ho L. NRP-1/CD304 expression in acute leukemia: a potential marker for minimal residual disease detection in precursor B-cell acute lymphoblastic leukemia. Am J Clin Pathol 2012; 137(1): 39–50
26. Solly F, Angelot F, Garand R, Ferrand C, Silles E, Schillinger F, Decobecq A, Billot M, Larosa F, Plouvier E, Deconinck E, Legrand F, Saas P, Rohrlich PS, Garnache-Ottou F. CD304 is preferentially expressed on a subset of B-lineage acute lymphoblastic leukemia and represents a novel marker for minimal residual disease detection by flow cytometry. Cytometry A 2012; 81A: 17–24
27. Wang W, Gao L, Li Y, Li ZL, Gong M, Huang FZ, Chen YR, Zhang CX, Gao YY, Ma YG. The application of CD73 in minimal residual disease monitoring using flow cytometry in B-cell acute lymphoblastic leukemia. Leuk Lymphoma 2016; 57(5): 1174–1181.
28. Wieten E, van der Linden-Schrever BE, Sonneveld E, Veerman AJ, Pieters R. CD73 (5'-nucleotidase) expression has no prognostic value in children with acute lymphoblastic leukemia. Leukemia 2011; 25(8): 1374–1376
29. Lucio P, Gaipa G, van Lochem EG, van Wering ER, Porwit-MacDonald A, Faria T, Bjorklund E, Biondi A, van den Beemd MW, Baars E, Vidriales B, Parreira A, van Dongen JJ, San Miguel JF, Orfao A. BIOMED-I concerted action report: flow cytometric immunophenotyping of precursor B-ALL with standardized triple-stainings. BIOMED-1 Concerted Action Investigation of Minimal Residual Disease in Acute Leukemia: International Standardization and Clinical Evaluation. Leukemia 2001; 15: 1185–1192
30. Chen JS, Coustan-Smith E, Suzuki T, Neale GA, Mihara K, Pui CH, Campana D. Identification of novel markers for monitoring minimal residual disease in acute lymphoblastic leukemia. Blood 2001; 97(7): 2115–2120

31. Coustan-Smith E, Sancho J, Behm FG, Hancock ML, Razzouk BI, Ribeiro RC, Rivera GK, Rubnitz JE, Sandlund JT, Pui CH, Campana D. Prognostic importance of measuring early clearance of leukemic cells by flow cytometry in childhood acute lymphoblastic leukemia. Blood 2002; 100(1): 52–58

SUPPLEMENTARY TABLES AND FIGURE

Supplementary Table 1. Patterns of expression of CD73, CD86 and CD304 on different subsets of normal bone marrow cells.

	CD73		CD86		CD304	
	MFI range (MFI step: 161)	**median nMFI (range)**	**MFI range (MFI step: 52)**	**median nMFI (range)**	**MFI range (MFI step: 90)**	**median nMFI (range)**
mature B-cells	N/A	N/A	**118–159**	**1 (0–1)**	**20–94**	**0 (0–1)**
T/NK cells	N/A	N/A	**107–151**	**0 (0–1)**	**19–49**	**0 (0–1)**
CD73-negative T/NK-cells	**20–44**	**0**	N/A	N/A	N/A	N/A
CD73-negative mature B-cells	**44–128**	**1 (0–1)**	N/A	N/A	N/A	N/A
CD73-positive T/NK-cells	366–699	3 (3–5)	N/A	N/A	N/A	N/A
CD73-positive mature B-cells	**656–3047**	**10 (4–19)**	N/A	N/A	N/A	N/A
plasma cells (PC)	N/A	N/A	**553–1063**	**10 (6–25)**	38–256	2 (1–3)
plasmacytoid dendritic cells (pDC)	N/A	N/A	157–264	2 (1–3)	**364–1968**	**10 (4–22)**
pre-B-I cells	16–50	0 (0–1)	112–225	1 (0–2)	44–161	1 (1–2)
pre-B-II cells	36–143	1 (0–1)	99–210	0 (0–2)	17–83	0.5 (0–1)
immature B-cells	34.8–178.9	1 (0–1)	102.5–158.0	0 (0–1)	21.6–73.8	0.5 (0–1)

MFI – median fluorescence intensity. Negative and positive reference cell populations for each of the three markers investigated were marked in bold.

Supplementary Table 2. Expression of CD73, CD86 and CD304 in different immunological subgroups of BCP-ALL as defined by the EGIL classification.

	pro-B-ALL	common-ALL	pre-B-ALL
CD73			
negative	4/6 (67%)	25/76 (33%)	8/26 (31%)
positive (nMFI≥2)	2/6 (33%)	51/76 (67%)	18/26 (69%)
overexpression (nMFI≥11)	0/6 (0%)	12/76 (16%)	4/26 (15%)
median nMFI (range)	1 (0–4)	3 (0–60)	3 (0–33)
median nMFI of positive (range)	2.5 (2–3)	6 (2–49)	4.5 (2–18)
median nMFI of overexpressed (range)	–	15.5 (11–49)	12.5 (12–18)
CD86			
negative	3/8 (38%)	29/69 (42%)	9/22 (41%)
positive (nMFI≥2)	5/8 (63%)	40/69 (58%)	13/22 (59%)
overexpression (nMFI≥11)	1/8 (13%)	7/69 (10%)	0/22 (0%)
median nMFI (range)	5 (1–44)	2 (0–24)	2 (0–7)
median nMFI of positive (range)	7 (5–44)	3 (2–24)	4 (2–7)
median nMFI of overexpressed (range)	44 (44)	13 (11–24)	–
CD304			
negative	10/13 (77%)	49/130 (38%)	23/57 (40%)
positive (nMFI≥2)	3/13 (23%)	81/130 (62%)	34/57 (60%)
overexpression (nMFI≥11)	0/13 (0%)	21/130 (16%)	13/57 (23%)
median nMFI (range)	1 (0–4)	2 (0–60)	3 (0–33)
median nMFI of positive (range)	2 (2–4)	5 (2–60)	7 (2–33)
median nMFI of overexpressed (range)	–	14 (11–60)	17 (11–33)

Results expressed as number of cases/total cases evaluated (percentage) unless otherwise specified.

Supplementary Table 3. Statistical significance of CD73, CD86 and CD304 expression in different immunological subgroups of BCP-ALL as defined by the EGIL classification.

A.		**common-ALL**	**pre-B-ALL**
CD73	pro-B-ALL	0.052	0.087
	common-ALL	–	2.537
CD86	pro-B-ALL	0.617	0.320
	common-ALL	–	2.252
CD304	pro-B-ALL	0.0007 *	0.0017 *
	common-ALL	–	2.150

B.		**common-ALL**	**pre-B-ALL**
CD73	pro-B-ALL	0.168	0.198
	common-ALL	–	0.749
CD86	pro-B-ALL	0.446	0.053
	common-ALL	–	0.208
CD304	pro-B-ALL	0.014 *	0.027 *
	common-ALL	–	0.794

A. Bonferroni-corrected p-values calculated for expression levels given in nMFI-based scale. The statistical significance ($p<0.05$) between specific pairs of immunological subgroups was marked with * (Mann-Whitney U test).
B. p-values calculated for expression levels based on the classical, 3-step notation (negative / dim / bright). The statistical significance ($p<0.05$) between specific pairs of immunological subgroups was marked with * (Pearson chi-square test).

Supplementary Table 4. Statistical significance of CD73, CD86 and CD304 expression in different genetic subgroups of BCP-ALL.

A.	**MLL-rearranged**	**ETV6-RUNX1**	**BCR-ABL1**	**TCF3-PBX1**	**hyperdiploidy**	**hypodiploidy**
CD73	0.097	5.508	N/A	N/A	4.067	N/A
CD86	0.618	2.325	1.673	N/A	0.614	N/A
CD304	0.012 *	0.009 *	0.520	N/A	0.974	1.489
B.	**MLL-rearranged**	**ETV6-RUNX1**	**BCR-ABL1**	**TCF3-PBX1**	**hyperdiploidy**	**hypodiploidy**
CD73	0.159	0.808	N/A	N/A	0.516	N/A
CD86	0.196	0.848	0.358	N/A	0.099	N/A
CD304	0.046 *	0.002 *	0.269	N/A	0.080	0.226

A. Bonferroni-corrected p-values calculated for expression levels given in nMFI-based scale. The statistical significance ($p<0.05$) between positive vs. negative cases for an individual genetic aberration was marked with * (Mann-Whitney U test).
B. p-values calculated for expression levels based on the classical, 3-step notation (negative / dim / bright).The statistical significance ($p<0.05$) between positive vs. negative cases for an individual genetic aberration was marked with * (Pearson chi-square test).

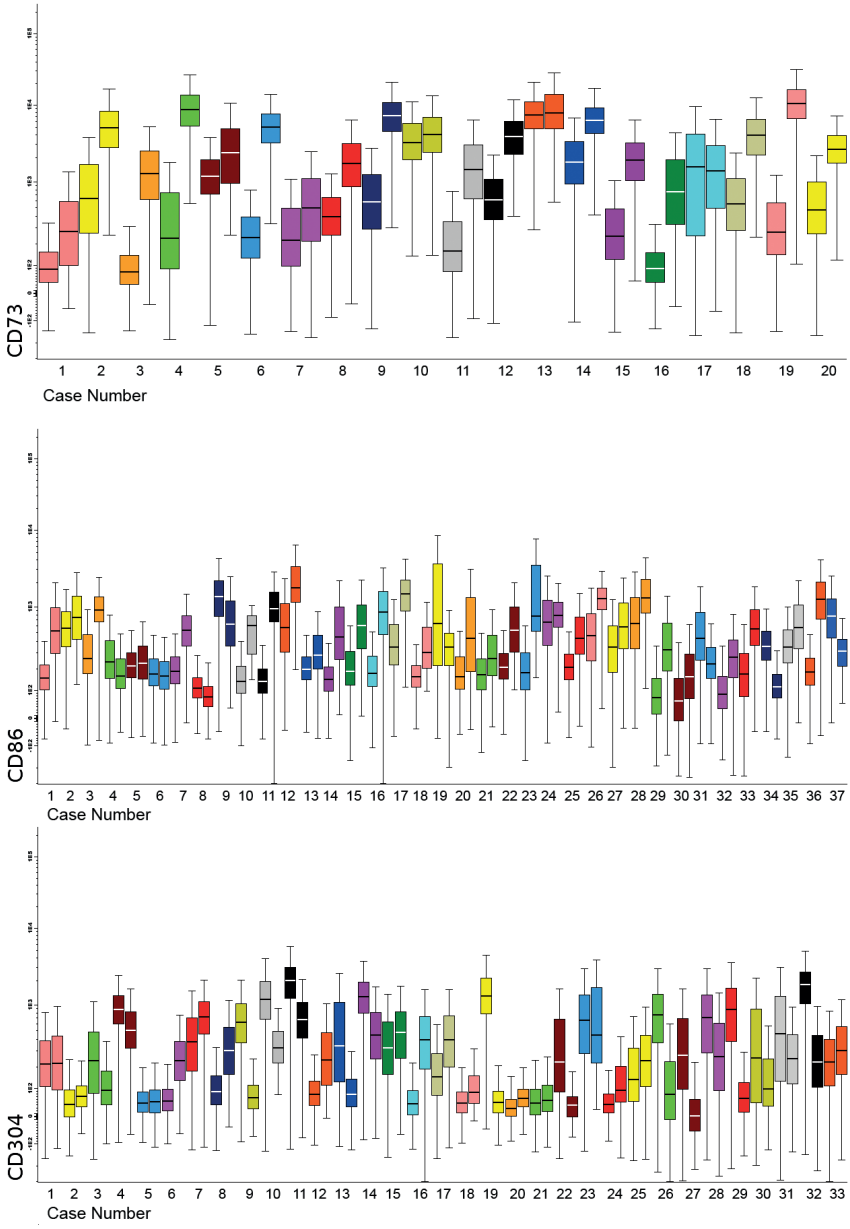

Supplementary Figure 1.

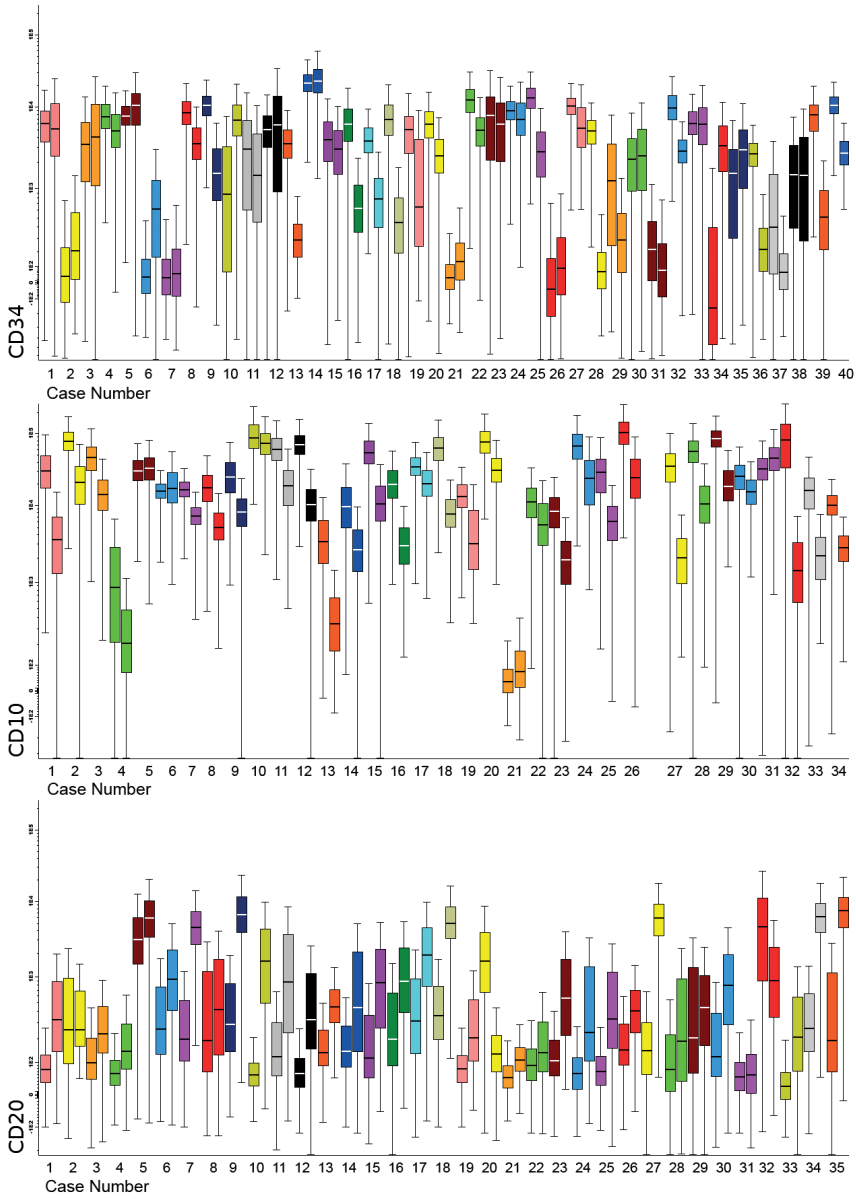

Supplementary Figure 1 (continued).

Expression of CD73, CD86, CD304 and other markers during follow-up. Adjacent bars of the same color represent the antigen expression level of the same BCP-ALL patient at diagnosis (left) and at day +15 of induction treatment (right).

Chapter 6

Standardized flow cytometry for highly sensitive MRD measurements in B-cell acute lymphoblastic leukemia

Prisca Theunissen[1#], Ester Mejstrikova[2#], Łukasz Sędek[3], Alita J. van der Sluijs-Gelling[4], Giuseppe Gaipa[5], Marius Bartels[6], Elaine Sobral da Costa[7], Michaela Kotrová[2], Michaela Nováková[2,6], Edwin Sonneveld[4,] Chiara Buracchi[5], Paola Bonaccorso[5], Elen Oliveira[7], Jeroen G. te Marvelde[1], Tomasz Szczepański[3], Ludovic Lhermitte[8], Ondrej Hrusak[2], Quentin Lecrevisse[9], Georgiana Emilia Grigore[10], Eva Froňková[2], Jan Trka[2], Monika Brüggemann[6], Alberto Orfao[9], Jacques J.M. van Dongen[1], and Vincent H.J. van der Velden[1], on behalf of the EuroFlow Consortium

[1]Department of Immunology, Erasmus MC, University Medical Center Rotterdam, Rotterdam, Netherlands; [2]CLIP - Childhood Leukaemia Investigation Prague, Department of Pediatric Hematology and Oncology, Second Faculty of Medicine, Charles University, University Hospital Motol, Prague, Czech Republic; [3]Department of Pediatric Hematology and Oncology, Zabrze, Medical University of Silesia (SUM), Katowice, Poland; [4]Dutch Childhood Oncology Group, The Hague, Netherlands; [5]Centro Ricerca Tettamanti, Clinica Pediatrica Università di Milano Bicocca, Monza (MB),Italy; [6]Department of Hematology, University of Schleswig-Holstein, Campus Kiel, Kiel, Germany; [7]Department of Pediatrics, Federal University of Rio de Janeiro, Rio de Janeiro, Brazil; [8]Department of Hematology, Hôpital Necker-Enfants-Malades (AP-HP) and UMR CNRS 8147, University of Paris Descartes, Paris, France; [9]Cancer Research Center (IBMCC-CSIC), Department of Medicine and Cytometry Service, University of Salamanca (USAL) and Institute of Biomedical Research of Salamanca (IBSAL), Salamanca, Spain; [10]Cytognos SL, Salamanca, Spain

# PT and EM equally contributed

Accepted for publication in Blood

ABSTRACT

A fully-standardized EuroFlow 8-color antibody panel and laboratory procedure was stepwise designed to measure minimal residual disease (MRD) in B-cell precursor (BCP) acute lymphoblastic leukemia (ALL) patients with a sensitivity of $\leq 10^{-5}$, comparable to real-time quantitative (RQ)-PCR-based MRD detection via antigen-receptor rearrangements.

Leukocyte markers and corresponding antibodies were selected based on their contribution in separating BCP-ALL cells from normal/regenerating BCP cells in multidimensional principal component analyses. After five multicenter design-test-evaluate-redesign phases with a total of 319 BCP-ALL patients at diagnosis, two 8-color antibody tubes were selected, which allowed separation between normal and malignant BCP cells in 99% of studied patients. These two tubes were tested with a new erythrocyte bulk-lysis protocol allowing acquisition of high cell numbers in 377 bone marrow follow-up samples of 178 BCP-ALL patients. Comparison with RQ-PCR-based MRD data showed a clear positive relation between the percentage concordant cases and the number of cells acquired. For those samples with >4 million cells acquired, concordant results were obtained in 93% of samples. Most discordances were clarified upon high-throughput sequencing of antigen-receptor rearrangements and re-analysis of flowcytometric data, resulting in an unprecedented concordance of 98% (97% for samples with MRD <0.01%).

In conclusion, the fully-standardized EuroFlow BCP-ALL MRD strategy is applicable to >98% of patients with sensitivities at least similar to RQ-PCR (≤10-5), if sufficient cells (>$4x10^6$) are evaluated.

INTRODUCTION

Most current treatment protocols for B-cell precursor (BCP) acute lymphoblastic leukemia (ALL) include minimal residual disease (MRD) measurements, generally based on PCR analysis of rearranged antigen receptor genes [1-3]. Although flow cytometry (FCM) can be used for MRD detection as well [4-9], studies so far indicate that the specificity and sensitivity of FCM MRD diagnostics is inferior to PCR-based MRD diagnostics [10-13]. Nevertheless, we and others have recently shown that the use of 6- or 7-color immunostainings combined with the introduction of new markers and new marker combinations significantly improved FCM MRD analysis in BCP-ALL patients [10,12]. These improvements were particularly related to specificity, whereas the sensitivity still appeared to be lower than for the PCR-based methods. To further improve FCM-based MRD diagnostics, more objective and efficient discrimination of BCP-ALL cells from normal BCP cells and improved sample preparation procedures for acquisition of larger numbers of cells are a prerequisite.

Eight-color immunostainings may contribute to improve flowcytometric MRD detection in BCP-ALL patients. Recently, an 8-color antibody tube was developed in the ALL-REZ-BFM 2002 trial [14]. This tube contained seven antibodies (CD10, CD19, CD20, CD22, CD34, CD45, CD38) and the nucleic acid dye Syto41 and gave concordant MRD results with PCR-MRD data in 86.5% of samples. A Chinese study reported an 8-color antibody tube (CD10, CD19, CD20, CD34, CD38, CD45, CD58, plus CD66c or CD13/CD33 or NG2/CD15) with a sensitivity of 0.001% in 81.6% of patients [8]. Shaver et al. elegantly analyzed the relative contribution that each marker and/or pair of markers made to detect MRD [15], and concluded that a single 8-color tube consisting of CD9, CD10, CD19, CD20, CD34, CD38, CD45, and CD58, could provide as much diagnostic utility as their existing three-tube panel with 12 markers.

Within the EuroFlow Consortium (EU-FP6, LSHB-CT-2006-018708), we aimed to design standardized 8-color immunophenotyping protocols for multicenter MRD measurement in BCP-ALL and to improve the sensitivity of the assay to $\leq 10^{-5}$ (at least comparable to PCR). First, in order to select the most informative markers in distinguishing BCP-ALL from normal BCP cells, we applied novel software tools and principal component-based analyses (PCA) [16, 17]. In each cycle of design-test-evaluate-redesign, the antibody tubes were tested on BCP-ALL samples and normal and/or regenerating bone marrow (BM), followed by assessment of the contribution of each antibody, until satisfactory results were obtained after five testing rounds. Second, a flowcytometric protocol for staining and acquisition of large numbers of cells (>4 million) was developed, allowing theoretical sensitivities of at least 0.001% ($\leq 10^{-5}$). Finally, the selected antibody tubes and standardized laboratory procedures were prospectively validated on follow-up samples from BCP-ALL patients, using the EuroMRD PCR-MRD method in parallel as gold standard [2].

MATERIALS AND METHODS

BCP-ALL patients and normal controls

Data were collected in seven EuroFlow centers. BM samples obtained from healthy donors or patients in whom no hematological malignancy could be detected (e.g. BM samples submitted for lymphoma staging, neuroblastoma staging) were used as control BM for normal/reactive BCP cells. BM samples obtained from pediatric ALL patients after induction therapy (day 78 of therapy) or one year after stop of therapy, proven to be MRD-negative by RQ-PCR analysis, were used as source of regenerating BCP. In the first part of the study (panel design and optimization), 319 BCP-ALL patients which were consecutively received during five design-test-evaluate-redesign phases (initial phase: n=69; phase 1: n=61; phase 2: n=28; phase 3: n=78; phase 4: n=83) were included. In the second part of the study (MRD analysis), 377 follow-up samples obtained from 178 BCP-ALL patients (day 15: n= 111; day 33: n= 139; day 78: n= 107; other time points: n=20) were included. Patient characteristics are summarized in Table 1. The institutional review board of each participating center approved this study and informed consent for study participation was obtained from each patient and/or his/her legal guardian.

Immunophenotyping MRD panel design

First, BM samples obtained from 69 BCP-ALL patients at diagnosis were stained with the EuroFlow BCP-ALL antibody panel (23 different antibodies in four 8-color tubes) [18]. The subsequently designed and optimized MRD tubes were tested during phase 1 to 4 on diagnostic BM samples from BCP-ALL patients using the standardized EuroFlow sample preparation and instrument set-up protocols [18,19]. Data were analyzed using Infinicyt software by comparing BCP-ALL cells with the nearest normal/reactive BCP subsets using APS plots (see Supplemental Methods) as illustrated in Figure 1 and Supplemental Figure 1 and 2. Regenerating BCP cells from 6 T-ALL patients were used as an additional negative control (Supplemental Figure 3).

Immunophenotyping MRD analyses

The finally selected BCP-ALL MRD tubes were evaluated on BM samples obtained during follow-up of BCP-ALL patients, using an optimized bulk-lysis protocol (see Results) [20]. BM samples were processed according to this new EuroFlow bulk-lysis protocol and subsequently stained using the regular EuroFlow protocol [19]. MRD analyses and interpretation were performed locally and data was subsequently sent to the BCP-ALL-MRD coordinator for central evaluation. Initial FCM-MRD data analysis was performed using two-dimensional dot plots for sequential gating of BCP-ALL cells, comparable to previous studies using 4-6 color stainings[10, 12]. For this study, we provisionally defined a minimum of

Table 1. Patient characteristics.

	Initial Phase		Phase 1		Phase 2		Phase 3		Phase 4		MRD phase	
Number	69		61		28		78		83		178	
Age (years)												
median	6		5		5		5		3		5	
min	0		1		1		0		0		0	
max	76		75		17		17		55		77	
Gender												
M	35	56%	40	66%	14	50%	46	59%	43	52%	94	53%
F	27	44%	21	34%	14	50%	32	41%	40	48%	84	47%
WBC (x10e9/L)												
median	13.4		8.2		13.7		10.9		15.9		8.5	
min	0.4		0.8		1.2		0.7		0.5		0.5	
max	818		87.6		312		595		1250		900	
No data	10		1		0		2		19		11	
Immunophenotype												
pro-B-ALL	8	13%	2	3%	4	14%	5	6%	6	7%	5	3%
common-ALL	44	73%	48	79%	20	71%	59	76%	56	67%	137	77%
pre-B-ALL	8	13%	11	18%	4	14%	13	17%	21	25%	35	20%
No data	7		0		0		1		0		1	
Genetic data[a]												
TEL-AML1	6	11%	15	27%	6	27%	11	16%	11	18%	45	26%
BCR-ABL	4	6%	1	2%	0	0%	3	4%	1	2%	4	2%
E2A-PBX1	0	0%	3	6%	0	0%	0	0%	0	0%	4	2%
MLL-AF4	4	6%	1	2%	2	7%	3	4%	4	6%	3	2%
MLL other	2	3%	1	2%	1	4%	1	1%	1	2%	2	1%
hyperdiplod	14	25%	27	48%	6	26%	26	37%	22	37%	67	43%
hypodiploid	0	0%	1	2%	1	4%	1	1%	1	2%	2	1%

[a] Genetic data were not available for all patients; percentages refer to positive patients per all analyzed patients.

10 clustered events to consider a sample as MRD positive (lower limit of detection, LOD) and a minimum of 40 clustered events for accurate quantitation of the MRD level (lower limit of quantitation, LLOQ) [2]. Inter-laboratory variability in data analysis was evaluated as described in the Supplemental Methods and Supplemental Figure 4).

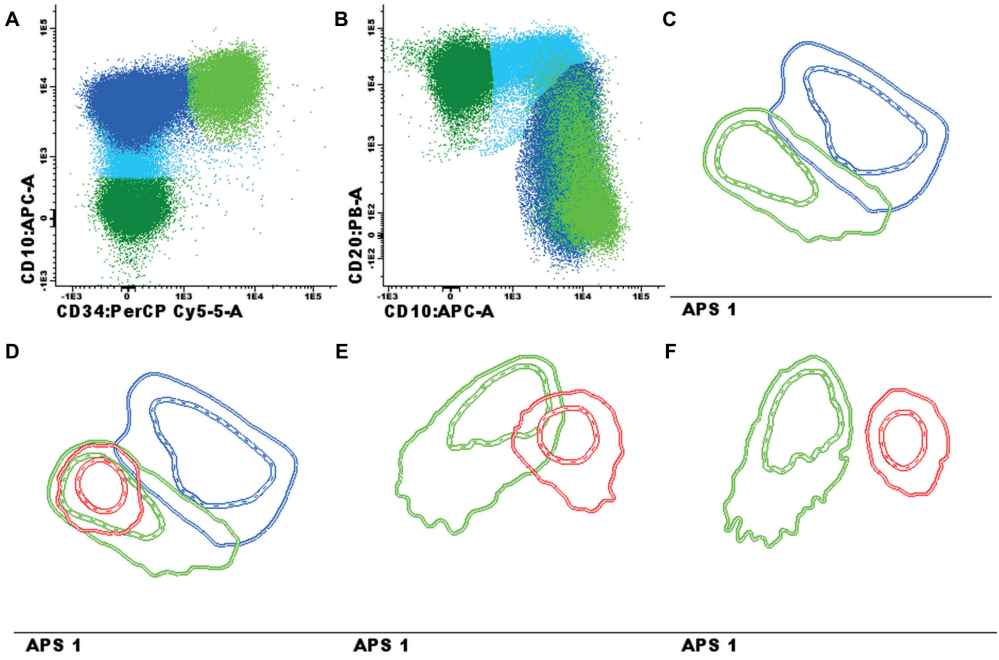

Figure 1. Data analysis strategy used to optimize the antibody panel for distinguishing between BCP-ALL cells and their nearest normal/reactive BCP counterpart.

First multiple normal/reactive BM samples and/or regenerating BM samples were merged (phase 1: n=7; phase 2: n=11; phase 3: n=14; phase 4: n=10) and CD19-positive B-cells were selected. These were subdivided in four B-cell subsets, based on the backbone markers (CD19/CD10/CD20/CD34/CD45): CD34+ pre-B-I cells (light green), CD34-/CD10+/CD20- to dim pre-B-II/immature cells (dark blue), CD34-/CD10+/CD20+ immature/transitional B-cells (light blue), and CD34-/CD10-/CD20+ mature B-cells (dark green). Dot plots of CD34 versus CD10 (**A.**) and CD10 versus CD20 (**B.**) are shown. The 1SD (dashed line) and 2SD lines (solid line) of the two most immature BCP subsets (pre-B-I (light green) and pre-B-II/immature (dark blue)) were displayed in an APS view, which was subsequently fixed (supervised; **C.**). Each individual BCP-ALL case was added to the fixed APS plot and the normal BCP population nearest to each of the BCP-ALL populations was defined (**D.**). The BCP-ALL cells and nearest normal BCP subset were then visualized in a separate (non-fixed and balanced) APS plot, one using the backbone markers only (**E.**) and one using all eight markers (**F.**), by plotting the 1SD curve and 2SD curves of the two populations. To prevent an influence of the number of cells on the PCA, we opted to use a balanced PCA, implying a fixed ratio between normal and pathological events. Finally, the separation between the two populations was scored, based on: no overlap between 2SD curves: 3 points; overlap of the 2SD curves: 2 points; overlap of the 2SD and the 1SD curve: 1 point; overlap of both 1SD curves: 0 points. An example of this scoring is shown in Supplemental Figure 1. It should be noted that the above described strategy was only used for optimizing the antibody panel for the BCP-ALL MRD tubes, and not for actual MRD analyses.

RQ-PCR-based MRD analyses

MRD levels were routinely determined by real-time quantitative PCR (RQ-PCR) analysis of rearranged immunoglobulin (IG) and/or T-cell receptor (TR) gene rearrangements in laboratories participating in the quality control rounds of the EuroMRD network (see www.EuroMRD.org) [3,22-26]. RQ-PCR data, performed in triplicate, were analyzed according to the EuroMRD guidelines, using the criteria to prevent false-negative MRD results [2]. Since application of these criteria might result in some false-positive RQ-PCR results [2], we performed next-generation sequencing (NGS) to confirm or to exclude the presence of MRD in discordant samples considered positive by RQ-PCR but negative by FCM.

NGS-based MRD analyses

NGS was generally performed as described previously [27]. Briefly, depending on the *IGH, TRG*, and/or *TRD* rearrangements applied as MRD targets in the RQ-PCR analysis, we performed a targeted approach: the follow-up samples were amplified using the multiplex primer set(s) of the relevant IG/TR locus only and data analysis was focussed on the specific junctional region sequence (i.e. the one used for RQ-PCR analysis). The primers for *TRG* were newly designed (Supplemental Table 1) and individual primer combinations from multiplex PCR were tested for sensitivity using NGS on diluted diagnostic ALL samples from patients with respective V and Jgamma segment combinations, all reaching the sensitivity of 10^{-5}. All data were finally scored as either MRD-positive or MRD-negative.

RESULTS

Design and optimization of 8-color MRD labeling for BCP-ALL

In the *initial phase*, five antibodies (CD19, CD45, CD34, CD10 and CD20) were upfront selected as backbone markers since they allow appropriate BCP gating as well as characterization of several BCP subpopulations, and are known to allow discrimination between normal BCP and BCP-ALL cells [10,28,29,30]. To evaluate which other markers could contribute to optimal separation of BCP-ALL cells from normal/reactive BCP cells, the EuroFlow BCP-ALL diagnosis panel [18] was applied to 69 BCP-ALL patients as well as to normal/reactive BM samples. Based on principal component analysis (visualized through APS plots) [16, 17, 19] of the BCP-ALL cells versus normal/reactive BCP cells (analyzed per tube), CD9, CD123, CD66c, CD81, CD24 and CD10 appeared to be markers that were most frequently differentially expressed (see Supplemental Figure 5). These markers were combined with the five backbone markers listed above and complemented with TdT and CD58, both previously reported to be of relevance for BCP-ALL MRD analyses [10,28,29,31]. The remaining open position was filled in with surface membrane (Sm) IgKappa/IgLambda, as

a potential exclusion maker for more mature BCPs. Fluorochrome positions were primarily determined based on the position of the involved markers in the EuroFlow BCP-ALL panel [18].

The resulting three *Phase-1* MRD tubes (Table 2) were subsequently tested on 61 consecutive BCP-ALL patients at diagnosis and the discriminatory power was evaluated by comparing the leukemic BCP with the nearest normal BCP subset in APS plots. Whereas both tube 1 and tube 3 gave good/fair separation in approximately 60% of cases, tube 2 was clearly less informative (fair/good separation in <35% of cases)(Figure 2). When the tube providing the best separation for each patient was selected, good/fair separation was observed in 77% of cases. Considering only tube 1 and 3, good/fair separation was still observed in 71% of cases. These data indicate that tube 1 and 3 had complementary value and confirm the limited value of tube 2.

To evaluate the relevance of each individual marker in discriminating BCP-ALL cells from normal/reactive BCP cells, those markers that received a weight over 10% in the first or second prinicipal component in an APS view of the nearest normal BCP cells and

Table 2. Development and design of the EuroFlow BCP-ALL MRD panel[a].

Phase	Violet laser		Blue laser				Red laser	
Initial[b]	**PB**	**PO**	**FITC**	**PE**	**PerCP Cy5.5**	**PECy7**	**APC**	**APC H7**
	CD20	CD45	CD58	CD66c	CD34	CD19	CD10	CD38
	CD9	CD45	TdT	CD13	CD34	CD19	CD22	CD24
	CD21	CD45	CD15/CD65	NG2	CD34	CD19	CD123	CD81
1	**PB**	**PO**	**FITC**	**PE**	**PerCP Cy5.5**	**PECy7**	**APC**	**APC H7**
	CD20	CD45	CD58	CD66c	CD34	CD19	CD10	CD38
	CD20	CD45	TdT	SmIgK/L	CD34	CD19	CD10	CD24
	CD20	CD45	CD9	CD123	CD34	CD19	CD10	CD81
2	**PB**	**PO**	**FITC**	**PE**	**PerCP Cy5.5**	**PE Cy7**	**APC**	**APC H7**
	CD20	CD45	CD9	CD22	CD34	CD19	CD10	CD38
	CD20	CD45	CD123	CD66c	CD34	CD19	CD10	CD24
3	**PB**	**PO**	**FITC**	**PE**	**PerCP Cy5.5**	**PE Cy7**	**APC**	**APC C750**
	CD20	CD45	CD9 (ML13)	CD66c/CD123	CD34	CD19	CD10	CD38
	CD20	CD45	CD58	CD22	CD34	CD19	CD10	CD81
4	**PB**	**PO**	**FITC**	**PE**	**PerCP Cy5.5**	**PE Cy7**	**APC**	**APC C750**
	CD20	CD45	CD81	CD66c/CD123	CD34	CD19	CD10	CD38
	CD20	CD45	CD81	CD73/CD304	CD34	CD19	CD10	CD38

[a] Markers that were changed as compared to the previous panel are marked grey.

[b] Only tube 1, 3 and 4 of the EuroFlow BCP-ALL diagnosis panel were evaluated, since most markers in tube 2 (Cyμ, SmIgK, SmIgL, SmIgM) were not expected to contribute to separation of normal and malignant BCP cells.

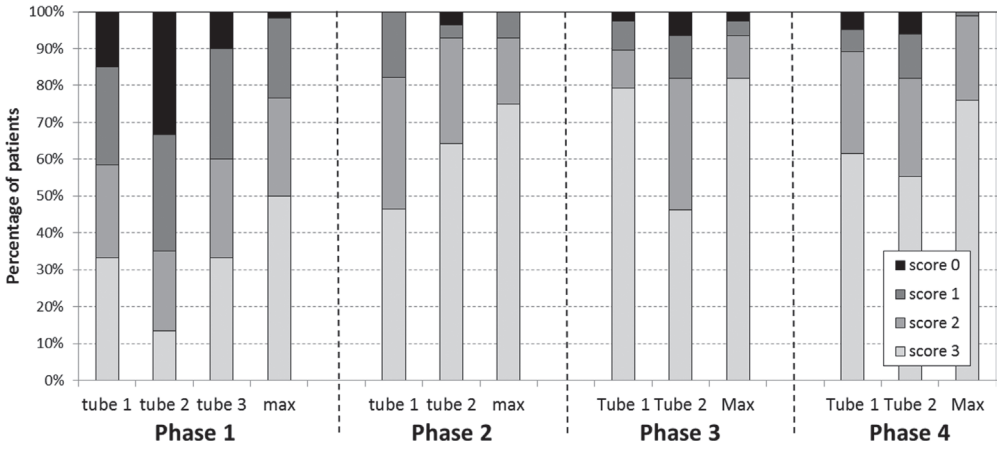

Figure 2. Power to distinguish BCP-ALL cells from their nearest normal BCP counterpart using the EuroFlow BCP-ALL MRD tubes.

Data reflect the percentage of patients that reached the specified score, obtained as described in Supplemental Figure 1. Briefly, for each patient BCP-ALL cells and their nearest normal BCP subset were visualized in a (non-fixed and balanced) APS plot showing the median, 1SD curves and 2SD curves for both populations. Each patient was subseqently scored as follows: no overlap between 2SD curves: 3 points; overlap of the 2SD curves: 2 points; overlap of the 2SD and the 1SD curve: 1 point; overlap of both 1SD curves: 0 points. Max refers to the maximal score of the individual tubes. Phase 1: seven normal/reactive BM samples and 61 BCP-ALL patients; Phase 2: seven normal BM samples, four regenerating BM samples, and 28 BCP-ALL patients; Phase 3: five normal/reactive BM samples, nine regenerating BM samples, and 78 BCP-ALL patients; Phase 4: ten normal/reactive BM samples and 83 BCP-ALL patients).

the BCP-ALL cells were selected. CD66c (80% of cases), CD9 (63%), and CD123 (55%) contributed most frequently.

Based on these Phase-1 BCP-ALL results, the panel was redesigned: CD58, TdT, SmIgK/L, and CD81 were (at least provisionally) excluded, whereas CD22, which might be important for gating of B-cells in case of CD19-targeting therapies, was included (Table 2).

The *Phase*-2 BCP-ALL MRD tubes were evaluated on diagnostic samples from 28 consecutive BCP-ALL patients. Good/fair separation between BCP-ALL cells and their nearest normal/reactive BCP counterpart was possible in approximately 75% of cases in both tubes (Figure 2), showing significant improvement over the Phase 1 tubes. If the best score of both tubes was used for each case, over 85% of BCP-ALL cases showed good/fair separation from the corresponding normal BCP subset and in only 3 cases (12%) separation was poor.

During Phase-2, additional studies were performed: 1) Because of non-optimal (relatively weak) CD9 (MEM61) staining, another CD9 clone (ML13) was evaluated with much stronger results; 2) Two newly available fluorochromes (APC-C750 and APC-A750) showed

lower background than APC-H7 (less binding to apoptotic cells; no binding to monocytes); 3) More detailed evaluation of the usefulness of CD81 versus CD24 (re-evaluation of Phase 1 data) showed that CD81 was more frequently differentially expressed between normal/reactive BCP cells and BCP-ALL cells and showed that CD81 in combination with only the backbone markers resulted in a higher percentage of cases with good separation than CD24 did (31% versus 20%); 4) Because CD66c and CD123 are both virtually negative on normal/reactive BCP cells, we tested whether these markers could be combined in the PE channel and concluded that background levels were not affected by combining these two markers (data not shown). Based on these data, the new CD9 clone was included in the MRD panel, APC-H7 was replaced by APC-C750/A750, CD24 was replaced by CD81, and CD66c and CD123 were combined into one fluorescence channel. The open FITC position was used for further evaluation of CD58. The combined data provided the Phase-3 BCP-ALL MRD tubes (Table 2).

The two *Phase-3* BCP-ALL MRD tubes were evaluated on 78 BCP-ALL patients. Overall, tube 1 resulted in good/fair separation in 90% of cases, whereas this was achieved in 82% of cases for tube 2 (Figure 2). In the three cases for which tube 1 did not result in good separation, normal/reactive BCP and BCP-ALL cells could be separated in tube 2, mainly due to differential expression of CD81. Further evaluation showed that CD38 (~35% of cases), CD66c/CD123 (~30%), and CD81 (~19%) improved the separation between normal/reactive and malignant BCP cells as compared to the five backbone markers only, whereas CD9, CD58 and CD22 had no or limited additional value. CD9 in tube 1 was therefore replaced by CD81-FITC (which demonstrated equally good staining patterns as CD81-APC-C750) and tube 2 was discarded.

Since in a few cases the evaluated MRD tubes did still not yet result in sufficient separation between normal/reactive and malignant BCP cells, we evaluated several other markers reported to be of potential interest for MRD analysis (e.g.: CD44-FITC, CD27-PE, CD164-FITC, CD73-PE, CD49f-FITC, CD200-PE, CD86-FITC, and Drebrin-PE) [32-36]. Based on initial testing on diagnostic BCP-ALL samples, CD73 and CD304 appeared to be most promising based on the level and frequency of overexpression (~20% for CD73 and ~40% for CD304) and their stability during follow-up (data not shown). Since it appeared not to be possible to combine these two markers with CD66c and CD123 in a single fluorescence channel (due to too high background levels), a second tube was designed; this tube was identical to tube 1 but with CD73/CD304 instead of CD66c/CD123 in the PE channel (Table 2).

The two *Phase-4* BCP-ALL MRD tubes were run on 83 consecutive diagnostic BCP-ALL samples. Overexpression of CD66c/CD123 or CD73/CD304 was observed in 45% and 46% of cases, respectively; 31% of cases did not show overexpression of either CD66c/CD123 or CD73/CD304. Tube 1 resulted in good/fair separation in 89% of cases, whereas this was

attained in 82% of cases for tube 2 (Figure 2). If the best score of both tubes was used, 99% of cases showed good/fair separation between the BCP-ALL cells and the nearest normal/reactive BCP subset. Therefore, tube 1 and tube 2 were complementary to each other and one might either decide at diagnosis which tube is best for monitoring the particular patient or use both tubes to have an extra internal control and more precise measurements. These two optimized tubes were considered to be final and ready for further evaluation in follow-up samples of BCP-ALL patients.

Optimization of the flowcytometric MRD sample preparation protocol

We aimed for a sensitivity of $\leq 10^{-5}$, at least comparable to the sensitivity reached in RQ-PCR-based MRD analysis. If a cluster of 10-40 BCP-ALL cells should be present to consider a sample as positive, one should acquire at least 4 million cells in order to reach the required sensitivity. Since the cellularity of BM samples obtained during the early phases of treatment is frequently low [37], staining whole BM samples using the regular EuroFlow protocols would not allow acquisition of millions of cells. We therefore designed and tested a new EuroFlow erythrocyte bulk-lysis procedure: sufficiently large volumes of BM, i.e. containing >10 million cells, are lysed and the leukocytes are subsequently resuspended in a small volume of washing buffer. This new protocol allowed staining of 10 million cells in 100 µl cell suspension per tube (Supplemental Table 2). Evaluation of this new protocol showed that the percentage of doublets did not increase, that the number of evaluable leukocytes increased significantly, and that there were no major differences in cellular composition as compared to the regular EuroFlow staining protocol (Figure 3). Given the large increase in the number of cells stained with this new approach, all antibody titers were re-evaluated; modifications appeared not to be necessary.

Evaluation of the EuroFlow BCP-ALL MRD tube

To evaluate whether the newly designed high-throughput EuroFlow BCP-ALL MRD strategy performed well, we tested the final MRD tubes on follow-up samples of BCP-ALL patients. Based on the immunophenotype of the BCP-ALL cells at diagnosis, one MRD tube was selected and subsequently used for MRD evaluation. First, flowcytometric MRD data obtained in 178 BCP-ALL patients were compared with routinely obtained PCR-MRD data. As shown in Figure 4A, the concordance between the FCM-MRD data and PCR-based MRD data was highly dependent on the number of cells acquired by flow cytometry. In addition, the sensitivity of FCM-MRD (percentage samples positive by both FCM and PCR relative to samples positive by PCR) significantly increased when higher cell numbers were acquired (Figure 4B). Therefore, only samples in which MRD could clearly be detected by FCM-MRD or samples which had sufficient cells acquired for reaching a sensitivity of $\leq 10^{-5}$ were included in the subsequent analyses. Based on a LLOQ of 40 events, at least $4x10^6$

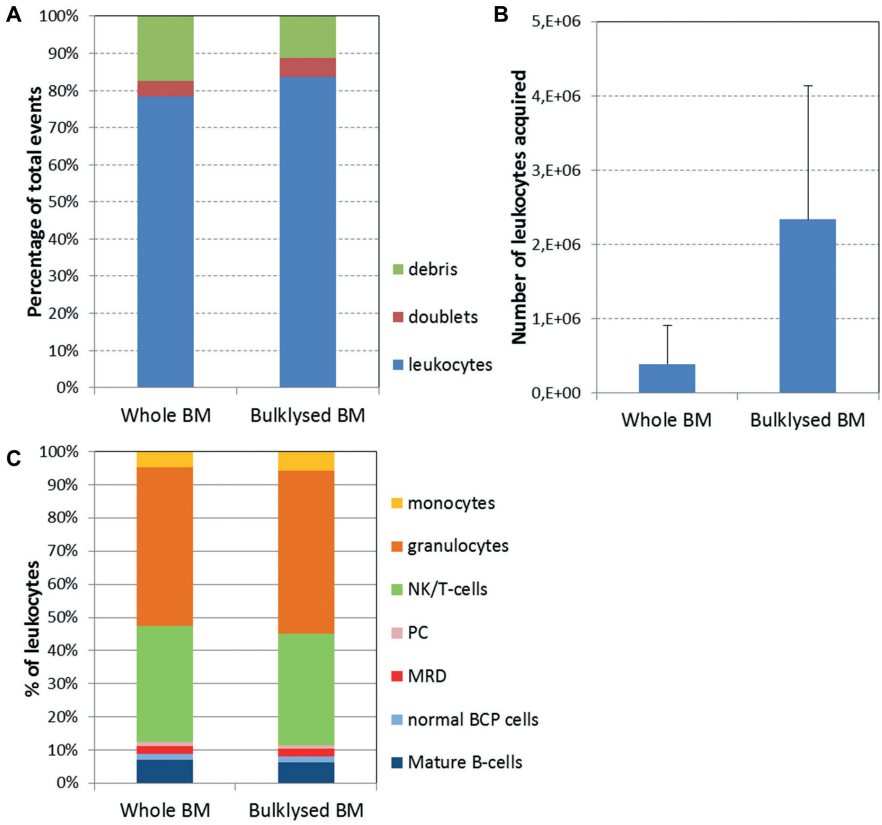

Figure 3. Evaluation of the EuroFlow bulk-lysis protocol.

BM samples (day 15: n=15; day 33: n=15; day 78: n=12) were stained with the standard EuroFlow protocol (FL) and with the EuroFlow bulk-lysis protocol (BL). **A.** Number of leukocytes, debris and doublets, calculated as percentage of acquired events. Using BL, significantly less debris (p=0.032 by paired t-test) and significantly more leukocytes (p=0.03 by paired t-test) were measured. There were no significant differences between the two methods for the percentage of doublets. **B.** Absolute number of leukocytes acquired. Using BL, on average 12-fold more leukocytes could be acquired (p<0.0001). Please note that we included relatively many day 15 samples in order to be able to evaluate the impact of the two methods on the MRD levels as well. However, these day 15 samples generally have a very low WBC; consequently, the number of leukocytes acquired after BL is still relatively low in a subset of samples. **C.** Distribution of leukocyte subpopulations, defined as percentage of leukocytes. By paired t-test (two-sided), small but statistically significant differences were observed for T/NK cells (mean: 24% versus 26%, p=0.0047), granulocytes (mean: 33% versus 38%, p<0.001) and monocytes (mean: 3.2% versus 4.5%, p<0,001) between FL and BL respectively, whereas no significant differences were observed for the remaining populations. Of note, in two samples MRD was only detected using BL (0.013% and 0.018%) but not using FL. In the 11 samples MRD positive by both methods, MRD levels were not significantly different from each other (paired t-test: p=0.30), with mean values of 6.3% and 6.7% by FL and BL method, respectively. Correlation analysis showed a Spearman r of 0.964 (95% CI: 00.857-0.991; p<0.0001).

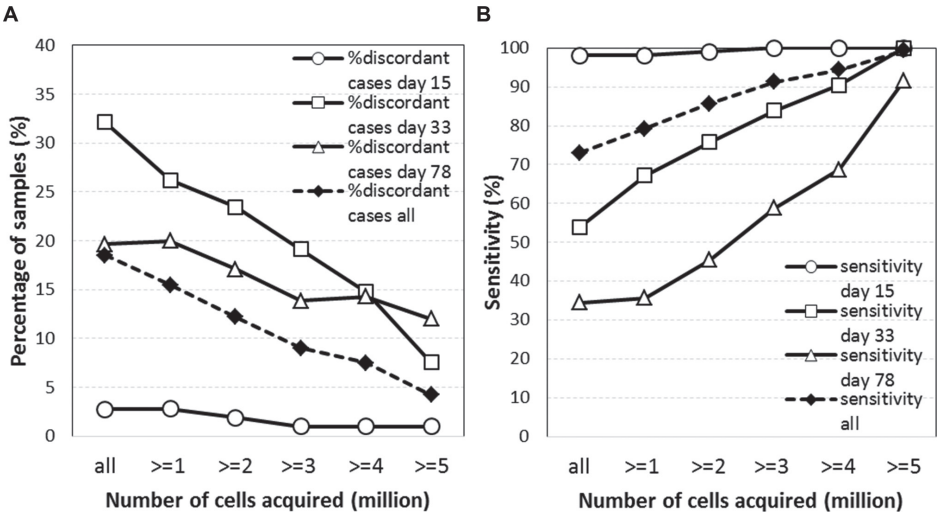

Figure 4. Performance of FCM-MRD versus PCR-based MRD is dependent on the number of acquired cells. **A.** The percentage of discordant cases by FCM-MRD and PCR-MRD is shown for individual time-points (day 15, day 33, and day 78) as well as for all samples together. Data are presented for variable numbers of acquired cells: all samples (independent of cell number) and samples with at least 1, 2, 3, 4, or 5 million cells acquired. **B.** The sensitivity of FCM-MRD relative to PCR-MRD is shown for individual time-points (day 15, day 33, and day 78) as well as for all samples together. Data are presented for variable numbers of acquired cells: all samples (independent of cell number; n=377) and samples with at least 1 (n=330), 2 (n=287), 3 (n=255), 4 (n=227), or 5 million cells (n=191) acquired. Sensitivity is calculated as the number of samples positive by both FCM and PCR divided by the total number of samples positive by PCR (i.e. the reference method).

cells should be acquired, which was possible in 227 out of 377 samples (60%). FCM-MRD data obtained in these patients was comparable to PCR-based MRD results in 93% of samples (Table 3 and Figure 5). All but one of the 17 discordant samples (seven FCM+/PCR- and ten FCM-/PCR+) had MRD levels $<10^{-4}$ (Supplemental Table 3). Bland–Altman analysis showed higher PCR-based MRD values with a mean difference of 0.34 log or factor 2.2 (Supplemental Figure 6).

Detailed evaluation of discordant cases

To evaluate the discordant cases, several additional analyses were performed. First, flow cytometry FCS data files were blindly distributed to four laboratories for re-analysis of the FCM-MRD data. Out of the seven cases initially scored positive by FCM-MRD and negative by PCR-MRD, six were interpreted as negative by all four centers upon FCM-MRD re-analysis, while one sample (day 15) was consistently scored positive by all four centers. Second, RQ-PCR-MRD data were checked for cases negative by FCM-MRD and positive by PCR-MRD. In eight of ten cases (all confirmed to be FCM-MRD negative by re-analysis

Table 3. Concordance between flowcytometric and molecular MRD data.[a]

	Day 15	Day 33	Day 78	Other TP	Total	%	%
Concordant							
FCM+/PCR+	102	47	11	9	169	74	93
FCM-/PCR-	1	5	31	4	41	18	
Discordant							
FCM-/PCR+	0	5	5	0	10	4	7
FCM+/PCR-	1	4	2	0	7	3	
Total	**104**	**61**	**49**	**13**	**227**	**100**	

[a] Only samples in which MRD could clearly be detected by FCM-MRD or samples which had at least $4x10^6$ cells acquired were included in the analyses. Based on a LLOQ of 40 events, this allowed a sensitivity of at least 10^{-5}.

in different centers), PCR-MRD data were considered positive based on a single well in a single target. To further evaluate whether this low-level positivity was potentially caused by nonspecific amplification, NGS was used to confirm the possible presence of the leukemia-specific antigen-receptor rearrangement. In seven out of nine available samples, NGS-MRD was negative, whereas MRD-positivity could be confirmed in the remaining two patients. Thus, 6/17 (35%) discordant cases were due to initial misinterpretation of the FCM-MRD data and at least 7/17 (41%) was due to over-interpretation of PCR-MRD data; the remaining 4 cases appeared to be truly discordant cases (Supplemental Table 3). After these additional evaluations the actual concordance increased to 98%. If only samples with MRD levels <0.01% were included, 97% gave concordant results.

DISCUSSION

After five phases of optimization, we finally selected two 8-color antibody tubes which only differed for the markers present in the PE channel (CD66c/CD123 versus CD73/CD304). These tubes are comparable with 8-color BCP-ALL MRD tubes recently used in other studies, since all proposed panels include CD19, CD10, CD20, CD34, and CD45. In our study, these markers were considered as backbone markers from start onwards, based on our previous experience [10, 12, 18, 28-30]. Also CD38 is present in all proposed panels and was proven to be relevant in our present study, as well as in the studies of Karawajew et al. [14] and Shaver et al [15]. The remaining two positions were completed with different markers: CD9, CD13/CD33, CD15/NG2, CD58 (two studies), CD66c (two studies), CD73, CD81, CD123, CD304, and a nucleic acid dye. In our analysis, CD9, CD58, and CD22 appeared be of limited value and were therefore discarded, while Shaver and colleagues, who also applied mathematical modelling systems, identified these as important MRD markers [15].

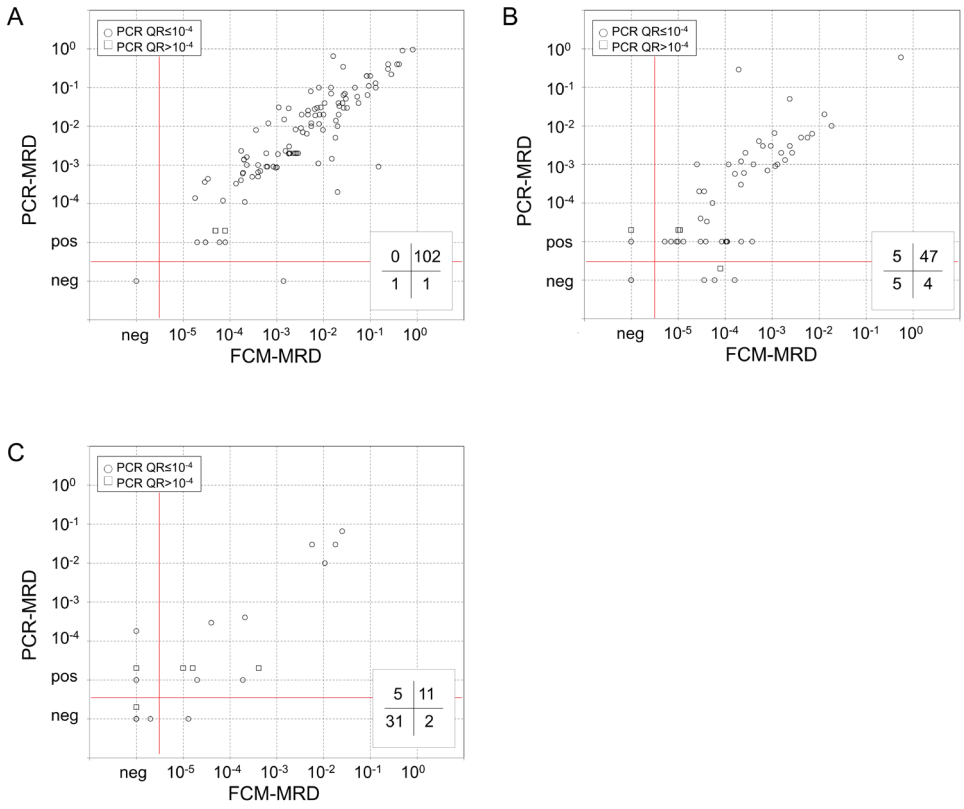

Figure 5. Comparison of MRD data obtained by 8-color EuroFlow flow cytometry and routinely obtained molecular MRD data.

Flowcytometric MRD data were compared with molecular MRD data and are shown for samples obtained at day 15 (**A**), day 33 (**B**), or day 78 (**C**). In the lower right part of each panel the number of FCM-/PCR+, FCM+/PCR+, FCM+/PCR-, and FCM-/PCR- is indicated. Only samples in which MRD could clearly be detected by FCM-MRD or samples which had sufficient cells acquired for reaching a sensitivity of $\leq 10^{-5}$ (i.e. $\geq 4 \times 10^{6}$ cells acquired) were included in the analyses. Based on a LOD of 10 events, the sensitivity of FCM-MRD was 2.5×10^{-6}; the quantitative range (based on a LLOQ of 40 events) was 10^{-5}. Consequently, FCM-MRD data between 2.5×10^{-6} and 10^{-5} should be considered as positive, but are below the limit of quantitation.

However, they did not test CD66c, CD73, CD123, or CD304 and the difference between the contribution of CD9 and CD81 in their study was limited [15]. CD15/NG2 might be relevant in ALL with *MLL* gene rearrangements, mainly occurring in infants [38]. These cases, however, are rare and frequently present with a pro-B-ALL immunophenotype which can relatively easily be distinguished from normal BCP cells and plasma cells [39]. In our study, we tested

and finally selected four markers that are frequently abnormally expressed on BCP-ALL cells: CD66c (associated with *BCR-ABL* and hyperdiploidy) [40, 41], CD123 (associated with hyperdiploidy [42]), CD73 [36], and CD304 (possibly associated with *TEL-AML1*) [33]. By combining two of these markers in a single fluorescence channel, abnormal expression could be identified in approximately 70% of BCP-ALL patients. Furthermore, in combination with the backbone markers and CD81, BCP-ALL cells could clearly be distinguished from normal BCP cells in virtually all patients. Thus, after multiple phases of multicenter testing of a wide range of leukocyte markers, antibody clones and fluorochrome-conjugated reagents using objective novel software tools, we were able to select two highly effective BCP-ALL MRD tubes.

It remains to be evaluated whether the designed BCP-ALL MRD tubes can also be used during antibody-based therapies. Especially Blinatumomab and CAR-T-cells (targeting CD19) may hamper the gating of BCP based on CD19. Although alternative gating strategies can be applied (e.g. based on CD10, CD34 and/or CD45), one could also decide to add CD24 and/or CD22 to the current tubes (transforming it into a 10-color tube) in MRD-based trials involving Blinatumomab [43]. Addition of CD24 and CD22 will also have the advantage that the earliest BCP cells, expressing CD24 and/or CD22 but not yet CD19 [44], can be identified; this may be of relevance for the identification of all BCP cells in regenerating BM samples.

In order to obtain MRD data with good sensitivity, acquisition of large numbers of cells appears to be a prerequisite. There is no consensus yet about the number of cells needed for a population. Most studies in BCP-ALL indicate a minimum number between 10 and 50 events, while a recent consensus report on MRD detection in multiple myeloma patients defined 20 and 50 cells as the LOD and LLOQ, respectively [21,14,45]. Consequently, a sensitivity of 10^{-5} (generally reached in PCR-MRD and NGS-MRD analysis) requires acquisition of $\geq 10^6$ cells, preferably $\geq 5x10^6$ cells. We therefore developed the new Euroflow bulk lysis protocol, allowing acquisition of such high cell numbers. Although the bulk lysis protocol contains several washing steps, which will likely result in some cell loss, there is no evidence for selective loss of BCP-ALL cells, given the high concordance between the final FCM-MRD results and the molecular MRD results. To our best knowledge, other FCM-MRD studies so far have not acquired $\geq 4x10^6$ events and therefore could not have reached the same sensitivity as shown here, although the study by the ALL-REZ-BFM 2002 trial group comes close [14]. Our data clearly shows that acquisition of large numbers of cells ($\geq 4x10^6$) is a prerequisite for obtaining good sensitivities and data which are truly comparable to PCR-MRD data.

We finally tested the newly designed and optimized BCP-ALL MRD tubes in combination with the bulk-lysis protocol on follow-up samples from BCP-ALL patients and compared the FCM-MRD data with PCR-MRD data. The concordance between both methods (in the absence of any cut-off) was extremely high (93%), and was significantly better than in

previous studies (82.3% [10] and 86.5% [14]). As mentioned above, this increased concordance is likely due to the higher sensitivity of the current study, resulting from the higher number of cells analyzed. Detailed evaluation of the discordant samples using NGS-based approaches showed that several discrepant cases were due to over-interpretation of the PCR-MRD data, as the involved leukemia-specific IG/TR rearrangements could not be detected by (qualitative) NGS analysis. Consequently, it is most likely that in these discordant cases the positive RQ-PCR MRD data, interpreted according to the EuroMRD criteria for prevention of false-negative MRD results, are due to non-specific amplification [2,10,47,47] and that these samples actually were MRD-negative.

Next to these "false-positive PCR-MRD" samples, part of the initially discordant cases could be explained by "false-positive FCM-MRD" results: samples were initially scored MRD-positive (generally at very low levels of <0.01%), but these samples were consistently scored MRD-negative upon blind re-analysis at four different centers. Interpretation of FCM-MRD data, especially at MRD levels <0.01%, is still expert-based and depends on the number of events in the suspected population, their distance from normal, and the homogeneity of the suspected population (clustering of suspected cells). Whereas the number of events may easily be defined, distance from normal, and homogeneity of the population are more complex to be objectively defined. Novel software tools, including automated gating approaches and maturation pathway analysis (Supplemental Figure 7), are currently being developed within the EuroFlow consortium and will facilitate FCM-MRD in BCP-ALL in the near future [37]. Preliminary maturation-based FCM-MRD data showed very good concordance with PCR-MRD data, although further improvements are needed for detection of low levels of MRD (<0.01%).

The NGS-MRD analyses and re-analyses of FCM-MRD data increased the concordance to an unprecedented rate of 98%; the remaining discordant cases are likely due to statistical variation around the detection limits of both assays [14]. Therefore, the here presented EuroFlow FCM-MRD strategy proved to be highly sensitive (at least comparable to PCR-MRD) and fast, and allows standardized quantification of MRD in virtually all BCP-ALL patients. By increasing the number of acquired cells to 10^7 (e.g. by running both tubes with $5x10^6$ cells), the sensitivity and robustness likely can even be further increased.

ACKNOWLEDGEMENTS

The research was performed within the EuroFlow Consortium, which started with an EU-FP6 grant (LSHB-CT-2006-018708) and obtained sustainability by protecting and licensing intellectual property, thereby obtaining royalties, which are exclusively being used for supporting the EuroFlow research program (chairmen: JJMvD and AO).

We gratefully acknowledge Tomas Kalina and the technicians of the Laboratory for Medical Immunology, Erasmus MC, for technical assistance. We thank Christa Homburg and colleagues for performing molecular MRD analyses of part of the Dutch patients. We thank Marieke Comans-Bitter for organizational support. EF was supported by the Grant Agency of the Czech Republic (GACR, project of Centre of Excellence No. P302/12/G101). LS, TS and PT were supported by ERA-NET PrioMedChild, grant 40-41800-98-027. EM was supported by Ministry of Health of the Czech Republic, grant nr. 15-28525A. MK was supported by the University Hospital Motol, Prague, Czech Republic (00064203). ECS, QL and AO acknowledge the Bilateral Cooperation Program between Coordenação de Aperfeiçoamento de Pessoal de Nível Superior CAPES (Brasília/Brazil) and Dirección General de Políticas Universitárias – Ministério de Educación, Cultura y Deportes DPGU (Madrid/Spain) (311/15). ESC acknowledges FAPERJ, Rio de Janeiro, Brazil (E26/110.105/2014; E26/102.191/2013) and Conselho Nacional de Desenvolvimento Científico e Tecnológico – CNPQ of Brazil (400194/2014-7). GG, CB and PB were supported by Fondazione Tettamanti. We gratefully acknowledge the contribution of the EuroClonality/EuroMRD NGS network (chair: A.W. Langerak) for support with the NGS data. The research for this manuscript was in part performed within the framework of the Erasmus Postgraduate School Molecular Medicine.

REFERENCES

1. Flohr T, Schrauder A, Cazzaniga G, Panzer-Grumayer R, van der Velden V, Fischer S, et al. Minimal residual disease-directed risk stratification using real-time quantitative PCR analysis of immunoglobulin and T-cell receptor gene rearrangements in the international multicenter trial AIEOP-BFM ALL 2000 for childhood acute lymphoblastic leukemia. Leukemia 2008; 22:771-782.
2. van der Velden VH, Cazzaniga G, Schrauder A, Hancock J, Bader P, Panzer-Grumayer ER, et al. Analysis of minimal residual disease by Ig/TCR gene rearrangements: guidelines for interpretation of real-time quantitative PCR data. Leukemia 2007; 21:604-611.
3. van der Velden VH, van Dongen JJ. MRD detection in acute lymphoblastic leukemia patients using Ig/TCR gene rearrangements as targets for real-time quantitative PCR. Methods Mol Biol 2009; 538:115-150.
4. Basso G, Veltroni M, Valsecchi MG, Dworzak MN, Ratei R, Silvestri D, et al. Risk of relapse of childhood acute lymphoblastic leukemia is predicted by flow cytometric measurement of residual disease on day 15 bone marrow. J Clin Oncol 2009; 27:5168-5174.
5. Borowitz MJ, Wood BL, Devidas M, Loh ML, Raetz EA, Salzer WL, et al. Prognostic significance of minimal residual disease in high risk B-ALL: a report from Children's Oncology Group study AALL0232. Blood 2015; 126:964-971.

6. Cheng SH, Lau KM, Li CK, Chan NP, Ip RK, Cheng CK, et al. Minimal residual disease-based risk stratification in Chinese childhood acute lymphoblastic leukemia by flow cytometry and plasma DNA quantitative polymerase chain reaction. PLoS One 2013; 8:e69467.
7. Stow P, Key L, Chen X, Pan Q, Neale GA, Coustan-Smith E, et al. Clinical significance of low levels of minimal residual disease at the end of remission induction therapy in childhood acute lymphoblastic leukemia. Blood 2010; 115:4657-4663.
8. Weng XQ, Shen Y, Sheng Y, Chen B, Wang JH, Li JM, et al. Prognostic significance of monitoring leukemia-associated immunophenotypes by eight-color flow cytometry in adult B-acute lymphoblastic leukemia. Blood Cancer J 2013; 3:e133.
9. Dworzak MN, Froschl G, Printz D, Mann G, Potschger U, Muhlegger N, et al. Prognostic significance and modalities of flow cytometric minimal residual disease detection in childhood acute lymphoblastic leukemia. Blood 2002; 99:1952-1958.
10. Denys B, van der Sluijs-Gelling AJ, Homburg C, van der Schoot CE, de Haas V, Philippe J, et al. Improved flow cytometric detection of minimal residual disease in childhood acute lymphoblastic leukemia. Leukemia 2013; 27:635-641.
11. Ryan J, Quinn F, Meunier A, Boublikova L, Crampe M, Tewari P, et al. Minimal residual disease detection in childhood acute lymphoblastic leukaemia patients at multiple time-points reveals high levels of concordance between molecular and immunophenotypic approaches. Br J Haematol 2009; 144:107-115.
12. Gaipa G, Cazzaniga G, Valsecchi MG, Panzer-Grumayer R, Buldini B, Silvestri D, et al. Time point-dependent concordance of flow cytometry and RQ-PCR inminimal residual disease detection in childhood acute lymphoblasticleukemia. Haematologica 2012; 97: 1582-1593.
13. Thorn I, Forestier E, Botling J, Thuresson B, Wasslavik C, Bjorklund E, et al. Minimal residual disease assessment in childhood acute lymphoblastic leukaemia: a Swedish multi-centre study comparing real-time polymerase chain reaction and multicolour flow cytometry. Br J Haematol 2011; 152:743-753.
14. Karawajew L, Dworzak M, Ratei R, Rhein P, Gaipa G, Buldini B, et al. Minimal residual disease analysis by eight-color flow cytometry in relapsed childhood acute lymphoblastic leukemia. Haematologica 2015; 100:935-944.
15. Shaver AC, Greig BW, Mosse CA, Seegmiller AC. B-ALL minimal residual disease flow cytometry: an application of a novel method for optimization of a single-tube model. Am J Clin Pathol 2015; 143:716-724.
16. Pedreira CE, Costa ES, Almeida J, Fernandez C, Quijano S, Flores J, et al. A probabilistic approach for the evaluation of minimal residual disease by multiparameter flow cytometry in leukemic B-cell chronic lymphoproliferative disorders. Cytometry A 2008; 73A:1141-1150.
17. Pedreira CE, Costa ES, Barrena S, Lecrevisse Q, Almeida J, van Dongen JJ, et al. Generation of flow cytometry data files with a potentially infinite number of dimensions. Cytometry A 2008; 73:834-846.

18. van Dongen JJ, Lhermitte L, Bottcher S, Almeida J, van der Velden VH, Flores-Montero J, et al. EuroFlow antibody panels for standardized n-dimensional flow cytometric immunophenotyping of normal, reactive and malignant leukocytes. Leukemia 2012; 26:1908-1975.
19. Kalina T, Flores-Montero J, van der Velden VH, Martin-Ayuso M, Bottcher S, Ritgen M, et al. EuroFlow standardization of flow cytometer instrument settings and immunophenotyping protocols. Leukemia 2012; 26:1986-2010.
20. Aalbers AM, van den Heuvel-Eibrink MM, Baumann I, Dworzak M, Hasle H, Locatelli F, et al. Bone marrow immunophenotyping by flow cytometry in refractory cytopenia of childhood. Haematologica 2015; 100:315-323.
21. Arroz M, Came N, Lin P, Chen W, Yuan C, Lagoo A, et al. Consensus guidelines on plasma cell myeloma minimal residual disease analysis and reporting. Cytometry B Clin Cytom 2016; 90:31-39.
22. van der Velden VHJ, Willemse MJ, van der Schoot CE, Hahlen K, van Wering ER, van Dongen JJM. Immunoglobulin kappa deleting element rearrangements in precursor-B acute lymphoblastic leukemia are stable targets for detection of minimal residual disease by real-time quantitative PCR. Leukemia 2002; 16:928-936.
23. van der Velden VHJ, Wijkhuijs JM, Jacobs DC, van Wering ER, van Dongen JJM. T cell receptor gamma gene rearrangements as targets for detection of minimal residual disease in acute lymphoblastic leukemia by real-time quantitative PCR analysis. Leukemia 2002; 16:1372-1380.
24. van der Velden VH, de Bie M, van Wering ER, van Dongen JJ. Immunoglobulin light chain gene rearrangements in precursor-B-acute lymphoblastic leukemia: characteristics and applicability for the detection of minimal residual disease. Haematologica 2006; 91:679-682.
25. Szczepanski T, van der Velden VHJ, Hoogeveen PG, De Bie M, Jacobs DCH, Van Wering ER, et al. V{delta}2-J{alpha} gene rearrangements are frequent in precursor-B-acute lymphoblastic leukemia but rare in normal lymphoid cells. Blood 2004; 103:3798-3804.
26. Bruggemann M, van der Velden VHJ, Raff T, Droese J, Ritgen M, Pott C, et al. Rearranged T-cell receptor beta genes represent powerful targets for quantification of minimal residual disease (MRD) in childhood and adult T-cell acute lymphoblastic leukemia (T-ALL). Leukemia 2004; 18:709-719.
27. Kotrova M, Muzikova K, Mejstrikova E, Novakova M, Bakardjieva-Mihaylova V, Fiser K, et al. The predictive strength of next-generation sequencing MRD detection for relapse compared with current methods in childhood ALL. Blood 2015; 126:1045-1047.
28. Lucio P, Gaipa G, van Lochem EG, van Wering ER, Porwit-MacDonald A, Faria T, et al. BIOMED-I concerted action report: flow cytometric immunophenotyping of precursor B-ALL with standardized triple-stainings. BIOMED-1 Concerted Action Investigation of Minimal Residual Disease in Acute Leukemia: International Standardization and Clinical Evaluation. Leukemia 2001; 15:1185-1192.
29. Lucio P, Parreira A, van den Beemd MW, van Lochem EG, van Wering ER, Baars E, et al. Flow cytometric analysis of normal B cell differentiation: a frame of reference for the detection of minimal residual disease in precursor-B-ALL. Leukemia 1999; 13:419-427.

30. Mejstrikova E, Fronkova E, Kalina T, Omelka M, Batinic D, Dubravcic K, et al. Detection of residual B precursor lymphoblastic leukemia by uniform gating flow cytometry. Pediatr Blood Cancer 2010; 54:62-70.
31. Veltroni M, De Zen L, Sanzari MC, Maglia O, Dworzak MN, Ratei R, et al. Expression of CD58 in normal, regenerating and leukemic bone marrow B cells: implications for the detection of minimal residual disease in acute lymphocytic leukemia. Haematologica 2003; 88:1245-1252.
32. Coustan-Smith E, Song G, Clark C, Key L, Liu P, Mehrpooya M, et al. New markers for minimal residual disease detection in acute lymphoblastic leukemia. Blood 2011; 117:6267-6276.
33. Solly F, Angelot F, Garand R, Ferrand C, Seilles E, Schillinger F, et al. CD304 is preferentially expressed on a subset of B-lineage acute lymphoblastic leukemia and represents a novel marker for minimal residual disease detection by flow cytometry. Cytometry A 2012; 81:17-24.
34. Vaskova M, Kovac M, Volna P, Angelisova P, Mejstrikova E, Zuna J, et al. High expression of cytoskeletal protein drebrin in TEL/AML1pos B-cell precursor acute lymphoblastic leukemia identified by a novel monoclonal antibody. Leuk Res 2011; 35:1111-1113.
35. Vaskova M, Mejstrikova E, Kalina T, Martinkova P, Omelka M, Trka J, et al. Transfer of genomics information to flow cytometry: expression of CD27 and CD44 discriminates subtypes of acute lymphoblastic leukemia. Leukemia 2005; 19:876-878.
36. Wang W, Gao L, Li Y, Li ZL, Gong M, Huang FZ, et al. The application of CD73 in minimal residual disease monitoring using flow cytometry in B-cell acute lymphoblastic leukemia. Leuk Lymphoma 2015:1-8.
37. van Dongen JJ, van der Velden VH, Bruggemann M, Orfao A. Minimal residual disease diagnostics in acute lymphoblastic leukemia: need for sensitive, fast, and standardized technologies. Blood 2015; 125:3996-4009.
38. Behm FG, Smith FO, Raimondi SC, Pui CH, Bernstein ID. Human homologue of the rat chondroitin sulfate proteoglycan, NG2, detected by monoclonal antibody 7.1, identifies childhood acute lymphoblastic leukemias with t(4;11)(q21;q23) or t(11;19)(q23;p13) and MLL gene rearrangements. Blood 1996; 87:1134-1139.
39. Jansen MW, Corral L, van der Velden VH, Panzer-Grumayer R, Schrappe M, Schrauder A, et al. Immunobiological diversity in infant acute lymphoblastic leukemia is related to the occurrence and type of MLL gene rearrangement. Leukemia 2007; 21:633-641.
40. Kalina T, Vaskova M, Mejstrikova E, Madzo J, Trka J, Stary J, et al. Myeloid antigens in childhood lymphoblastic leukemia: clinical data point to regulation of CD66c distinct from other myeloid antigens. BMC Cancer 2005; 5:38.
41. Kiyokawa N, Iijima K, Tomita O, Miharu M, Hasegawa D, Kobayashi K, et al. Significance of CD66c expression in childhood acute lymphoblastic leukemia. Leuk Res 2014; 38:42-48.
42. Djokic M, Bjorklund E, Blennow E, Mazur J, Soderhall S, Porwit A. Overexpression of CD123 correlates with the hyperdiploid genotype in acute lymphoblastic leukemia. Haematologica 2009; 94:1016-1019.

43. Cherian S, Miller V, McCullouch V, Dougherty K, Fromm JR, Wood BL. A novel flow cytometric assay for detection of residual disease in patients with B-lymphoblastic leukemia/lymphoma post anti-CD19 therapy. Cytometry B Clin Cytom 2016.
44. van Lochem EG, van der Velden VHJ, Wind H, te Marvelde JG, Westerdaal NAC, van Dongen JJM. Immunophenotypic Differentiation Patterns of Normal Hematopoiesis in Human Bone Marrow: reference patterns for age-related changes and disease-induced shifts. Clinical Cytometry 2004; 60B:1-13.
45. Wood BL. Principles of minimal residual disease detection for hematopoietic neoplasms by flow cytometry. Cytometry B Clin Cytom 2016; 90:47-53.
46. Fronkova E, Muzikova K, Mejstrikova E, Kovac M, Formankova R, Sedlacek P, et al. B-cell reconstitution after allogeneic SCT impairs minimal residual disease monitoring in children with ALL. Bone Marrow Transplant 2008; 42:187-196.
47. van der Velden VH, Wijkhuijs JM, van Dongen JJ. Non-specific amplification of patient-specific Ig/TCR gene rearrangements depends on the time point during therapy: implications for minimal residual disease monitoring. Leukemia 2008; 22:641-644.

SUPPLEMENTAL METHODS & FIGURES

SUPPLEMENTAL METHODS

Flowcytometric analysis

Flowcytometric (FCM) data were acquired using BD Biosciences FACS Diva software (BD Biosciences, Erembodegem, BE) and further analyzed using Infinicyt software (Cytognos, Salamanca, ES). In addition to the classical 2-dimensional dot plots, the Infinicyt sofware allows visualization of the data using the Automatic Population Separator (APS) graphical representation. Such APS is based on principal component analysis (PCA) with bi-dimensional graphical representations of Principal Component (PC) X versus PC Y. On the basis of such APS representation, information about the separation between two populations is obtained through definition of median and/or mean ± standard deviations (SD) borders together with information about the most informative (versus redundant) parameters [1-4]. To prevent the number of normal cells influencing the PCA, we opted to use a previously reported balanced PCA [2], implying a fixed ratio between normal and pathological events. Briefly, data on normal or regenerating B-cell precursor (BCP) cells were obtained from a merge of 7 to 14 different data-files, each corresponding to a normal or regenerating bone marrow (BM) sample. From this merged file, a pool of 28.000 to 1.124.900 normal/regenerating BCP events was obtained. Next, each BCP-ALL case (generally 5000 events/case) was merged with this normal/regenerating BCP cells pool in a balanced ratio of 1/1 of normal/leukemic events. Finally, a PCA transformation was calculated to achieve the maximum variance ('distance') between the normal/regenerating BCP cells and the leukemic cells for each individual BCP-ALL patient. Therefore, by using the balanced APS the composition of the sample (number of events) will not have an impact on the final results [1-4]. Of note, the above described strategy was only used for optimizing the antibody panel for the BCP-ALL MRD tubes, and not for actual MRD analyses.

Bulk lysis evaluations

To allow acquisition of sufficient numbers of cells (up to 5 million per tube), a bulk-lysis protocol [5] was optimized. Initial testing (washing buffer (PBS) with 0.5% BSA or 4% BSA; with or without a FACSLysing step after the final staining) showed that washing buffer with 0.5% BSA in combination with a FACSLysing step resulted in best results (lowest percentage of debris). To evaluate whether the optimized bulk-lysis procedure does not result in selective loss of certain populations (especially normal or malignant B-cells), 42 follow-up samples of BCP-ALL patients (day 15, n=15; day 33, n=15; and day 79, n=15) were stained using the EuroFlow BCP-ALL MRD tube (either tube 1 or 2, dependent on the immunophenotype

at diagnosis). For each sample, staining was performed in two ways: (1) using 50 ul whole BM, stain, FACSLysing, wash (i.e. the regular EuroFlow protocol); and (2) using 100 ul of bulk-lysed BM, stain, FACSLysing, wash (i.e. the EuroFlow bulk-lysis protocol). Data were analyzed with respect to the total number of events acquired, the percentage debris and doublets (% of all events), the number of leukocytes, and percentages of leukocyte subpopulations (% of leukocytes). Statistical evaluation (using GraphPad Prism 5, La Jolla, CA) of potential differences between the two methods was performed using the paired t-test; the correlation of MRD levels as determined by both methods was evaluated using the Spearman's r test

Re-analysis of FCM-MRD data

To evaluate the inter-laboratory (inter-observer) variability in FCM-MRD, 27 electronic data files (FCS) of 27 BCP-ALL patients during follow-up were selected based on variable levels of MRD (as determined by PCR-MRD). These data were distributed, together with the corresponding diagnostics file, amongst six EuroFlow laboratories participating in this study and analyzed blinded. Data were reported to the principal investigator (VHJvdV) who further analyzed the data using GraphPad Prism 5. Correlations between the FCM-MRD data of the individual laboratories and the median FCM-MRD value of the seven laboratories were analyzed using the Speaman's r test.

SUPPLEMENTAL FIGURES AND TABLES

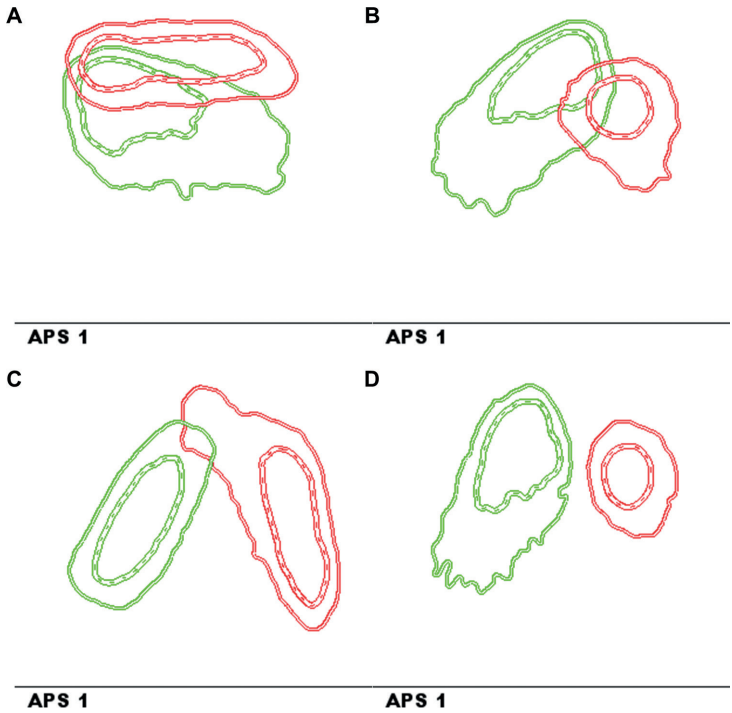

Supplemental Figure 1. Scoring system for discrimination of normal and leukemic B-cell BCP cells.
First, data from multiple normal/reactive BM samples and regenerating BM samples were used to define four particular B-cell subsets. The two most immature BCP subsets were displayed in an APS view, which was subsequently fixed (supervised). Each individual BCP-ALL case was added to the fixed APS plot and the normal BCP population nearest to the BCP-ALL cells was defined. The BCP-ALL cells and nearest normal BCP subset were then visualized in a separate (non-fixed and balanced) APS plot. Data are presented as 1SD curves (dashed lines) and 2SD curves (solid lines) for the normal/reactive BCP cells (green lines) and the BCP-ALL cells (red lines). Scoring was performed as follows: overlap of both 1SD curves: 0 points (**A**.); overlap of the 2SD and the 1SD curve: 1 point (**B**.); overlap of the 2SD curves only: 2 points (**C**.); no overlap between 2SD curves: 3 points (**D**.).

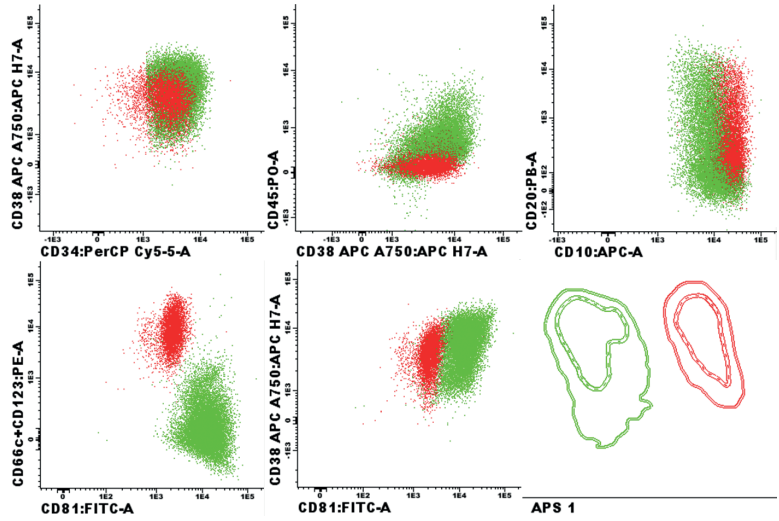

A 3 points

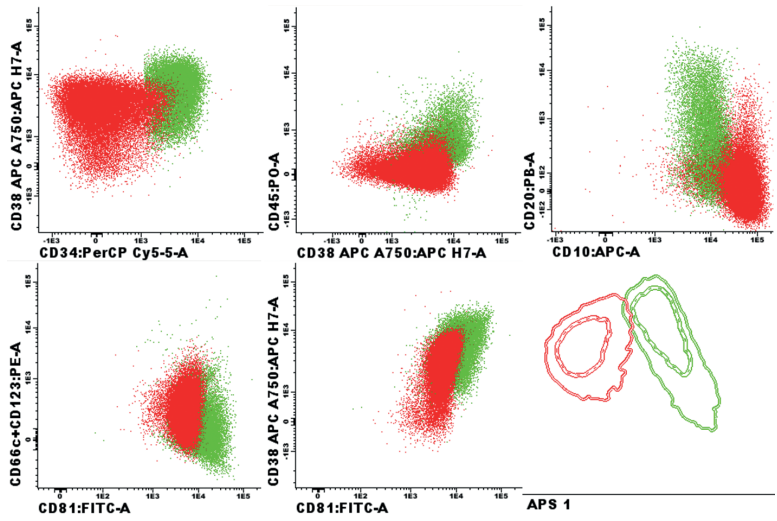

B 2 points

Supplemental Figure 2. Representative examples of different scores for discrimination of normal and leukemic BCP cells. Scoring was performed as described in Supplemental Figure 1 for four BCP-ALL patients. The green dots, 1 SD contour (dashed line), and 2 SD contour (solid lines) represent normal/regenerating BCP cells, whereas the red dots, 1 SD contour (dashed line), and 2 SD contour (solid lines) represent BCP-ALL cells. **A.** BCP-ALL case receiving 3 points based on the APS view. In the classical dot plot showing CD66c/123 versus CD81, indeed complete separation between the BCP-ALL cells and normal/regenerating BCP cells can be observed. **B.** BCP-ALL case receiving 2 points based on the APS view, with some overlap between the two 2SD curves. In the classical dot plots showing CD34 versus CD38 or CD10 versus CD20, indeed good separation between the BCP-ALL cells and normal/regenerating BCP cells can be observed, but there is some overlap.

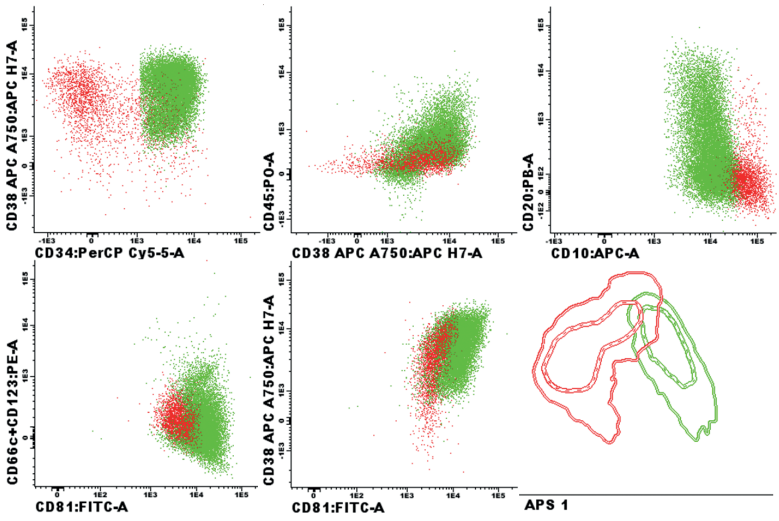

C 1 point

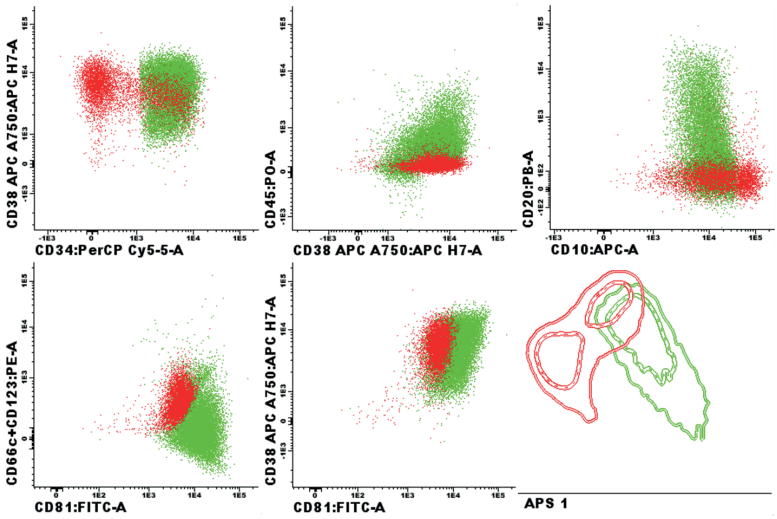

D 0 points

Supplemental Figure 2 (continued). Representative examples of different scores for discrimination of normal and leukemic BCP cells.

C. BCP-ALL case receiving 1 point based on the APS view. In the classical dot plot showing CD38 versus CD34, part of the BCP-ALL cells separates well from the normal/regenerating BCP cells, but a part of the BCP-ALL cells clearly overlaps with normal/regenerating BCP cells. Also in the CD10 versus CD20 dot plot there is some separation, but also overlap. **D.** BCP-ALL case receiving 0 points based on the APS view. The BCP-ALL population appeared to be heterogeneous, with part of the BCP-ALL cells clearly different from normal/regenerating BCP cells, but also part of the BCP-ALL cells clearly overlapping with the normal BCP cells. In agreement with this, in none of the classical dot plots good separation between the various BCP-ALL cells and normal/regenerating BCP cells was observed.

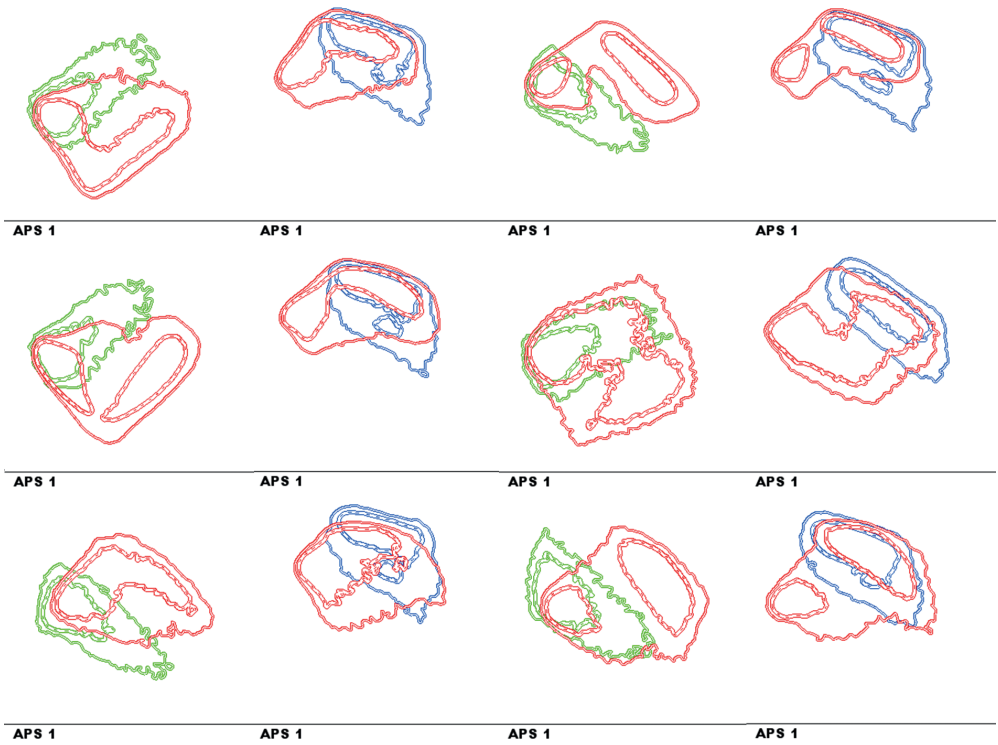

Supplemental Figure 3. BCP cells present in follow-up samples of T-ALL patients overlap with normal/ regenerating BCP cells – proof of validity of scoring system.

BM samples from six T-ALL patients were obtained at day 78 and stained with the EuroFlow BCP-ALL MRD tube 1 (final) according to the EuroFlow BCP-ALL MRD protocol. CD19+ BCP cells (red) were gated and compared with two early normal/regenerating BCP subsets (green: pre-B-I-cells; blue: pre-B-II and immature B-cells). Since BCP cells in the T-ALL patients are heterogeneous (the total BCP population, including pre-B-I, pre-B-II, and immature cells, is shown), part of the BCP cells present in the T-ALL patients show overlap with the most immature normal BCP subset (green), whereas the other BCP cells in the T-ALL sample show overlap with the more mature normal BCP subset (blue). Consequently, in all cases this would result in a scoring of zero points.

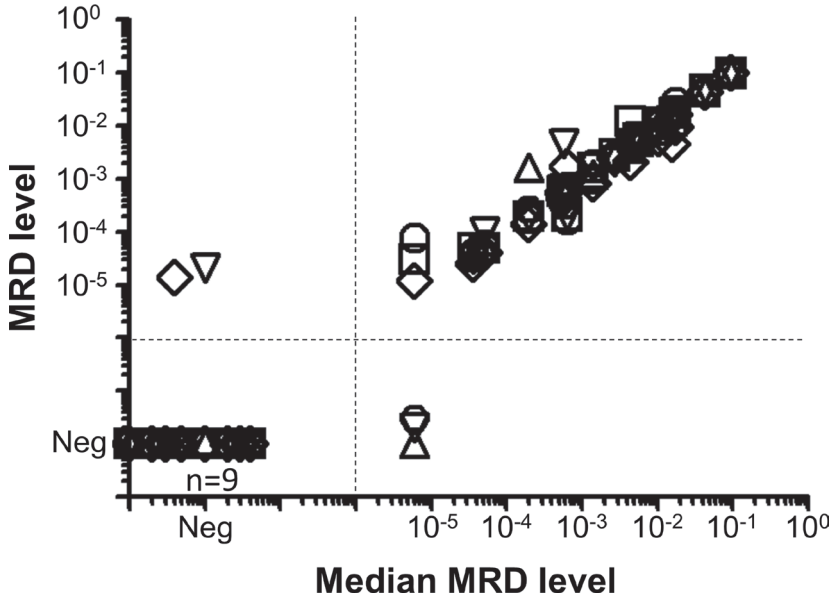

Supplemental Figure 4. Inter-laboratory variability in FCM-MRD data analysis.

Correlation between median FCM-MRD data and FCM-MRD data obtained in the six participating laboratories. Resulting Spearman r values (median FCM-MRD data versus FCM-MRD data from individual laboratory) were 0.9376, 0.9503, 0.9558, 0.9546, 0.9334, and 0.9583, respectively ($p<0.001$ for all six comparisons) (mean±SD of six laboratories: 0.95±0.01). The qualitative concordance was 100%, 100%, 96.3%, 92.6%, 96.3%, and 100%, respectively (mean±SD of six laboratories: 98.7%±1.7%). The different symbols represent different laboratories. The dashed lines represent the borders between negative FCM-MRD data and positive FCM-MRD data.

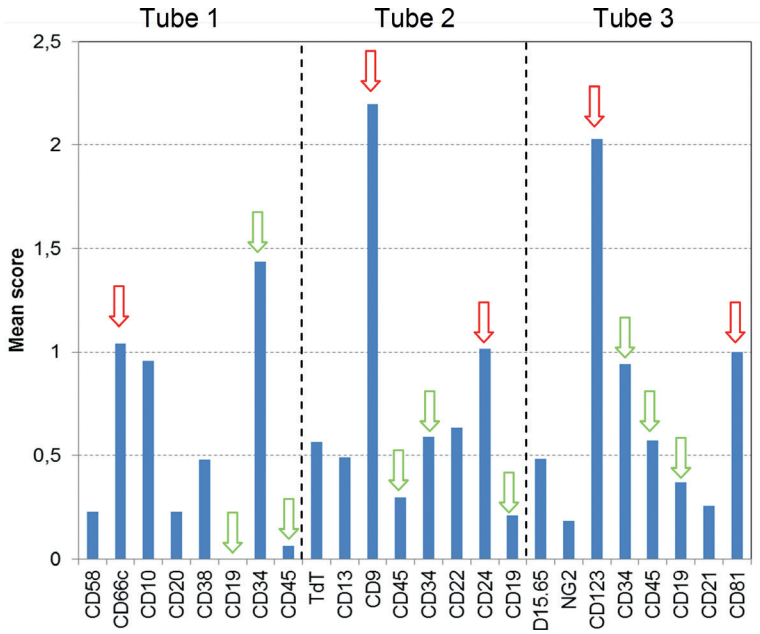

Supplemental Figure 5. Contribution of individual markers to discriminating between BCP-ALL cells and normal/reactive BCP cells.

The EuroFlow BCP-ALL diagnosis panel (tube 1, 3, and 4) was applied to 69 patients with BCP-ALL as well as to normal/reactive bone marrow samples. Data from each individual tube was analyzed by principal component analysis (APS plots), showing BCP-ALL cells and normal BCP-cells. Markers were scored based on their relative contribution to the separation in the APS plot: the top ranked marker received 3 points, the second ranked marker 2 points, the third 1 point; other markers did not get any points. For each evaluated marker, the mean score is shown. CD9, CD123, CD66c, CD81 and CD24 (marked by the red arrows) appeared to be markers that were most frequently differentially expressed between leukemic and normal/reactive BCP cells. The green arrows refer to the backbone markers (CD45, CD19, CD34) of the EuroFlow BCP-ALL diagnosis panel.

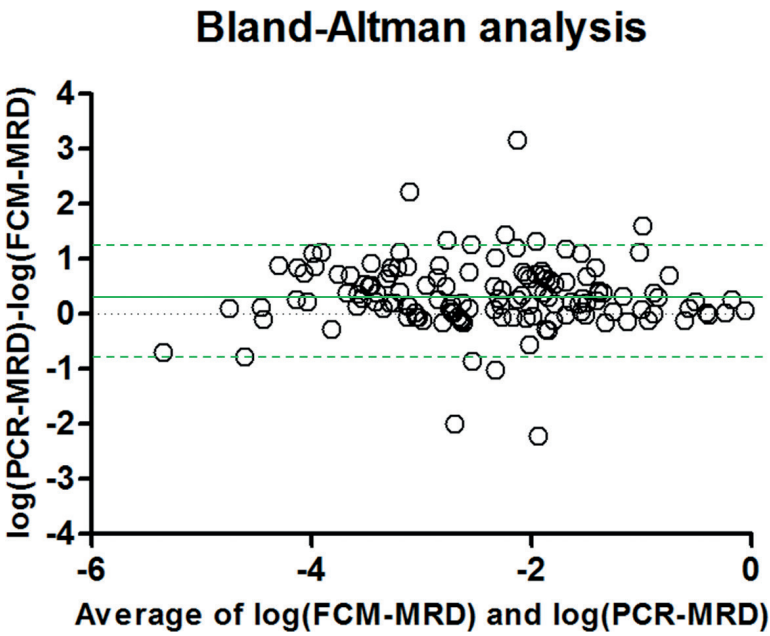

Supplemental Figure 6. Bland-Altman analysis of all samples with quantitative MRD data obtained by both FCM and PCR.

MRD data were first log10-transformed. The Bland–Altman difference plot showed a mean difference of 0.34 log (or factor 2.2; solid green line). The dashed green lines indicate the upper and lower 95% limits of agreement (-0.87-1.15). These data are comparable to previous studies comparing FCM and PCR (mean difference of 0.20 log; 95% limits of agreement from -0.72 to 1.13) [6] and may in part be explained by the use of mononuclear cells for the PCR-MRD data and whole BM for the FCM-MRD data in the present study.

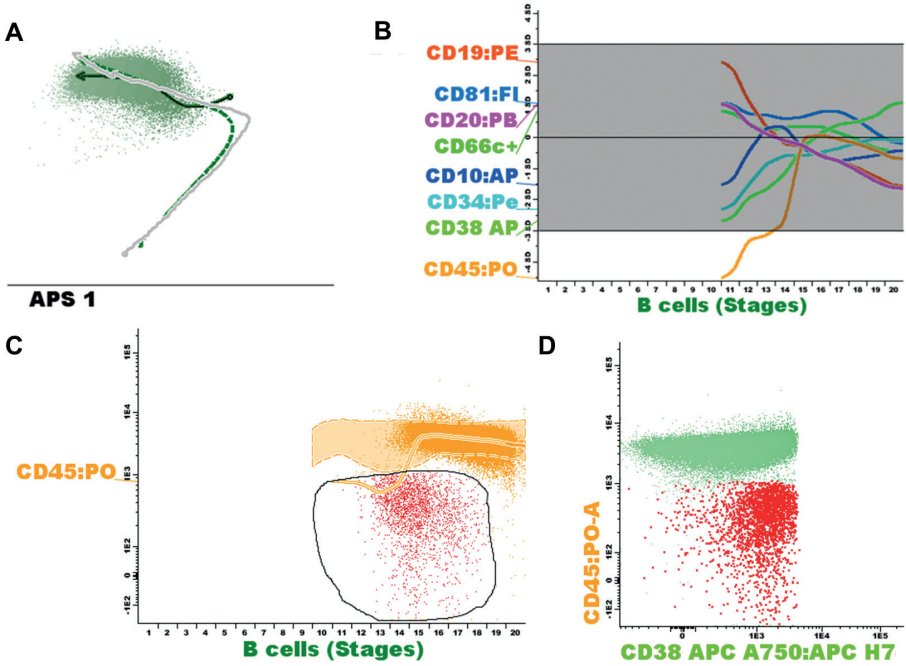

Supplemental Figure 7. Example of maturation-based FCM-MRD analysis.

FCM-MRD data were obtained from a BCP-ALL patient at day 33 of treatment as described in the Materials and Methods section. After gating on CD19+ cells and exclusion of debris and doublets (based on scatter characteristics), the resulting B-cells were compared with the maturation profile of normal/regenerating B-cells, obtained from six normal and five regenerating (day 78, MRD-PCR negative) BM samples (**A.**). The resulting maturation plot (**B.**) shows the normalized expression data, where the x-axis shows the various stages of B-cell development and the y-axis shows the level of abnormality (Grey zone: 2SD range of normal/reactive and regenerating BM). Since CD45 expression appeared to be abnormal, a maturation plot was made for CD45 only (**C.**). The orange curve shows the maturation pathway (2SD range) of the normal/reactive and regenerating BCP cells. The dots represent the data from the patient. Cells displaying aberrant phenotypes fall outside the normal maturation pathway and are gated and subsequently shown in classical dotplots (**D.**). The gated cells (indicated in red; green is other (normal) B-cells) clearly show an abnormal immunophenotype, as is demonstrated by their position outside the normal reference images (in green and yellow). The BCP-ALL cells represented 0.13% of all leukocytes.

Supplemental Table 1. Primers used for next-generation sequencing of TCRG rearrangements.

System	Oligo Name	Oligo Sequence (5' to 3')
TRG	forward primer Vg1	GTAAAACGACGGCCAGAAATCTAATTAAAAATGATTCTGGG
	forward primer Vg2	GTAAAACGACGGCCAGAAATCTAATTGAAAATGACTCTGGG
	forward primer Vg3-5	GTAAAACGACGGCCAGAAATCTAATTGAAAATGATTCTGGG
	forward primer Vg4	GTAAAACGACGGCCAGGAAATCTTATTGAAAATGACTCTGGA
	forward primer Vg8	GTAAAACGACGGCCAGAAAATCTAATTGAACGTGACTCTGG
	forward primer Vg9	GTAAAACGACGGCCAGCAATGTAGAGAAACAGGACATAGCTA
	forward primer Vg10	GTAAAACGACGGCCAGCGTAGAGAAAGAAGACATGGCC
	forward primer Vg11	GTAAAACGACGGCCAGAAGTTCTTAGAGAAAGAAGATGAGGTG
	reverse primer Jg1Jg2	CAGGAAACAGCTATGACTGTTGTTCCACTGCCAAAGAG
	reverse primer JgP1	CAGGAAACAGCTATGACAGGTGAAGTTACTATGAGCTTAGT
	reverse primer JgP2	CAGGAAACAGCTATGACAGGCGAAGTTACTATGAGCCTAGT
	reverse primer JgP	CAGGAAACAGCTATGACCGGGACCAAATACCTTGATTTT

Target-specific sequences are depicted in black colour, universal adaptors for second round of PCR are in red.

Supplemental Table 2. EuroFlow Standard Operating Protocol (SOP) for Bulk Lysis for MRD panels[a]

1. Transfer the sample containing at least 10 x 10^6 nucleated cells for each MRD tube to be stained to a 50 mL Falcon tube. Do not use more than 2 mL of sample per 50 mL of lysing solution. If more sample need to be processed (i.e. starting cells concentration is low), use several 50 mL tubes.
2. Fill the tube up to reach 50 mL volume with Pharm Lyse solution (diluted to 1X in dH2O and at room temperature - RT) or in-house made NH4CL working solution.
3. Mix well and incubate for 15 min in a roller or sample-shaker device.
4. Centrifuge at 800 g for 10 min and remove the supernatant using a Pasteur pipette or a vacuum system without disturbing the cell pellet. Alternatively, the supernatant can be decanted and drops attached to the rim of the tube can be sucked away using a paper towel. Typically, 300 µL of cell suspension should remain in the tube.
5. Add 2 mL of PBS + 0.09% of NaN3 + 0.5 % of BSA and resuspend the cell pellet vigorously.
6. Complete the volume of the tube containing the cell suspension up to 50 mL final volume with PBS + 0.09% of NaN3 + 0.5 % of BSA.
7. Mix well.
8. Centrifuge at 800 g for 5 min and remove the supernatant using a Pasteur pipette or a vacuum system, without disturbing the cell pellet. Alternatively, the supernatant can be decanted and drops attached to the rim of the tube can be sucked away using a paper towel.
9. Resuspend the cell pellet in 2 mL of PBS + 0.09% of NaN3 + 0.5 % of BSA. Mix well and transfer this volume to a 5 mL polystyrene round-bottom Falcon tube ("FACS tube").
10. Wash the 50 mL Falcon tube with 2 mL of PBS + 0.09% of NaN3 + 0.5 % of BSA more to recover cells that might have been left in the original tube. Add this volume to the 5 mL Falcon tube containing the rest of the sample transferred in step 9.
11. Centrifuge at 540 g for 5 min and remove the supernatant by decanting or using a Pasteur pipette. If the remaining cell volume is lower than 300 µL, PBS + 0.09% of NaN3 + 0.5 % of BSA will be added to reach a volume of at least 300 µL.
12. In case multiple 50 mL tubes were used (because it was needed to lyse large sample volumes) the cell suspensions from the same sample should be combined at this moment, before adjusting cell concentration. Try to keep the final volume low, so that, in case that cell concentration needs to be adjusted as indicated in the next step, it can be easily done by diluting with the recommended buffer.
13. Adjust the final cells concentration to 1 x 10^5 cells / µL, by resuspending the pellet with PBS + 0.09% of NaN3 + 0.5 % of BSA.
14. Use 100 µL (i.e. 10 million cells) of the cell suspension per each tube to be stained.

[a] For up-to-date EuroFlow protocols please see www.EuroFlow.org.

Supplemental Table 3. Original MRD data and data of additional evaluations of those 17 cases that initially showed discordant results between flowcytometric MRD analysis and RQ-PCR-based MRD analysis.

Sample	Initial FCM analysis (%)	Final FCM analysis (%)	RQ-PCR data	NGS target(s)	NGS MRD	Conclusion
Day 15						
PRA 0597	0.14	0,09	negative	no material		Remains discordant [a]
Day 33						
PRA 0993	0.016	negative	negative	*TRD*	neg	Concordant after flow consensus
MON042	negative	negative	pos, <10e-4	*IGH*	negative	Concordant, RQPCR false positive
TH16466	negative	negative	pos, <10e-4	*IGH*	negative	Concordant, RQPCR false positive
TH16836	0.0036	negative	negative	*TRD*	negative	Concordant after flow consensus
TH17174	0.006	negative	negative	*TRD*	negative	Concordant after flow consensus
ROT16666	negative	negative	pos, <5x10e-4	no material		Remains discordant
ROT 16643	negative	negative	pos, <5x10e-4	*IGH*	negative	Concordant, RQPCR false positive
ROT16278	negative	negative	pos, <5x10e-4	*IGH*	positive	Remains discordant
ROT16434	0,008	negative	negative	*IGH*	negative	Concordant after flow consensus
Day 78						
TH16297	0.0002	negative	negative	*IGH*	negative	Concordant after flow consensus
TH16415	negative	negative	pos, <5x10e-4	*IGH*	negative	Concordant, RQPCR false positive
TH16539	negative	negative	pos, <10e-4	*TRD*	negative	Concordant, RQPCR falsely positive
TH16651	negative	negative	pos, <10e-4	*TRD*	negative	Concordant, RQPCR false positive
TH17068	0.00013	negative	negative	*IGH*	negative	Concordant after flow consensus
PRA 0530	negative	negative	1.8e-4	*IGH/IGH*	positive	Remains discordant
ROT 16506	negative	negative	pos, <5x10e-4	*IGH/TRG*	negative	Concordant, RQPCR false positive

[a] Sample was positive by RQ-PCR analysis of *BCR-ABL*

REFERENCES

1. Kalina T, Flores-Montero J, van der Velden VH, Martin-Ayuso M, Bottcher S, Ritgen M*, et al.* EuroFlow standardization of flow cytometer instrument settings and immunophenotyping protocols. *Leukemia* 2012; 26:1986-2010.
2. Pedreira CE, Costa ES, Almeida J, Fernandez C, Quijano S, Flores J*, et al.* A probabilistic approach for the evaluation of minimal residual disease by multiparameter flow cytometry in leukemic B-cell chronic lymphoproliferative disorders. *Cytometry A* 2008; 73A:1141-1150.
3. Pedreira CE, Costa ES, Barrena S, Lecrevisse Q, Almeida J, van Dongen JJ*, et al.* Generation of flow cytometry data files with a potentially infinite number of dimensions. *Cytometry A* 2008; 73:834-846.
4. Pedreira CE, Costa ES, Lecrevisse Q, van Dongen JJ, Orfao A, EuroFlow C. Overview of clinical flow cytometry data analysis: recent advances and future challenges. *Trends Biotechnol* 2013; 31:415-425.
5. Aalbers AM, van den Heuvel-Eibrink MM, Baumann I, Dworzak M, Hasle H, Locatelli F*, et al.* Bone marrow immunophenotyping by flow cytometry in refractory cytopenia of childhood. *Haematologica* 2015; 100:315-323.
6. Denys B, van der Sluijs-Gelling AJ, Homburg C, van der Schoot CE, de Haas V, Philippe J*, et al.* Improved flow cytometric detection of minimal residual disease in childhood acute lymphoblastic leukemia. *Leukemia* 2013; 27:635-641.

Chapter 7

General Discussion

GENERAL DISCUSSION

In this thesis, we studied the role of both leukemic and newly generated normal B-cells in children with B-cell precursor acute lymphoblastic leukemia (BCP-ALL). We therefore focused on the leukemic B-cell population at BCP-ALL diagnosis, the recovery of the B-cell system during and after BCP-ALL therapy and the improvement of flow cytometric minimal residual disease (MRD) detection by the development of a new protocol for flow cytometric MRD detection.

BCP-ALL CLONES AND THEIR DISTRIBUTION

Although the exact pathogenesis of BCP-ALL is unclear, the development of BCP-ALL is characterized by an initiating genetic lesion, often a chromosomal translocation, which is followed by the acquisition of structural variations and sequence mutations [1]. The order of genetic events resulting in the development of overt BCP-ALL is best described for patients with an *ETV6-RUNX1* translocation.

ETV6-RUNX1 translocations can already develop in utero, since they could be traced back in neonatal blood spots in at least 50% of the *ETV6-RUNX1*-positive BCP-ALL patients [2-4]. The *ETV6-RUNX1* translocation causes an arrest in B-cell development and permanent activity of the recombination-activating gene (RAG) enzymes [5]. This continuous RAG-enzyme activity mediates ongoing immunoglobulin (IG) or T-cell receptor (TR) gene rearrangements, but also deletions (or other types of structural variations) in genes that do not encode immune receptors. This could be deduced from the presence of recombination signal sequence (RSS) motifs and nontemplated sequences at the sites of the deletion break points [5]. Finally, on top of the *ETV6-RUNX1* translocation and the genomic deletions, single nucleotide variants (SNVs) are acquired [6]. Presumably, this is not, as previously thought, a linear process in which a leukemic stem cell population is successively replaced by new clones without self-renewing capacity, but rather a process of clonal branching within the leukemic stem cell population itself (Figure 1). In the latter model, acquisition of advantageous genetic lesions in the ancestral clone leads to new clones with self-renewing capacity, as well as 'non-stem cell' clones that form dead ends in the evolutionary tree [7,8]. Selective pressure, for example caused by different phases of therapy or changes in microenvironment, determines which clones will disappear, which will grow out as dominant clones, and which will survive as subclones. Consequently, the clonal diversity and the relative dominance of clones can vary during development and progression of BCP-ALL [7]. This is in accordance with studies on paired diagnosis-relapse samples (using IG/TR gene rearrangements or copy number

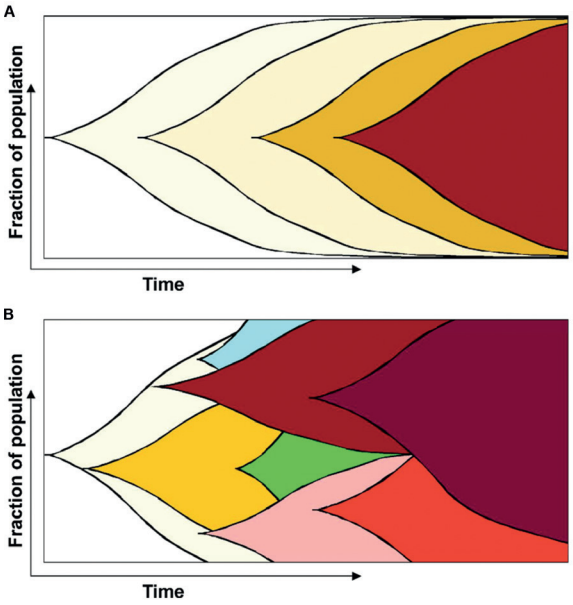

Figure 1.
Schematic view of clonal evolution. Different colors represent different clones.
A. Linear model in which new, advantageous genetic lesions occur successively, resulting in the replacement of the ancestral clone by the new clone.
B. Branch-like model in which genetically divergent clones co-exist and can change in size over time, dependent on the positive selection pressure (Marusyk et al., Biochim. Biophys. Acta, 2011) [8].

alterations (CNAs) as read-out), which showed that small subclones at diagnosis can develop into major clones at relapse (Figure 2) [9-13].

The genetic heterogeneity in a BCP-ALL population does however not directly translate into immunophenotypic subpopulations [8]. Immunophenotypic heterogeneity is common, but mostly comprises only a few subpopulations, often characterized by bimodal expression of TdT, CD34 and/or cylgμ. The immunophenotypic subpopulations within a BCP-ALL patient do not differ from each other with regard to their IG/TR gene rearrangement profile or genetic aberrancies [7,14].

The maximum number of genetically distinct clones that can be found within one BCP-ALL patient differs between studies, depending on the technique that was used. Studies which tracked BCP-ALL subclones based on their CNAs, used a limited number of pre-selected CNAs. Therefore, any other CNA or mutation was not registered, and the total number of subclones underestimated [5,7]. Studies which used PCR-based methods to analyze *IGH* gene rearrangements in BCP-ALL found, when excluding infants with an *MLL*-rearrangement (which are known to be highly oligoclonal), a maximum of 9 clonal rearrangements per patient [15]. A study which used next generation sequencing (NGS) to analyze *IGH* gene rearrangements detected up to thousands of clonal rearrangements in

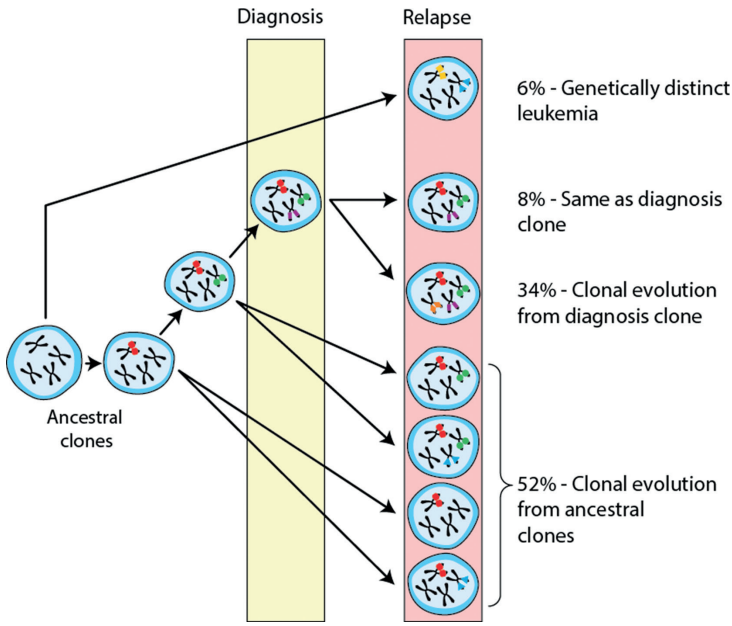

Figure 2.
Clonal relationship of diagnosis and relapse samples in ALL. The majority of relapse cases have a clear relationship to the diagnosis leukemic clone, either arising through the acquisition of additional genetic lesions or, more commonly, arising from an ancestral (prediagnosis) clone. In the latter scenario, the relapse clone acquires new lesions while retaining some but not all of the lesions found in the diagnostic sample. In only a minority of ALL cases does the relapse clone represent the emergence of a genetically distinct and thus unrelated second leukemia (Mullighan et al., Science, 2008) [11].

a single patient [16]. In this thesis, we found, by using NGS-based IG/TR gene rearrangement analysis, up to 171 clonal *IGH* gene rearrangements per patient (Chapter 2). Also for the other IG/TR gene rearrangements, we detected relatively high numbers of clonal rearrangements per patient. Although the number of clonal rearrangements is not directly representative for the number of clones (one leukemic cell can harbor multiple IG and/or TR gene rearrangements and can be mono-allelic or bi-allelic for a specific type of IG/TR gene rearrangement), NGS-based IG/TR gene rearrangement analysis shows that the number of subclones that can be present in a single BCP-ALL patient is higher than previously found with PCR-based IG/TR gene rearrangement analysis.

NGS-based IG/TR gene rearrangement analysis might be able to replace PCR-based methods in MRD detection. In this case, all leukemic clones, even the very minor subclones, can be identified in bone marrow (BM) or peripheral blood (PB) at diagnosis and subsequently retraced in follow up samples. Since all IG/TR gene rearrangements in a follow up sample are sequenced, patient-specific assays are not needed anymore [16,17]. However, certain technical issues are still hindering adequate NGS-based IG/TR gene rearrangement analysis. First, it is

difficult to discriminate between IG/TR gene rearrangements derived from small subclones and IG/TR gene rearrangements derived from normal B-cell and T-cell clones in a diagnosis sample (Chapter 2). Therefore, thresholds above which IG/TR gene rearrangements can reliably be regarded as leukemic should be carefully determined, thereby taking into account the cell input, the specific clinical setting (e.g. normal lymphocyte clones might be larger in regenerating BM or in case of infection), and age (in adult PB, non-leukemic B-cell and T-cell clones are frequently observed). Second, disproportionate amplification in super-multiplex PCR reactions prior to NGS can cause problems with the quantification of clonal IG/TR gene rearrangements. DNA barcoding techniques (in which barcodes are appended to each DNA template molecule before PCR amplification) or single cell NGS could circumvent this disproportional amplification [18]. Finally, before NGS-based MRD detection can be implemented in routine practice, full standardization and subsequent validation by scientifically independent laboratories is required [19]. The EuroClonality and EuroMRD consortia are currently optimizing NGS-based IG/TR gene rearrangement analysis (e.g. by developing new primers and bioinformatics strategies), after which the standardized NGS protocol will be validated via multi-laboratory testing rounds [19]. However, even if these technical problems can be overcome, it still needs to be elucidated whether NGS will be of additional value in BCP-ALL MRD monitoring, i.e. whether the monitoring of all clonal IG/TR gene rearrangements rather than a few major clonal IG/TR gene rearrangements will lead to improved assessment of treatment effectiveness and better relapse prediction. So far, PCR-based monitoring of a few major clonal IG/TR gene rearrangements present at diagnosis (index clones with a frequency >5%), has resulted in a 5-year cumulative relapse incidence of the Standard Risk and Medium Risk patients of only 6% respectively 8% and a loss of all MRD targets in only 10% within the relapsed patients [12,20]. In the future, retrospective studies in which samples of relapsed patients are re-analyzed by NGS-based MRD detection could determine whether these patients would have been stratified in a higher risk group (with a potentially decreased risk of relapse) if NGS-based MRD detection had been applied. Alternatively, NGS-based IG/TR gene rearrangement analysis could be used to acquire a complete overview of all leukemic IG/TR gene rearrangements present at diagnosis, after which the rearrangements with the lowest degree of oligoclonality could be selected as MRD targets for fully standardized PCR-based MRD detection during follow up.

An important aim of this thesis was to study the tissue distribution of clones and subclones in BCP-ALL patients (Chapter 2). Different BCP-ALL clones can have different functional properties, for example with regard to quiescence, drug sensitivity and angiogenic, proliferative or immunogenic potential [7,8]. Therefore, the degree of dissemination could also vary between clones. Previous studies, using mice models, found that CXCL12/CXCR4 interactions play a major role in the retention of ALL cells in the BM microenvironment

and that administration of CXCR4 antagonists mobilized ALL cells into PB [21-23]. However, only limited research was performed on the distribution of different ALL clones in BM and PB in humans. A previous study using Southern blot to study IG/TR gene rearrangements in paired BM-PB samples reported that subclonal *IGH* gene rearrangements found in BM were not always found in the corresponding PB sample in oligoclonal BCP-ALL patients [24]. However, this absence of clonal IG/TR gene rearrangements in PB could at least partly be explained by the limited sensitivity of the Southern blot technique (5-10%). Using NGS-based IG/TR gene rearrangement analysis, we found that almost all clones disseminate homogeneously via PB throughout the BM compartment (Chapter 2). This finding implies that any sample, i.e. taken from PB or any location in BM, could be used for NGS-based selection of MRD targets.

RECOVERY OF THE NORMAL B-CELL SYSTEM

Traditionally, immunophenotypic B-cell precursor (BCP) differentiation can be divided into a pro-B (CD22+CD19-CD34+), pre-B-I (CD19+CD10highCD34+), pre-B-II-Large (CD19+CD10+CD34-CD20high), pre-B-II-Small (CD19+CD10+CD34-CD20low) and immature (CD19+CD10+Igκ/λ+) stage [25-27]. By using EuroFlow-based multiparametric analysis, we were capable of visualizing the BCP differentiation as one continuum (Chapter 4). This way, transition phases that formed the missing links between the pre-B-I and pre-B-II-Large stage as well as the pre-B-II-Large and pre-B-II-Small I B-cell stage were identified.

After differentiation in BM, BCPs are released in PB as transitional B-cells, which mature in the lymphoid tissues and spleen to become naive mature, natural effector and memory B-cells [28]. In healthy infants, the BCP population in BM consists of all BCP subsets, but the mature B-cell population in PB consists mainly of transitional B-cells and naive mature B-cells (Figure 3) [29]. Around the age of four years old, the mature B-cell subsets, including the natural effector B-cell subset and memory B-cell subset, are present in a ratio that is more comparable to that in healthy adults [29]. In healthy individuals, the absolute number of naive B cells is regulated by BM output, apoptosis, antigen-independent homeostatic proliferation and further maturation after antigen encounter (Figure 4). Homeostatic proliferation of naive mature B-cells consists of 1 to 2 cell cycles, expanding the naive B-cell compartment maximally two to four fold [30,31]. The balance between the output of B-cells from BM and peripheral expansion of naive mature B-cells is tightly controlled in order to maintain a diverse naive B-cell receptor (BCR) repertoire.

By comparing BCPs and mature B-cells of healthy children with those of children treated for BCP-ALL, we gained new insights into the recovery of the B-cell system during and

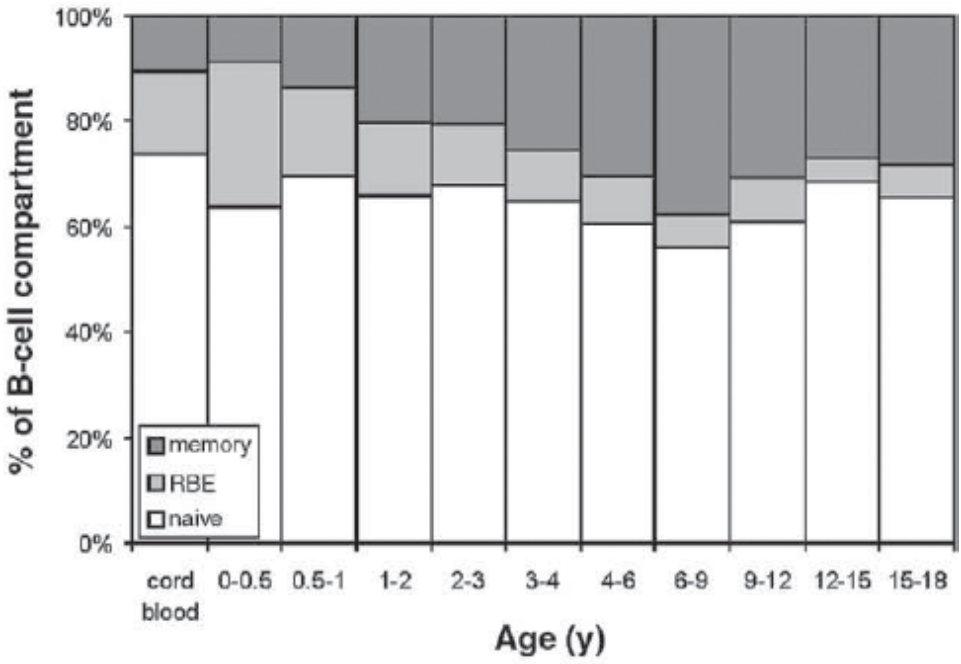

Figure 3.
B-cell subset distribution within the mature B-cell population during childhood. RBE: recent BM emigrants (transitional B-cells) (Van Gent et al., Clin. Immunol., 2009) [29].

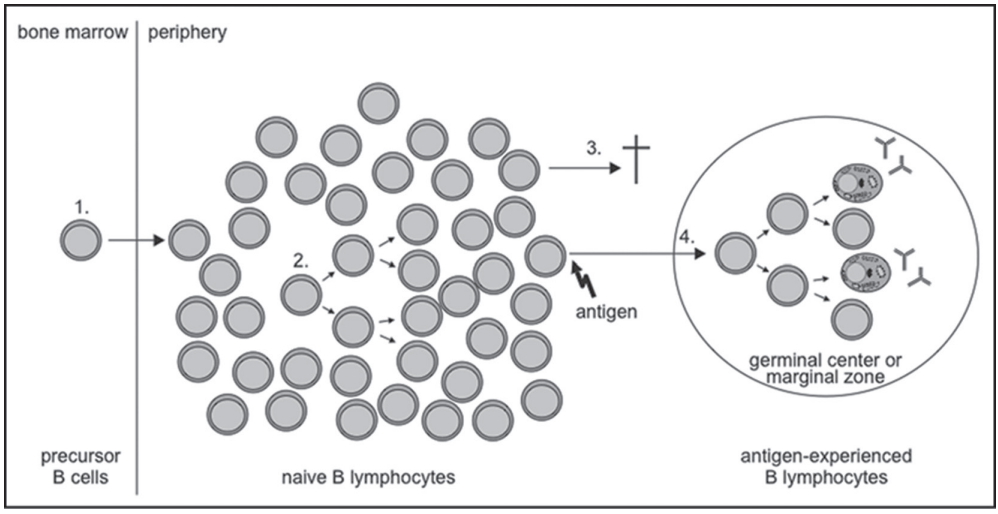

Figure 4.
The absolute number of naive mature B-cells in PB is the result of four processes: output of newly generated mature B-cells from BM (1), homeostatic proliferation of naive mature B-cells (2), apoptosis (3) and further maturation upon antigen encounter(4) (Van Zelm, Cell Cycle, 2007) [30].

after BCP-ALL therapy. First, we found that previously unknown CD34-/dim pre-B-I cells, which were rare in BM of healthy children, are abundantly present in regenerating BM of children treated for BCP-ALL (Chapter 4). We speculated that these CD34-/dim pre-B-I cells might represent pre-B-I cells that are negatively selected based on two unproductive *IGH* gene rearrangements and are consequently pre-apoptotic. By sampling at the time the regenerating BCPs simultaneously reach the stage of negative pre-B-I cell selection (like a 'wave'), the amount of CD34-/dim pre-B-I cells is relatively large. Alternatively, the CD34-/dim pre-B-I cells are not pre-apoptotic, negatively selected cells, but part of a parallel maturation pathway. According to this theory, a part of the pre-B-I cells follows a parallel maturation pathway in which CD34 expression is downregulated before a functional *IGH* gene rearrangement, and consequently cyIgμ, has been formed (Figure 5). This parallel maturation pathway might, for yet unknown reasons, be preferred under regeneration conditions, resulting in a relatively large number of CD34-/dim pre-B-I cells. One year after end of therapy, the frequency of the CD34-/dim pre-B-I cells had normalized to that in BM from healthy children (Chapter 4). Second, we found that the B-cell maturation pattern during the first year posttreatment was strikingly similar to that during initial B-cell development in healthy infants, i.e. we found a delayed formation of classical CD38dim naive mature B-cells, natural effector B-cells and memory B-cells shortly after treatment (Chapter 3). In contrast, a relatively high percentage of CD38high naive B-cells was observed in the first six months posttreatment. These cells represent pre-naive B-cells, an intermediate stage between the CD38bright transitional B-cells and the classical CD38dim naive mature B-cells [32,33]. High percentages of pre-naive B-cells were previously found in neonates and in patients after stem cell transplantation [32-34]. We can therefore conclude that, during constitution or reconstitution of the B-cell system, including reconstitution after BCP-ALL therapy, B-cell maturation does initially not pass the pre-naive B-cell stage. Third, we showed that B-cell reconstitution after BCP-ALL treatment was a result of increased *de novo* early BCP generation, rather than the result of enhanced proliferation within a BCP subset or within the naive mature B-cell subset (Chapter 3). Moreover, also when therapy was still ongoing, profound B-lymphopenia did not lead to enhanced proliferation of residual naive B-cells. In contrast, lymphopenia as a result of certain immune deficiency disorders (such as specific variants of ataxia telangiectasia or common variable immune deficiency disorder) does lead to compensatory proliferation of naive mature B-cells [35,36]. However, since B-cell reconstitution cannot take place in these immunodeficient patients (due to an arrest in B-cell differentiation), compensatory proliferation might only under these circumstances be used as a last resort to increase the number of B-cells.

Our findings on the recovery of the B-cell system in children during and after BCP-ALL therapy can have clinical implications. First, the immunophenotype of newly identified CD34-/dim pre-B-I cells, found in regenerating BM during BCP-ALL therapy, overlapped

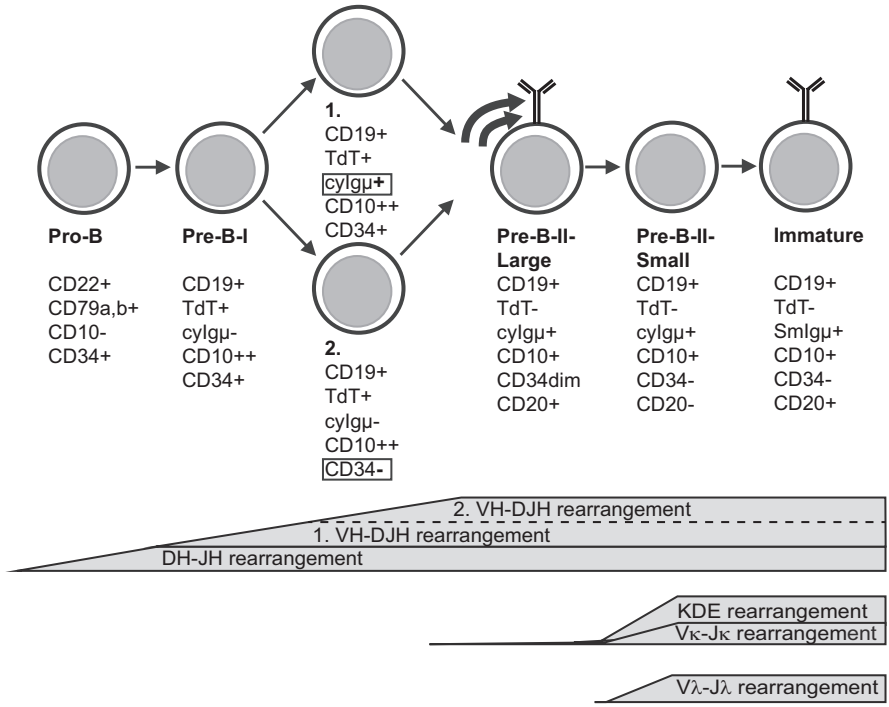

Figure 5.
Hypothetical model of two parallel routes of immunophenotypic BCP differentiation. In the classical route (1), a functional complete *IGH* gene rearrangement (and consequently cylgμ) is formed before CD34 is downregulated. In the alternative route (2), which could be the route of preference during BCP regeneration, CD34 is already downregulated before a functional complete *IGH* gene rearrangement has been formed.

with leukemic cells in a significant part of the patients (Chapter 4). These CD34-/dim pre-B-I cells should be carefully discriminated from residual BCP-ALL cells in order to prevent false-positive MRD results. It is therefore recommended to use regenerating BM (with abundant CD34-/dim pre-B-I cells) as reference in flow cytometric MRD measurements. Second, the infant-like B-cell maturation after end of therapy implies a temporary absence of the memory B-cell compartment and thus a temporary decreased humoral immunity (Chapter 3). Moreover, although part of the tissue plasma cells might survive BCP-ALL treatment, previous studies showed that plasma cells do not produce protective levels of immunoglobulins anymore in a significant part of the posttreatment patients [37,38]. The temporary lack of serum immunoglobulins and the partial loss of vaccine-induced memory indicate that administration of intravenous immunoglobulins (IVIGs) during and shortly after therapy and revaccination after end of therapy might be beneficial. The effect of IVIG administration during BCP-ALL treatment is still unclear and might even have an adverse effect, since IVIGs could potentially suppress the generation of new B-cells by a negative feedback mechanism. To determine the protective effect of IVIGs in

children treated for BCP-ALL, patients currently included in the DCOG ALL11 protocol are randomized into a group with and a group without IVIG administration during treatment. The need for revaccination after BCP-ALL treatment is also still under debate, since data on immunoglobulin levels against vaccine-preventable diseases during BCP-ALL treatment are conflicting [38-42].

IMPROVEMENT OF FLOW CYTOMETRIC MRD DETECTION

To optimize antibody panels for flow cytometric MRD measurement, many studies have focused on the identification of new MRD markers. Based on cell surface proteome analysis and genome-wide gene expression profiles of leukemic cells, several new candidate markers were found [43, 44]. Markers are only suited for flow cytometric MRD detection if they are aberrantly expressed in a significant part of the BCP-ALL patients, if their expression level clearly deviates from that on normal BCPs and if their expression pattern remains stable during follow up. Early during follow up, particularly the glucocorticoids in the induction therapy can cause modulation of marker expression levels [45,46]. This phenomenon, also called glucocorticoid-induced immunophenotypic shift, was amongst others observed for B-cell markers CD34, CD10, CD20 and CD45 [45]. In this thesis, we studied whether CD73, CD86 and CD304 could be useful in flow cytometric MRD detection in BCP-ALL patients. Since we found that these markers are clearly overexpressed on leukemic cells in a substantial number of BCP-ALL patients and that they are relatively stable during treatment (Chapter 5), these markers could be suitable for inclusion in a BCP-ALL MRD antibody panel.

As discussed in Chapter 1, different techniques can be used for MRD detection in BCP-ALL (i.e. NGS, PCR and flow cytometry), each with its own advantages and disadvantages. For adequate MRD detection, a sensitivity of at least 10^{-4} and preferably down to 10^{-5} is required. This requirement is met by PCR-based IG/TR gene rearrangement analysis, which is currently the gold standard in Europe for MRD detection in BCP-ALL patients [47,48]. The sensitivity of 4 to 6-color flow cytometric MRD detection generally reaches 10^{-4} [19], but the concordance between 4 to 6-color flow cytometry and PCR can be rather poor below a level of 10^{-3} (Figure 6) [49-51]. In this thesis we selected, based on our results on CD73, CD86 and CD304 and our previous studies, a number of potentially useful MRD markers. These markers were evaluated in multiple testing rounds, resulting in the design of a novel 8-color MRD antibody panel (Chapter 6). This antibody panel allowed for improved discrimination between leukemic cells and normal BCPs. Also, we optimized the sample processing procedure, so that a much higher number of cells ($\geq 4x10^6$) could be acquired (Chapter 6). Together, the newly developed MRD antibody panel in combination with the

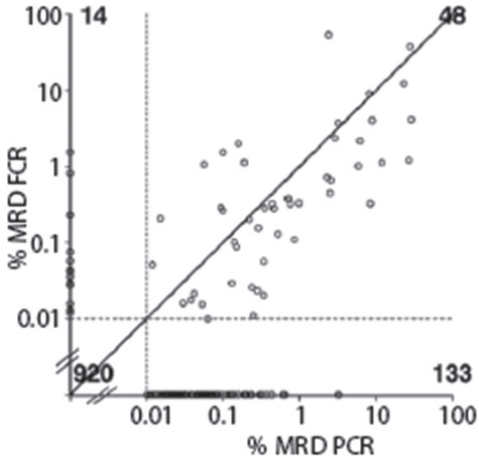

Figure 6.
Example of comparison of MRD levels measured by the PCR-based method and 4-color flow cytometry at day 78 after start of treatment (Gaipa et al., Haematologica, 2012) [49]. FCR = flow cytometry.

acquisition of sufficient cells resulted in a sensitivity of $\leq 10^{-5}$, in turn leading to a very high concordance (98%) with PCR-based MRD detection (Chapter 6).

To implement a technique into clinical practice, also other requirements, such as broad availability, easy implementation, applicability in the vast majority of patients, a short turnaround time and the possibility to standardize, should be fulfilled [19]. To meet these requirements, some aspects of flow cytometric MRD detection still need to be improved. First, the interpretation of flow cytometric data should become easier and more objective. This could be achieved by using automatic analysis tools, which are currently in development within the EuroFlow Consortium. These tools can take into account all markers at the same time and determine the 'distance' between the potential leukemic cells and normal BCPs. Second, antibody panels with a slightly adapted composition should be available for patients who are treated with antibody therapy. For example, in patients treated with Blinatumomab (which targets CD19), CD19 cannot be used as a gating marker. Replacement of CD19 with CD22 or CD24 could resolve this problem.

DIAGNOSTIC RECOMMENDATIONS

So far, the sensitivity of flow cytometric MRD detection has always been poorer than that of PCR-based MRD detection. Still, flow cytometry has been used as a complementary method to PCR-based IG/TR gene rearrangement analysis, since its rapid turnaround time allows for early assessment of the therapy response and consequently early identification of HR patients (MRD levels $>10^{-3}$), i.e. before the results of PCR-based IG/TR gene

rearrangement analysis become available [52]. In this thesis, we showed that flow cytometric MRD detection can reach a sensitivity of ≤10^{-5} and can be highly standardized. Therefore, concerning sensitivity and standardization, flow cytometric MRD detection performed according to the newly designed protocol can now meet and further improve the criteria as set by PCR-based MRD detection. Since flow cytometric MRD detection has specific advantages compared to PCR-based MRD detection, i.e. a rapid turnaround time, additional information on the normal B-cell compartment, and small effects of clonal evolution, we believe that PCR-based MRD detection can and should be replaced by EuroFlow-based, 8-color flow cytometry in the near future.

In the meanwhile, the role of NGS in BCP-ALL MRD detection should be further investigated. It can be expected that the current technical problems of NGS-based MRD detection concerning quantification as well as discrimination between leukemic and background IG/TR gene rearrangements will eventually be resolved by NGS methods that do not require 'pre-PCRs' and by databases with 'background-thresholds' for each clinical situation and cell input, respectively. In that case, NGS-based MRD detection may potentially be preferred above flow cytometric MRD detection, since NGS requires a lower cell number (which is especially advantageous in the context of low-cellular follow up samples) and circumvents the problem of immunophentypic shifts, while it still enables monitoring of almost all subclones (in contrast to PCR-based MRD detection). The next step would then be to compare NGS-based MRD monitoring of a large number of clonal IG/TR gene rearrangements versus PCR-based MRD monitoring of a selected number of clonal IG/TR gene rearrangements. Importantly, standardization of NGS-based MRD detection is currently ongoing. However, the use of NGS-based MRD detection in BCP-ALL patients is at the current stage of development not yet recommended.

REFERENCES

1. Hunger SP, Mullighan CG. Acute Lymphoblastic Leukemia in Children. N Engl J Med 2015 Oct 15; 373(16): 1541-1552.
2. Wiemels JL, Cazzaniga G, Daniotti M, Eden OB, Addison GM, Masera G, et al. Prenatal origin of acute lymphoblastic leukaemia in children. Lancet 1999 Oct 30; 354(9189): 1499-1503.
3. Zuna J, Madzo J, Krejci O, Zemanova Z, Kalinova M, Muzikova K, et al. ETV6/RUNX1 (TEL/AML1) is a frequent prenatal first hit in childhood leukemia. Blood 2011 Jan 6; 117(1): 368-369; author reply 370-361.
4. McHale CM, Wiemels JL, Zhang L, Ma X, Buffler PA, Guo W, et al. Prenatal origin of TEL-AML1-positive acute lymphoblastic leukemia in children born in California. Genes Chromosomes Cancer 2003 May; 37(1): 36-43.

5. Papaemmanuil E, Rapado I, Li Y, Potter NE, Wedge DC, Tubio J, et al. RAG-mediated recombination is the predominant driver of oncogenic rearrangement in ETV6-RUNX1 acute lymphoblastic leukemia. Nat Genet 2014 Feb; 46(2): 116-125.
6. Gawad C, Koh W, Quake SR. Dissecting the clonal origins of childhood acute lymphoblastic leukemia by single-cell genomics. Proc Natl Acad Sci U S A 2014 Dec 16; 111(50): 17947-17952.
7. Anderson K, Lutz C, van Delft FW, Bateman CM, Guo Y, Colman SM, et al. Genetic variegation of clonal architecture and propagating cells in leukaemia. Nature 2011 Jan 20; 469(7330): 356-361.
8. Marusyk A, Polyak K. Tumor heterogeneity: causes and consequences. Biochim Biophys Acta 2010 Jan; 1805(1): 105-117.
9. Choi S, Henderson MJ, Kwan E, Beesley AH, Sutton R, Bahar AY, et al. Relapse in children with acute lymphoblastic leukemia involving selection of a preexisting drug-resistant subclone. Blood 2007 Jul 15; 110(2): 632-639.
10. Li A, Zhou J, Zuckerman D, Rue M, Dalton V, Lyons C, et al. Sequence analysis of clonal immunoglobulin and T-cell receptor gene rearrangements in children with acute lymphoblastic leukemia at diagnosis and at relapse: implications for pathogenesis and for the clinical utility of PCR-based methods of minimal residual disease detection. Blood 2003 Dec 15; 102(13): 4520-4526.
11. Mullighan CG, Phillips LA, Su X, Ma J, Miller CB, Shurtleff SA, et al. Genomic analysis of the clonal origins of relapsed acute lymphoblastic leukemia. Science 2008 Nov 28; 322(5906): 1377-1380.
12. Szczepanski T, Willemse MJ, Brinkhof B, van Wering ER, van der Burg M, van Dongen JJ. Comparative analysis of Ig and TCR gene rearrangements at diagnosis and at relapse of childhood precursor-B-ALL provides improved strategies for selection of stable PCR targets for monitoring of minimal residual disease. Blood 2002 Apr 1; 99(7): 2315-2323.
13. Szczepanski T, van der Velden VH, Raff T, Jacobs DC, van Wering ER, Bruggemann M, et al. Comparative analysis of T-cell receptor gene rearrangements at diagnosis and relapse of T-cell acute lymphoblastic leukemia (T-ALL) shows high stability of clonal markers for monitoring of minimal residual disease and reveals the occurrence of second T-ALL. Leukemia 2003 Nov; 17(11): 2149-2156.
14. Obro NF, Marquart HV, Madsen HO, Ryder LP, Andersen MK, Lausen B, et al. Immunophenotype-defined sub-populations are common at diagnosis in childhood B-cell precursor acute lymphoblastic leukemia. Leukemia 2011 Oct; 25(10): 1652-1657.
15. Beishuizen A, Verhoeven MA, van Wering ER, Hahlen K, Hooijkaas H, van Dongen JJ. Analysis of Ig and T-cell receptor genes in 40 childhood acute lymphoblastic leukemias at diagnosis and subsequent relapse: implications for the detection of minimal residual disease by polymerase chain reaction analysis. Blood 1994 Apr 15; 83(8): 2238-2247.
16. Gawad C, Pepin F, Carlton VE, Klinger M, Logan AC, Miklos DB, et al. Massive evolution of the immunoglobulin heavy chain locus in children with B precursor acute lymphoblastic leukemia. Blood 2012 Nov 22; 120(22): 4407-4417.

17. Faham M, Zheng J, Moorhead M, Carlton VE, Stow P, Coustan-Smith E, et al. Deep-sequencing approach for minimal residual disease detection in acute lymphoblastic leukemia. Blood 2012 Dec 20; 120(26): 5173-5180.
18. Georgiou G, Ippolito GC, Beausang J, Busse CE, Wardemann H, Quake SR. The promise and challenge of high-throughput sequencing of the antibody repertoire. Nat Biotechnol 2014 Feb; 32(2): 158-168.
19. van Dongen JJ, van der Velden VH, Bruggemann M, Orfao A. Minimal residual disease diagnostics in acute lymphoblastic leukemia: need for sensitive, fast, and standardized technologies. Blood 2015 Jun 25; 125(26): 3996-4009.
20. Pieters R, de Groot-Kruseman H, Van der Velden V, Fiocco M, van den Berg H, de Bont E, et al. Successful Therapy Reduction and Intensification for Childhood Acute Lymphoblastic Leukemia Based on Minimal Residual Disease Monitoring: Study ALL10 From the Dutch Childhood Oncology Group. J Clin Oncol 2016 Jun 6.
21. Juarez J, Dela Pena A, Baraz R, Hewson J, Khoo M, Cisterne A, et al. CXCR4 antagonists mobilize childhood acute lymphoblastic leukemia cells into the peripheral blood and inhibit engraftment. Leukemia 2007 Jun; 21(6): 1249-1257.
22. Shen W, Bendall LJ, Gottlieb DJ, Bradstock KF. The chemokine receptor CXCR4 enhances integrin-mediated in vitro adhesion and facilitates engraftment of leukemic precursor-B cells in the bone marrow. Exp Hematol 2001 Dec; 29(12): 1439-1447.
23. Arnaud MP, Vallee A, Robert G, Bonneau J, Leroy C, Varin-Blank N, et al. CD9, a key actor in the dissemination of lymphoblastic leukemia, modulating CXCR4-mediated migration via RAC1 signaling. Blood 2015 Oct 8; 126(15): 1802-1812.
24. Beishuizen A, Verhoeven MA, Hahlen K, van Wering ER, van Dongen JJ. Differences in immunoglobulin heavy chain gene rearrangmeent patterns between bone marrow and blood samples in childhood precursor B-acute lymphoblastic leaukemia at diagnosis. Leukemia 1993 Jun; 7(6): 60-63.
25. van Zelm MC, van der Burg M, de Ridder D, Barendregt BH, de Haas EF, Reinders MJ, et al. Ig gene rearrangement steps are initiated in early human precursor B cell subsets and correlate with specific transcription factor expression. J Immunol 2005 Nov 1; 175(9): 5912-5922.
26. Noordzij JG, de Bruin-Versteeg S, Comans-Bitter WM, Hartwig NG, Hendriks RW, de Groot R, et al. Composition of precursor B-cell compartment in bone marrow from patients with X-linked agammaglobulinemia compared with healthy children. Pediatr Res 2002 Feb; 51(2): 159-168.
27. Ghia P, ten Boekel E, Sanz E, de la Hera A, Rolink A, Melchers F. Ordering of human bone marrow B lymphocyte precursors by single-cell polymerase chain reaction analyses of the rearrangement status of the immunoglobulin H and L chain gene loci. J Exp Med 1996 Dec 1; 184(6): 2217-2229.
28. Pieper K, Grimbacher B, Eibel H. B-cell biology and development. J Allergy Clin Immunol 2013 Apr; 131(4): 959-971.
29. van Gent R, van Tilburg CM, Nibbelke EE, Otto SA, Gaiser JF, Janssens-Korpela PL, et al. Refined characterization and reference values of the pediatric T- and B-cell compartments. Clin Immunol 2009 Oct; 133(1): 95-107.

30. van Zelm MC, van der Burg M, van Dongen JJ. Homeostatic and maturation-associated proliferation in the peripheral B-cell compartment. Cell Cycle 2007 Dec 1; 6(23): 2890-2895.
31. van Zelm MC, Szczepanski T, van der Burg M, van Dongen JJ. Replication history of B lymphocytes reveals homeostatic proliferation and extensive antigen-induced B cell expansion. J Exp Med 2007 Mar 19; 204(3): 645-655.
32. Lee J, Kuchen S, Fischer R, Chang S, Lipsky PE. Identification and characterization of a human CD5+ pre-naive B cell population. J Immunol 2009 Apr 1; 182(7): 4116-4126.
33. Sims GP, Ettinger R, Shirota Y, Yarboro CH, Illei GG, Lipsky PE. Identification and characterization of circulating human transitional B cells. Blood 2005 Jun 1; 105(11): 4390-4398.
34. Small TN, Keever CA, Weiner-Fedus S, Heller G, O'Reilly RJ, Flomenberg N. B-cell differentiation following autologous, conventional, or T-cell depleted bone marrow transplantation: a recapitulation of normal B-cell ontogeny. Blood 1990 Oct 15; 76(8): 1647-1656.
35. Driessen GJ, Ijspeert H, Weemaes CM, Haraldsson A, Trip M, Warris A, et al. Antibody deficiency in patients with ataxia telangiectasia is caused by disturbed B- and T-cell homeostasis and reduced immune repertoire diversity. J Allergy Clin Immunol 2013 May; 131(5): 1367-1375 e1369.
36. Driessen GJ, van Zelm MC, van Hagen PM, Hartwig NG, Trip M, Warris A, et al. B-cell replication history and somatic hypermutation status identify distinct pathophysiologic backgrounds in common variable immunodeficiency. Blood 2011 Dec 22; 118(26): 6814-6823.
37. van Tilburg CM, Sanders EA, Rovers MM, Wolfs TF, Bierings MB. Loss of antibodies and response to (re-) vaccination in children after treatment for acute lymphocytic leukemia: a systematic review. Leukemia 2006 Oct; 20(10): 1717-1722.
38. Lehrnbecher T, Schubert R, Allwinn R, Dogan K, Koehl U, Gruttner HP. Revaccination of children after completion of standard chemotherapy for acute lymphoblastic leukaemia: a pilot study comparing different schedules. Br J Haematol 2011 Mar; 152(6): 754-757.
39. Ercan TE, Soycan LY, Apak H, Celkan T, Ozkan A, Akdenizli E, et al. Antibody titers and immune response to diphtheria-tetanus-pertussis and measles-mumps-rubella vaccination in children treated for acute lymphoblastic leukemia. J Pediatr Hematol Oncol 2005 May; 27(5): 273-277.
40. Patel SR, Ortin M, Cohen BJ, Borrow R, Irving D, Sheldon J, et al. Revaccination of children after completion of standard chemotherapy for acute leukemia. Clin Infect Dis 2007 Mar 1; 44(5): 635-642.
41. Zengin E, Sarper N. Humoral immunity to diphtheria, tetanus, measles, and hemophilus influenzae type b in children with acute lymphoblastic leukemia and response to re-vaccination. Pediatr Blood Cancer 2009 Dec; 53(6): 967-972.
42. Zignol M, Peracchi M, Tridello G, Pillon M, Fregonese F, D'Elia R, et al. Assessment of humoral immunity to poliomyelitis, tetanus, hepatitis B, measles, rubella, and mumps in children after chemotherapy. Cancer 2004 Aug 1; 101(3): 635-641.
43. Mirkowska P, Hofmann A, Sedek L, Slamova L, Mejstrikova E, Szczepanski T, et al. Leukemia surfaceome analysis reveals new disease-associated features. Blood 2013 Jun 20; 121(25): e149-159.

44. Coustan-Smith E, Song G, Clark C, Key L, Liu P, Mehrpooya M, et al. New markers for minimal residual disease detection in acute lymphoblastic leukemia. Blood 2011 Jun 9; 117(23): 6267-6276.
45. Dworzak MN, Gaipa G, Schumich A, Maglia O, Ratei R, Veltroni M, et al. Modulation of antigen expression in B-cell precursor acute lymphoblastic leukemia during induction therapy is partly transient: evidence for a drug-induced regulatory phenomenon. Results of the AIEOP-BFM-ALL-FLOW-MRD-Study Group. Cytometry B Clin Cytom 2010 May; 78(3): 147-153.
46. van Wering ER, Beishuizen A, Roeffen ET, van der Linden-Schrever BE, Verhoeven MA, Hahlen K, et al. Immunophenotypic changes between diagnosis and relapse in childhood acute lymphoblastic leukemia. Leukemia 1995 Sep; 9(9): 1523-1533.
47. van der Velden VH, Cazzaniga G, Schrauder A, Hancock J, Bader P, Panzer-Grumayer ER, et al. Analysis of minimal residual disease by Ig/TCR gene rearrangements: guidelines for interpretation of real-time quantitative PCR data. Leukemia 2007 Apr; 21(4): 604-611.
48. van der Velden VH, van Dongen JJ. MRD detection in acute lymphoblastic leukemia patients using Ig/TCR gene rearrangements as targets for real-time quantitative PCR. Methods Mol Biol 2009; 538: 115-150.
49. Gaipa G, Cazzaniga G, Valsecchi MG, Panzer-Grumayer R, Buldini B, Silvestri D, et al. Time point-dependent concordance of flow cytometry and real-time quantitative polymerase chain reaction for minimal residual disease detection in childhood acute lymphoblastic leukemia. Haematologica 2012 Oct; 97(10): 1582-1593.
50. Denys B, van der Sluijs-Gelling AJ, Homburg C, van der Schoot CE, de Haas V, Philippe J, et al. Improved flow cytometric detection of minimal residual disease in childhood acute lymphoblastic leukemia. Leukemia 2013 Mar; 27(3): 635-641.
51. Malec M, van der Velden VH, Bjorklund E, Wijkhuijs JM, Soderhall S, Mazur J, et al. Analysis of minimal residual disease in childhood acute lymphoblastic leukemia: comparison between RQ-PCR analysis of Ig/TcR gene rearrangements and multicolor flow cytometric immunophenotyping. Leukemia 2004 Oct; 18(10): 1630-1636.
52. Basso G, Veltroni M, Valsecchi MG, Dworzak MN, Ratei R, Silvestri D, et al. Risk of relapse of childhood acute lymphoblastic leukemia is predicted by flow cytometric measurement of residual disease on day 15 bone marrow. J Clin Oncol 2009 Nov 1; 27(31): 5168-5174.

Addendum

ABBREVIATIONS

AL	Acute leukemia
ALL	Acute lymphoblastic leukemia
ASO	Allele-specific oligonucleotide
ADCC	Antibody dependent cellular cytotoxicity
ATM	Ataxia-telangiectasia-mutated protein
BCP-ALL	B-cell precursor acute lymphoblastic leukemia
BCP	B-cell precursors
BCR	B-cell receptor
BM	Bone marrow
CSR	Class switch-recombination
CDC	Complement dependent cytotoxicity
CNA	Copy number alteration
Cy	Cytoplasmic
D	Diversity
Dx	Diagnosis
DNA-PKcs	DNA-dependent protein kinase catalytic subunit
FC / FCM	Flow cytometry
GC	Germinal center
HR	High Risk
IG	Immunoglobulin
IVIG	Intravenous immunoglobulin
J	Joining
LAIP	Leukemia-associated immunophenotype
LSC	Leukemic stem cell
MR	Medium Risk
MRD	Minimal residual disease
MNC	Mononuclear cell
NGS	Next generation sequencing

nMFI	Normalized median fluorescence intensity
PB	Peripheral blood
PC	Plasma cell
pDC	Plasmacytoid dendritic cell
RCT	Read count threshold
RQ-PCR	Real-time quantitative PCR
RAG	Recombinase activating gene
RSS	Recombination signal sequence
SNV	Single nucleotide variant
SHM	Somatic hypermutation
SB	Southern blot
SR	Standard Risk
SCT	Stem cell transplantation
Sm	Surface membrane
TR	T-cell receptor
TdT	Terminal deoxynucleotidyl transferase
V	Variable

SUMMARY

B-cell precursors (BCPs) in the bone marrow (BM) differentiate through the pro-B, pre-B-I, pre-B-II-Large, pre-B-II-Small, and Immature stages to become mature B-cells, which express a functional B-cell receptor (BCR) and circulate through the peripheral blood (PB) and lymphoid tissues. The mature B-cell population in PB can be subdivided into a translational B-cell, naive mature B-cell, natural effector B-cell, memory B-cell and plasmablast subset. Plasmablasts mature into plasma cells, which are able to secrete immunoglobulins that are similar to their BCR. During BCP differentiation, the BCR is generated through a process called V(D)J-recombination, which allows for the creation of a wide variety of BCRs and consequently the recognition of a large number of antigens.

In patients with B-cell precursor acute lymphoblastic leukemia (BCP-ALL), a BCP is arrested in a particular BCP differentiation stage and transformed into a malignant cell. Subsequently, clonal expansion takes place, resulting in suppression of the normal hematopoiesis in BM. Each year, approximately 100 new cases of pediatric BCP-ALL are diagnosed in the Netherlands. The general prognosis for children with BCP-ALL is good, with a cure rate of approximately 90%. However, depending on clinical features, specific genetic aberrancies and treatment response, the prognosis differs between individual patients. The strongest prognostic factor is the level of residual leukemic cells, i.e. minimal residual disease (MRD), during the first 3 months of treatment. To detect MRD, different methods can be used, i.e. flow cytometry, PCR-based immunoglobulin/T-cell receptor (IG/TR) gene rearrangement analysis, and next generation sequencing (NGS)-based IG/TR gene rearrangement analysis. Depending on the MRD level, patients are stratified in a Standard Risk, Medium Risk or High Risk treatment arm. Patients with a standard risk receive less intense therapy, resulting in a significant reduction of drug-induced morbidity, whereas patients with a medium and high risk receive more intense therapy to increase the cure rate.

The aim of this thesis was to study the role of both leukemic and newly generated normal B-cells in children with BCP-ALL.

First, we focused on the leukemic B-cell population at BCP-ALL diagnosis. As a result of clonal evolution during disease development and progression, a BCP-ALL population can consist of multiple clones. Different clones may have different properties and might be differently distributed within the body. In **Chapter 2**, we aimed to study the distribution of all leukemic clones, including the small subclones, throughout the BM and PB compartments. For this purpose we used NGS-based analysis of IG/TR gene rearrangements in paired BM samples and paired BM-PB samples from BCP-ALL patients at diagnosis. We found a high number of clonal IG/TR gene rearrangements per patient, indicating that a BCP-ALL population can contain more subclones than previously

thought. Importantly, we showed that the relative quantity of IG/TR gene rearrangements within the total (rearranged) BCP-ALL population was generally equal between different locations within the BM compartment and between the BM and the PB compartments. Therefore, we conclude that almost all BCP-ALL clones, even the small subclones, are fairly homogeneously distributed throughout the BM and PB compartments at diagnosis (albeit that the frequencies in total mononuclear cells may be lower in PB because of the presence of remaining normal leukocytes).

BCP-ALL treatment destroys, besides the targeted leukemic cells, also the normal B-cell compartment. In **Chapter 3**, we studied the reconstitution of the B-cell compartment in both BM and PB in patients treated for BCP-ALL. We showed that, during treatment intervals, regenerating BCPs maximally reached the pre-B-II-Large stage and were therefore not capable of supplying the PB with new mature B-cells. Also, we found that the maturation pattern during B-cell reconstitution in patients after end of therapy, was strikingly similar to that during initial B-cell development in healthy infants. Finally, we showed that B-cell reconstitution was the result of increased *de novo* generation of the earliest BCPs, rather than the result of enhanced proliferation within a BCP subset or the naive mature B-cell subset. Consequently, a naive B-cell population with broad BCR repertoire will be rebuild. Together, these data indicate that, after an infant-like memory B-cell deficit in the first 6 to 12 months after treatment, a B-cell compartment similar to that in healthy children will be reestablished in posttreatment BCP-ALL patients.

Flow cytometric MRD detection at time points of BCP regeneration (during treatment intervals) can be difficult, due to potential immunophenotypic overlap between residual leukemic cells and regenerating BCPs. In **Chapter 4**, we obtained detailed data on the immunophenotypic maturation of regenerating BCPs in BM from treated BCP-ALL patients by using 8-color immunostainings and novel EuroFlow-based multiparameter software tools and compared these with the immunophenotypic maturation of BCPs in BM from healthy children. We found a previously unknown (expanded) immunophenotypic BCP subset in the regenerating BCP population, which consisted of pre-B-I cells with a negative to dim CD34 expression. Due to their 'aberrant' immunophenotype, these BCPs could potentially be mistaken for residual leukemic cells, which could further complicate flow cytometric MRD detection at time points of BCP regeneration. Additionally, by studying the immunophenotypic maturation of normal BCPs in healthy children, we identified two additional maturation stages which could be regarded as transition stages in between the conventional BCP differentiation stages.

To implement flow cytometry as first choice for MRD detection in BCP-ALL, a sensitivity of $\leq 10^{-4}$ should be achieved. Therefore, an improved immunophenotypic identification of leukemic cells and an increased acquisition of cells per follow up time point is required. To improve the identification of leukemic cells in a background of normal BCPs, new markers

that are differentially expressed on normal BCP and leukemic cells are needed. In **Chapter 5**, we studied the expression of CD73, CD86 and CD304 in a large cohort of pediatric BCP-ALL patients, included in multiple laboratories of the international EuroFlow Consortium. We showed that these markers were overexpressed in a substantial part of the BCP-ALL patients and that expecially CD73 was relatively stable during the first phase of treatment. Inclusion of these markers in BCP-ALL MRD antibody panels may therefore contribute to improved flow cytometric MRD analysis. In **Chapter 6**, we designed, via four testing- and evaluation rounds, an optimized 8-color antibody panel (in which CD73 and CD304 were included), and developed a sample processing procedure for the acquisition of large cell numbers ($\geq 4x10^6$ per tube). The final flow cytometric BCP-ALL MRD detection protocol was fully standardized and tested in parallel to PCR-based MRD detection in multiple laboratories participating in the EuroFlow Consortium. The data from this study showed that the new protocol was applicable to >98% of the patients and reached a sensitivity of $\leq 10^{-5}$, which is comparable to (or even better than) real-time quantitative (RQ)-PCR-based MRD detection. Importantly, concordant results between flow cytometric and PCR-based MRD measurements were obtained in an unprecedented >98% of the samples.

Since the sensitivity of flow cytometric MRD detection now at least equals that of PCR-based MRD detection and since flow cytometry has additional advantages, we finally conclude, in **Chapter 7**, that implementation of EuroFlow-based 8-color flow cytometry as primary MRD detection method in children with BCP-ALL can be recommended.

SAMENVATTING

Voorloper B-cellen in het beenmerg (BM) differentiëren via de pro-B, pre-B-I, pre-B-II-Large, pre-B-II-Small en Immature stadia tot rijpe B-cellen, die een functionele B-cel receptor (BCR) tot expressie brengen en door het perifere bloed (PB) en de lymfoide weefsels circuleren. De rijpe B-cel populatie in PB kan onderverdeeld worden in een transitional, naive mature, natural effector, memory B-cel en plasmablast subset. Plasmablasten rijpen verder uit tot plasma cellen, welke immunonglobulines secreteren die gelijk zijn aan hun BCR. De BCR wordt gedurende de B-cel differentiatie gevormd door middel van een proces genaamd V(D)J recombinatie, hetgeen zorgt voor de vorming van een grote diversiteit aan BCRs en daarmee de herkenning van een groot aantal antigenen.

In patiënten met B-cell precursor acute lymphoblastic leukemia (BCP-ALL) is een BCP geblokkeerd in een specifiek differentiatie stadium en getransformeerd tot een maligne cel. Vervolgens treedt klonale expansie op, met onderdrukking van de normale hematopoiese in het BM tot gevolg. In Nederland worden er elk jaar ongeveer 100 nieuwe gevallen van BCP-ALL bij kinderen gerapporteerd. De prognose van kinderen met BCP-ALL is over het algemeen goed met een overlevingspercentage van ongeveer 90%. De prognose verschilt echter per patiënt, afhankelijk van klinische karakteristieken, specifieke genetische afwijkingen en de respons op behandeling. De sterkste prognostische factor is het aantal leukemische cellen dat nog aanwezig is gedurende de eerste drie maanden na het starten van de therapie, hetgeen minimale restziekte (MRD) wordt genoemd. Voor de detectie van MRD kunnen verschillende methoden worden gebruikt, namelijk flowcytometrie, PCR-gebaseerde immunoglobuline/T-cel receptor (IG/TR) gen herschikking analyse en next generation sequencing (NGS)-gebaseerde IG/TR gen herschikking analyse. Aan de hand van het MRD niveau worden patiënten ingedeeld in een standaard risico, middelhoog risico of hoog risico groep. Patiënten met een laag risico krijgen minder intense therapie, resulterend in significant minder bijwerkingen, terwijl patiënten met een middelhoog of hoog risico zwaardere therapie krijgen om de kans op genezing te vergroten.

Het doel van dit proefschrift was om in kinderen met BCP-ALL de rol van zowel de leukemische als nieuw gegenereerde normale B-cellen te bestuderen.

We richtten ons hierbij eerst op de leukemische B-cel populatie op het moment van diagnose. Ten gevolge van klonale evolutie gedurende de ontwikkeling en progressie van BCP-ALL, kan de BCP-ALL populatie uit meerdere klonen bestaan. Deze klonen kunnen verschillende eigenschappen hebben en zich potentieel in verschillende mate door het lichaam verspreiden. In **Hoofdstuk 2** hadden we als doel om de verspreiding van alle leukemische klonen, inclusief de kleine subklonen, over het BM en PB compartiment te onderzoeken. Hiervoor gebruikten we NGS-gebaseerde analyse van IG/TR gen herschikkingen in gepaarde BM monsters en gepaarde BM-PB monsters, afgenomen op

het moment van diagnose. We vonden een groot aantal IG/TR gen herschikkingen per patiënt, hetgeen erop duidt dat een BCP-ALL populatie uit meer subklonen kan bestaan dan voorheen werd gedacht. Ook toonden we aan dat de relatieve hoeveelheid IG/TR gen herschikkingen binnen de totale (herschikte) BCP-ALL populatie gelijk was tussen verschillende BM locaties en tussen BM en PB. Daarom kunnen we concluderen dat bijna alle BCP-ALL klonen, inclusief de kleine subklonen, behoorlijk homogeen verspreid zijn over het BM en PB compartiment op het moment van diagnose (hoewel de frequenties binnen de totale mononucleaire cellen lager kunnen zijn in PB vanwege de aanwezigheid van resterende normale leukocyten).

De behandeling van BCP-ALL vernietigt, naast de beoogde leukemische cellen, ook het normale B-cel compartiment. In **Hoofdstuk 3** onderzochten we de heropbouw van het B-cel compartiment in zowel BM als PB van patiënten die behandeld worden voor BCP-ALL. We lieten zien dat, tijdens therapie intervallen, regenererende BCPs maximaal het pre-B-II-Large stadium bereikten en daarom het PB tijdens therapie niet van nieuwe mature B-cellen konden voorzien. Daarnaast vonden we dat het maturatie patroon tijdens B-cel reconstitutie in patiënten na beëindiging van therapie gelijk was aan dat tijdens de initiële opbouw van het B-cel systeem in gezonde pasgeborenen. Tenslotte toonden we aan dat het herstel van het B-cel compartiment na BCP-ALL therapie het resultaat was van *de novo* regeneratie van de meest vroege voorloper B-cellen, en niet van compensatoire proliferatie in een BCP subset of de naive mature B-cel subset. Hierdoor zal opnieuw een naïeve B-cel populatie met een breed BCR repertoire ontstaan. Deze data wijzen erop dat, na het tijdelijk gebrek aan geheugen B-cellen in de eerste 6 tot 12 maanden na de therapie, een B-cel compartiment gelijk aan dat in gezonde kinderen gevormd zal worden in patiënten die BCP-ALL therapie hebben ondergaan.

Flowcytometrische MRD detectie op tijdstippen waarop BCP regeneratie plaatsvindt (gedurende therapie intervallen) wordt bemoeilijkt door mogelijke immunofenotypische overlap tussen resterende leukemische cellen en regenererende BCPs. In **Hoofdstuk 4** verzamelden we gedetailleerde data over de immunofenotypische maturatie van regenererende BCPs in BM van behandelde BCP-ALL patiënten, door gebruik te maken van 8-kleuren flowcytometrie en nieuwe EuroFlow-gebaseerde multiparameter software tools, en vergeleken deze met de immunofenotypische maturatie van BCPs in BM van gezonde kinderen. We vonden een tot nu toe onbekende (geëxpandeerde) immunofenotypische BCP subset in de regenererende BCP populatie, welke bestond uit pre-B-I cellen met negatieve tot zwakke expressie van CD34. Door dit 'afwijkende' immunofenotype kunnen deze regenererende BCPs potentieel foutief aangezien worden voor resterende leukemische cellen, hetgeen flowcytometrische MRD detectie op tijdstippen van BCP regeneratie nog complexer kan maken. Daarnaast identificeerden we, door tevens de immunofenotypische maturatie van normale BCPs in gezonde kinderen

te onderzoeken, twee extra normale BCP differentiatie stadia, welke beschouwd kunnen worden als overgangsfasen tussen de conventionele BCP differentiatie stadia.

Om flowcytometrie als eerste keus voor MRD detectie bij kinderen met BCP-ALL te implementeren, zal een sensitiviteit van $\leq 10^{-4}$ behaald moeten worden. Daarvoor is een verbeterde immunofenotypische identificatie van leukemische cellen en een toegenomen acquisitie van cellen per follow up tijdstip vereist. Om de identificatie van leukemische cellen in een achtergrond van normale BCPs te verbeteren zijn nieuwe markers nodig, die verschillend tot expressie komen op normale BCPs en leukemische cellen. In **Hoofdstuk 5** onderzochten we de expressie van CD73, CD86 en CD304 in een groot cohort kinderen met BCP-ALL, geïncludeerd in verschillende laboratoria behorend tot het EuroFlow Consortium. We vonden dat deze markers overexpressie toonden op leukemische cellen in een substantieel deel van de BCP-ALL patiënten en dat vooral CD73 relatief stabiel bleef gedurende de eerste fase van therapie. Inclusie van deze markers in een BCP-ALL MRD antistof panel kan daarom mogelijk bijdragen aan verbeterde flowcytometrische MRD detectie. In **Hoofdstuk 6** ontwierpen we, via vier test-en-evaluatie rondes, een optimaal 8-kleuren antistof panel (waarin CD73 en CD304 werden geïncludeerd), en ontwikkelden we een monster verwerkingsprocedure waarmee grote cel aantallen verkregen konden worden ($\geq 4x10^6$ cellen). Het uiteindelijke flowcytometrische BCP-ALL MRD detectie protocol werd volledig gestandaardiseerd en, in parallel met PCR-gebaseerde MRD detectie, getest in meerdere laboratoria participerend in het EuroFlow Consortium. De resultaten van deze studie lieten zien dat het nieuwe protocol toepasbaar was bij >98% van de patiënten en een sensitiviteit behaalde van $\leq 10^{-5}$, hetgeen vergelijkbaar is met (of zelfs beter is dan) de sensitiviteit van real-time quantitative (RQ)-PCR gebaseerde detectie van IG/TR gen herschikkingen. Concordante MRD resultaten werden, voor het eerst, verkregen in >98% van de monsters.

Omdat de sensitiviteit van flowcytometrie die van PCR op zijn minst evenaart en flowcytometrie extra voordelen heeft, concludeerden we ten slotte in **Hoofdstuk 7** dat implementatie van EuroFlow-gebaseerde 8-kleuren flowcytometrie als primaire methode voor MRD detectie bij kinderen met BCP-ALL kan worden aanbevolen.

DANKWOORD

Graag wil ik de volgende personen bedanken voor hun bijdrage aan de totstandkoming van dit proefschrift.

Allereerst wil ik mijn promotor, professor Jacques van Dongen, bedanken. Beste Jacques, hartelijk dank dat je me het vertrouwen hebt gegeven om binnen jouw groep te promoveren. Jouw kritische, maar altijd positieve en onderbouwende commentaren hebben mij enorm geholpen. Onze brainstorm-sessies, waarin jouw enthousiasme inspirerend werkte, zal ik zeker gaan missen.

Daarnaast gaat mijn dank uit naar mijn co-promotor, Vincent van der Velden. Beste Vincent, heel erg bedankt voor de begeleiding en de tijd die je voor mij hebt vrijgemaakt. Door jouw vriendelijkheid en behulpzaamheid schroomde ik nooit je om advies of hulp te vragen. Ik bewonder je kalmte en optimisme, ook in tijden van drukte, en ik heb ontzettend veel van je geleerd.

Beste Mirjam van der Burg, bedankt voor het optreden als secretaris van de kleine commissie en het kritisch nalezen van mijn proefschrift. Professor Tomasz Szczepański, thank you very much for participating in my reading committee, and also for your kind support during the earlier stages of my PhD project. Professor Michel Zwaan, ook u bedankt voor uw deelname aan de kleine commissie. Professor Pieter Sonneveld, professor Ellen van der Schoot en professor Arjan Lankester, veel dank voor het zitting nemen in de grote commissie.

Dear colleagues from the EuroFlow consortium, thanks to all of you for our fruitful, but also very enjoyable collaboration. Professor Alberto Orfao, I greatly appreciated your input and comments on my manuscripts. Ester Mejstrikova, Tomas Kalina, Giuseppe Gaipa and Quentin Lecrevisse, thank you for the successful cooperation between the laboratories, the useful discussions and your great hospitality. It was a real pleasure to work with you. Dear Michaela and Lukasz, thanks a lot for your support and, almost equally important, the fun we had during our meetings all over Europe. I hope we will stay in touch!

Valerie de Haas en Edwin Sonneveld, bedankt voor jullie ondersteuning vanuit het SKION, mijn aanvragen voor extra patiëntmateriaal of -informatie waren jullie nooit te veel. Beste Alita, ontzettend bedankt voor je inzet en je hulp, jouw enthousiasme werkte zeer aanstekelijk.

Auke Beishuizen en de verpleegkundigen en analisten van de afdeling kinderoncologie, ontzettend bedankt voor jullie inspanningen met betrekking tot het bewaren en doorsturen van extra patiëntmateriaal. Malek Faham, thanks a lot for your help on the next generation sequencing study. Andrew Stubbs, thank you for the collaboration between our lab and the department of Bioinformatics. Beste David, wat een geluk voor mij dat ik jouw kennis en vaardigheden op het gebied van de informatica tot mijn beschikking had.

Dank dat je altijd klaar stond om 'even' langs te komen om een 'kleine' verandering in de pipeline door te voeren.

Beste professor Peter Katsikis en collega's van de afdeling Immunologie, bedankt voor de fijne tijd op de afdeling. In het bijzonder dank aan de (oud-) analisten van de LLD groep: Henk, Jeroen, Romana, Claudia, Stefan, Jeanet, André, Gonnie, Jolanda, Jane, Patricia, Rianne en Maaike. Heel erg bedankt voor jullie bijdrage aan het labwerk in dit proefschrift en jullie hulp in het algemeen. Beste Daniëlle, Bibi en Erna, de opmaak van dit proefschrift heb ik in alle vertrouwen aan jullie over kunnen laten. Daniëlle, heel erg bedankt voor je tijd en inzet!

Beste Suzanne, nogmaals dank voor de bijdrage die jij als student aan een van mijn projecten hebt geleverd. Lieve Anouk, ook jij was een student van grote waarde. Dank je voor je inzet en hulp, maar zeker ook voor je gezelligheid!

Beste (oud-) OIO's en postdoc's, bedankt voor de leuke tijd en de mentale ondersteuning. Pauline, Fabian en Magda, wat heb ik het getroffen met jullie als kamergenootjes! Lieve Wouter, naast leverancier van koffie, ook altijd in voor een borrel met mij! Dear Cristina and Katharina, thanks for the fun I had with both of you. Lieve Malou, bedankt voor de leuke koffiepauzes en goede gesprekken. Marieke, wat fijn dat ik de laatste maanden bij jou kon wonen. Lieve Christina, Jorn, Willem-Jan, Wendy, Martine, Jenna, Chris, Sandra, Jan-Piet, Wida, Simar, Marlieke, Christopher, Hanna Kok, Britt, Marjolein, Liza, Anne, Hanna IJspeert, Daphne, Ruud en Diana, bedankt voor de gezelligheid op de afdeling, maar ook tijdens onze borrels en avondjes uit.

Lieve Anna en Alice, lieve paranimfen, wat hebben we samen veel meegemaakt! Bedankt dat ik alles met jullie kon delen. Wat goed dat wij elkaar getroffen hebben!

Lieve vriendjes en vriendinnetjes van RSKV Erasmus, wat fijn dat ik bij jullie cluppie hoor! De feestjes, activiteiten en oh ja…het korfballen zelf waren een zeer welkome afleiding van de promotie-stress. Bedankt hiervoor!

Lieve Annemieke, Eva, Berb, Saar, Inge en Maud, samen JC Harrie, samen de gezelligste! Bedankt meiden! Lieve Irene, wat een geluk dat je in Rotterdam bent komen wonen, ik had onze avondjes uit niet willen missen! Lieve Feline, Andrea en Michelle, ongeacht de tijd ertussen is het altijd goed en vertrouwd als we elkaar weer zien, en dat zal zeker zo blijven. Bedankt voor jullie vriendschap! Lieve Anouk, ook jij bedankt, onze vriendschap van al minstens 20 jaar koester ik enorm.

Lieve familie, lieve Ruby, wat fijn dat ik jullie heb, ik kan jullie niet missen! Lieve oma, ik weet hoe trots je op mij bent en ik wil je ervoor bedanken dat je altijd aan mij denkt. Lieve Toon, Niek en Tom, de liefste ouders en het beste broertje. Jullie zijn er altijd voor mij, bedankt voor jullie onvoorwaardelijke steun en liefde.

CURRICULUM VITAE

Personal details

Name:	Prisca Theunissen
Date of birth:	21 June 1987
Place of birth:	Bilzen, Belgium
Nationality:	Dutch

Education

2005-2011	Master of Science: Medicine Maastricht University, Maastricht
1999-2005	VWO Gymnasium ('Cum laude') Jeanne d'Arc College, Maastricht

Research experience

Sep 2011 - Dec 2016	PhD study 'Normal and malignant B-cells in acute lymphoblastic leukemia: insight into clonal distribution, minimal residual disease and normal B-cell recovery. ' Department of Immunology, Erasmus MC, Rotterdam (promotor prof.dr. Jacques van Dongen and co-promotor dr. Vincent van der Velden)

Relevant internships

Mar 2011 – Jul 2011	Final internship Internal Medicine Atrium Medisch Centrum, Heerlen
Oct 2010 – Feb 2011	Research Internship 'Celkernruptuur bij laminopathieën ten gevolge van lamine A/C genmutatie'. Department of Molecular Cell Biology, Maastricht University, Maastricht (supervisor dr. Jos Broers)
Dec 2008 – Feb 2009	Internship Internal Medicine ('Excellent') Academische Ziekenhuis Maastricht, Maastricht

Internships abroad

Apr 2009 – May 2009	Internship Ear, Nose and Throat Medicine University of Pretoria/ Steve Biko Academic Hospital, Pretoria, South Africa
Sep 2008 – Nov 2008	Hepato-pancreato-biliary surgery University College London/University College London Hospital (UCLH), London, United Kingdom

Courses (additional to PhD portfolio)

- Course Tropical Medicine (extra-curricular), Maastricht University, Maastricht
- Course Pathology: musculoskeletal system and thorax/abdomen (extra-curricular), Maastricht University, Maastricht
- Reanimation course, Nederlandse Reanimatie Raad, Maastricht

Secundary activities

- PhD-committee Department of Immunology
- Member Student Evaluation Committee, Maastricht University, Maastricht
- Program coordinator Studentenkamer Festival, Maastricht
- Member student society SV KoKo, Maastricht

PHD PORTFOLIO

Name PhD student:	Prisca Theunissen
Erasmus MC Department:	Immunology
Research School	Molecular Medicine
PhD period:	September 2011 – December 2016
Supervisor:	Dr. Vincent H.J. van der Velden
Promotor:	Prof. dr. Jacques J.M. van Dongen

General courses

2013	English biomedical writing and communication, Erasmus MC, Rotterdam
2012	Management voor Promovendi en Post-docs, NIBI, Utrecht

Specific courses

2015	Galaxy Course, Department of Bioinformatics and MolMed postgraduate school, Erasmus MC, Rotterdam
2013	Advanced Flow Cytometry course, BD Biosciences, Erasmus MC, Rotterdam
2012	Annual course Advanced Immunology, MolMed postgraduate school, Erasmus MC, Rotterdam
2012	Biomedical Research Techniques, MolMed postgraduate school, Erasmus MC, Rotterdam

Seminars and workshops

2012	Infinicyt workshop
2011	Medical Immunology, Department of Immunology, Erasmus MC, Rotterdam and Avans Hogeschool, Utrecht
2011-2014	Annual MolMed day (4x)

Conferences and presentations

2014	56th American Society of Hematology Annual Meeting, San Francisco, United States (poster presentation)
2014	9th Biennial Childhood Leukemia Symposium, Prague, Czech Republic (poster presentation)
2013	18th Congress of the European Hematology Association, Stockholm, Sweden (poster presentation)

2011/2014	Nederlandse Vereniging voor Immunologie (NVVI) Annual Meeting, Noordwijkerhout, The Netherlands (2x; poster presentations)

Other meetings and presentations

2012-2015	EuroFlow Consortium meetings, Praag/Katowice/Rotterdam/ Porto/Milaan/Salamanca 10x); oral presentations)
2015	Nederlandse Vereniging voor Immunologie (NVVI) Lunteren Meeting, Lunteren, The Netherlands
2013	European Scientific foundation for Laboratory Hemato Oncology Symposium, Rotterdam, The Netherlands

Other

2013	SMWBO Exam
2011-2015	Seminars department of Immunology
2011-2015	Journal club department of Immunology

Teaching

2013-2015	Supervision Bachelor thesis (2x), Erasmus MC, Rotterdam
2012-2013	Medicine for scholars (2x), Erasmus MC, Rotterdam
2011-2015	Assistant histology teaching (8 cycles), Erasmus MC, Rotterdam

PUBLICATIONS

1. **Theunissen PMJ**, van Zessen D, Stubbs AP, Faham M, Zwaan M, van Dongen JJM, van der Velden VHJ. Antigen receptor sequencing of paired bone marrow samples shows homogeneous distribution of acute lymphoblastic leukemia subclones. *Submitted*

2. **Theunissen PMJ**, van den Branden A, van der Sluijs-Gelling A, de Haas V, Beishuizen A, van Dongen JJM, van der Velden VHJ. Understanding the reconstitution of the B-cell compartment in bone marrow and blood after treatment for B-cell precursor acute lymphoblastic leukemia. *Submitted to Br J Haematol (minor revisions)*

3. **Theunissen PMJ**, Sędek Ł, de Haas V, Szczepański T, van der Sluijs-Gelling A, Mejstrikova E, Nováková M, Kalina T, Lecrevisse Q, Orfao A, Lankester AC, van Dongen JJM, van der Velden VHJ. Detailed immunophenotypic analysis of B-cell precursors in regenerating bone marrow of children treated for acute lymphoblastic leukemia reveals new subsets: implications for minimal residual disease detection. *Submitted*

4. Sędek Ł, **Theunissen PMJ**, Sobral da Costa E, van der Sluijs-Gelling A, Mejstrikova E, Gaipa G, Sonsala A, Twardoch M, Oliveira E, Nováková M, Buracchi C, van Dongen JJM, Orfao A, van der Velden VHJ, Szczepański T. Pattern of expression of CD73, CD86 and CD304 in normal vs. leukemic B-cell precursors: utility as stable minimal residual disease markers for treatment monitoring in childhood B-cell precursor acute lymphoblastic leukemia. *Submitted*

5. **Theunissen PMJ**, Mejstrikova E, Sędek Ł, van der Sluijs-Gelling A, Gaipa B, Bartels M, Sobral da Costa E, Kotrová M, Nováková M, Sonneveld E, Buracchi C, Bonaccorso P, Oliveira E, te Marvelde JG, Szczepański T, Lhermitte L, Hrusak O, Lecrevisse Q, Grigore GE, Froňková E, Trka J, Brüggemann M, Orfao A, van Dongen JJM, van der Velden VHJ. Standardized flow cytometry for highly sensitive MRD measurements in B-cell acute lymphoblastic leukemia. *Accepted for publication in Blood*